Optimal Performance of Advanced Radiating Structures

Ehrenborg, Casimir

2019

Document Version:
Publisher's PDF, also known as Version of record

Optimal Performance of Advanced Radiating Structures

Casimir Ehrenborg

Doctoral Dissertation
Electromagnetic Theory

Lund University
Lund, Sweden
2019

Doctoral dissertation which, by due permission of the Faculty of Engineering, Lund University, will be publicly defended on May 24, 2019, at 9:15 a.m. in lecture hall E:1406, John Ericssons väg 4, Lund, for the degree of Doctor of Philosophy in Engineering in Electromagnetic Theory.

Department of Electrical and Information Technology
Electromagnetic Theory Group
Lund University
P.O. Box 118, S-221 00 Lund, Sweden

Series of licentiate and doctoral theses
ISSN 1654-790X; No. 122
ISBN 978-91-7895-117-8 (print)
ISBN 978-91-7895-118-5 (digital)

Typeset in Computer Modern 10 pt using LaTeX and BibTeX.
Printed in Sweden by *Tryckeriet i E-huset*, Lund University, Lund.
April, 2019

"The man who moves a mountain begins by carrying away small stones."

-Confucius: The Analects

Abstract

Requirements on radiating structures are constantly increasing, demand for faster speed, smaller size, and higher reliability drives today's technical development. However, for electrically small structures, less than half-a-wavelength in size, performance is fundamentally limited by physical size. This thesis explores how to construct and calculate physical bounds for advanced antennas and complex environments that are in use in modern communication today. Previously, physical bounds have mainly been formulated for single feed, single resonance antennas in free space. However, in modern communication settings antennas are much more advanced. In all cellular networks after the third generation of mobile networks (3G) Multiple-Input-Multiple-Output (MIMO) systems are being utilized, where antennas have multiple feeds. Formulating physical bounds for these antennas is not trivial due to classically limited performance metrics, such as the Q-factor, being difficult to define or calculate. It is not only the antennas themselves that are more advanced, antennas are also used in implants, medical devices, meta materials, and in plasmonics. Calculating physical bounds in these scenarios require new methods that reliably predict accurate results for all different types of materials.

In this thesis a method for constructing physical bounds for general MIMO antennas is presented. By idealizing the channel and representing the antenna by the equivalent currents excited across it, a bound can be calculated with convex current optimization. It is shown that that bound is effectively reached by exciting different sets of modes depending on what constraints are put on the optimization. Different shapes and sub-regions are analyzed using the strength of these modes.

A new method for calculating stored energy and Q-factor in the presence of complex media is presented and investigated. By viewing the antenna as a dynamic system the Method of Moments (MoM) impedance equation can be formulated as a state space model. The energy stored within in such a model is identified as the stored energy. This method can be generalized to dispersive and inhomogeneous media.

Populärvetenskaplig Sammanfattning (in Swedish)

Antenner förekommer överallt i vår vardag. Den fullständiga uppkopplingen via våra telefoner och datorer vi utnyttjar idag har blivit en extremt viktig del av vårt sammhälle. I dagsläget ser den trenden ut att bara öka, med fler och fler enheter i bruk, och mycket annan elektronik som behöver kommunicera med internet. Med denna ökning i volym kommer nya krav på uppkopplingshastigheten och mängden data som överförs. För detta krävs bättre antenndesigner.

I dagsläget är en stor del av antenndesign baserat på ingenjörsmässiga tummregler och tidskrävande simuleringar. Att automatisera eller effektivisera den processen är något som skulle frigöra en stor mängd tid för många högutbildade inom telecom industrin. Denna avhandling undersöker en viktig del i den processen kallad fysiska begränsningar för antenner. Fysiska begränsningar är optimala gränser för prestanda hos antenner. De konstrueras genom att på förhand räkna ut hur bra det är möjligt för en antenn att fungera, givet en viss storlek. De kan användas både som ett mål i automatiserad antenndesign eller som ett riktmärke för hur mycket prestanda det finns kvar att utvinna för en designer.

Dessa fysiska begränsingar räknas ut genom att representera en antenn med de strömmar den har möjlighet att inducera i ett visst område. Dessa strömmar används som variabler i optimeringsproblem som maximerar antennprestanda. Genom att skriva dessa optimeringsproblem på konvex form kan vi garantera att en optimal lösning finns. Konvexa problem är sådana problem som alltid har ett unikt minimum värde, de kan enkelt beskrivas som kurvor med endast en dal. Att hitta minimum värdet av en sådan kurva är ett problem som går att lösa. Denna metod har tidigare används för att räkna ut maximal bandbredd, strålningsfokusering, eller effektivitet för en antenn.

Tidigare har denna typ av begränsningar framförallt existerat för enkla antenntyper i frirymd. I dagens användarscenarion är antenntyper mycket mer avancerade än så. För all telefonkommunikation från 4G och framåt används flera antenner tillsammans för att sända en större mängd data. Nästan alla antenner byggs på dielektriska material eller används i närheten av förlustmaterial, så som kroppen. Denna avhandling fokuserar på att skapa fysiska begränsningar för dessa mer avancerade antenntyper. Multipelantennsystem undersöks genom att idealisera vissa parametrar för att kunna beskriva antennerna på en form där strömoptimering kan användas. Fysiska begränsningar för antenner i förlustmaterial konstrueras genom att beskriva antennen som ett dynamiskt system och därigenom kunna utvärdera dess bandbredd utan att behandla vissa antennbegrepp som är svåra att definiera i komplexa material.

Preface

This thesis summarizes the research I have carried out over the past five years at the Department of Electrical and Information Technology, Lund University, Sweden. The thesis starts with a brief summary of the research topics covered in the papers. This is followed by the papers which are organized to follow the order in which the introduction has been written.

List of Included Papers

I. M. Capek, L. Jelinek, K. Schab, M. Gustafsson, B.L.G. Jonsson, F. Ferrero, and C. Ehrenborg,
"Optimal Planar Electric Dipole Antenna."
IEEE Antennas and Propagation Magazine, to be published.

Contributions of the author: The author of this thesis was part of the collaborative workshop and discussions that resulted in this paper. He has simulated some of the examples in section III and written the accompanying text.

II. C. Ehrenborg, and M. Gustafsson,
"Fundamental bounds on MIMO antennas."
IEEE Antennas and Wireless Propagation Letters, Vol. 15, No. 1, pp. 21–24, IEEE, 2018.

Contributions of the author: The author of this thesis is the main contributor to this paper, setting up and running the simulations, and writing the paper. The paper has been written under the supervision of the second author.

III. C. Ehrenborg, and M. Gustafsson,
"Physical Bounds and Radiation Modes for MIMO Antennas."
Technical Report TEAT-7265, Electromagnetic Theory Department of Electrical and Information Technology, 2018.[1]

Contributions of the author: The author of this thesis is the main contributor to this paper, setting up and running the simulations, and writing the paper. The paper has been written under the supervision of the second author.

[1] Submitted for publication

IV. C. Ehrenborg, M. Gustafsson, and M. Capek,
"Analysis of Energy Modes for MIMO Antennas."
Technical Report TEAT-7266, Electromagnetic Theory Department of Electrical and Information Technology, 2019.[2]

Contributions of the author: The author of this thesis is the main contributor to this paper. He has set up and run all of the simulations. He has written the paper. Miloslav Capek has written the simulation software used for one of the examples. The paper has been written under the supervision of the second author.

V. K. Schab, L. Jelinek, M. Capek, C. Ehrenborg, D. Tayli,
G.A.E. Vandenbosch, M. Gustafsson,
"Energy Stored by Radiating Systems."
IEEE Access, Vol. 6, pp. 10553–10568, IEEE, 2018.

Contributions of the author: The author of this thesis has participated in the collaborative workshop and discussions resulting in this paper. He has run some of the simulations illustrating the theory presented and written the text discussing those results.

VI. M. Gustafsson, and C. Ehrenborg,
"State-Space Models and Stored Electromagnetic Energy for Antennas in Dispersive and Heterogeneous Media."
Radio Science, Vol. 52, No. 11, pp. 1325–1343, 2017.

Contributions of the author: The author of this thesis has co-written this paper with Mats Gustafsson. He has run some of the simulations and written much of the text. Mats Gustafsson has developed the theory of the paper.

[2]To be submitted for publication

Other Publications by the Author

The author of this dissertation is also the author or co-author of the following publications which are related to but not considered part of the dissertation:

VII. G. Wolgast, C. Ehrenborg, A. Israelsson, J. Helander, E. Johansson, and H. Manefjord, "Wireless body area network for heart attack detection [Education Corner]" *IEEE Antennas and Propagation Magazine*, Vol. 58, No. 5, pp. 84-92, IEEE, 2016.

VIII. M. Gustafsson, D. Tayli, C. Ehrenborg, M. Cismasu, S. Nordebo, "Antenna current optimization using MATLAB and CVX." *FERMAT*, Vol. 15, No. 5, pp. 1–29, 2016.

IX. C. Ehrenborg, M. Gustafsson, "Physical Bounds and Automatic Design of Antennas Above Ground Planes." *2016 URSI International Symposium on Electromagnetic Theory (EMTS)*, pp. 233–235, Helsinki, Finland, 2016.

X. M. Nedic, C. Ehrenborg, Y. Ivanenko, A. Ludvig-Osipov, S. Nordebo, A. Luger, B.L.G. Jonsson, D. Sjöberg, M. Gustafsson, "Herglotz Functions and Applications in Electromagnetics," In: *Advances in Mathematical Methods for Electromagnetics.* Edited by K. Kobayashi and P. Smith. 22 pages, IET, 2019. *In press*

XI. A. Ludvig-Osipov, J. Lundgren, C. Ehrenborg, Y. Ivanenko, A. Ericsson, M. Gustafsson, B.L.G. Jonsson, D. Sjöberg, "Fundamental Bounds on Extraordinary Transmission with Experimental Validation." *arXiv preprint arXiv:1810.07669*, 2018.[3]

[3]Submitted for publication

Acknowledgments

First and foremost I would like to thank Prof. Mats Gustafsson, my supervisor, not only for being an amazing and inspiring teacher, but also for being a good friend. Thanks also to Prof. Daniel Sjöberg, my co-supervisor, for putting an insane amount of effort into all his endeavors and always being fun. I have been honored to teach electromagnetic theory with Prof. Anders Karlsson and Prof. Gerhard Kristensson, both of whom have shown me how fun and rewarding teaching can be. I gratefully acknowledge the Swedish Foundation for Strategic Research (SSF) whose funding of the project Complex analysis and convex optimization for EM design made this PhD possible.

I would like to thank the SSF group, Prof. Lars Jonsson, Prof. Sven Nordebo, and Prof. Annemarie Luger, as well as Yevhen Ivanenko, Andrei Osipov, and Dr. Mitja Nedic, for collaborating with me and their patience in explaining mathematical concepts. I would like to congratulate the group: Prof. Miloslav Capek, Prof. Kurt Schab, Prof. Lukas Jelinek, Prof. Fabien Ferrero, and Prof. Guy Vandenbosch, for equally fruitful and frustrating discussion and collaboration. It was my pleasure to attend all of our workshops and host you at my parents summer house.

I am eternally grateful for the company of my colleagues, who have made this journey extremely entertaining and who have supported me all the way through. Johan Lundgren, thank you for making me cry with laughter all the time, and for making sure I have gotten into much better physical health. Dr. Jakob Helander, thank you for putting life in a good perspective and making me feel better about myself. Dr. Doruk Tayli, thank you for bringing the Mediterranean flare to everyday work life and all the wonderful discussions, or arguments as the case may be. Christian Nelson, thank you for having the best stories. Thank you also to Dr. Andreas Ericsson, Dr. Iman Vakili, Dr. Marius Cismasu, Dr. Alexander Bondarik, Dr. Gabriele Costanza, Dr. Mikael Henriksson and Niklas Wingren.

Finally, I would like to thank my friends and family, for always believing in me. Most specially my parents, Christian Ehrenborg and Prof. Ewa Ehrenborg, for always pushing me to reach my full potential. A special thank you to Irene Geijselaers for helping me with the figures in this thesis and keeping me calm while writing it.

Lund, April 2019

Casimir Ehrenborg

Acronyms and Abbreviations

3G	Third Generation Mobile Networks
4G	Fourth Generation Mobile Networks
5G	Fifth Generation Mobile Networks
AToM®	Antenna Toolbox for MATLAB
CM	Characteristic Mode
CVX®	Matlab Software for Disciplined Convex programming
EFIE	Electric Field Integral Equation
FBW	Fractional Bandwidth
IoT	Internet of Things
MATLAB®	Matrix Laboratory
MIMO	Multiple Input Multiple Output
MFIE	Magnetic Field Integral Equation
MoM	Method of Moments
PEC	Perfect Electric Conductor
PMCHWT	Poggio-Miller-Chan-Harrington-Wu-Tsai
QCQP	Quadratically Constrained Quadratic Programming
RFID	Radio Frequency Identification Programming
Rx	Receiver
SNR	Signal to Noise Ratio
SVD	Singular Value Decomposition
Tx	Transmitter

Contents

Part I: Introduction and Research Overview

Casimir Ehrenborg

1 Background and Motivation

Antennas are more and more becoming an integral part of all user electronics. As our society becomes fully connected the need for high speed communication between devices is becoming more pressing [1, 21, 111]. With the emergence of Internet of Things (IoT) many more devices will be connected and contain antennas [50]. This, in conjunction with user demand, puts ever more pressing requirements on high data rates and information transfer. While much of this is achieved by clever communication schemes, the demand on antenna performance increases as well. Being able to design antennas achieving as much performance as possible is therefore very desirable. This naturally leads to the question: *How good is it possible to make an antenna?* This is the question this thesis aims to answer.

Antennas are implemented in many different environments, in the case of base stations or tv-antennas, space and miniaturization is not a pressing issue. In these cases antennas can be designed at their natural size, *i.e.*, around half-a-wavelength or larger. However, many antennas are placed within devices, such as mobile phones or Bluetooth headphones, where space is at a premium. Here, the antennas compete with other vital components, such as batteries, connectors, screens *etc.*, for design space. In these cases it becomes imperative to be able to effectively place and utilize the space allotted to antenna design. This is schematically shown in Fig. 1a, where only a sub-region of the device is dedicated to antenna design. For such a scenario the question can therefore be formulated as: *Where should my design region be placed and what are the possibilities for my antenna design within it, in the presence of this environment.* Knowing this type of information prior to designing an antenna has many uses. It gives an upper limit for what is possible for the designer; they need not waste valuable time and effort trying to achieve specifications handed down to them that are not possible. It can be used as a goal or stopping criterion for optimization; when I am this close to the limit it is not worth investing more time or effort. Such information can be used to implement automated antenna design, where software carries out much of the basic or rough antenna design, reducing cost.

Before the work carried out in this thesis there already existed a wealth of work investigating the problem of calculating optimal antenna performance [13, 20, 22, 24, 40, 41, 51, 57, 60, 63, 66, 68, 81, 84, 94, 112, 116, 120, 122, 130]. These papers dealt mainly with calculating the optimal performance of simple, single feed, single resonance, antennas in free space. These idealizations makes the mathematical problem easier to define, more tractable, and have served the antenna community well in scenarios where they are reasonable approximations of reality. However, in modern communication settings antenna design complexity has surpassed what many of these optimal limits are capable of describing. Since the advent of the Fourth Generation Mobile Networks (4G) communication network, antennas are designed to have several inputs or elements that work together to maximize the bit-rate transferred [27, 45, 54, 79, 97, 104]. For these types of an-

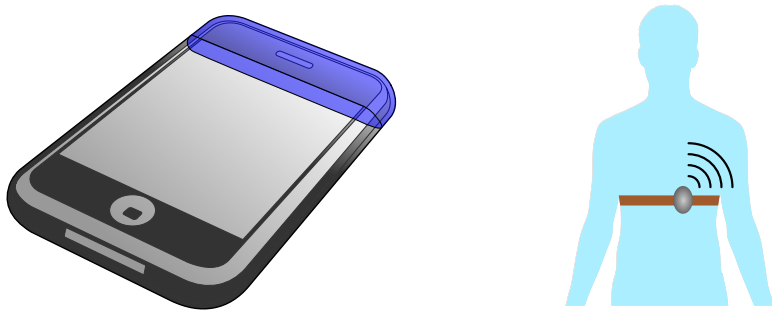

(a) (b)

Figure 1: (a) Schematic illustration of one of the possible regions within a mobile phone dedicated to antenna design. (b) Illustration of a body area network operating on the human body.

tennas, known as MIMO antennas, past optimal limits are not applicable. Many devices and antennas also operate close to, or inside, of the human body, see Fig. 1b. Most of the previous limits for optimal performance are based on the assumption that the antenna is operating in free space, and therefore become inaccurate in the presence of complex media. This thesis aims to begin to investigate how to construct optimal limits, or *physical bounds*, for more advanced radiating systems, specifically MIMO antennas and antennas inside of complex media.

1.1 Research Overview

From our intuitive understanding of the term optimal it might be logical to assume that this value is close to unobtainable and only achieved by complex and brilliant designs. However, an important part of calculating a bound for antenna performance is that it should be "tight". In this context that implies that the bound is as close as possible to reality, a bound which is far away from what can be achieved is less useful. In Paper I of this thesis, an overview of how to reach the physical bounds for small antennas with simple antenna designs is presented.

MIMO systems function based on the relationship between two sets of antennas, typically a base station and a device. In both of these the antennas are antennas with more than one input [104]. This makes it difficult to construct general physical bounds for MIMO antennas. Previously, this has been done for spherical surfaces [45, 54, 102] or through information theoretical approaches [9, 35–37, 39, 49, 80, 87, 93, 97, 98, 100, 101, 118, 128]. However, it is interesting to consider how much performance can be gained from antenna design. In Fig. 1a it can be seen that antennas are restricted to much more confined regions in many applications. Physical bounds must therefore treat arbitrary design regions. Papers II, and III illustrate how to calculate a general physical bound for

a MIMO antenna, and investigate how that physical bound behaves.

Modal analysis through Characteristic Modes (CM) is a very popular method for antenna design [10, 16, 69, 71, 91, 92, 96]. By analyzing the natural resonances on a structure it is possible to gain an intuitive understanding of how to design an antenna that most efficiently excites those resonances, or modes. In Papers III and IV it is shown that current distributions contributing to optimal performance can be analyzed in terms of different sets of modes depending on what criteria are placed on the optimization. How to effectively excite these to generate the best MIMO performance is investigated as well.

One of the most enigmatic quantities for antennas is known as stored electromagnetic energy [11,14,15,23,43,53,105,108,108,125]. Stored energy is important due to its connection to the bandwidth of an antenna, one of the most important performance quantities. In Paper V an overview of how to define and calculate stored energy is presented, dealing mainly with a historical perspective, focusing on single resonance antennas in free space. In Paper VI a method for calculating stored energy in complex media is presented, providing an important cornerstone in constructing physical bounds for on/in-body antennas.

1.2 Structure

The introduction to this thesis is structured as follows. First in Sec. 2 the concept of bounding antenna performance is introduced and a brief summary of what has been done before the initialization of this work is presented. Then in Sec. 3 the concept of MIMO antennas is introduced and how to construct performance bounds for them is detailed. Finally, in Sec. 4 stored electromagnetic energy is discussed and methods for calculating it in the presence of complex media is presented.

2 Optimal Antenna Performance and Physical Bounds

Performance quantities of antennas are limited in certain applications [20, 22, 63, 66, 127, 130]. Specifically when the antenna size is smaller than the wavelength it is operating at. This issue naturally leads to the investigation of the extent of these limits. Some of these performance quantities, such as bandwidth, gain, and efficiency, are calculated through convex expressions [59]. A convex function is a function with an unique minimum value (or an unique maximum value in the concave case), and all local minima of the function are also global minima [7]. What this is equivalent to is that the true extremal value of these functions is unique. Therefore, it is possible to calculate the bounding values of these performance quantities. This can be done for many other types of systems such as cloaking devices or periodic structures, these limits are known, in general, as Physical or Fundamental bounds [33, 56, 60, 63].

Historically the pursuit of physical bounds has been extensive. Perhaps most famously the Chu bound [20] for Q-factor and bandwidth has permeated the antenna community widely. This bound limits the Q-factor of omni-directional antennas, effectively providing a lower limit for any electrically small antenna that can be circumscribed by the considered sphere. These bounds were extended to consider antennas of arbitrary shape [57], utilizing the polarizability of a structure to limit its Q-factor and gain. However, bounding other antenna quantities require more general methods, one such method is convex current optimization [59, 63]. With the advent of this method it is possible to create fundamental limitations for any antenna quantity that can be described by a convex function.

Previously, these physical bounds have mostly been calculated for single resonance, single feed, antennas in free space. Antenna quantities in such a configuration can often be calculated through quadratic forms which can be evaluated with little computational cost [63]. While such expressions lend themselves to antenna optimization and generation, antennas used in modern communications have become much more complex, often including several feeders and placed in close proximity to complex materials. The goal of this thesis is to investigate the possibility of bounding the performance of these more complex antenna types and configurations.

2.1 Electrical size

Antenna size is often classified in terms of its electrical size, *i.e.*, it's size in terms of wavelengths. The generalized way of quantifying the antenna size is to consider the radius a of the smallest sphere circumscribing the antenna structure. The electrical size is measured as the wavenumber $k = \frac{2\pi}{\lambda}$ of the operating frequency times the radius, ka, where λ is the wavelength. This is a unit less quantity that lets us describe an antenna independent of its operating frequency or physical size. Many phenomena and quantities scale with electrical size, such as Q-factor, efficiency, and directivity.

2.2 Q-Factor

One of the most commonly bounded parameters for antennas is the Q-factor [103]. The Q-factor or *quality factor* is a parameter which describes how long a system can stay oscillating without extra energy being supplied. A system with high Q will oscillate for a longer time whereas a system with low Q-factor will dissipate its energy quickly. It can conceptually be defined as the ratio of stored energy in the system over the dissipated power per cycle. This concept works well for most resonant systems such as springs, coils, electromagnetic cavities, and pendulums. For these types of systems a high Q-factor is often desirable as one would like the system to keep oscillating with as little input as possible [103]. However, for antennas the object is the opposite. Here, we (usually) want to radiate as much

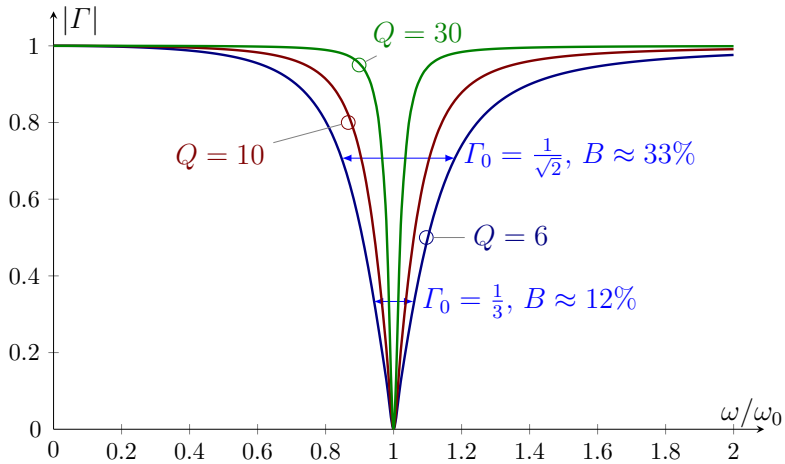

Figure 2: Magnitude of the reflection coefficient $|\Gamma|$ for RLC circuits with resonance frequency ω_0 and Q-factors $Q = \{6, 10, 30\}$. The fractional bandwidths for the $Q = 6$ case with threshold levels $\Gamma_0 = \{1/\sqrt{2}, 1/3\}$ are $B \approx \{0.33, 0.12\}$ [59, 63].

energy as possible to our surrounding, minimizing the energy stored around the antenna, and therefore unavailable for communication.

For an antenna the tuned Q-factor is defined as [75]

$$Q = \frac{2\omega \max\{W_\mathrm{e}, W_\mathrm{m}\}}{P_\mathrm{d}}, \tag{1}$$

where $\omega = 2\pi f$ is the angular frequency, f is the frequency, W_e and W_m are the stored electric and magnetic energies, respectively, and P_d is the dissipated power. The dissipated power is defined as all power lost in the system and can be divided as,

$$P_\mathrm{d} = P_\mathrm{r} + P_\Omega, \tag{2}$$

where P_r is the radiated power, and P_Ω are the conduction and dielectric losses in the antenna. By defining the tuned Q-factor in (1) as the maximum of the two types of stored energy its value is ensured even for antennas not operating at resonance. Because the difference between the two energies is the same as the cost of tuning the antenna to resonance with an ideal lumped circuit component, *i.e.*, an inductance or capacitance. The Q-factor can also be defined as

$$Q_\mathrm{ut} = \frac{\omega(W_\mathrm{e} + W_\mathrm{m})}{P_\mathrm{d}}. \tag{3}$$

This is sometimes referred to as the untuned Q-factor, where the average of the two stored energies is taken as the energy to define the Q-factor. At resonance the tuned and untuned Q-factors are equal.

The Q-factor has special significance for antennas due to its connection to bandwidth, see Fig. 2. For a single resonance, single input, antennas the Q factor is inversely proportional to the fractional bandwidth B [103, 138],

$$B \propto \frac{1}{Q}. \tag{4}$$

The bandwidth of an antenna is defined as the frequency range in which the antenna adequately accepts electromagnetic waves, and is calculated from the fractional bandwidth by multiplying it with the center frequency of the frequency band. This is commonly defined based on a threshold level Γ_0 of the reflection coefficient. For narrow-banded single resonance systems the relation between the fractional bandwidth and the Q-factor becomes explicit [138],

$$Q_{\mathrm{FBW}} = \frac{2\Gamma_0}{\sqrt{1-\Gamma_0^2}}\frac{1}{B}. \tag{5}$$

One of the most useful methods for calculating the Q-factor of an antenna was presented by Yaghjian and Best in [138]. It is an approximation based on the frequency derivative of the antenna input impedance Z_{in} when tuned to resonance by a lumped inductor or capacitor,

$$Q_{\mathrm{Z}'} = \frac{\omega}{2R_{\mathrm{in}}}\left|\frac{\partial Z_{\mathrm{in}}}{\partial \omega}\right|, \tag{6}$$

where R_{in} is the input resistance. This approximation is particularly useful due to the ease of its evaluation. It also serves as a comparison to stored energy results throughout this thesis as its calculation is not based on the evaluation of stored energy.

2.3 Current Optimization

The physical bounds most commonly referred to in this thesis have been calculated using *current optimization*. Current optimization functions by letting the equivalent currents that could be induced in the antenna volume be the optimization variables [59]. Given full control of these currents any possible antenna shape within the volume can be represented. If the expression that is optimized is a convex function, this implies that if a minimum is found it represents the best possible solution for any antenna that can be constructed within the volume. These currents are not necessarily realizable using physical feeding structures, see Fig. 3, but they do still provide an upper bound to the currents that can be excited by an antenna constructed in the design region.

To numerically perform this optimization the currents and antennas need to be represented by a method that lends itself to fast and efficient evaluation. For antennas, and small antennas specifically, a method well suited to this purpose is MoM. MoM is an integral equation based method that computes the currents of

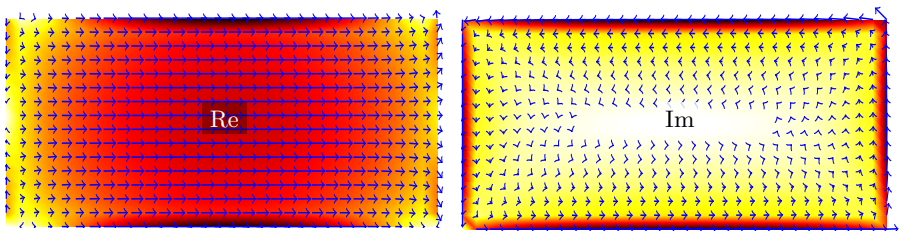

Figure 3: The optimal current distribution for the maximization of gain over Q-factor optimization problem for an aspect ratio $2:1$, $ka = 0.31$ plate. To the left the real part of the current distribution is a dipole current and to the right the imaginary part is a loop current [59].

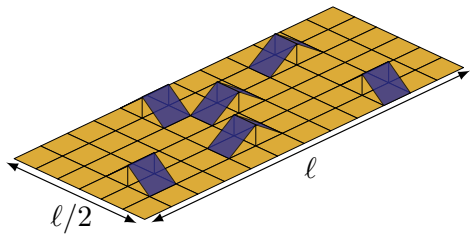

Figure 4: An $\ell \times \ell/2$ plate typical for many small antenna simulations. On the plate are shown rooftop basis functions that are used to approximate the current density that flows across it.

an object based on its excitation [44, 70, 129]. The current density on the antenna is expanded in basis functions $\boldsymbol{\psi}_n(\boldsymbol{r})$,

$$\boldsymbol{J}(\boldsymbol{r}) = \sum_{n=1}^{N} I_n \boldsymbol{\psi}_n(\boldsymbol{r}), \tag{7}$$

with expansion coefficients I_n, see Fig. 4. The main equation within this method takes the form,

$$\mathbf{ZI} = \mathbf{V}, \tag{8}$$

where $\mathbf{Z}$ is the impedance matrix, $\mathbf{I}$ is the current matrix with elements I_n, and $\mathbf{V}$ is the excitation matrix. The impedance matrix $\mathbf{Z}$ maps how the current on every part of the antenna connects to itself and the other currents present on it. If the excitation is known the currents can be found by inverting this matrix. The construction and inversion of this matrix carries with it a plethora of numerical details and difficulties [19, 70], which will not be discussed in this thesis. The power of this method, from an optimization perspective, is the fact that the evaluation of many antenna quantities essentially come for free after the matrices have been constructed. Many performance quantities can be calculated directly from the matrices in (8). For example, the radiated power is calculated

as the quadratic form of the radiation matrix, which, for loss-less structures is the real part of the impedance matrix, $\mathbf{R}_\mathrm{r} = \mathrm{Re}\{\mathbf{Z}\}$,

$$P_\mathrm{r} = \frac{1}{2}\mathbf{I}^\mathrm{H}\mathbf{R}_\mathrm{r}\mathbf{I}. \tag{9}$$

Quadratic forms can be evaluated quickly and efficiently, and are used in explicit optimization routines such as Quadratically Constrained Quadratic Programming (QCQP) [7]. From (8) the resonance of the antenna can be analyzed through the imaginary part of the impedance matrix, known as the reactance matrix $\mathbf{X} = \mathrm{Im}\{\mathbf{Z}\}$, where zero reactance in the input impedance at the frequency of operation defines resonance. $\mathbf{X}$ also defines the electric and magnetic energy matrices [59],

$$\mathbf{X}_\mathrm{e} = \frac{\omega}{2}\left(\frac{\partial \mathbf{X}}{\partial \omega} - \frac{\mathbf{X}}{\omega}\right), \tag{10}$$

$$\mathbf{X}_\mathrm{m} = \frac{\omega}{2}\left(\frac{\partial \mathbf{X}}{\partial \omega} + \frac{\mathbf{X}}{\omega}\right). \tag{11}$$

The matrices $\mathbf{X}_\mathrm{e}$, $\mathbf{X}_\mathrm{m}$ and $\mathbf{R}_\mathrm{r}$ can be used in (1) to give the expression for the Q-factor, for the loss-loss case, in MoM matrices,

$$Q = \frac{\max\{\mathbf{I}^\mathrm{H}\mathbf{X}_\mathrm{e}\mathbf{I}, \mathbf{I}^\mathrm{H}\mathbf{X}_\mathrm{m}\mathbf{I}\}}{\mathbf{I}^\mathrm{H}\mathbf{R}_\mathrm{r}\mathbf{I}}. \tag{12}$$

The optimization problems that calculate the physical bounds, on *e.g.*, Q-factor or efficiency, can be written directly on convex form or be formulated as QCQP taking the following form [51, 55, 59, 78],

$$\begin{aligned} \text{maximize} \quad & \mathbf{I}^\mathrm{H}\mathbf{A}\mathbf{I} \\ \text{subject to} \quad & \mathbf{I}^\mathrm{H}\mathbf{B}\mathbf{I} \leq 1 \\ & \mathbf{I}^\mathrm{H}\mathbf{C}\mathbf{I} = 0 \\ & \mathbf{D}\mathbf{I} = \boldsymbol{d}, \end{aligned} \tag{13}$$

where the matrices $\mathbf{A}$, $\mathbf{B}$, $\mathbf{C}$, $\mathbf{D}$, and the vector $\boldsymbol{d}$ are general quantities that can be replaced with the matrices above in order to create the physical bound of interest. Here the currents are the variables of the problem, making matrix inversion of (8) unnecessary. Depending on what matrices are put into (13), these problems are usually solved by their dual formulation [7].

2.4 Gain over Q Bound

The problem formulation (13) lets us investigate performance limits tailored to specific applications. In this subsection a brief summary of how to calculate one of the most prolific performance bounds, the gain over Q bound, using current optimization, is presented [59].

To maximize gain over Q, the Q-factor must be minimized, however, (12) is not a convex function and as such cannot be minimized directly. Therefore we must formulate a convex function that can be maximized. Consider the partial gain of an antenna, calculated as [75],

$$G(\hat{\boldsymbol{k}}, \hat{\boldsymbol{e}}) = \frac{4\pi P(\hat{\boldsymbol{k}}, \hat{\boldsymbol{e}})}{P_{\mathrm{r}} + P_{\Omega}}, \tag{14}$$

where $\hat{\boldsymbol{k}}$ is the direction of radiation, $\hat{\boldsymbol{e}}$ is the polarization of the radiation, and $P(\hat{\boldsymbol{k}}, \hat{\boldsymbol{e}})$ is the radiation intensity for that direction and polarization.

The value of (14) in a certain direction is known as the gain, and it is equal to the directivity for a loss-less antenna. The radiation intensity can be calculated in a certain direction by

$$P(\hat{\boldsymbol{k}}, \hat{\boldsymbol{e}}) = \frac{1}{2\eta_0} |\mathbf{F}^{\mathrm{H}}\mathbf{I}|^2, \tag{15}$$

where $\mathbf{F}$ is the radiation vector in the $\hat{\boldsymbol{k}}$ direction with polarization $\hat{\boldsymbol{e}}$. Dividing the partial gain (14) with the Q-factor (1), and inserting the MoM matrices, gives an expression that can be maximized,

$$\frac{G(\hat{\boldsymbol{k}}, \hat{\boldsymbol{e}})}{Q} = \frac{4\pi |\mathbf{F}^{\mathrm{H}}\mathbf{I}|^2}{\eta_0 \max\{\mathbf{I}^{\mathrm{H}}\mathbf{X}_{\mathrm{e}}\mathbf{I}, \mathbf{I}^{\mathrm{H}}\mathbf{X}_{\mathrm{m}}\mathbf{I}\}}. \tag{16}$$

The maximization of (16) can either be written as a maximization of the numerator or a minimization of the denominator. Here, we will choose the second and write the convex optimization problem [55]

$$\begin{aligned} &\text{minimize} && \max\{\mathbf{I}^{\mathrm{H}}\mathbf{X}_{\mathrm{e}}\mathbf{I}, \mathbf{I}^{\mathrm{H}}\mathbf{X}_{\mathrm{m}}\mathbf{I}\} \\ &\text{subject to} && \mathbf{F}^{\mathrm{H}}\mathbf{I} = -\mathrm{j}, \end{aligned} \tag{17}$$

where restricting the number inside the absolute square, $\mathbf{F}^{\mathrm{H}}\mathbf{I}$ is the same as restricting the square, $|\mathbf{F}^{\mathrm{H}}\mathbf{I}|^2$. This is a convex problem that can be solved by inputting it on this form into freely available solvers, such as Matlab Software for Disciplined Convex Programming (CVX) [7, 48, 59], given that the problem is tractable, *i.e.*, be of reasonable size. The optimal currents of this problem are shown in Fig. 3. These currents will not always give minimum Q-factor for all antennas. However, electrically small antennas have, in general, dipole-like radiation patterns. It is possible to form a convex optimization problem on the form of (17) that minimizes the Q-factor for a given radiation pattern, in this way giving a lower bound for Q for small antennas [12, 55]. This type of formulation opens the possibility to form other types of problems that calculate bounds for other performance quantities for small antennas [51, 81].

2.5 Reaching the Physical Bounds

A pressing issue for all physical bounds that have been established for antennas are whether or not they are tight. The Chu bound deals with the optimal Q-factor for radiating structures defined by their circumscribing sphere [20]. This

bound sets a lower limit for the Q-factor for any structure that can be constructed within the sphere [3, 6, 64, 65, 83, 84]. While being a seminal work and one that is used to this day, the issue with this bound is that most antenna structures do not fully utilize the volume of the sphere. A typical modern antenna, where bandwidth performance is an issue, is printed on a substrate [38]. This means that the Chu bound of that antenna is much lower than what is actually achievable on that surface. Consequently, the Chu bound is not well suited as, *e.g.*, a stopping criterion in optimization. This deficiency lead to the investigation and development of tighter physical bounds that bound the performance of arbitrarily shaped radiators [34, 57, 58, 121–123, 126, 127, 136, 137].

Verification of these bounds is done by simulating known antenna designs and verifying their relation to the bound [4, 5, 58]. Their validity is predicated on the fact that no antennas that are constructed in the considered volume have better performance than the bound. However, one way to further validate this is to consider heuristically optimized antennas. Techniques, such as, genetic algorithms, particle swarm, Monte Carlo simulations, and others, have been utilized successfully in antenna design [73, 86, 106, 107, 109]. These non-deterministic algorithms are well suited for antenna design problems where a large number of solutions produce acceptable results. By running these for many points along the physical bounds its possible to show solutions that approach the bound for every frequency point, see Fig. 5. In Paper I it is shown that simple antenna designs can be made to approach the bound as long as the antennas are electrically small. One of those simple antenna designs for small planar antennas that reach the physical bound is the meanderline, as seen in Fig. 5.

3 Physical Bounds for MIMO Antennas

Utilizing multiple antennas in concert was one of the big technological leaps forward with the introduction of the 4G cellular network, resulting in much higher data rates [27]. Today the use of MIMO has become ubiquitous in communication systems, being implemented in wireless LAN, 4G, and the soon to come Fifth Generation Mobile Networks (5G) systems [27, 99, 104, 111]. The principle of MIMO is to create several paths between the receiver and transmitter antenna sets by including multiple antennas in each. When the channel describing the propagation between the two sets is known or estimated it is possible to allocate power to the different paths in an efficient manner that increases the overall bit-rate sent through the link [26, 79, 99, 104].

Physical limits for the optimal performance of MIMO systems has previously mainly been studied from an information theoretical perspective [35, 37, 39, 87, 118]. Where ideal antenna design has been considered and limits on different channel models are studied [9, 93, 128], or on how to calculate a bound on the number of degrees of freedom in a MIMO system [36, 49, 97, 98], as well as bounds for antenna selection [100] or beamsteering within a channel [28]. Before the work carried out in this thesis, spherical modes and geometries had been

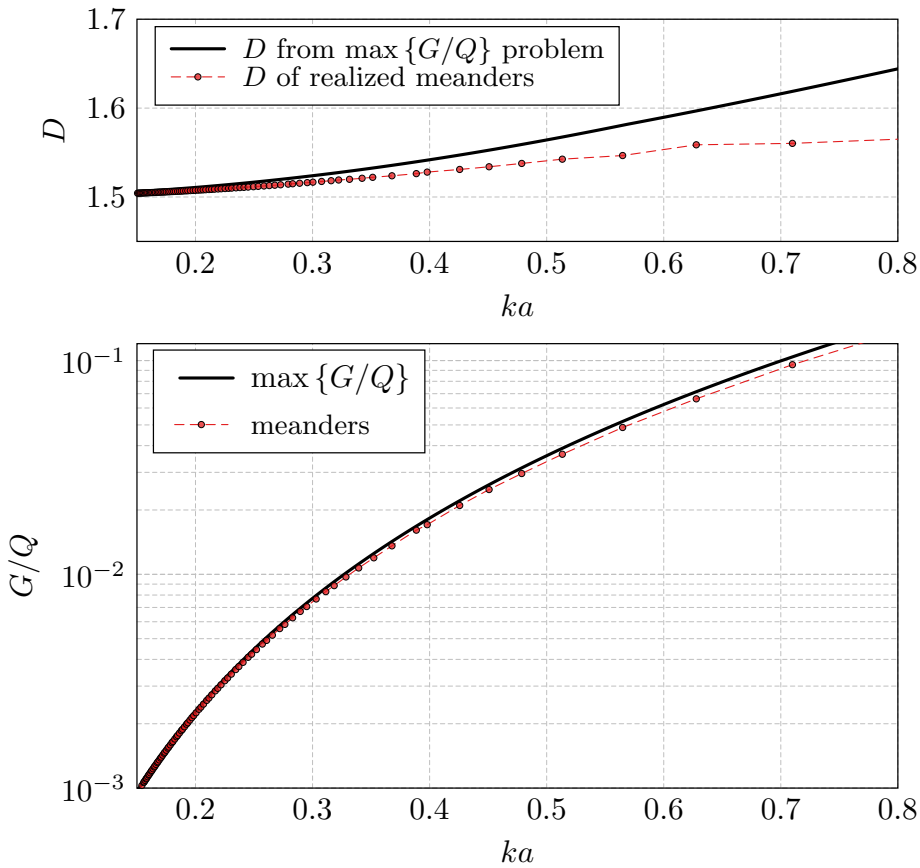

Figure 5: The G/Q bound for an aspect ratio 2 : 1 plate for different sizes, as well as realized meander line structures and how they relate to the bound. The meander lines have been optimized using a genetic algorithm, and the details of their parametrization can be found in Paper I. In the top graph the directivity of the bound is shown and how the directivity of the meander lines relate to it. The meander lines have been optimized for maximum G/Q.

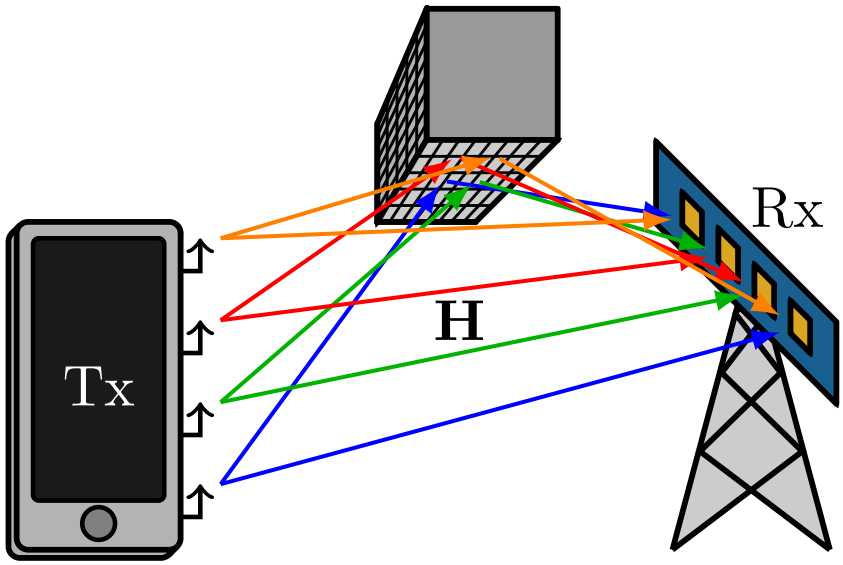

Figure 6: Schematic illustration of a MIMO channel where each of the path ways between one input antenna on the transmitting set to an output antenna on the receiving set make up the channel matrix between them.

considered, much in the same way as the early bounds for the Q-factor were established [45, 54, 102]. Superdirective antennas and optimal antenna characteristics for more arbitrary geometries have been considered as well [80, 101]. However, to construct a tighter bound, arbitrary geometries with constrained antennas must be considered. This was carried out in Papers II, III, and IV. A brief summary of the basics of MIMO antennas and the method used to bound them follows in this section.

3.1 MIMO

A simple MIMO system, depicted in Fig. 6, with N transmitting antennas, M receiving antennas, and additive noise is described by the equation [104]

$$\mathbf{y} = \mathbf{H}\mathbf{x} + \mathbf{n}, \tag{18}$$

where $\mathbf{y}$ is a $M \times 1$ matrix containing the received signals, $\mathbf{H}$ is a $M \times N$ matrix describing the channel between the two sets of antennas, $\mathbf{x}$ is a $N \times 1$ matrix containing the transmitted signals, and $\mathbf{n}$ is a $M \times 1$ matrix containing the noise in each receiver. The maximal capacity that can be sent through this channel is defined as when the mutual information between the received signal $\mathbf{y}$ and the transmitted signal $\mathbf{x}$ is maximized [29, 104]. This reduces to maximizing the

differential entropy of the received signal $\mathbf{y}$ [26], for which we have the expression

$$C = \max_{\mathrm{Tr}(\mathbf{A})=1} \log_2 \det(\mathbf{1} + \frac{P}{N_0}\mathbf{H}\mathbf{A}\mathbf{H}^{\mathrm{H}}), \tag{19}$$

where

$$\mathbf{A} = \frac{1}{2}\mathcal{E}\left\{\mathbf{x}\mathbf{x}^{\mathrm{H}}\right\} \tag{20}$$

is the covariance matrix of the transmitted signals, P is the input power, and N_0 is the noise spectral power density. In a typical MIMO link the channel $\mathbf{H}$ varies over time [104] and a statistical average is taken over all its variations in (19), here, we consider the case of a fixed channel for simplicity. The capacity calculated in (19) has the units bits/(s Hz) and is referred to as the spectral efficiency [104]. To gain the true capacity of the system, *i.e.*, how many bits per second can be transmitted through the link, the spectral efficiency must be multiplied by the systems bandwidth. The spectral efficiency can alternatively been interpreted as the capacity of a system with a frequency flat bandwidth of 1 Hz [104]. Note that all spectral power quantities are normalized to the 1 Hz bandwidth, as in [104].

There are many different scenarios in which MIMO is utilized, sometimes the channel is unknown to the transmitter and the maximization of (19) is difficult to achieve, or simply carried out with equal power distribution [104]. Ideally the channel is estimated so that power can be allocated optimally to the different antennas. This is the case that is considered throughout this thesis as the body of work deals with bounding the performance of MIMO antennas, and not in the optimal power allocation for different channel scenarios. If the channel is known to the receiver, the optimal power allocation can be found using an algorithm known as water filling [26, 104]. This algorithm is based on performing a Singular Value Decomposition (SVD) of the channel matrix $\mathbf{H}$. Each singular value illustrates how much loss there is when transmitting through the mode associated with it, where, in the simplest case, a mode is a connection between one antenna in the transceiver and one antenna in receiver. A large singular value is associated with low loss, or a strong channel, and a small value with high loss, or a weak channel. The SVD of the channel rewrites (19) as,

$$\begin{aligned} C &= \max_{\mathrm{Tr}(\mathbf{A})=1} \log_2 \det(\mathbf{1} + \frac{P}{N_0}\mathbf{U}\mathbf{\Sigma}\mathbf{V}^{\mathrm{H}}\mathbf{A}\mathbf{V}\mathbf{\Sigma}^{\mathrm{H}}\mathbf{U}^{\mathrm{H}}) \\ &= \max_{\mathrm{Tr}(\mathbf{A})=1} \log_2 \det(\mathbf{1} + \frac{P}{N_0}\mathbf{\Sigma}\mathbf{V}^{\mathrm{H}}\mathbf{A}\mathbf{V}\mathbf{\Sigma}^{\mathrm{H}}), \end{aligned} \tag{21}$$

where $\mathbf{U}$ and $\mathbf{V}$ are unitary matrices, and $\mathbf{\Sigma}$ is matrix containing the singular values σ_n of the channel matrix. The exterior unitary matrix $\mathbf{U}$ can be discarded as it does not change the value of the determinant. The optimal power allocation in $\mathbf{A}$ for a diagonal $\mathbf{\Sigma}$ makes the product $\mathbf{V}^{\mathrm{H}}\mathbf{A}\mathbf{V}$ a diagonal matrix [104], giving

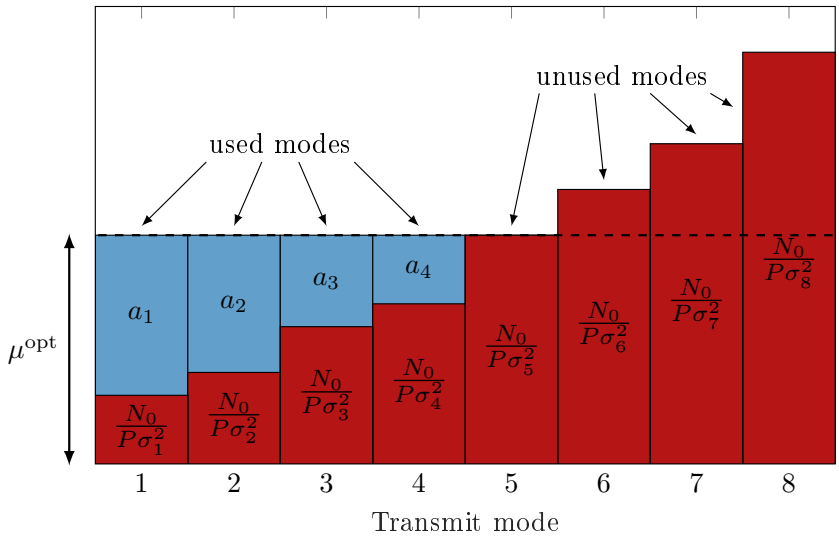

Figure 7: Schematic illustration of the water filling algorithm. The value μ^{opt} shows the optimal "water" level for the power allocation, a_n , $n = 1, \ldots, 4$ are the power allocation levels in the used modes, and N_n , $n = 1, \ldots, 8$ illustrates the amount of loss in each mode.

the simpler optimization problem,

$$C = \max_{\sum_{n=1}^{r} a_n = 1} \sum_{n=1}^{r} \log_2(1 + \frac{P}{N_0}\sigma_n^2 a_n), \tag{22}$$

where r is the rank of the channel matrix, and $a_n \geq 0$ is the power allocation to each of those paths. The optimal distribution of a_n can be found using the water filling algorithm [26, 104]. This algorithm functions by calculating the optimal filling level μ^{opt}, see Fig. 7, and allocating energy to each path way to match that level. This level is calculated for each step of the algorithm p as [104],

$$\mu_{\text{p}} = \frac{1}{p}\left(1 + \frac{N_0}{P}\sum_{n=1}^{p}\frac{1}{\sigma_n^2}\right), \; p \leq r, \tag{23}$$

where p can maximally be increased to the rank of the channel matrix r. The allocation levels are calculated as,

$$a_n = \mu_{\text{p}} - \frac{N_0}{P\sigma_n^2}, \; n = 1, 2, \ldots, p \leq r. \tag{24}$$

This algorithm starts by only allocating power into the first mode, if the last value of a_n is non-negative, the iteration count p is increased by one and the next mode is included. This is carried out until the algorithm tries to fill a mode

with negative power, corresponding to mode number 5 in Fig. 7, at which point the algorithm is terminated and the previous iterations power allocation vector is the optimal solution.

3.2 Bounding MIMO Antennas

Constructing physical bounds for MIMO antennas is a not a trivial problem. There are several considerations that must be taken into account.

- First, there are two sets of antennas that depend intimately on each other to function, typically a base station and a hand-held device, see Fig. 6. In this case the designer would most likely design one of these independently of the other. Optimizing both simultaneously yields specific link to link scenarios that do not model a general case.

- Second, optimizing over the input signals to the ports of the antenna, which is traditionally done in information theoretical approaches [26, 104], does not let us manipulate the antenna design and truly bound the performance available from it.

- Third, the main performance quantity of MIMO antennas, capacity, is evaluated in the covariance of the input signals, increasing the computational complexity of the expressions that must be evaluated.

- Finally, the antennas are constructed from several elements and ports which make concepts such as Q-factor, which we traditionally use to quantify antenna performance [138], hard to define.

To deal with these issues a simplified version of the original problem can be considered. We rely on the fact that any idealization we perform will constitute a relaxation of the original problem, therefore providing a bound to the optimal performance.

First consider two sets of antennas, in a typical communication scenario one of these sets is inside a device, and the other on a base station, see Fig. 6. The base station antenna is typically electrically large and comprising of many elements. Designing those types of antennas carry with them requirements and difficulties relating to feeding network efficiency, line of sight blocking, *etc.* [18, 104, 117]. Because they are electrically large, they are not harshly limited by their physical size. The other set of antennas, on the other hand, are limited by its size. Because of their position within a device, they are competing with other components for design space, often making them electrically small [17, 38, 135]. This carries with it implicit restrictions on bandwidth, efficiency and directivity. Therefore it is interesting to compute physical bounds for this set of antennas.

A general physical bound for MIMO antennas must be applicable for any antenna. The nature of a MIMO system, that it depends on two different sets of antennas, is contradictory to that aim. We resolve this by idealizing one of

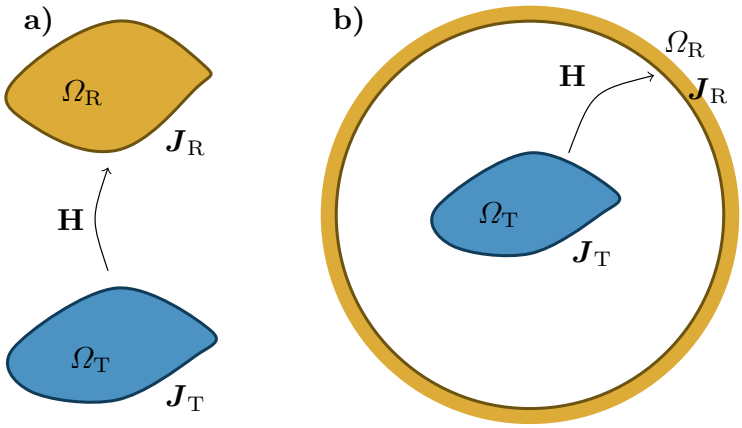

Figure 8: Schematic illustration of the difference between a normal channel **a** and an idealized channel **b**. The typical channel **a** is made up of a receiving and transmitting set of antennas, here depicted as general bodies Ω_{R} and Ω_{T}. Each has a current densities, $\boldsymbol{J}_{\mathrm{R}}$ and $\boldsymbol{J}_{\mathrm{T}}$, respectively, that is induced across them. In the idealized channel **b** the receiver Ω_{R} is fully enveloping the transmitter and the current density $\boldsymbol{J}_{\mathrm{R}}$ is described by the spherical modes in the far-field [30].

the sets of antennas, in this way making a bound for a link between any MIMO antenna to an idealized antenna. We choose the transmitting antenna as the one we will bound, and idealize the receiving set, see Fig. 8. This is done by representing the receiver as the spherical modes in the far-field [46, 47, 54, 62]. This is equivalent to having the receiver accept all energy radiated from the transmitter, essentially making it the best possible receiver. Spectral efficiency is measured in the diversity of the spherical modes that are radiated. A scenario that this can be likened to is an antenna situated in a room where the walls are covered by smart surfaces, as was suggested in [74]. This methodology has the added benefit of greatly reducing the computational cost of the problem as the receiver does not need to be meshed and can be evaluated analytically. In this case no scattering phenomena or statistical models are used for the channel. These can be included at added numerical cost but do not contribute to the fundamental analysis of the problem [46, 47].

As described in Sec. 3.1, typically, analysis and optimization of MIMO systems are done by controlling the signals fed to the transmitting antenna. However, this is done with the assumption that the antennas are already designed and fixed. Essentially the methodology is to maximize bit rate through an information theoretical approach given a set of transmitting antennas. What we are interested in when constructing an antenna bound is the amount of performance to be gained from efficient antenna design. Therefore, the problem must be reformulated to include the design of the antennas as a variable. An antenna feed induces currents on the element which radiate, in current optimization, the method outlined in

Sec. 2.3, the currents are the optimization variables representing the antenna. Each port n on the antenna induces a current across it,

$$\mathbf{I}_n = \mathbf{T}_n \mathbf{x}_n, \tag{25}$$

where $\mathbf{T}_n$ is the matrix describing the map between the port and the current. Each of these currents contribute to a total current across the structure. We model our antenna and the currents that flow on it with MoM. The idealized channel matrix is therefore the matrix that connects the MoM basis functions on the antenna to the spherical modes in the far-field. This matrix is called $\mathbf{S}$ and is a map between the MoM basis functions and the spherical vector wave expansion [119]. With that channel matrix we can formulate the maximal capacity problem (19) when controlling the inputs to the antennas $\mathbf{x}_n$ as,

$$\begin{aligned}
\text{maximize}_{\mathbf{x}_n} \quad & \log_2 \det\left(\mathbf{1} + \gamma \mathbf{S}\mathbf{T}\mathbf{A}\mathbf{T}^{\mathrm{H}}\mathbf{S}^{\mathrm{H}}\right) \\
\text{subject to} \quad & \frac{1}{2}\mathcal{E}\left\{\mathbf{I}_n^{\mathrm{H}}\mathbf{R}_{\mathrm{r}}\mathbf{I}_n\right\} = p_n, \qquad n = 1, \ldots, N \\
& \mathbf{I}_n = \mathbf{T}_n \mathbf{x}_n, \\
& \mathbf{A} = \frac{1}{2}\mathcal{E}\left\{\mathbf{x}_n \mathbf{x}_n^{\mathrm{H}}\right\}, \\
& \sum_{n=1}^{N} p_n = 1,
\end{aligned} \tag{26}$$

where $\mathbf{T} = [\mathbf{T}_1, \mathbf{T}_2, \ldots \mathbf{T}_N]$ is the collection of all the maps between the ports and their respective currents, $\gamma = P/N_0$ is the total Signal-to-Noise Ratio (SNR), and each port is limited by its radiated power. This problem is not convex, and therefore difficult for us to solve, however, it can be relaxed to a convex problem. Let us begin by adding the conditions restricting the input power of the ports together,

$$\begin{aligned}
\text{maximize}_{\mathbf{x}_n} \quad & \log_2 \det\left(\mathbf{1} + \gamma \mathbf{S}\mathbf{T}\mathbf{A}\mathbf{T}^{\mathrm{H}}\mathbf{S}^{\mathrm{H}}\right) \\
\text{subject to} \quad & \sum_{n=1}^{N} \frac{1}{2}\mathcal{E}\left\{\mathbf{I}_n^{\mathrm{H}}\mathbf{R}_{\mathrm{r}}\mathbf{I}_n\right\} = 1 \\
& \mathbf{I}_n = \mathbf{T}_n \mathbf{x}_n, \\
& \mathbf{A} = \frac{1}{2}\mathcal{E}\left\{\mathbf{x}_n \mathbf{x}_n^{\mathrm{H}}\right\}.
\end{aligned} \tag{27}$$

This problem can be reformulated into a convex optimization problem through semi-definite relaxation [7]. Semi-definite relaxation is well suited to optimizing MIMO antennas as it is based on reformulating the problem in the correlation matrix of the variables. In our case spectral efficiency is already formulated in the covariance of the input signals (20). We need only to reformulate the problem so that it is written in the covariance of the currents on the antenna in order to use current optimization, as discussed in Sec. 2.3. Introduce the covariance of

the currents $\mathbf{P} = \frac{1}{2}\mathcal{E}\left\{\mathbf{I}\mathbf{I}^{\mathrm{H}}\right\}$ such that,

$$\mathbf{P} = \frac{1}{2}\mathcal{E}\left\{ \begin{pmatrix} \mathbf{I}_1 & \mathbf{I}_2 & \cdots & \mathbf{I}_N \end{pmatrix} \begin{pmatrix} \mathbf{I}_1^{\mathrm{H}} \\ \mathbf{I}_2^{\mathrm{H}} \\ \vdots \\ \mathbf{I}_N^{\mathrm{H}} \end{pmatrix} \right\} = \frac{1}{2}\sum_{n=1}^{N} \mathcal{E}\left\{\mathbf{T}_n \mathbf{x}_n \mathbf{x}_n^{\mathrm{H}} \mathbf{T}_n^{\mathrm{H}}\right\} = \mathbf{T}\mathbf{A}\mathbf{T}^{\mathrm{H}}. \tag{28}$$

The covariance can be applied to the quadratic forms restricting (27) since they are scalar quantities giving,

$$\begin{aligned} \sum_{n=1}^{N} \frac{1}{2}\mathcal{E}\left\{\mathbf{I}_n^{\mathrm{H}} \mathbf{R}_{\mathrm{r}} \mathbf{I}_n\right\} = \sum_{n=1}^{N} \frac{1}{2}\operatorname{Tr}\mathcal{E}\left\{\mathbf{I}_n^{\mathrm{H}} \mathbf{R}_{\mathrm{r}} \mathbf{I}_n\right\} = \sum_{n=1}^{N} \frac{1}{2}\operatorname{Tr}\mathcal{E}\left\{\mathbf{R}_{\mathrm{r}} \mathbf{I}_n \mathbf{I}_n^{\mathrm{H}}\right\} \\ = \frac{1}{2}\operatorname{Tr}(\mathbf{R}_{\mathrm{r}}\mathbf{T}\mathbf{A}\mathbf{T}^{\mathrm{H}}) = \operatorname{Tr}(\mathbf{R}_{\mathrm{r}}\mathbf{P}), \end{aligned} \tag{29}$$

where the trace $\operatorname{Tr}(\cdot)$ can be applied to scalar quantities as well, and its cyclic property has been utilized. The problem formulated in the currents is now written as,

$$\begin{aligned} \text{maximize} \quad & \log_2 \det\left(\mathbf{1} + \gamma \mathbf{S}\mathbf{P}\mathbf{S}^{\mathrm{H}}\right) \\ \text{subject to} \quad & \operatorname{Tr}(\mathbf{R}_{\mathrm{r}}\mathbf{P}) = 1 \\ & \mathbf{P} \succeq 0, \\ & \operatorname{rank}(\mathbf{P}) = N, \end{aligned} \tag{30}$$

where the restriction on the rank of $\mathbf{P}$ is due to the number of ports in the MIMO antenna. This is still not a convex problem due to this finite rank restriction. The semi-definite relaxation is done by dropping this rank constraint [7], effectively allowing an infinite amount of feeders to be placed in order to find the optimal solution. Finally giving a convex problem that can be solved to find an upper bound on the optimal spectral efficiency,

$$\begin{aligned} \text{maximize} \quad & \log_2 \det\left(\mathbf{1} + \gamma \mathbf{S}\mathbf{P}\mathbf{S}^{\mathrm{H}}\right) \\ \text{subject to} \quad & \operatorname{Tr}(\mathbf{R}_{\mathrm{r}}\mathbf{P}) = 1 \\ & \mathbf{P} \succeq 0. \end{aligned} \tag{31}$$

We have now formulated the optimal spectral efficiency on a form where the two sets of antennas are the spherical modes in the far-field, for the receiver, and the currents on the transmitting antenna, described by the MoM basis functions. Both of these two sets can be arbitrarily large. If the SNR is scaled with the number of channels that this implies, the optimal spectral efficiency is unbounded [30, 104]. In this case we consider the SNR to be fixed and therefore the optimal spectral efficiency converges. The analytical solution to this optimization problem can be found by rewriting $\mathbf{R}_{\mathrm{r}} = \mathbf{S}^{\mathrm{H}}\mathbf{S}$ [119] and utilizing the cyclic property of the trace,

$$\operatorname{Tr}(\mathbf{R}_{\mathrm{r}}\mathbf{P}) = \operatorname{Tr}(\mathbf{S}\mathbf{P}\mathbf{S}^{\mathrm{H}}) = \operatorname{Tr}(\mathbf{Q}), \tag{32}$$

where $\mathbf{Q} = \mathbf{S}\mathbf{P}\mathbf{S}^{\mathrm{H}}$. This is the trace of the same matrix as is found in the spectral efficiency expression, therefore (31) can be written as,

$$\begin{aligned} &\text{maximize} && \log_2 \det\left(\mathbf{1} + \gamma\mathbf{Q}\right) \\ &\text{subject to} && \mathrm{Tr}(\mathbf{Q}) = 1 \\ & && \mathbf{Q} \succeq 0. \end{aligned} \tag{33}$$

The problem (33) now has the variable $\mathbf{Q}$ and is not constrained by any conditions that differentiate between the different modes. The analytical solution to such a MIMO channel is simply equal energy distribution in every channel, giving the optimal spectral efficiency,

$$\log_2 \det\left(\mathbf{1} + \gamma\mathbf{Q}\right) = \log_2(1 + \gamma\frac{1}{N})^N \approx \frac{\gamma}{\log 2},\ N \to \infty \tag{34}$$

where N is the dimension of $\mathbf{Q}$, and log is the natural logarithm. This presents a fundamental bound, only dependent on SNR, to an unconstrained MIMO antenna.

The bound calculated by (31) is obviously not very realistic since no constraints have been put on the antenna, letting the solution have unlimited losses and infinitely narrow bandwidth, for example. This can be remedied by adding constraints to the optimization problem to include what limits are put on different design variables. Some of these parameters are well defined such as ohmic losses that can be modeled by the Gram matrix of the MoM basis,

$$P_\Omega = \frac{1}{2}\mathcal{E}\left\{\mathbf{I}^{\mathrm{H}}\mathbf{R}_\Omega\mathbf{I}\right\} = \mathrm{Tr}(\mathbf{R}_\Omega\mathbf{P}), \tag{35}$$

where $\mathbf{R}_\Omega = R_{\mathrm{s}}\mathbf{\Psi}$, $\mathbf{\Psi}$ is the Gram matrix, and R_{s} is the surface resistance in $\Omega/\square$. Where as other parameters, such as the Q-factor are more difficult to define for MIMO antennas. Consider the perspective presented in (26) where each antenna port is restricted individually. Each port has a well defined Q-factor when considered individually, these can serve as a bandwidth restriction for each port,

$$\begin{aligned} &\frac{1}{2}\mathbf{I}_n^{\mathrm{H}}\mathbf{X}_{\mathrm{e}}\mathbf{I}_n = Q\omega p_n, \quad n = 1, \ldots, N \\ &\frac{1}{2}\mathbf{I}_n^{\mathrm{H}}\mathbf{X}_{\mathrm{m}}\mathbf{I}_n = Q\omega p_n, \quad n = 1, \ldots, N, \end{aligned} \tag{36}$$

where p_m is the power allocation to each port. These conditions can be relaxed in the same manner as before by adding them together and rewriting them in the covariance of the total current density,

$$\begin{aligned} &\mathrm{Tr}(\mathbf{X}_{\mathrm{e}}\mathbf{P}) = Q\omega \\ &\mathrm{Tr}(\mathbf{X}_{\mathrm{m}}\mathbf{P}) = Q\omega. \end{aligned} \tag{37}$$

This relaxation guarantees that the bound that is created always encompasses the original problem restricted by the individual port Q-factors. Although the direct

connection between bandwidth and the Q-factor of the total current density is not determined, this means that the bandwidth of the system is still implicitly restricted. The equality signs in (36) enforce resonance for each of the ports, in (37) this means resonance for the total current. However, in MIMO antennas such a concept is not necessarily desirable and can be dropped by adding the two conditions together or replacing the equality with an inequality.

These constraints can now be added to (31) to create a bound for a specific set of design criteria,

$$\begin{aligned} \text{maximize} \quad & \log_2 \det\left(\mathbf{1} + \gamma \mathbf{S}\mathbf{P}\mathbf{S}^{\mathrm{H}}\right) \\ \text{subject to} \quad & \mathrm{Tr}((\mathbf{X}_{\mathrm{e}} + \mathbf{X}_{\mathrm{m}})\mathbf{P}) \leq 2Q\omega \\ & \mathrm{Tr}(\mathbf{X}\mathbf{P}) = 0 \\ & \mathrm{Tr}(\mathbf{R}_{\Omega}\mathbf{P}) \leq \delta \\ & \mathrm{Tr}(\mathbf{R}_{\mathrm{r}}\mathbf{P}) = 1 \\ & \mathbf{P} \succeq 0, \end{aligned} \tag{38}$$

where $\delta = P_{\Omega}/P_{\mathrm{r}}$ is the dissipation factor [66]. Additional constraints can be added to this problem to investigate other quantities. The problem (38) is non-trivial because it is a semi-definite programming problem, since such problems are formulated in the correlation matrix they contain the square of the number of unknowns typically considered. To put this in perspective to the quadratic forms that are usually optimized in current optimization, see Sec. 2.3, take a typical small antenna discretized in MoM. If the antenna is meshed rectangularly with 40×40 elements its total number of unknowns are $n \approx 3200$, a manageable size for quadratic forms. However, if such an antenna is considered in (38) the number of unknowns is close to $n^2/2 \approx 5 \cdot 10^6$. In Paper II this issue is addressed by performing a model order reduction in the form of a basis change. The currents on the antenna are expanded in different sets of modes, such as characteristic modes [16], energy modes [59], and radiation modes [110]. Only the most dominant modes are included in the optimization, constituting a model order reduction. This method enables the problem to be solved by readily available solvers, such as CVX, and can be input on the form of (38). However, for convergence the required number of included spherical modes and current modes still make the problem computationally demanding and time consuming. This makes it difficult to run electrically larger problems, or investigating greater solution spaces such as embedded antennas.

In Fig. 9 problem (38) has been solved in CVX for an $\ell \times \ell/2$ loss-less plate, see Fig. 4. The size of the plate and the restricting Q-factor has been swept to create a Pareto tradeoff curve between the two. It is clear that a significant amount of performance is lost in comparison to the ideal spectral efficiency (34). We can also see that the solution is not realizable below the lower bound for Q for the plate. The shape of that curve is followed for the spectral efficiency as the size of the plate is increased.

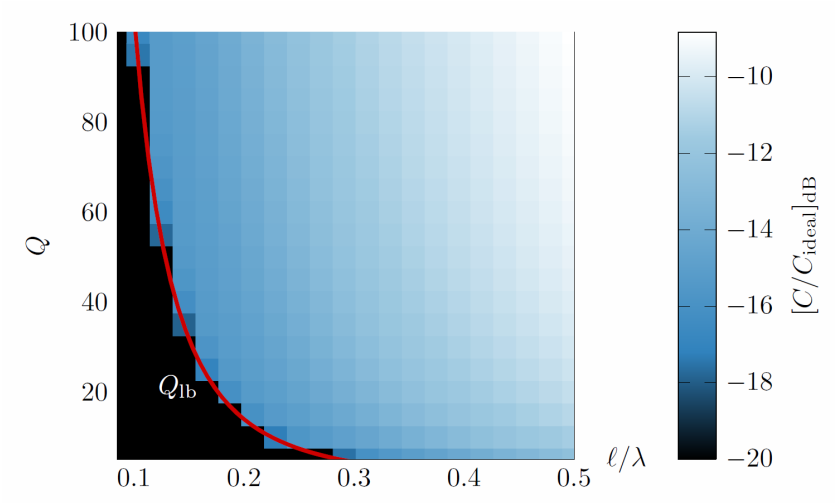

Figure 9: The Pareto tradeoff curve between Q and size in terms of spectral efficiency loss in comparison with the ideal for an aspect ratio 2 : 1 plate. The SNR has been set to $\gamma = 50$. The lower bound for Q is drawn separately, and solutions below it are unfeasible.

3.3 Modal Analysis of MIMO Antennas

A method to handle larger, more computationally demanding problems, such as (38), is to develop tailored solution methods or codes. This was done in Papers III and IV by investigating the problem when it is only restricted by one condition other than the power normalization. This method is predicated on the matrix in the condition being positive semi-definite, to allow certain decompositions to be used. The condition (35) has a positive semi-definite matrix defining it, since the ohmic losses are modeled by the Gram matrix. The Q-factor restriction is more difficult because $(\mathbf{X}_{\mathrm{e}} + \mathbf{X}_{\mathrm{m}})$ are, in general, indefinite. However, for small electrical sizes, $\ell < \lambda/2$, they are positive semi-definite [59].

The bound is constructed by formulating a dual problem to the initial optimization problem. A dual problem calculates a bound on the value of the original problem, the difference between the two values is known as the duality gap [7]. In this case the duality gap was verified to be zero by solving the original problem in CVX, where possible. The dual was constructed by taking a linear combination between the two conditions restricting the optimization and using the fact that a problem with less constraints will always have a greater solution. This problem is then be solved by utilizing the good properties of the matrices in the conditions to calculate the SVD of the optimal channel. The optimal spectral efficiency is found by water filling [104].

In this solution the singular values of the optimal channel are constructed based on the ratio of the linear combination of the two conditions, which is swept

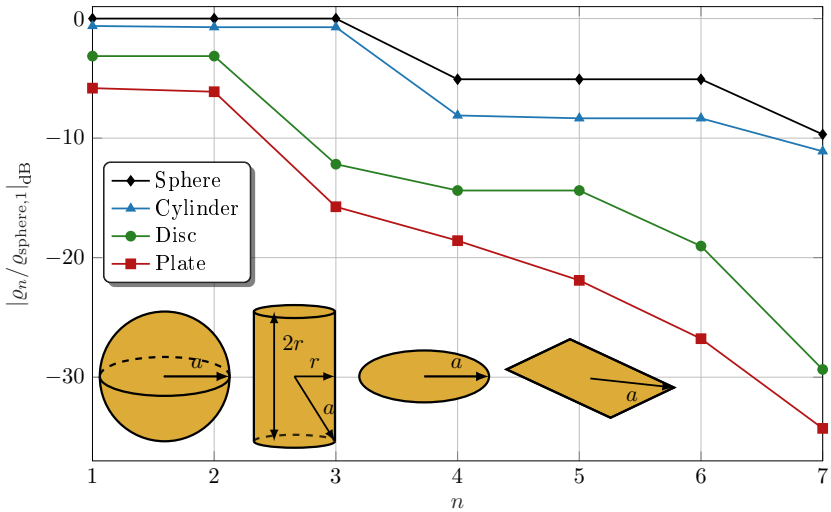

Figure 10: Radiation mode strength of different shapes normalized to the first spherical mode. All shapes have size $ka = 1$.

in order to find the optimal channel. The important factor in the expression for the singular values is the eigenvalues of the generalized eigenvalue problem between the component matrices in the condition. If the ohmic losses in the antenna was chosen, the eigenvalues that affect the solution are calculated from,

$$\mathbf{R}_{\text{r}}\mathbf{I}_n = \varrho_n \mathbf{R}_\Omega \mathbf{I}_n, \tag{39}$$

where ϱ_n are the eigenvalues representing the strength of the modes, and $\mathbf{I}_n$ are the mode currents. The modes that this eigenvalue problem produce are known as radiation modes [110]. The greater number of strong radiation modes that a structure has, the larger diversity it will be able to induce in its optimal channel, for a problem restricted by the ohmic losses, and therefore higher optimal spectral efficiency. This analysis is powerful for antenna design as the matrices in (39) are mainly dependent on the geometry of the structure. It is, through this expression, possible to *a priori* compare different structures or geometries viability as MIMO antennas by studying their radiation mode strengths. Equivalently, if we consider an optimization restricted by other parameters, the matrices involved create a different set of modes that predict structural viability based on those metrics, *e.g.*, energy modes [59] in the case of the stored energy condition with the matrices $(\mathbf{X}_{\text{e}}+\mathbf{X}_{\text{m}})$, see Paper IV. This type of analysis is similar to the degrees of freedom analysis that has previously been investigated for MIMO systems [36, 49, 97, 98].

In Fig. 10 the radiation mode strength of different shapes has been plotted normalized to the first radiation mode of the sphere. Here, we can see how much worse different shapes are at inducing the radiation modes compared to the sphere. All shapes are contained within the sphere and have size $ka = 1$. The cylinder, for example, a popular antenna design for omnidirectional arrays [77,

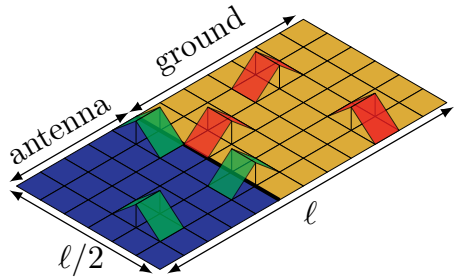

Figure 11: Sub-division of the plate in Fig. 4 into an antenna region and ground region, as illustrated in Fig. 1b. Where the basis functions representing the currents in the antenna region can be controlled [59].

82, 90], has similar mode strengths for the first three modes. Whereas the planar shapes, such as a plate or disc, have much weaker modes. Notice also the mode grouping that occurs, where radiation modes for the sphere and cylinder come in groups of three, whereas the only grouping that occurs for the planar shapes are the first two which correspond to the dipole modes.

The geometry that affects the strength of the radiation modes in (39) is not restricted to different shapes. Embedded antennas fed by sub-regions can be analyzed using the same metric. Reformulating the optimization problem in only the controlled currents of the sub-region, can be done by the Schur compliment [139], see Fig. 11. Divide the MoM matrices into block matrices relating to antenna and ground regions [59]. Consider the MoM matrix equation $\mathbf{ZI} = \mathbf{V}$,

$$\begin{pmatrix} \mathbf{Z}_{\mathrm{aa}} & \mathbf{Z}_{\mathrm{ag}} \\ \mathbf{Z}_{\mathrm{ga}} & \mathbf{Z}_{\mathrm{gg}} \end{pmatrix} \begin{pmatrix} \mathbf{I}_{\mathrm{a}} \\ \mathbf{I}_{\mathrm{g}} \end{pmatrix} = \begin{pmatrix} \mathbf{V}_{\mathrm{a}} \\ \mathbf{0} \end{pmatrix}, \tag{40}$$

where subscript a denotes the controlled or antenna region, and subscript g denotes the ground region. $\mathbf{Z}_{\mathrm{aa}}$ and $\mathbf{Z}_{\mathrm{gg}}$ connects the antenna and ground regions to themselves, and $\mathbf{Z}_{\mathrm{ag}}$ and $\mathbf{Z}_{\mathrm{ga}}$ connect between the antenna and ground regions. The system is only fed in the controlled region. It is possible to eliminate the ground currents from (40) by rewriting the second equation as,

$$\mathbf{I}_{\mathrm{g}} = -\mathbf{Z}_{\mathrm{gg}}^{-1}\mathbf{Z}_{\mathrm{ga}}\mathbf{I}_{\mathrm{a}} = \mathbf{Z}_{\mathrm{t}}\mathbf{I}_{\mathrm{a}}. \tag{41}$$

This new matrix $\mathbf{Z}_{\mathrm{t}}$ is then used to rewrite all MoM matrices on a form that only acts on the antenna currents. Take for example the reactance matrix $\mathbf{X}$,

$$\begin{aligned} \mathbf{I}_{\mathrm{a}}\mathbf{X}\mathbf{I}_{\mathrm{a}} &= \mathbf{I}_{\mathrm{a}}^{\mathrm{H}}\mathbf{X}_{\mathrm{aa}}\mathbf{I}_{\mathrm{a}} + \mathbf{I}_{\mathrm{a}}^{\mathrm{H}}\mathbf{X}_{\mathrm{ag}}\mathbf{I}_{\mathrm{g}} + \mathbf{I}_{\mathrm{g}}^{\mathrm{H}}\mathbf{X}_{\mathrm{ga}}\mathbf{I}_{\mathrm{a}} + \mathbf{I}_{\mathrm{g}}^{\mathrm{H}}\mathbf{X}_{\mathrm{gg}}\mathbf{I}_{\mathrm{g}} \\ &= \mathbf{I}_{\mathrm{a}}^{\mathrm{H}}(\mathbf{X}_{\mathrm{aa}} + 2\,\mathrm{Re}\{\mathbf{X}_{\mathrm{ag}}\mathbf{Z}_{\mathrm{t}}\} + \mathbf{Z}_{\mathrm{t}}^{\mathrm{H}}\mathbf{X}_{\mathrm{gg}}\mathbf{Z}_{\mathrm{t}})\mathbf{I}_{\mathrm{a}} = \mathbf{I}_{\mathrm{a}}^{\mathrm{H}}\mathbf{X}_{\mathrm{p}}\mathbf{I}_{\mathrm{a}}. \end{aligned} \tag{42}$$

By doing this (38) can be rewritten in terms of a controlled sub-region of a larger shape, enabling the investigation of embedded antennas. This is investigated in

Paper III for MIMO antennas restricted by radiation efficiency and in Paper IV for MIMO antennas with bandwidth conditions.

In principal (38) is not limited to electrically small antennas once any conditions related to Q or stored energy is discarded. This enables the investigation of electrically large antennas, however, computational issues do arise. A direct MoM solver, as has been used throughout this thesis, is not well suited to simulate electrically large structures due to the amount of unknowns. This quickly makes assembling, and handling the matrices describing the antenna computationally unfeasible. However, this is mainly an issue for dense matrices, such as the impedance matrix $\mathbf{Z}$. The gram matrix describing the ohmic losses $\mathbf{R}_\Omega = R_\mathrm{s}\mathbf{\Psi}$, for example, is a sparse matrix and can be stored efficiently for very large structures. The radiation matrix $\mathbf{R}_\mathrm{r}$ can similarly also be constructed in a computationally efficient way. By decomposing it in the matrix connecting the MoM basis functions to the spherical modes $\mathbf{S}$, it can be written as a product between low rank matrices, $\mathbf{R}_\mathrm{r} = \mathbf{S}^\mathrm{H}\mathbf{S}$, and evaluated accurately for much less computational cost compared to the classical construction [119]. This enables the investigation of the problem with restricted losses for large electrical sizes.

An interesting metric to study when investigating size is the number of degrees of freedom available for different geometries. In principle this number serves as an estimate of how many different modes can be induced on the object. We define this as the number of viable modes with an eigenvalue greater than one. This can be normalized to the number of available modes per unit area on the object [74, 98]. Which is defined for a sphere as [67]

$$2L(L+2) \approx 2ka(ka+2) \approx 2(ka)^2\,,\; ka \to \infty. \tag{43}$$

Which can be put in relation to the area of an object by rewriting ka in the area of the sphere A,

$$2(ka)^2 = \frac{k^2 A}{2\pi} = \frac{2\pi A}{\lambda^2}. \tag{44}$$

This gives us an analytical measure of the number of degrees of freedom a shape has. Normalizing the number of effective modes for a shape with this number gives a measure of how many effective modes are being induced per area. This gives a metric to compare different shapes to see if they effectively utilize their surface area, such an analysis was carried out in Paper III.

4 Stored Electromagnetic Energy

Stored electromagnetic energy is interesting to define due to its appearance in the calculation of the Q-factor (1), and therefore its role in estimating bandwidth for antennas [75]. However, it is, in general, a difficult quantity to define due to the vague separation between stored and radiating fields. The stored energy commonly refers to the energy of the reactive fields surrounding the antenna, the energy that is neither radiated nor reflected back by the system. In the

circuit analog this is the energy stored by reactive circuit elements within the system [134].

There exists many different ways of evaluating stored energy, all of them with benefits and drawbacks. One general theme is the dependence on size. Most methods of calculating stored energy agree for single resonance, electrically small antennas. However, for electrically large antennas or antennas in the presence of complex materials there are greater differences. In Paper V the existing methods are divided into three broad categories:

- Stored energy evaluated from field quantities
- Stored energy evaluated from currents
- Stored energy calculated from a system perspective

Each of which are briefly touched upon here. There are different metrics on which to judge these methods, *e.g.*, how well they function as a physical definition of an energy quantity or how numerically efficient their evaluation is. However, as stated in Sec. 1 the motivation of this thesis is to further develop antenna optimization. One of the main factors that are needed for these quantities to be useful in optimization is fast and efficient evaluation. Therefore, expressions that fulfill these requirements have been the focus of the work conducted in this thesis.

4.1 Stored Energy Evaluated from Field Quantities

These methods are based around calculating the total stored energy in the field and subtracting away the energy that is radiated. The energy density of a field is evaluated as its absolute value squared [32, 76, 88]. The most common way to remove the radiated energy is to subtract the far-field amplitude $\boldsymbol{F}$, *i.e.*, the energy that is radiated to infinity [31, 41, 42, 52, 89, 108, 138],

$$W_{\text{stored}} = \frac{1}{4}\int_{\mathbb{R}^3} \epsilon_0|\boldsymbol{E}(\boldsymbol{r})|^2 + \mu_0|\boldsymbol{H}(\boldsymbol{r})|^2 - 2\epsilon_0\frac{|\boldsymbol{F}(\hat{\boldsymbol{r}})|^2}{|\boldsymbol{r}|^2}\,\mathrm{d}V. \tag{45}$$

Other methods calculating the stored energy through field quantities are also based on the idea of subtracting the energy which travels away from the antenna, utilizing the Poynting vector instead of the far-field amplitude [20, 22, 24, 25]. For the evaluation of (45) we must calculate the field in all space making the numerical evaluation of this expression cumbersome. Additionally the far-field amplitude is quiescent in general dispersive media, making these methods mostly applicable for antennas in free space.

4.2 Stored Energy Evaluated from Currents

Evaluating stored energy from the antenna current density synergizes well with simulation methods such as MoM and are used extensively in current optimization [12, 55, 59, 78]. Here, the antenna is typically represented by an equivalent current distribution from which stored energy can be calculated. For Perfect Electric Conductor (PEC) antennas in free space many of these methods condense to the same expression, calculating stored energy from the frequency derivative of the reactance matrix,

$$W_{\text{stored}} = \frac{1}{4}\mathbf{I}^{\text{H}}\frac{\partial \mathbf{X}}{\partial \omega}\mathbf{I}. \tag{46}$$

This expression was first proposed by Harrington and Mautz [72]. It is analogous to the stored energy of a lumped circuit, if the MoM matrices are replaced with circuit impedance matrices [115]. Other current based methods are derived from representing the subtraction of the far-field in terms of the currents instead [125], or as in Paper VI representing the antenna as a dynamic system. Both of these and other [40] methods that converge to (46) for the simple case have the common problem that $\mathbf{X}$ becomes indefinite for electrically large structures and therefore cannot calculate stored energy for them. Stored energy has also been evaluated using time domain methods, where the separation between radiated and stored fields can be made clear [14].

4.3 Stored Energy Calculated from a System Perspective

Methods that fall under this categorization view the antenna as an input-output relationship which can be represented by something for which we can calculate stored energy. Most poignant of these being circuit synthesis, where the antenna is represented by a circuit that produces the same input impedance response as the antenna. The stored energy can be estimated by calculating the energy stored in the equivalent circuit elements. These circuits can be synthesized by different methods, *e.g.*, Brune synthesis [8, 134]. Other examples of this methodology is the Chu bound where the wave impedances of spherical modes is represented by lumped circuit elements [20, 120, 122]. Here, it is important that the circuit synthesized is a minimal representation of the input impedance. Because it is possible to synthesize circuits with hidden reactive elements, such as the Zöbel circuit, see Paper V, that do not affect the input impedance response of the system, the stored energy estimation can vary wildly for inaccurately synthesized circuits.

4.4 Stored Energy in Complex Media

Most ways of calculating stored energy have been constructed for antennas in free space. However, many antennas operate close to, or insider of complex media.

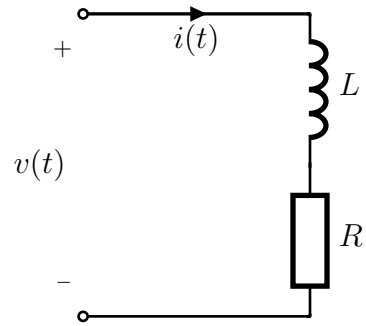

Figure 12: A lumped inductor and resistor circuit.

Application areas such as body area networks, mobile phones, in-body antennas, submarines or plasmonics [2, 95, 131], all need to consider the media their antennas are operating in the vicinity of during the design process. Due to the design process of such antennas often being complicated [85, 95, 113, 114], developing quick and efficient optimization is important. To facilitate that process a rigorous method for calculating stored energy is needed. Methods designed for free space can serve as relatively good indicators for stored energy in complex media. However, they often struggle with particularly difficult cases, such as dispersion or media with resonances close to the resonance frequency of the antenna. In Paper VI a method for calculating stored energy in dispersive and inhomogeneous media is presented. The method is based on representing the antenna as a dynamic system through a state-space method and using the methodology presented in [132, 133] to calculate the energy stored in such a dynamic system. The strength of this method is how it is generalized from free space to complex media. The same procedure is followed as if it is derived for free space, extending the matrices describing the system to encompas the complex behaviour of the materials involved. Here follows a brief derivation of the state-space model for stored energy for an antenna in free space.

4.5 State-Space model for Stored Energy

To illustrate the state-space model lets first consider a much simpler dynamic system than an antenna. Consider the lumped circuit in Fig. 12. The power in this system can be computed by multiplying the voltage v and the current i together,

$$p = vi = iL\frac{\partial i}{\partial t} + Ri^2 = \frac{\partial}{\partial t}\left(\frac{Li^2}{2}\right) + Ri^2, \tag{47}$$

where we have used the well known constitutive relations for an inductor $v_{\mathrm{L}} = L\frac{\partial i}{\partial t}$, and a resistance $v_{\mathrm{R}} = Ri$. The energy of the system can be calculated by

integrating the power over time,

$$W(\tau) = \int_{-\infty}^{\tau} p(t)\,\mathrm{d}t = \int_{-\infty}^{\tau} L\frac{\partial i}{\partial t} i + Ri^2\,\mathrm{d}t = \frac{1}{2}Li^2(\tau) + \int_{-\infty}^{\tau} Ri^2\,\mathrm{d}t, \tag{48}$$

where we have used partial integration and the common assumption of quiescent currents at early times $i(-\infty) = 0$. The first term in (48) is recognizable as the energy stored in an inductor and the second term is the dissipated energy in the resistance. For a time harmonic signal, $i(t) = \mathrm{Re}\{I_0 \mathrm{e}^{\mathrm{j}\omega t}\}$ and $v(t) = \mathrm{Re}\{V_0 \mathrm{e}^{\mathrm{j}\omega t}\}$, the stored magnetic energy W_m in the inductor can therefore be calculated as [134]

$$W_\mathrm{m} = \frac{1}{T}\int_0^T \frac{1}{2}Li^2(t)\,\mathrm{d}t = \frac{1}{4}L|I_0|^2, \tag{49}$$

where T is the time period. The time-average stored energy in a capacitor is similarly

$$W_\mathrm{e} = \frac{1}{4}C|V_0|^2 = \frac{1}{4\omega^2 C}|I_0|^2. \tag{50}$$

This is indicative of how to calculate the stored energy of a general dynamic system. In (47) it is the term with a partial time derivative which describes the storage function of the system.

Suppose we have a circuit network characterized by its input impedance Z_in. The input impedance can be separated into a resistive and a reactive part. The resistive part relates to the energy dissipation and the reactive part relates to energy stored. For a lumped circuit network we have the relation [134],

$$Z_\mathrm{in} = R_\mathrm{in} + \mathrm{j}X_\mathrm{in} = \frac{2P_\mathrm{d} + 4\mathrm{j}\omega(W_\mathrm{m} - W_\mathrm{e})}{|I_\mathrm{in}|^2}, \tag{51}$$

where R_in and X_in are the input resistance and reactance, respectively, P_d is the dissipated power, W_m and W_e are the stored magnetic and electric energies, respectively, and I_in is the input current. Here, the reactance of the system is proportional to the difference between the energy stored magnetically, in the inductors, and electrically, in the capacitors. For a more general system one can relate the currents $\mathbf{I}$ and the voltages $\mathbf{V} = \mathbf{ZI}$ through the impedance matrix $\mathbf{Z}$ using Kirchoff's laws. The impedance matrix can be decomposed into its resistance $\mathbf{R}$, inductance $\mathbf{L}$, and capacitance $\mathbf{C} = \mathbf{C}_\mathrm{i}^{-1}$ matrices [115],

$$\mathbf{Z} = \mathbf{R} + \mathrm{j}\mathbf{X} = \mathbf{R} + \mathrm{j}\omega\mathbf{L} + \frac{1}{\mathrm{j}\omega}\mathbf{C}_\mathrm{i} = \mathbf{R} + s\mathbf{L} + \frac{1}{s}\mathbf{C}_\mathrm{i}, \tag{52}$$

where $s = \mathrm{j}\omega$ is the Laplace parameter. The impedance matrix (52) is a second order state-space model for the input impedance $Z_\mathrm{in} = V_\mathrm{in}/I_\mathrm{in}$ with the input $\mathbf{V} = \mathbf{B}V_\mathrm{in}$ and output $I_\mathrm{in} = \mathbf{B}^\mathrm{T}\mathbf{I}$, where $\mathbf{B}$ defines the port position of the circuit. However, to define the stored energy of a system it is convenient to use the state-space model of the first order [133]. This can be done by the introduction of the

voltage state $\mathbf{U} = \frac{1}{s}\mathbf{C}_\mathrm{i}\mathbf{I}$,

$$s\begin{pmatrix}\mathbf{L} & \mathbf{0}\\ \mathbf{0} & \mathbf{C}\end{pmatrix}\begin{pmatrix}\mathbf{I}\\ \mathbf{U}\end{pmatrix} + \begin{pmatrix}\mathbf{R} & \mathbf{1}\\ -\mathbf{1} & \mathbf{0}\end{pmatrix}\begin{pmatrix}\mathbf{I}\\ \mathbf{U}\end{pmatrix} = \begin{pmatrix}s\mathbf{L}+\mathbf{R} & \mathbf{1}\\ -\mathbf{1} & s\mathbf{C}\end{pmatrix}\begin{pmatrix}\mathbf{I}\\ \mathbf{U}\end{pmatrix}. \tag{53}$$

Because we are evaluating time harmonic frequency domain quantities, multiplication by the frequency variable s is synonymous with a time-derivative in the time domain. This lets us identify the first matrix in (53) as the stored energy term analogous to that of the inductor in (47). Hence, the time-average stored energy of the system is obtained by the quadratic form

$$W = \begin{pmatrix}\mathbf{I}\\ \mathbf{U}\end{pmatrix}^\mathrm{T}\begin{pmatrix}\mathbf{L} & \mathbf{0}\\ \mathbf{0} & \mathbf{C}\end{pmatrix}\begin{pmatrix}\mathbf{I}\\ \mathbf{U}\end{pmatrix} = \frac{1}{4}\mathbf{I}^\mathrm{H}\mathbf{L}\mathbf{I} + \frac{1}{4\omega^2}\mathbf{I}^\mathrm{H}\mathbf{C}_\mathrm{i}\mathbf{I}, \tag{54}$$

where the voltage state $\mathbf{U}$ has been substituted back to gain a quadratic form in the current. Here, we see similarities with the expressions (49) and (50). Stored energy in many other linear systems can be determined analogously [133].

Now we can consider a simple PEC antenna in free space modeled by MoM. The impedance equation (8), describes the system and is written as,

$$\mathbf{Z}\mathbf{I} = \left(s\mu_0\mathbf{L} + \frac{1}{s\epsilon_0}\mathbf{C}_\mathrm{i}\right)\mathbf{I} = s\mu_0\mathbf{L}\mathbf{I} + \mathbf{U} = \mathbf{V}, \tag{55}$$

where $\mathbf{L}$ and $\mathbf{C}_\mathrm{i}$ are now MoM matrices, and the voltage state $\mathbf{U} = \frac{1}{s\epsilon_0}\mathbf{C}_\mathrm{i}\mathbf{I}$ now includes the permittivity. This system is only slightly different from that of the lumped circuit in (52), and stored energy can be calculated for it in the same way as in (54). However, the $\mathbf{L}$ and $\mathbf{C}_\mathrm{i}$ matrices have frequency dependence that cannot be neglected. It is possible to approximate it as a linear dependence which is estimated by differentiating the matrices with regards to the laplace variable. This gives the energy expression,

$$\begin{aligned} W &= \frac{\mathrm{Re}}{4}\begin{pmatrix}\mathbf{I}\\ \mathbf{U}\end{pmatrix}^\mathrm{H}\begin{pmatrix}\mu_0(\mathbf{L}+\mathrm{j}\omega\mathbf{L}') & \mathbf{0}\\ \mathbf{0} & \epsilon_0(\mathbf{C}+\mathrm{j}\omega\mathbf{C}')\end{pmatrix}\begin{pmatrix}\mathbf{I}\\ \mathbf{U}\end{pmatrix}\\ &= \frac{\mathrm{Re}}{4}\big(\mu_0\mathbf{I}^\mathrm{H}(\mathbf{L}+\mathrm{j}\omega\mathbf{L}')\mathbf{I} + \epsilon_0\mathbf{U}^\mathrm{H}(\mathbf{C}+\mathrm{j}\omega\mathbf{C}')\mathbf{U}\big)\\ &\simeq \frac{\mathrm{Re}}{4}\mathbf{I}^\mathrm{H}\big(\mu_0(\mathbf{L}+\mathrm{j}\omega\mathbf{L}') + \frac{1}{\omega^2\epsilon_0}(\mathbf{C}_\mathrm{i}-\mathrm{j}\omega\mathbf{C}_\mathrm{i}')\big)\mathbf{I} = \frac{1}{4}\mathbf{I}^\mathrm{H}\frac{\partial\mathbf{X}}{\partial\omega}\mathbf{I}, \end{aligned} \tag{56}$$

where $\mathbf{C}' = -\mathbf{C}\mathbf{C}_\mathrm{i}'\mathbf{C}$ is used. This expression can be extended to complex media by the inclusion of more advanced material models in ϵ and μ. These can be expressed in terms of Lorentz resonances on the form [76, 124],

$$\epsilon(s) = \epsilon_\infty + \frac{\alpha^2}{\beta^2 + \gamma s + \delta s^2} \tag{57}$$

where ϵ_∞ is the instantaneous response, and $\alpha, \beta, \gamma, \delta$ are the Lorentz parameters describing the materials frequency dependence. By changing the parameters

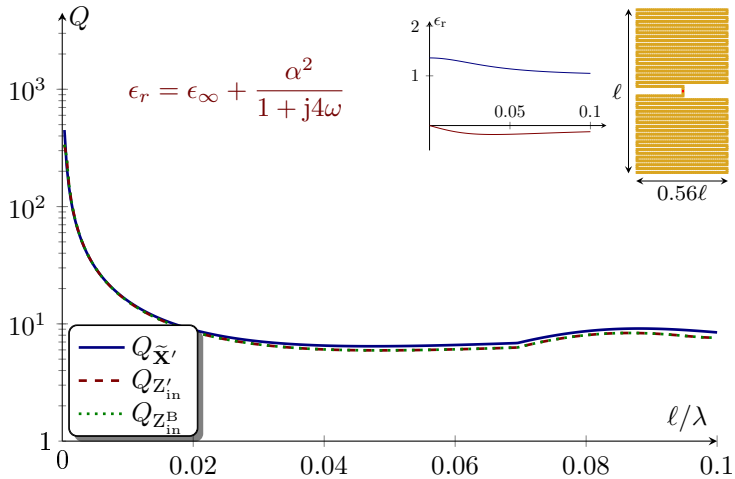

Figure 13: A meanderline antenna from [4] of size $\ell \times 0.56\ell$ simulated in homogeneous Debye medium with relative permittivity depicted in the inset. Three different Q-factors have been calculated for the antenna. The Q-factor derived from the states space model $Q_{\widetilde{\mathbf{X}}'}$, from Brune synthesis $Q_{Z^{\mathrm{B}}_{\mathrm{in}}}$ [8], and from the differentiation of the impedance matrix $Q_{Z'_{\mathrm{in}}}$ [61, 138].

in (57) the model can be reduced to a variety of different material models, *e.g.*, the Debye ($\delta = 0$) or Drude ($\beta = 0$) models. To handle these new frequency dependent terms new states, similar to the voltage state $\mathbf{U}$, are introduced and their relation to each other and the previous states extend the matrices in (56). This procedure is detailed in Paper VI. In Fig. 13 a meander line embedded in Debye media is depicted. Here we can see that the state-space model agrees well with the Q-factor calculated from circuit synthesis [8] and differentiation of the input impedance [138].

5 Conclusions

In this thesis a new and novel method for calculating physical bounds for MIMO antennas is presented. These bounds calculate the optimal performance for an antenna in an ideal channel, therefore providing a bound to the performance of implemented MIMO antennas. While these bounds are idealized and might be difficult to verify experimentally they do mirror the operating scenario of electrically small MIMO antennas. The radiation pattern of such antennas are, in general, relatively omnidirectional. Using the ideal spherical channel to bound their performance is therefore relatively close to their operating scenario since they rely on radiating in any direction to excite multipath propagation. It is also shown that this method of constructing physical bounds for MIMO antennas

gives insight into what modes are efficient for inducing optimal performance. Depending on what conditions are put on the optimization problem, different modes relating to those conditions induce optimal performance for the antenna. This has the potential to provide insight into how to effectively design MIMO antennas. The optimization problem presented is not limited to small electrical sizes. For larger electrical sizes it is shown how the effective modes could be used to investigate the number of degrees of freedom for a device. In this way predicting if a geometry was an effective use of volume and surface area.

The second part of this thesis dealt with the theoretical problem of stored electromagnetic energy. First providing an overview and categorization of previously existing methods, and then introducing a new method for calculating stored energy in complex media. This method has the possibility to calculate stored energy for an antenna in any background, as long as the antenna itself is electrically small. This method is stable for many difficult to handle scenarios, such as resonant dispersive media, or piecewise homogeneous media.

6 Future Work

The work carried out in this thesis is a first step to providing useful physical bounds for MIMO antennas and antennas in complex media. The method for calculating physical bounds for MIMO antennas can be extended to include channel characteristics and more realistic scenarios. It is also an interesting prospect to run the optimization problem on real antenna structures and large arrays to utilize the modal analysis that is derived from it. This connects back to investigating how these bounds compare to designed antenna performance, both in simulation and measurement.

For complex media, developing MoM code that can efficiently simulate user scenarios involving antennas in complex media is essential to calculating physical bounds using the stored energy expressions presented in this thesis. With such a code it would be interesting to formulate and investigate a procedure for calculating physical bounds for implantable antennas. This could prove very useful for performing automatic optimization of in-body and on-body antennas.

References

[1] ITU-R WP5D. Minimum requirements related to technical performance for imt-2020 radio interface(s), 2017.

[2] S. Arslanagic, R. W. Ziolkowski, and O. Breinbjerg. Analytical and numerical investigation of the radiation and scattering from concentric metamaterial cylinders excited by an electric line source. *Radio Sci.*, **42**(6), 2007.

[3] S. R. Best. A low Q electrically small magnetic (TE mode) dipole. *IEEE Antennas Wirel. Propag. Lett.*, **8**, pp. 572–575, 2009.

[4] S. R. Best. Electrically small resonant planar antennas: Optimizing the quality factor and bandwidth. *IEEE Antennas Propag. Mag.*, **57**(3), pp. 38–47, Jun. 2015.

[5] S. R. Best. A comparison of the cylindrical folded helix Q to the Gustafsson limit. In *2009 3rd European Conference on Antennas and Propagation*, pp. 2554–2557. IEEE, 2009.

[6] S. R. Best and D. L. Hanna. A performance comparison of fundamental small-antenna designs. *IEEE Antennas Propag. Mag.*, **52**(1), pp. 47–70, 2010.

[7] S. P. Boyd and L. Vandenberghe. *Convex Optimization*. Cambridge Univ. Pr., 2004.

[8] O. Brune. Synthesis of a finite two-terminal network whose driving-point impedance is a prescribed function of frequency. *MIT J. Math. Phys.*, **10**, pp. 191–236, 1931.

[9] A. G. Burr. Capacity bounds and estimates for the finite scatterers MIMO wireless channel. *IEEE J. Sel. Areas Commun.*, **21**(5), pp. 812–818, Jun. 2003.

[10] M. Cabedo-Fabres, E. Antonino-Daviu, A. Valero-Nogueira, and M. Bataller. The theory of characteristic modes revisited: A contribution to the design of antennas for modern applications. *IEEE Antennas Propag. Mag.*, **49**(5), pp. 52–68, 2007.

[11] M. Capek and L. Jelinek. Comments on 'On stored energies and radiation Q'. *IEEE Trans. Antennas Propag.*, 2015. (in press).

[12] M. Capek, M. Gustafsson, and K. Schab. Minimization of antenna quality factor. *IEEE Trans. Antennas Propag.*, **65**(8), pp. 4115–4123, 2017.

[13] M. Capek and L. Jelinek. Optimal composition of modal currents for minimal quality factor Q. *IEEE Trans. Antennas Propag.*, **64**(12), pp. 5230–5242, 2016.

[14] M. Capek, L. Jelinek, and G. A. E. Vandenbosch. Stored electromagnetic energy and quality factor of radiating structures. *Proc. R. Soc. A*, **472**(2188), 2016.

[15] C. J. Carpenter. Electromagnetic energy and power in terms of charges and potentials instead of fields. *IEE Proc. A*, **136**(2), pp. 55–65, 1989.

[16] Y. Chen and C.-F. Wang. *Characteristic Modes: Theory and Applications in Antenna Engineering*. John Wiley & Sons, 2015.

[17] Z. N. Chen. *Antennas for portable devices*. John Wiley & Sons, 2007.

[18] Z. N. Chen and K. M. Luk, editors. *Antennas for base stations in wireless communications*. McGraw-Hill, 2009.

[19] W. C. Chew, M. S. Tong, and B. Hu. *Integral Equation Methods for Electromagnetic and Elastic Waves*, volume 12. Morgan & Claypool, 2008.

[20] L. J. Chu. Physical limitations of omni-directional antennas. *J. Appl. Phys.*, **19**, pp. 1163–1175, 1948.

[21] Cisco Visual Networking Index. Global mobile data traffic forecast update, 2014–2019. *White Paper, Feb.*, **1**, 2015.

[22] R. E. Collin. Minimum Q of small antennas. *J. Electromagnet. Waves Appl.*, **12**, pp. 1369–1393, 1998.

[23] R. E. Collin and S. Rothschild. Reactive energy in aperture fields and apperture Q. *Canadian Journal of Physics*, **41**(12), pp. 1967–1979, 1963.

[24] R. E. Collin and S. Rothschild. Evaluation of antenna Q. *IEEE Trans. Antennas Propag.*, **12**, pp. 23–27, Jan. 1964.

[25] V. A. Counter. Miniature cavity antenna. Technical Report 2, Microwave Lab, 1948. Contract No. W28-099-ac-382.

[26] T. M. Cover and J. A. Thomas. *Elements of information theory*. John Wiley & Sons, 2012.

[27] E. Dahlman, S. Parkvall, and J. Skold. *4G: LTE/LTE-advanced for mobile broadband*. Academic press, 2013.

[28] W. Dai, Y. Liu, and B. Rider. Quantization bounds on grassmann manifolds and applications to MIMO communications. *IEEE Trans. Inf. Theory*, **54**(3), pp. 1108–1123, Mar. 2008.

[29] P. F. Driessen and G. J. Foschini. On the capacity formula for multiple input-multiple output wireless channels: A geometric interpretation. *IEEE Trans. on Communication*, **47**(2), pp. 173–176, Feb. 1999.

[30] C. Ehrenborg and M. Gustafsson. Fundamental bounds on MIMO antennas. *IEEE Antennas Wireless Propag. Lett.*, **17**(1), pp. 21–24, Jan. 2018.

[31] R. L. Fante. Quality factor of general ideal antennas. *IEEE Trans. Antennas Propag.*, **17**(2), pp. 151–155, Mar. 1969.

[32] R. P. Feynman, R. B. Leighton, and M. Sands. *The Feynman Lectures on Physics*. Addison-Wesley, Reading, MA, 1965.

[33] R. Fleury, J. Soric, and A. Alù. Physical bounds on absorption and scattering for cloaked sensors. *Physical Review B*, **89**(4), pp. 045122, Jan. 2014.

[34] H. D. Foltz and J. S. McLean. Limits on the radiation Q of electrically small antennas restricted to oblong bounding regions. In *IEEE Antennas and Propagation Society International Symposium*, volume 4, pp. 2702–2705. IEEE, 1999.

[35] M. Franceschetti, O. Dousse, D. N. C. Tse, and P. Thiran. Closing the gap in the capacity of wireless networks via percolation theory. *IEEE Trans. Inf. Theory*, **53**(3), pp. 1009–1018, Mar. 2007.

[36] M. Franceschetti, M. D. Migliore, and P. Minero. The capacity of wireless networks: Information-theoretic and physical limits. *IEEE Trans. Inf. Theory*, **55**(8), pp. 3413–3424, Aug. 2009.

[37] M. Franceschetti. *Wave Theory of Information*. Cambridge University Press, 2017.

[38] K. Fujimoto and H. Morishita. *Modern Small Antennas*. Cambridge University Press, 2013.

[39] B. N. Getu and J. B. Andersen. The MIMO cube - a compact MIMO antenna. *IEEE Trans. Wireless Communications*, **4**(3), pp. 1136–1141, 2005.

[40] W. Geyi. A method for the evaluation of small antenna Q. *IEEE Trans. Antennas Propag.*, **51**(8), pp. 2124–2129, 2003.

[41] W. Geyi. Physical limitations of antenna. *IEEE Trans. Antennas Propag.*, **51**(8), pp. 2116–2123, Aug. 2003.

[42] W. Geyi. *Foundations of Applied Electrodynamics*. John Wiley & Sons, 2011.

[43] W. Geyi. Stored energies and radiation Q. *IEEE Trans. Antennas Propag.*, **63**(2), pp. 636–645, 2015.

[44] W. C. Gibson. *The Method of Moments in Electromagnetics*, volume 1. Chapman & Hall/CRC London, UK, 2008.

[45] A. A. Glazunov, M. Gustafsson, and A. Molisch. On the physical limitations of the interaction of a spherical aperture and a random field. *IEEE Trans. Antennas Propag.*, **59**(1), pp. 119–128, 2011.

[46] A. A. Glazunov, M. Gustafsson, A. Molisch, and F. Tufvesson. Physical modeling of multiple-input multiple-output antennas and channels by means of the spherical vector wave expansion. *IET Microwaves, Antennas & Propagation*, **4**(6), pp. 778–791, 2010.

[47] A. A. Glazunov, M. Gustafsson, A. Molisch, F. Tufvesson, and G. Kristensson. Spherical vector wave expansion of gaussian electromagnetic fields for antenna-channel interaction analysis. *IEEE Trans. Antennas Propag.*, **3**(2), pp. 214–227, 2009.

[48] M. Grant and S. Boyd. CVX: Matlab software for disciplined convex programming, version 2.1. http://cvxr.com/cvx, Dec. 2018.

[49] F. K. Gruber and E. A. Marengo. New aspects of electromagnetic information theory for wireless and antenna systems. *IEEE Trans. Antennas Propag.*, **56**(11), pp. 3470–3484, Nov. 2008.

[50] J. Gubbi, R. Buyya, S. Marusic, and M. Palaniswami. Internet of things (IoT): A vision, architectural elements, and future directions. *Future generation computer systems*, **29**(7), pp. 1645–1660, 2013.

[51] M. Gustafsson, M. Capek, and K. Schab. Trade-off between antenna efficiency and Q-factor. *IEEE Trans. Antennas Propag.*, **67**(4), pp. 2482–2493, Apr. 2019.

[52] M. Gustafsson and B. L. G. Jonsson. Antenna Q and stored energy expressed in the fields, currents, and input impedance. *IEEE Trans. Antennas Propag.*, **63**(1), pp. 240–249, 2015.

[53] M. Gustafsson and B. L. G. Jonsson. Stored electromagnetic energy and antenna Q. *Prog. Electromagn. Res. (PIER)*, **150**, pp. 13–27, 2015.

[54] M. Gustafsson and S. Nordebo. On the spectral efficiency of a sphere. *Prog. Electromagn. Res.*, **67**, pp. 275–296, 2007.

[55] M. Gustafsson and S. Nordebo. Optimal antenna currents for Q, superdirectivity, and radiation patterns using convex optimization. *IEEE Trans. Antennas Propag.*, **61**(3), pp. 1109–1118, 2013.

[56] M. Gustafsson and D. Sjöberg. Sum rules and physical bounds on passive metamaterials. *New Journal of Physics*, **12**(043046), pp. 1–18, 2010.

[57] M. Gustafsson, C. Sohl, and G. Kristensson. Physical limitations on antennas of arbitrary shape. *Proc. R. Soc. A*, **463**, pp. 2589–2607, 2007.

[58] M. Gustafsson, C. Sohl, and G. Kristensson. Illustrations of new physical bounds on linearly polarized antennas. *IEEE Trans. Antennas Propag.*, **57**(5), pp. 1319–1327, May 2009.

[59] M. Gustafsson, D. Tayli, C. Ehrenborg, M. Cismasu, and S. Nordebo. Antenna current optimization using MATLAB and CVX. *FERMAT*, **15**(5), pp. 1–29, 2016.

[60] M. Gustafsson, M. Cismasu, and B. L. G. Jonsson. Physical bounds and optimal currents on antennas. *IEEE Trans. Antennas Propag.*, **60**(6), pp. 2672–2681, 2012.

[61] M. Gustafsson and C. Ehrenborg. State-space models and stored electromagnetic energy for antennas in dispersive and heterogeneous media. *Radio Sci.*, **52**, 2017.

[62] M. Gustafsson and S. Nordebo. Characterization of MIMO antennas using spherical vector waves. *IEEE Trans. Antennas Propag.*, **54**(9), pp. 2679–2682, 2006.

[63] M. Gustafsson, D. Tayli, and M. Cismasu. *Physical bounds of antennas*, pp. 1–32. Springer-Verlag, 2015.

[64] T. V. Hansen, O. S. Kim, and O. Breinbjerg. Stored energy and quality factor of spherical wave functions–in relation to spherical antennas with material cores. *IEEE Trans. Antennas Propag.*, **60**(3), pp. 1281–1290, 2012.

[65] T. V. Hansen, O. S. Kim, and O. Breinbjerg. Properties of sub-wavelength spherical antennas with arbitrarily lossy magnetodielectric cores approaching the Chu lower bound. *IEEE Trans. Antennas Propag.*, **62**(3), pp. 1456–1460, 2014.

[66] R. F. Harrington. Effect of antenna size on gain, bandwidth and efficiency. *Journal of Research of the National Bureau of Standards – D. Radio Propagation*, **64D**, pp. 1–12, Jan. – Feb. 1960.

[67] R. F. Harrington. *Time Harmonic Electromagnetic Fields.* McGraw-Hill, New York, NY, 1961.

[68] R. F. Harrington. Antenna excitation for maximum gain. *IEEE Trans. Antennas Propag.*, **13**(6), pp. 896–903, Nov. 1965.

[69] R. Harrington. Characteristic modes for antennas and scatterers. In R. Mittra, editor, *Numerical and Asymptotic Techniques in Electromagnetics*, volume 3 of *Topics in Applied Physics*, pp. 51–87. Springer Berlin Heidelberg, 1975.

[70] R. F. Harrington. *Field Computation by Moment Methods.* Macmillan, New York, NY, 1968.

[71] R. F. Harrington and J. R. Mautz. Theory of characteristic modes for conducting bodies. *IEEE Trans. Antennas Propag.*, **19**(5), pp. 622–628, 1971.

[72] R. F. Harrington and J. R. Mautz. Control of radar scattering by reactive loading. *IEEE Trans. Antennas Propag.*, **20**(4), pp. 446–454, 1972.

[73] R. L. Haupt and D. H. Werner. *Genetic algorithms in electromagnetics*. John Wiley & Sons, 2007.

[74] S. Hu, F. Rusek, and O. Edfors. The potential of using large antenna arrays on intelligent surfaces. In *2017 IEEE 85th Vehicular Technology Conference (VTC Spring)*, pp. 1–6, Jun. 2017.

[75] IEEE145-1993. *IEEE Standard Definition of Terms for Antennas*. Antenna Standards Committee of the IEEE Antennas and Propagation Society, Mar. 1993.

[76] J. D. Jackson. *Classical Electrodynamics*. John Wiley & Sons, New York, NY, third edition, 1999.

[77] I. Jayakumar, R. Garg, B. Sarap, and B. Lal. A conformal cylindrical microstrip array for producing omnidirectional radiation pattern. *IEEE Trans. Antennas Propag.*, **34**(10), pp. 1258–1261, Oct. 1986.

[78] L. Jelinek and M. Capek. Optimal currents on arbitrarily shaped surfaces. *IEEE Trans. Antennas Propag.*, **65**(1), pp. 329–341, 2017.

[79] M. A. Jensen and J. W. Wallace. A review of antennas and propagation for MIMO wireless communications. *IEEE Trans. Antennas Propag.*, **52**(11), pp. 2810–2824, Nov. 2004.

[80] M. A. Jensen and J. W. Wallace. Capacity of the continuous-space electromagnetic channel. *IEEE Trans. Antennas Propag.*, **56**(2), pp. 524–531, Feb. 2008.

[81] B. L. G. Jonsson, S. Shi, L. Wang, F. Ferrero, and L. Lizzi. On methods to determine bounds on the Q-factor for a given directivity. *IEEE Trans. Antennas Propag.*, **65**(11), pp. 5686–5696, 2017.

[82] L. Josefsson and P. Persson. *Conformal Array Antenna Theory & Design*. Wiley-IEEE Press, 2006.

[83] O. Kim. Low-Q electrically small spherical magnetic dipole antennas. *IEEE Trans. Antennas Propag.*, **58**(7), pp. 2210–2217, Jul. 2010.

[84] O. Kim. Minimum Q electrically small antennas. *IEEE Trans. Antennas Propag.*, **60**(8), pp. 3551–3558, Aug. 2012.

[85] A. Kiourti and K. S. Nikita. A review of implantable patch antennas for biomedical telemetry: Challenges and solutions [wireless corner]. *IEEE Antennas Propag. Mag.*, **54**(3), pp. 210–228, Jun. 2012.

[86] S. Koziel and S. Ogurtsov. *Antenna design by simulation-driven optimization*. Springer, 2014.

[87] L. Kundu. *Information-Theoretic Limits on MIMO Antennas*. PhD thesis, North Carolina State University, 2016.

[88] L. D. Landau, E. M. Lifshitz, and L. P. Pitaevskiĭ. *Electrodynamics of Continuous Media*. Pergamon Press, Oxford, second edition, 1984.

[89] C. Levis. A reactance theorem for antennas. *Proceedings of the IRE*, **45**(8), pp. 1128–1134, 1957.

[90] R. J. Mailloux. *Phased array antenna handbook*. Artech house, 2017.

[91] D. Manteuffel and R. Martens. A concept for MIMO antennas on small terminals based on characteristic modes. In *International Workshop on Antenna Technology (iWAT)*, 2011.

[92] R. Martens, E. Safin, and D. Manteuffel. Inductive and capacitive excitation of the characteristic modes of small terminals. In *2011 Loughborough Antennas Propagation Conference*, Nov. 2011.

[93] M. R. McKay and I. B. Collings. General capacity bounds for spatially correlated rician MIMO channels. *IEEE Trans. Inf. Theory*, **51**(9), pp. 3121–3145, Sep. 2005.

[94] J. S. McLean. A re-examination of the fundamental limits on the radiation Q of electrically small antennas. *IEEE Trans. Antennas Propag.*, **44**(5), pp. 672–676, May 1996.

[95] F. Merli, L. Bolomey, J. Zurcher, G. Corradini, E. Meurville, and A. Skrivervik. Design, realization and measurements of a miniature antenna for implantable wireless communication systems. *IEEE Trans. Antennas Propag.*, **59**(10), pp. 3544–3555, 2011.

[96] Z. Miers, H. Li, and B. K. Lau. Design of bandwidth-enhanced and multiband MIMO antennas using characteristic modes. *IEEE Antennas Wirel. Propag. Lett.*, **12**, pp. 1696–1699, 2013.

[97] M. D. Migliore. On the role of the number of degrees of freedom of the field in MIMO channels. *IEEE Trans. Antennas Propag.*, **54**(2), pp. 620–628, Feb 2006.

[98] M. Migliore. On electromagnetics and information theory. *IEEE Trans. Antennas Propag.*, **56**(10), pp. 3188–3200, Oct. 2008.

[99] A. F. Molisch. *Wireless Communications*. John Wiley & Sons, New York, NY, second edition, 2011.

[100] A. F. Molisch, M. Z. Win, and J. H. Winters. Capacity of MIMO systems with antenna selection. In *ICC 2001. IEEE International Conference on Communications. Conference Record (Cat. No.01CH37240)*, volume 2, pp. 570–574, Jun. 2001.

[101] M. L. Morris, M. Jensen, J. W. Wallace, et al. Superdirectivity in MIMO systems. *IEEE Trans. Antennas Propag.*, **53**(9), pp. 2850–2857, 2005.

[102] S. Nordebo, M. Gustafsson, and G. Kristensson. On the capacity of the free space antenna channel. In *IEEE Antennas and Propagation Society International Symposium 2006,*, pp. 3105–3108. IEEE Press, 2006.

[103] T. Ohira. What in the world is Q? *IEEE Microw. Mag.*, **17**(6), pp. 42–49, Jun. 2016.

[104] A. Paulraj, R. Nabar, and D. Gore. *Introduction to Space-Time Wireless Communications*. Cambridge University Press, Cambridge, 2003.

[105] V. G. Polevoi. Maximum energy extractable from an electromagnetic field. *Radiophysics and Quantum Electronics*, **33**(7), pp. 603–609, 1990.

[106] Y. Rahmat-Samii and E. Michielssen. *Electromagnetic Optimization by Genetic Algorithms*. Wiley Series in Microwave and Optical Engineering. John Wiley & Sons, 1999.

[107] E. Rajo-Iglesias and O. Quevedo-Teruel. Linear array synthesis using an ant-colony-optimization-based algorithm. *IEEE Antennas Propag. Mag.*, **49**(2), pp. 70–79, Apr. 2007.

[108] D. R. Rhodes. Observable stored energies of electromagnetic systems. *Journal of the Franklin Institute*, **302**(3), pp. 225–237, 1976.

[109] J. Robinson and Y. Rahmat-Samii. Particle swarm optimization in electromagnetics. *IEEE Trans. Antennas Propag.*, **52**(2), pp. 397 – 407, Feb. 2004.

[110] K. R. Schab. *Modal analysis of radiation and energy storage mechanisms on conducting scatterers*. PhD thesis, University of Illinois at Urbana-Champaign, 2016.

[111] M. Shafi, A. F. Molisch, P. J. Smith, T. Haustein, P. Zhu, P. De Silva, F. Tufvesson, A. Benjebbour, and G. Wunder. 5G: A tutorial overview of standards, trials, challenges, deployment, and practice. *IEEE J. Sel. Areas Commun.*, **35**(6), pp. 1201–1221, Jun. 2017.

[112] M. Shahpari and D. V. Thiel. Fundamental limitations for antenna radiation efficiency. *IEEE Trans. Antennas Propag.*, **66**(8), pp. 3894–3901, Aug. 2018.

[113] A. K. Skrivervik and F. Merli. Design strategies for implantable antennas. In *2011 Loughborough Antennas Propagation Conference*, pp. 1–5, Nov. 2011.

[114] A. K. Skrivervik. Implantable antennas: The challenge of efficiency. In *2013 7th European Conference on Antennas and Propagation (EuCAP),*, pp. 3627–3631. IEEE, 2013.

[115] W. E. Smith. The energy storage of a prescribed impedance. *Proceedings of the Royal Society of New South Wales*, **102**, pp. 203—-218, 1969.

[116] C. Sohl and M. Gustafsson. A priori estimates on the partial realized gain of Ultra-Wideband (UWB) antennas. *Quart. J. Mech. Appl. Math.*, **61**(3), pp. 415–430, 2008.

[117] W. L. Stutzman and G. A. Thiele. *Antenna Theory and Design*. John Wiley & Sons, New York, NY, second edition, 1998.

[118] P. S. Taluja and B. L. Hughes. Fundamental capacity limits on compact MIMO-OFDM systems. In *IEEE International Conference on Communications (ICC)*, pp. 2547–2552, Jun. 2012.

[119] D. Tayli, M. Capek, L. Akrou, V. Losenicky, L. Jelinek, and M. Gustafsson. Accurate and efficient evaluation of characteristic modes. *IEEE Trans. Antennas Propag.*, pp. 1–10, 2018.

[120] H. L. Thal. New radiation Q limits for spherical wire antennas. *IEEE Trans. Antennas Propag.*, **54**(10), pp. 2757–2763, Oct. 2006.

[121] H. L. Thal. Gain and Q bounds for coupled TM-TE modes. *IEEE Trans. Antennas Propag.*, **57**(7), pp. 1879–1885, Jul. 2009.

[122] H. L. Thal. Q Bounds for Arbitrary Small Antennas: A Circuit Approach. *IEEE Trans. Antennas Propag.*, **60**(7), pp. 3120–3128, 2012.

[123] G. Thiele, P. Detweiler, and R. Penno. On the lower bound of the radiation Q for electrically small antennas. *IEEE Trans. Antennas Propag.*, **51**(6), pp. 1263–1269, Jun. 2003.

[124] J. G. van Bladel. *Electromagnetic Fields*. IEEE Press, Piscataway, NJ, second edition edition, 2007.

[125] G. A. E. Vandenbosch. Reactive energies, impedance, and Q factor of radiating structures. *IEEE Trans. Antennas Propag.*, **58**(4), pp. 1112–1127, 2010.

[126] G. A. E. Vandenbosch. Simple procedure to derive lower bounds for radiation Q of electrically small devices of arbitrary topology. *IEEE Trans. Antennas Propag.*, **59**(6), pp. 2217–2225, 2011.

[127] J. Volakis, C. C. Chen, and K. Fujimoto. *Small Antennas: Miniaturization Techniques & Applications*. McGraw-Hill, New York, NY, 2010.

[128] B. Wang, J. Zhang, and A. Host-Madsen. On the capacity of MIMO relay channels. *IEEE Trans. Inf. Theory*, **51**(1), pp. 29–43, 2005.

[129] J. J. H. Wang. *Generalized Moment Methods in Electromagnetics: Formulation and Computer Solution of Integral Equations*. John Wiley & Sons, New York, NY, 1991.

[130] H. A. Wheeler. Fundamental limitations of small antennas. *Proc. IRE*, **35**(12), pp. 1479–1484, 1947.

[131] H. A. Wheeler. Fundamental limitations of a small VLF antenna for submarines. *IRE Trans. on Antennas and Propagation*, **6**, pp. 123–125, 1958.

[132] J. C. Willems. Dissipative dynamical systems part I: General theory. *Arch. Rational Mech. Anal.*, **45**(5), pp. 321–351, 1972.

[133] J. C. Willems. Dissipative dynamical systems part II: Linear systems with quadratic supply rates. *Arch. Rational Mech. Anal.*, **45**(5), pp. 352–393, 1972.

[134] O. Wing. *Classical Circuit Theory*. Springer, New York, 2008.

[135] K.-L. Wong. *Planar Antennas for Wireless Communications*. John Wiley & Sons, New York, NY, 2003.

[136] A. D. Yaghjian, M. Gustafsson, and B. L. G. Jonsson. Minimum Q for lossy and lossless electrically small dipole antennas. *Prog. Electromagn. Res.*, **143**, pp. 641–673, 2013.

[137] A. D. Yaghjian and H. R. Stuart. Lower bounds on the Q of electrically small dipole antennas. *IEEE Trans. Antennas Propag.*, **58**(10), pp. 3114–3121, 2010.

[138] A. D. Yaghjian and S. R. Best. Impedance, bandwidth, and Q of antennas. *IEEE Trans. Antennas Propag.*, **53**(4), pp. 1298–1324, 2005.

[139] F. Zhang. *The Schur complement and its applications*, volume 4. Springer Science & Business Media, 2006.

Part II: Included Papers

Paper I

Optimal Planar Electric Dipole Antenna

Miloslav Capek, Lukas Jelinek, Kurt Schab, Mats Gustafsson,
B.L.G. Jonsson, Fabien Ferrero, and Casimir Ehrenborg

Accepted as: M. Capek, L. Jelinek, K. Schab, M. Gustafsson, B.L.G. Jonsson, F. Ferrero, and C. Ehrenborg, "Optimal Planar Electric Dipole Antenna," *IEEE Antennas and Propagation Magazine*, to be published.

Abstract

Considerable time is often spent optimizing antennas to meet specific design metrics. Rarely, however, are the resulting antenna designs compared to rigorous physical bounds on those metrics. Here we study the performance of optimized planar meander line antennas with respect to such bounds. Results show that these simple structures meet the lower bound on radiation Q-factor (maximizing single resonance fractional bandwidth), but are far from reaching the associated physical bounds on efficiency. The relative performance of other canonical antenna designs is compared in similar ways, and the quantitative results are connected to intuitions from small antenna design, physical bounds, and matching network design.

1 Introduction

Antenna parameters such as gain, Q-factor, and efficiency are limited by the geometry made available for a given design. Given bounds on these parameters under certain constraints, a designer can rapidly assess the feasibility of design requirements. This feasibility assumes the existence of an "optimal antenna" design which approaches the bounds on certain specified parameters. Synthesis of an optimal antenna is not a trivial task, and it remains to be demonstrated how an antenna designed to be optimal in one parameter (*e.g.*, radiation Q-factor) performs relative to bounds on other parameters (*e.g.*, efficiency). The goal of this paper is to discuss the synthesis and analysis of optimal antennas starting from classical antenna topologies.

Many strategies have been employed to optimize antennas. Heuristic optimization methods such as genetic algorithms [30, 50] and particle swarm optimization have the advantage of generating design geometries outside of the antenna designer's usual catalog [13, 42, 49]. Such techniques have been used to design optimal antennas with radiation Q-factors very close to the physical bounds [10], though the resulting designs are computationally expensive to produce and offer only rough insight into guidelines for designing optimal antennas in volumes with arbitrary shapes and electrical size. Conversely, canonical antenna designs were shown [3, 23] to reach the lower bound on radiation Q-factor, but the question remains whether these designs represent optimal solutions over arbitrary electrical sizes and whether they are optimal in other parameters, *e.g.*, radiation efficiency and input impedance. The cost of matching an optimal antenna design to arbitrary impedances is also unclear, regardless if matching is performed on the antenna itself or through external networks.

In this paper we study whether there exists a simple "recipe" for an optimal planar antenna (Throughout this paper, the term planar means to lie in a plane.) with respect to radiation Q-factor and radiation efficiency. In doing so, we ask whether, when prescribed with some form factor and electrical size, a simple design can be readily employed to achieve an antenna whose properties are sufficiently close to their bounds. The strategy adopted here is to optimize

parameterizations of canonical antenna geometries known for good behavior in certain parameters. The examples studied here give quantifiable results to this end, *i.e.*, how to design certain kinds of optimal antennas.

Along the way, we address the crossover of optimality of antennas across different performance parameters, *e.g.*, do minimum radiation Q-factor antennas have inherently high radiation efficiency? Also discussed are the impacts of certain constraints, particularly those related to an antenna's input impedance, on optimized parameters.

We stress out that this work differs significantly from other works on antenna optimization through parametric, heuristic, or metaheuristic means which typically involves the iterative evaluation and modification of designs until a local optimum or design goal is reached. Here, instead, we focus on designing antenna performance with respect to physical bounds, which provide an absolute measure in judging the quality of the synthesized design.

2 Minimum Radiation Q-Factor of Planar TM Antennas

We begin by studying the synthesis of electrically small dipole-like (TM) antennas with minimal radiation Q-factor Q_{rad} (see Box 1 and Box 2). This leads to increased impedance bandwidth, however, the lower bound on radiation Q-factor increases rapidly as an antenna design region becomes smaller (see Box 2). Thus, obtaining low Q-factor Q_{rad} is a key objective and challenge in the design of electrically small antennas.

2.1 Synthesis of Meander Line Antennas

Drawing from the prevalence of meander line antennas in applications requiring electrically small planar antennas [16, 63], as well as previous work studying their optimality in radiation Q-factor [3], we focus on determining whether meander lines present a consistent, simple solution, to obtaining minimum radiation Q-factor at arbitrary frequencies within rectangular design regions. Here, and throughout Section 3, we specify a rectangular design region of fixed aspect ratio ($L/W = 2$). The impact of varying aspect ratios is demonstrated and discussed in Section 2.2.

From the many possible meander line shapes (for example, rectangular, triangular, sinusoidal [16]) we have chosen the simple parametrization from Fig. 1. Thin wire versions of such antennas were previously shown to reach the lower bound on radiation Q-factor Q_{rad} for their corresponding rectangular design regions with electrical sizes near $ka = 0.3$ [3]. Here, we use the parameterization in Fig. 1 to optimize the meander line antenna for resonance by requiring the magnitude of the normalized input reactance $X_{\text{in}}/R_{\text{in}}$ to be smaller than a specified tolerance, $|X_{\text{in}}/R_{\text{in}}| < 10^{-3}$. This procedure is repeated at many frequencies

Box 1. Q-Factor

The Q-factor of an antenna system tuned to resonance (equality of mean magnetic and mean electric energy) is defined as [31]

$$Q = \frac{2\omega W_{\mathrm{sto}}}{P_{\mathrm{rad}} + P_{\mathrm{diss}}}, \tag{1}$$

where W_{sto} represents the cycle mean stored energy, while P_{rad} and P_{diss} denote cycle mean radiated and dissipated powers, respectively. In single-resonance systems, lower Q-factor implies larger fractional impedance bandwidth B by an inverse relationship [9, 14, 67]

$$B \sim Q^{-1}. \tag{2}$$

Evaluated at a single frequency via (1), Q-factor thus becomes a convenient measure of the frequency selectivity of a system [7, 9, 11, 12, 14, 17, 19, 20, 25, 29, 52, 62, 67]. Calculation of a system's Q-factor can be carried out by a variety of approaches, from impedance-based techniques [67] to methods based on the evaluation of stored energy directly [10, 62]. All of these approaches generally agree for electrically small, narrow-band antennas, see [53] for complete discussion and bibliography.

The radiation Q-factor Q_{rad}, in which only radiated power is considered, can be expressed in terms of Q in (1) and radiation efficiency η (see Box 3, (5)) as

$$Q_{\mathrm{rad}} = Q/\eta \sim (B\eta)^{-1}. \tag{3}$$

(electrical sizes, values of ka) to obtain a set of antenna designs, each resonant at a specific frequency. The Q-factors Q_{rad} of the resulting designs were then calculated in AToM [1] and compared to the bounds discussed in Box 2. The comparison is shown in Fig. 2. Note that the value of Q-factor Q_{rad} is just weakly dependent on dissipation factor (see Box 3) provided that dissipation is not exceedingly high.

In order to verify the computed data in Fig. 2, an antenna design sample with $ka = 0.42$ was scaled to 1.4 GHz and fabricated on a 25 μm-thick Polyimide film with 17 μm-thick copper foil bonded by an 25 μm-thick acrylic adhesive ($\varepsilon_{\mathrm{r}} = 4$) . Thanks to the very thin profile of the substrate as compared to wavelength, the effect of dielectric can be neglected for a radiation Q-factor evaluation. The input impedance of the prototype was measured using a differential technique [48] and has been used to estimate the Q-factor via the Q_{Z} formula [67]. Radiation efficiency of the antenna was measured via a multiport near-field method [51] and was used to evaluate radiation Q-factor, and its confidence interval of width equal to two times the standard deviation, see triangular marker and corresponding error bar in Fig. 2.

Figure 2 illustrates that a simple parametrization, such as the one from Fig. 1, is able to closely approach the radiation Q-factor bound limited to TM radiation $Q_{\mathrm{rad}}^{\mathrm{lb,TM}}$ (see Box 2) in the entire frequency range of electrically small an-

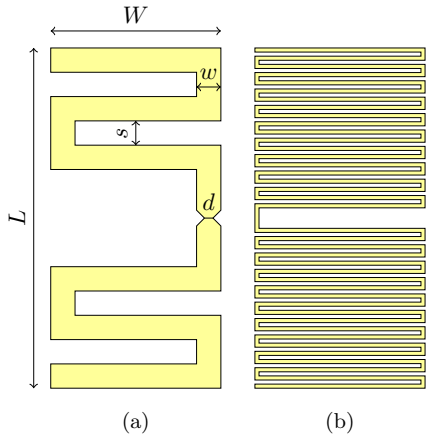

Figure 1: Panel (a) shows a parameterization of a meander line antenna used in this work. The antenna is fed via delta gap source along a horizontal line cutting the center of the meander line. The feeding region contains a taper between the feeding strip of width d and the meander line of width w. The angle of the taper's cut is 45°. Throughout the paper $d = \min(w, L/40)$ in order to keep the feeding region realistically narrow. Panel (b) shows a meander line antenna design "M1" from [3] within the parametrization used in this paper.

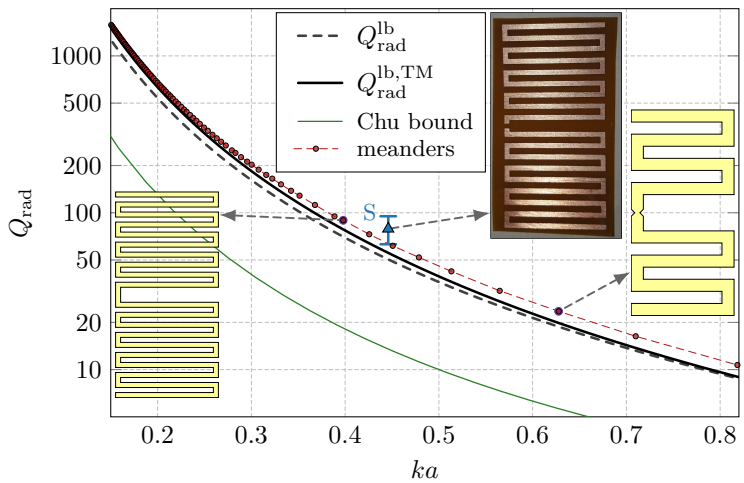

Figure 2: Radiation Q-factors of self-resonant meander line antennas simulated as made of PEC (markers) and the lower bound on radiation Q-factor (see Box 1) corresponding to a rectangular region bounding the meander line. All meander lines are designed using the parameterization in Fig. 1 with $w/s = 1$ and $L/W = 2$. The defining parameters of all meandered dipoles are depicted in Fig. 3. A triangular marker with a corresponding error bar represents measured radiation Q-factor of selected meander line design.

Box 2. Lower Bounds on Radiation Q-Factor

The approximate inverse proportionality between the Q-factor and the fractional bandwidth (see Box 1) induced considerable effort in lowering the Q-factor for spherical [9, 12, 38, 40, 58, 63] and arbitrarily shaped antennas [8, 22, 26, 56, 59, 64, 66]. The sole focus on the radiation Q-factor Q_{rad} in these works avoids the undesired possibility of reducing Q-factor Q by degrading radiation efficiency.

For electrically small antennas, the lower bound on the Q_{rad}, here denoted as $Q_{\mathrm{rad}}^{\mathrm{lb}}$, is a combination of electric and magnetic dipoles [5, 8, 9, 34, 40]. In general, it is challenging to excite such a current with a single feeding position see [32, Sec. IV] for related discussion. A constrained minimization which is more representative for single port antennas is to restrict the radiation to TM (electric dipole) modes, yielding the lower bound $Q_{\mathrm{rad}}^{\mathrm{lb,TM}}$, see, *e.g.*, [24].
The importance of Q-factor bounds arises from two key properties. First, the Q-factor bound represents the physical lower bound among all possible currents contained within the considered region. It thus presents an absolute measure against which to compare the performance of different antenna designs. Practical feasibility of designing antennas which reach various bounds remains an open question. Second, both $Q_{\mathrm{rad}}^{\mathrm{lb}}$ and $Q_{\mathrm{rad}}^{\mathrm{lb,TM}}$ scale approximately as $(ka)^{-3}$ for electrically small antennas ($ka < 1$), *cf.*, [35]. Here k is the free-space wavenumber and a is the radius of the smallest circumscribing sphere. This $(ka)^{-3}$ scaling is the root cause of the limited bandwidth in electrically small antennas. The associated geometry coefficients for certain shapes are shown in Table 1, where η_0 denotes free-space impedance and R_{s} denotes surface resistance.

tennas. From this, it is possible to conclude that a complex design (*e.g.*, the parameterizations found in [44]) is not needed to reach the lower bound.

The absolute lower bound for radiation Q-factor $Q_{\mathrm{rad}}^{\mathrm{lb}}$ is unreachable by this meander line antenna since its planar geometry and single feed scenario does not allow for an efficient excitation of combined TE and TM radiation. This contrasts to three-dimensional (*e.g.*, spherical) geometries [5, 58], where the dual mode behavior can be realized by a single feed network.

Parameters of the self-resonant designs from Fig. 2 are shown in Fig. 3. Design curves are fitted to the optimized parameters using a polynomial fit with good agreement. While some of the curves from Fig. 3 can be found in [16] for several parametrization, here all the designing curves are related back to Fig. 2 in which the Q-factor Q_{rad} is minimized. The presented data series can therefore be used for designing meandered dipoles approaching lower bounds on radiation Q-factor for TM antennas. It should, however, be noted that design curves from Fig. 3 depends on the used parametrization and are valid only for $L/W = 2$ and $w/s \approx 1$.

Table 1: Lower bounds on radiation Q-factors and efficiency in the limit of electrical size $ka \to 0$ for a sphere, a cylindrical tube, a rectangle, a thin strip dipole and a square loop.

	$(ka)^3 Q_{\mathrm{rad}}^{\mathrm{lb}}$	$(ka)^3 Q_{\mathrm{rad}}^{\mathrm{lb,TM}}$	$(ka)^4 \eta_0 / R_{\mathrm{s}} \delta$
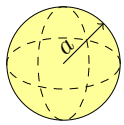	1	$\frac{3}{2}$	3
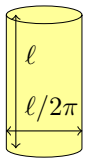	4.5	4.6	59
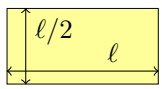	4.3	5.2	42
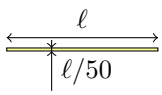	16	16	3400
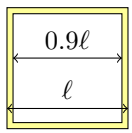	5.3	7.4	130

2.2 Varying Aspect Ratios

Meander line antennas, introduced in the previous section, are now studied for various L/W and w/s aspect ratios and compared against the fundamental bounds calculated for each form factor.

In all cases, the value of radiation Q-factor Q_{rad} is normalized with respect to the minimal TM radiation Q-factor. Generally, Fig. 4 shows that the minimal values can closely be approached for various L/W aspect ratios. Slightly better performance is observed for higher L/W ratios, however, at the cost of higher absolute bound on radiation Q-factor see top panel of Fig. 4.

With respect to the varying w/s ratio, slightly better performance is observed for higher values, *i.e.*, wider metallic strips. The differences become negligible for small values of ka, see Fig. 5. Notice, however, that this behavior is substantially changed when ohmic losses are introduced, mainly since the spatial proximity of out-of-phased currents degrades the radiation and enhance the ohmic losses [4].

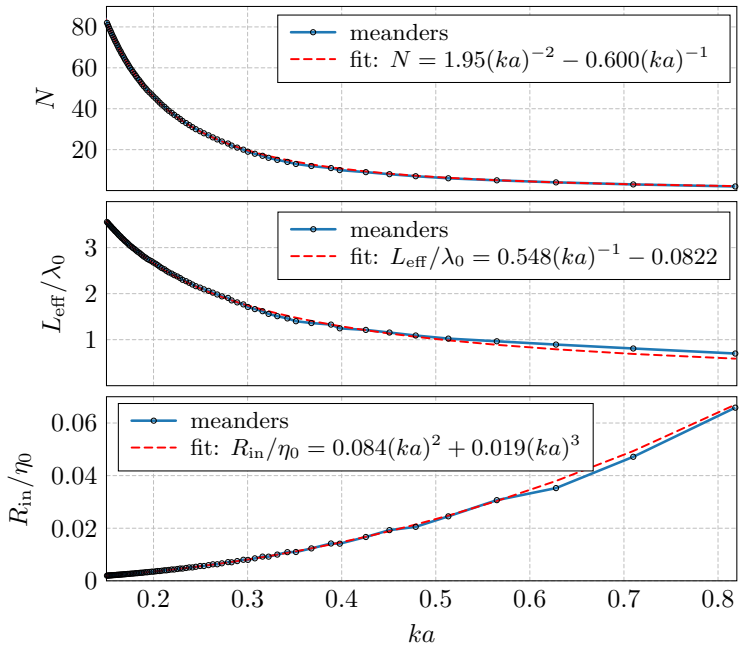

Figure 3: Design curves for the meander line antennas from Fig. 1. The panels show consecutively total number of meanders N, total length of the strip L_{eff} normalized to free-space wavelength, and input resistance R_{in} normalized to free-space impedance. In all cases $w/s = 1$, $L/W = 2$ and PEC are considered. One meander line ($N = 1$) consists of two horizontal strips and vertical connections, *i.e.*, meander line antennas in Fig. 1 have 3 and 20 meanders, respectively.

2.3 The Impact of Impedance Matching on Q-Factor Q_{rad}

The designs obtained above are all self resonant ($X_{\text{in}} \approx 0$), but no constraint was placed on the value of the input resistance R_{in}. In most practical cases, the objective antenna input resistance is not driven by any antenna consideration but is set by the radio frequency electronic equipment to be interfaced with a particular antenna. Transmission lines and active receivers based on Low Noise Amplifiers (LNA) often require matching to 50 Ω. However, where devices with complex impedances are used, antenna resonance may not be ideal for conjugate matching and maximum power transfer. For example, a typical Power Amplifier (PA) output impedance is complex [65], with an input resistance lower than 50 Ω and an inductive (positive) reactive component. Similarly, passive RFID receivers based on Schottky diode rectifiers typically exhibit input resistances lower than 50 Ω and strong capacitive (negative) reactance [39]. Examples of nominal impedances Z_0 for these systems are listed in Table 2.

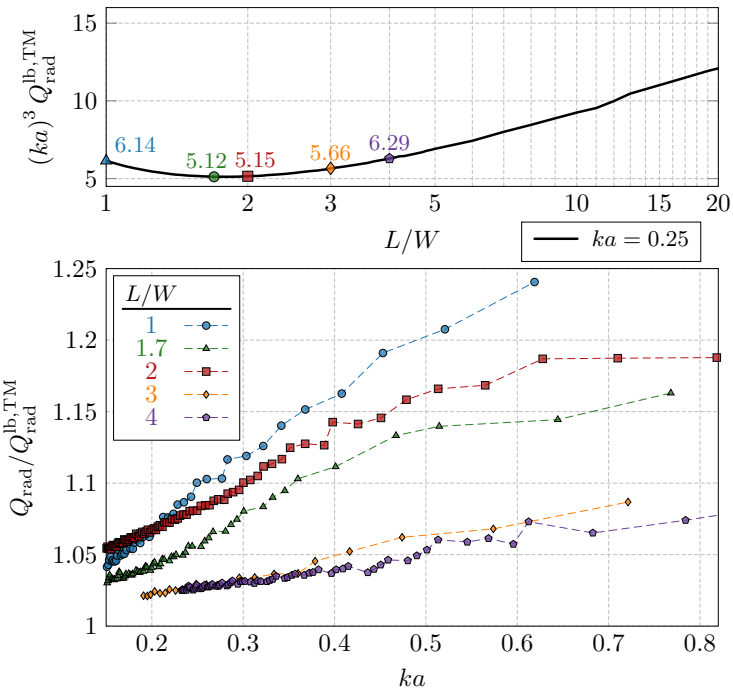

Figure 4: Radiation Q-factor performance of PEC self-resonant meandered dipoles from Fig. 2 for various L/W aspect ratios. The radiation Q-factor is normalized to fundamental bound for a rectangular region which is shown in the top panel as a function of the aspect ratio. The minimum of the fundamental bound is found around ratio $L/W \approx 5/3$. Generally, the higher the L/W ratio, the closer the meander lines are to the bound, however, at the cost of increasing absolute value of radiation Q-factor.

Table 2: Three impedances of practical significance for antenna system design.

System	Input impedance Z_0
Power amplifier (PA)	$15 + \mathrm{j}50\,\Omega$
RFID chip (passive RX)	$20 - \mathrm{j}200\,\Omega$
Low-noise amplifier (LNA)	$50\,\Omega$

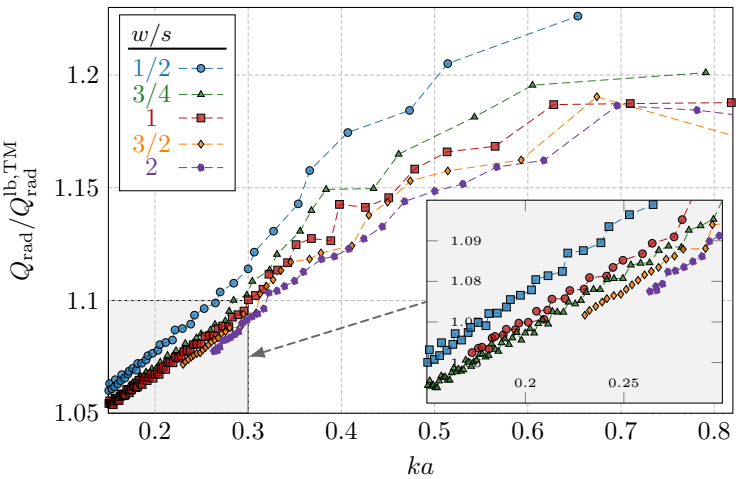

Figure 5: The same study as in Fig. 4 done for various ratios of meander line width w to spacing s.

Antennas may be designed to have input impedances which conjugate match a desired load. However, any of the designs shown in Fig. 2 can be conjugate matched to an arbitrary complex impedance Z_0 through an L-network consisting of two reactive components [47]. In many instances, the stored energies within these reactances will raise the radiation Q-factor of the system. To assess the cost of this form of simple matching, we select the design in Fig. 2 corresponding to self resonance at $ka = 0.479$. A set of lossless networks was generated to conjugate match the antenna to arbitrary complex impedances and the matched radiation Q-factors were calculated. A typical frequency dependence of this cost is depicted in Fig. 6 while the dependence on matching impedance is depicted in Fig. 7. We observe that it is generally possible to transform the resonant antenna impedance to an arbitrary real value with minimal increase in radiation Q-factor, except when small resistance and high reactance is required. As expected, adding a reactive component to the real-valued (resonant) antenna impedance necessarily increases radiation Q-factor, though this increase is on the order of 30% for the most extreme of the three test impedances (RFID) examined here. Additionally, Fig. 6 shows that it is often possible to move slightly away from the self-resonant frequency and lower the overall radiation Q-factor by a small amount. Nonetheless, the minimum radiation Q-factor of the matched antenna is, for practical values of the matching impedance, within the vicinity of the self-resonance of the antenna.

The importance of Q-factor is its relation to fractional bandwidth which is predicated on simple, single resonance behavior [67]. We demonstrate that the low variance in Q-factor corresponds to consistent realized bandwidth when L-networks are used to conjugate match an antenna to an arbitrary impedance. Figure 8 shows the power delivered P_{del} to the meander line antenna studied

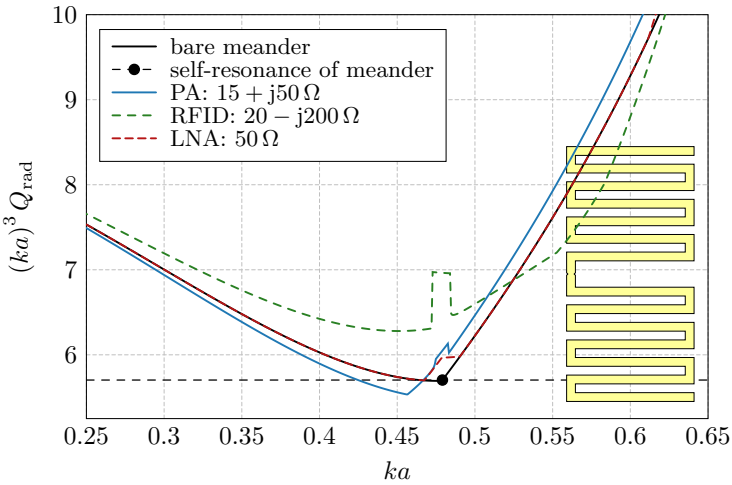

Figure 6: Matched radiation Q-factor of a selected meander line antenna for several impedance matching scenarios listed in Table 2. Matching to each impedance is accomplished via a two-element reactive L-network, see inset in Fig. 7 for a schematic. In cases when several L-networks exist for a given matching impedance, the network with the lowest stored energy has been used. Abrupt jumps of the matched radiation Q-factor curves result from non-existence of matching by two inductances in certain frequency ranges. This double inductance matching is the most favorable scenario for a capacitive antenna.

above using a matched source ($Z_0 = R_{\mathrm{in}}$) as well as with L-networks designed to match the antenna to the three complex impedances of practical interest in Table 2. In each case, a network tunes the antenna to the desired (possibly complex) impedance at its natural resonant frequency. The frequency profile of the mismatch factor [6, 47]

$$\tau = \frac{P_{\mathrm{del}}}{P_{\mathrm{cm}}} = \frac{4R_{\mathrm{in}}^{\mathrm{m}} R_0}{|Z_{\mathrm{in}}^{\mathrm{m}} + Z_0|^2} \tag{4}$$

is nearly identical in all four cases, in agreement with the predictions based on the relatively invariant Q-factor across these cases. Here, $Z_{\mathrm{in}}^{\mathrm{m}}$ is the antenna impedance including the tuning network, P_{del} is the power delivered to the antenna, and P_{cm} is the power delivered under a conjugate match condition. It is necessary to point out that we have assumed non-dispersive matching impedances, *i.e.*, $\partial Z_0/\partial\omega = 0$. In practice, the matching impedance may be dispersive within the band of interest, in which case the relation between Q-factor and bandwidth described in [67] ceases to be valid. However, inclusion of a dispersive load impedance may not necessarily cause major changes to the realized bandwidth due to the already heavily frequency-dependent nature of the impedance of high Q-factor antennas. Despite this simplification, when generating Fig. 8, lumped inductors and capacitors in each tuning network are modeled

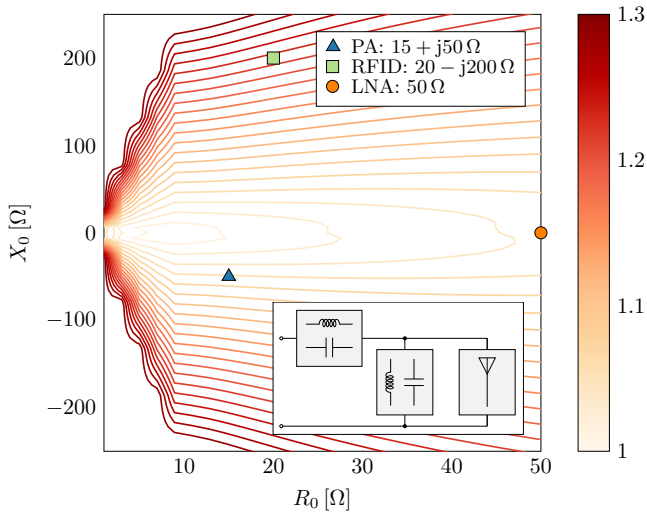

Figure 7: Matched radiation Q-factor of a selected meander line antenna for varying complex matching impedance normalized to radiation Q-factor of bare antenna. For each complex impedance, the meander line is conjugate matched at its self-resonance (circle mark in Fig. 6, $ka \approx 0.479$) using the lossless L-network matching circuit with lowest Q-factor. The markers denote the three impedances from Fig. 6 and Table 2.

as frequency dependent impedances.

The results in Figs. 7 and 8 numerically suggest that there is little cost in bandwidth to match a self-resonant antenna to arbitrary impedances. However, further considerations reveal why it is of practical importance to design an antenna with a given impedance, rather than relying on this form of matching. First, the use of lumped components increases complexity and cost of an antenna system and the required component values for the L-networks described in this section may not be realizable. Second, lumped components made of any practical, lossy material (*e.g.*, metallic inductors) increase the net loss in an antenna system while not adding any potential radiation mechanism. This guarantees a decrease in overall efficiency, particularly in high Q-factor antennas [57]. Additionally, tunability or the use of broadband multiple resonance matching may benefit from the design of an antenna with specific impedance characteristics, *e.g.*, to increase the radiation resistance [2, 3].

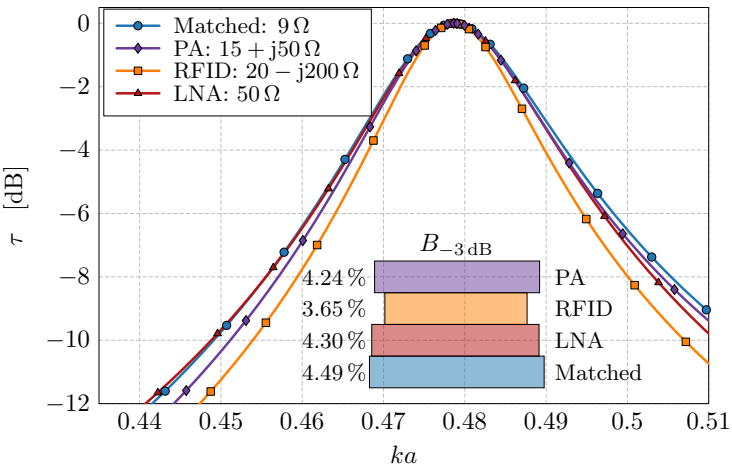

Figure 8: Frequency dependence of normalized power delivered $P_{\mathrm{del}}/P_{\mathrm{cm}}$ to the meander line studied in Figs. 6 and 7. The separate curves correspond to devices exhibiting the three practically relevant impedances from Table 2 and to a device with impedance corresponding to that of the meander line at its self-resonance ("Matched"). In each case, the antenna is conjugate matched using an L-network at its self resonant frequency, $ka \approx 0.479$. The -3 dB bandwidths 50% power delivered bandwidths $B_{-3\ \mathrm{dB}}$ for each scenario are also listed.

3 Radiation Efficiency of Q-Optimal Antennas

The previous section demonstrated that meander line antennas are nearly optimal with respect to radiation Q-factor, including the cases when matching to realistic complex impedances is desired. This section studies how these antennas perform with respect to another critical antenna metric: radiation efficiency (see Box 3). Specifically, we examine their performance with respect to radiation efficiency bounds (see Box 4).

Before presenting the radiation efficiency of matched meander line antennas it is necessary to deal with losses in the matching circuit since, similarly to the case of Q-factor, any matching circuit with finite losses will worsen the overall efficiency of the antenna system. Throughout this section we will assume that all matching networks are composed of lossless capacitors and lossy inductors[1]. The inductors are further assumed to be planar, made of the same material (metallic sheet, surface resistivity R_{s}) as the antenna itself. Under such restrictions it is possible to estimate the loss added by a matching network quite precisely using data from Fig. 9, which shows the normalized reactance, $\left(10^3/ka_L\right)\left(R_{\mathrm{s}}/\eta_0\right)\left(X_{\mathrm{L}}/R_{\mathrm{L}}\right)$, of several spiral inductors as a function of

[1] Q-factors of lossy capacitors are typically much higher than those of lossy inductors.

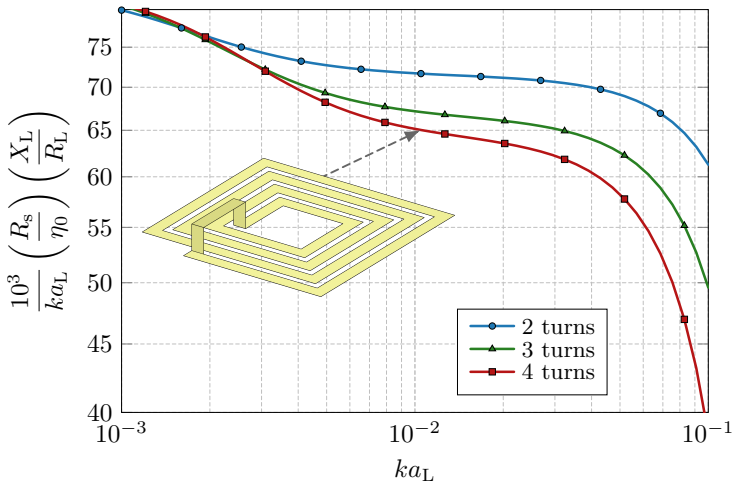

Figure 9: Normalized reactances of selected rectangular spiral inductors. The quantities X_{L}, R_{L}, and R_{s} denote input reactance, input resistance, and surface resistance, respectively. The radius a_{L} defines the smallest sphere circumscribing the inductor.

their electrical size. Here η_0 denotes the free space impedance. The normalized reactance in Fig. 9 is independent on surface resistance R_s and, at small electrical size, just weakly dependent on number of turns and frequency, consistent with classical relations for helical air-core inductors [41]. A conservative value $\left(10^3/ka_{\mathrm{L}}\right)\left(R_{\mathrm{s}}/\eta_0\right)\left(X_{\mathrm{L}}/R_{\mathrm{L}}\right) = 66$ will be used in this section to determine losses of all inductors within the L-matching network, assuming further that inductors are always ten times smaller in electrical size than the antenna, *i.e.*, $a_L = a/10$. This last assumption enforces the use of an electrically small, approximately lumped element, matching network.

Lossy elements with the above mentioned specifications are used to match the meander studied in Figs. 6–8 to impedance $Z_0 = 50\,\Omega$ over a band of interest near the meander line's self-resonant frequency. The resulting radiation Q-factor and efficiency (here presented in the form of dissipation factor, δ) are depicted in Fig. 10 as functions of frequency (scaled as electrical size ka). The figure reiterates the previously-observed near-optimal performance of meander line antennas with respect to radiation Q-factor, but, surprisingly, shows a rather poor performance with respect to radiation efficiency. This metric is, at the self-resonance frequency of the antenna, almost one order of magnitude worse than the value of the physical bound (see Box 4). Similarly to radiation Q-factor, dissipation factor reaches its minimum in the vicinity of the resonance frequency, at least in the case of realistic values of matching impedances used here.

Within the used normalization of dissipation factor and radiation Q-factor, it is reasonable to represent the data from Fig. 10 as a two dimensional curve (radiation Q-factor vs. dissipation factor) parametrized by frequency, see Fig. 11. The

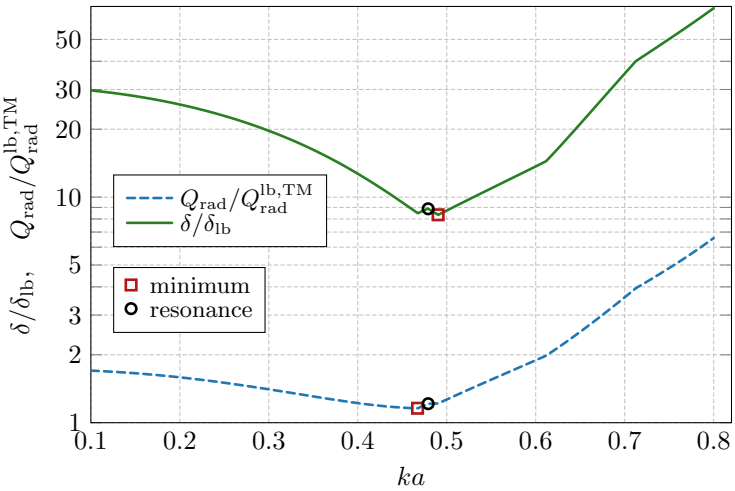

Figure 10: Normalized radiation Q-factor and normalized dissipation factor of a selected meander line antenna matched to 50 Ω over a range of frequencies (scaled here as electrical size ka). The self-resonance of the antenna ($ka = 0.47$) is denoted on each trace with a circular marker while the minimum of each trace is also marked. The same data are also plotted as a curve parameterized by frequency in Fig. 11.

figure also shows the Pareto front (represented by the black line) evaluated by the method from [18], which demonstrates the optimal trade-off between radiation Q-factor and dissipation factor for the given design geometry and frequency. The Pareto front has been evaluated at $ka = 0.5$, but, due to the used normalization, it is almost independent of electrical size. The Pareto front was evaluated for a combination of TM and TE modes which, as normalized to the TM bound $Q_{\mathrm{rad}}^{\mathrm{lb,TM}}$, gives values lower than one. The reason for this particular normalization is that TM bounds represent meaningful limit of one-port planar antennas.

The two-dimensional plot in Fig. 11 represents a complete comparison of various antenna designs with respect to matched efficiency and matched radiation Q-factor. An example of such comparison is shown in Fig. 12, where the normalized and frequency-parameterized Q–δ curves are drawn for several small antenna designs within the same design specifications[2]. Figure 12 clearly presents the superior performance in efficiency and Q-factor of simple meander line antennas shown in Fig. 1 with respect to other designs. It also shows that although there exist other meander lines which perform slightly better in radiation efficiency (Palmier pastry type, [43]) this improvement costs much in the radiation Q-factor. In conclusion, simple meander line antennas present the best trade-off between radiation Q-factor and dissipation factor from the depicted antennas

[2]The bounding geometry, material parameters, and restrictions on matching network topology and losses are all kept constant across each design.

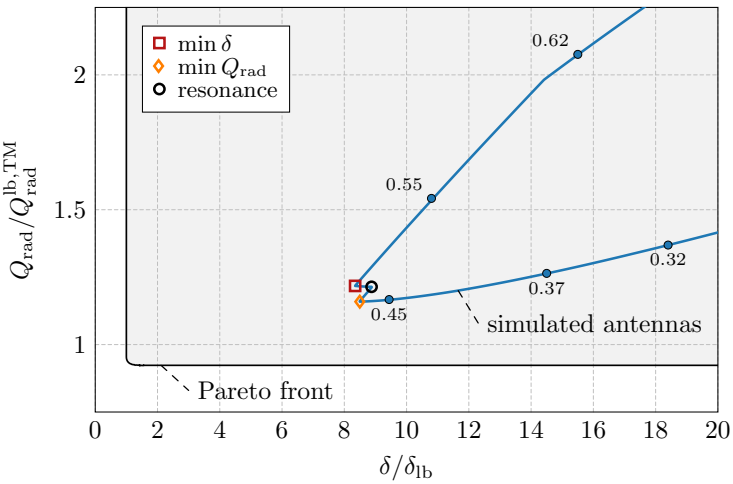

Figure 11: A two-dimensional view of the lower bounds on dissipation factor and radiation Q-factor. A black solid curve denotes the Pareto front describing the trade-off between these quantities and the corresponding feasible region (shaded). The data from Fig. 10 are drawn as a curve parameterized by frequency, with the relevant points in Fig. 10 being similarly marked. The circle markers along the curve representing the simulated antenna show the electrical size ka.

when matching to real impedances is demanded. As in the previous section, we note that the use of more advanced matching topology (*e.g.*, folding or impedance transformer) may benefit from alternative antenna designs.

Figures 11 and 12 show that the considered antenna structures, which are close to optimal in radiation Q-factor, are far away from the efficiency bounds. This is puzzling since resonant modes optimal in radiation Q-factor and efficiency are similar in nature. However, there are important differences. Radiation Q-factor restricted to TM modes is minimized by separation of charges and inducing dipole like currents [24]. These modes can be tuned to resonance by inducing edge loops along the structure. TM efficiency, on the other hand, is minimized by inducing homogeneous currents [54]. These are similar in nature to the dipole like currents minimizing Q-factor, but the loop currents which minimize TE Q-factor and maximize TE efficiency are fundamentally different. Where low Q-factor loops tend to be confined towards the edges of the structure, high efficiency loops are spread across the whole area [18, Fig. 4]. Such loop currents are naturally restricted as an original simply connected object fully filling a prescribed bounding box is perforated, forcing the current distribution into more inhomogeneous forms. Thus, low Q-factor loops are tolerant of alterations to a structure whereas high efficiency loops are harshly disrupted.

In Fig. 13, the optimal resonant Q-factor and dissipation factor are plotted normalized to the corresponding bounds of a rectangular plate. Data for different shapes made by removing portions of the plate are shown. The currents on

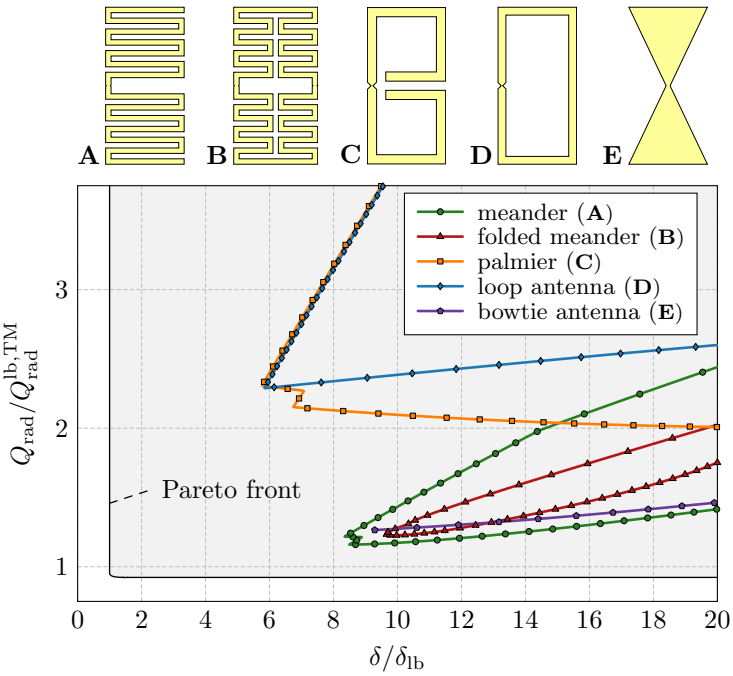

Figure 12: Two dimensional frequency parametrized plot representing the physical bound and several antennas. The matching impedance equals to $50\,\Omega$. The tip of each curve lies in the vicinity of resonance or anti-resonance of the antenna. The electrical sizes at the resonance or anti-resonance frequency are: A ($ka = 0.48$, res.), B ($ka = 0.85$, res.), C ($ka = 0.50$, res.), D ($ka = 0.59$, anti-res.), E (no resonance).

the structures in Fig. 13 have been calculated with current optimization without physical feeding. It is clear that removing metal does not greatly affect the achievable radiation Q-factor, at worst reducing it to the TM-only bound. However, when metal is removed from the plate the loss factor is significantly increased, especially for small electrical sizes. Thus, while optimal radiation Q-factor and radiation efficiency modes are fairly similar, removing design space has a much greater effect on the loss factor than the Q-factor in relation to the physical bounds. This can be seen in Fig. 13 where the loss factor of the optimal resonant currents is very high for the structures with slots in them. Consider the meander line antenna which has significantly higher loss factor at electrical sizes $ka < 0.4$, here the loop modes are extremely disrupted, however, the Q-factor is hardly affected. The sharp change in the meander line's loss at around $ka = 0.6$ is due to its resonance, where it is possible to induce a resonant dipole mode on the structure. This example illustrates a fundamental challenge in designing efficient small resonant antennas: many of the strategies normally utilized to induce resonance, such as meandering, harshly limit the achievable efficiency.

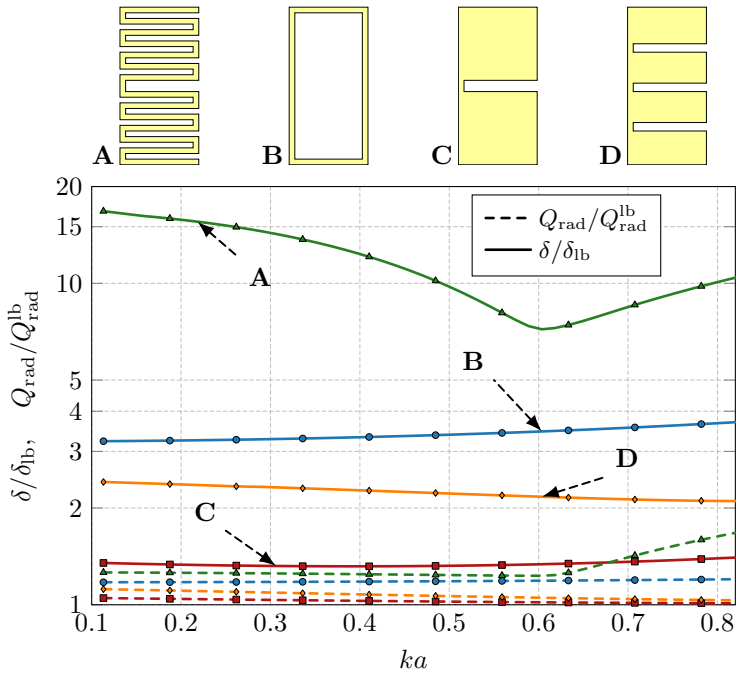

Figure 13: Illustration of how much different metrics deteriorate when a solid plate is permuted. The figure shows four generic shapes, a single slot, three slots, a meander line, and a loop. The ratio between optimal loss factor for different geometries and the optimal loss factor for the full plate are shown in solid lines. The ratio between the optimal mixed mode Q-factor for the same geometries and the optimal mixed mode Q-factor of the full plate are shown in dashed lines.

4 Antennas Optimal in Other Parameters

Determining the best possible Q-factor can be formulated as a minimization problem. Therefore it is possible to add different or additional constraints to such an optimization. So far, in this paper, we have considered the constraints of efficiency and impedance matching. Another type of constraints are different kinds of field-shaping requirements of near and/or far-fields [21, 36]. For small antennas it is well known that the radiated far-field tends to resemble a dipole pattern, meander line antenna treated in this paper being no exception, see Fig. 14. However, with these types of Q-factor optimization procedures it is possible to determine the Q-factor cost, to have the antenna radiating with a certain front-to-back ratio or (super-) directivity in a given direction. These classes of bounds indicate that for a limited bandwidth cost it is possible to

Box 3. Radiation Efficiency

The radiation efficiency of an antenna is defined as

$$\eta = \frac{P_{\mathrm{rad}}}{P_{\mathrm{rad}} + P_{\mathrm{diss}}} = \frac{1}{1+\delta}, \tag{5}$$

where, as in (1), P_{rad} and P_{diss} are radiated and ohmic dissipated power, respectively, and $\delta = P_{\mathrm{diss}}/P_{\mathrm{rad}}$ is the dissipation factor [27]. Along with bandwidth radiation efficiency is a key antenna performance parameter, particularly in electrically small systems where it is known to decrease rapidly with antenna size.

For objects with homogeneous loss properties, *e.g.*, uniform surface resistance or conductivity, the dissipation factor δ is a linear function of those properties. As such, values of dissipation factor can be normalized by surface resistivity for ease of comparison.

extend, *e.g.*, the directivity beyond the traditional dipole pattern, see [15,21,36, 37,46,55,68,69].

To illustrate bounds on superdirectivity, Q-factor optimization for a given directivity described in [21,36], was solved for a small antenna with length to width ratio of 2:1, infinitesimal thickness, and electrical sizes $ka \in \{0.2, 0.5, 0.8\}$. The bounds for low directivities are identical to the lower bound on the Q-factor, where the radiation pattern changes from that of an elliptically polarized dipole with $D \approx 1.5$ to that of a Huygens source with directivity just below $D = 3$ and the main beam pointing in the direction of the longest side [7]. Higher directivities require quadrupole and higher order modes which increases the Q-factor rapidly [9]. The direction of the main beam changes from the longest side of the antenna to an endfire pattern along the shortest side at $Q_{\mathrm{rad}}/Q_{\mathrm{rad}}^{\mathrm{lb,TM}} \approx 3$ as indicated by circles in Fig. 15.

Much like bounds on other parameters (*e.g.*, efficiency), it is an open problem if the directivity-constrained limits are reachable for all sizes and desired directivity, even under idealized lossless conditions. As a demonstration of one possible high directivity, low Q-factor design, a three port array composed of a meander line and a loop structure with optimized feeding is presented in relation to the bounds, see Fig. 15. However, high directivity for single port antennas remains, as of yet, far from the bound and new designs ideas that allow a high directivity with larger bandwidth are desired.

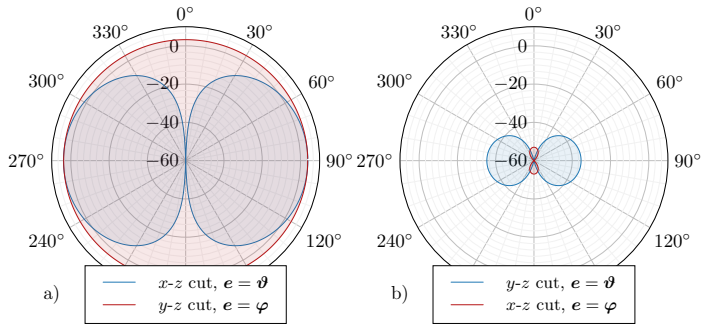

Figure 14: Directivity (in dB scale) with respect to an isotropic radiator of a meander line antenna depicted in Fig. 2 as the very right inset. Antenna is placed in x-z plane, with a longer side aligned with z-direction.

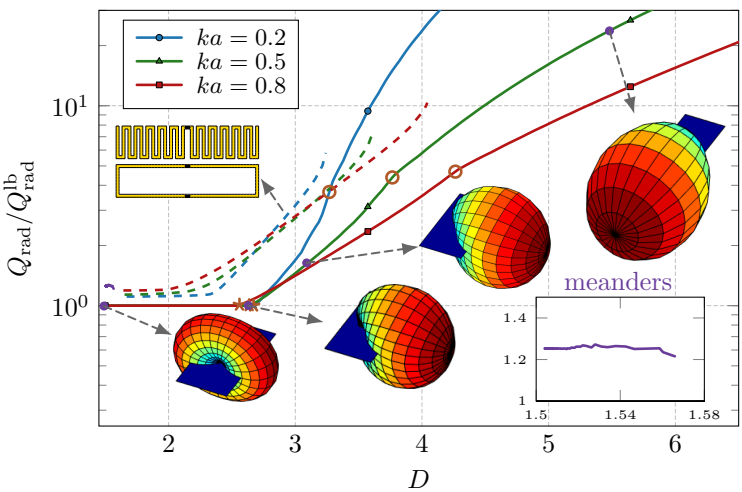

Figure 15: The cost in Q-factor for a desired directivity in a lossless 2:1 shaped antenna. The three line colors represent electrical sizes $ka = \{0.2, 0.5, 0.8\}$ and the radiation patterns correspond to the $ka = 0.5$ case for the optimal current. All Q- vs D-values for the meander lines of Fig. 2 are represented in purple, and the relevant region is zoomed in the right bottom inset. Dashed curves show the results for an array composed of a meander line antenna element with one feed and a loop antenna element with two feeds.

Box 4. Lower Bounds to Dissipation Factor

Two different paradigms for minimization of dissipation factor exist. The first assumes that tuning or general impedance matching of the antenna can be performed in a lossless manner. Under this assumption, the optimal current density minimizing dissipation factor is the result of a generalized eigenvalue problem [27, 28, 54, 61]. Such lower bounds were shown to scale with electrical size as $(ka)^{-2}$ and are straightforward to calculate. Their major drawback, however, is that, by neglecting matching network losses, the resulting dissipation factors are overly optimistic and unachievable by realistic designs where some form of matching is required [57].

One solution to the aforementioned drawback is a paradigm in which the optimal currents are calculated while taking into account the dissipation cost of achieving resonance or general matching [33, 57]. Dissipation factors coming from this second paradigm are generally closer to realistic designs and scale with electrical size as $(ka)^{-4}$ [18,33,45,60]. Lower bounds to tuned dissipation factor for several selected shapes are shown in Table 1.

5 Conclusion

The possibilities how to approach the fundamental bounds on selected antenna metrics were investigated. A planar region of rectangular form factor was considered. It was observed that the lower bound on Q-factor with radiation restricted to TM modes only is closely approached by a meander line antenna for a broad range of electrical sizes. The optimal design parameters were depicted and various aspect ratios of the bounding rectangle were studied together with selected ratios of the strip and slot widths. The simulated results were verified by a measurement of a fabricated prototype. The impedance matching and its impact on the Q-factor of the antenna was studied, concluding that the effect of the impedance matching on radiation Q-factor is minor and, in some cases, that matching the antenna slightly away from its self-resonance can even decrease its Q-factor. Radiation efficiency of the meander line antennas optimal in Q-factor was evaluated, taking into account ohmic losses dissipated in the matching circuit. It was observed that the radiation efficiency of the studied meander line antennas is far from an upper bound of a rectangular patch. Several other planar antennas were similarly evaluated against fundamental bounds yielding consistent conclusions: synthesizing antenna designs which approach the upper bound on radiation efficiency is more difficult than designing those which reach the lower bound on Q-factor. The reason was identified in the high sensitivity of radiation efficiency to the perturbation of ideal constant current density. Namely, when an initial structure fully filling the prescribed bounding box is perforated (as is done in a practical synthesis procedure), the performance of maximum efficiency current distributions drops much faster than that of a minimum Q-factor distribution.

Finally, a Pareto-type bound between Q-factor and directivity has been calculated and compared to meander line antennas. An attempt has been made to find an antenna with reasonably low Q-factor and directivity higher than that of an electric dipole type antenna. Nevertheless, no planar antenna with one feed fulfilling these contradictory constraints was found. This task and its feasibility remains as a subject for ongoing research.

The fundamental bounds, *i.e.*, the lower bounds on Q-factor, the upper bounds on radiation efficiency, the Pareto-optimality between Q-factor and efficiency, or Q-factor and directivity, were demonstrated to be powerful tools for judging the performance of the radiating devices. If the realistic designs are compared to the fundamental bounds, designer can assess how far from the optima the design is, therefore, if further improvement is needed. Furthermore, incremental progress in design improvement can be put into context by considering the remaining distance between an antenna's realized performance and the fundamental bounds. It is the normalized ratio of the actual device's performance to the fundamental bounds what reveals the real quality of the design.

References

[1] Antenna Toolbox for MATLAB (AToM), 2017.

[2] S. Best. Small and fractal antennas. In C. A. Balanis, editor, *Modern Antenna Handbook*, pp. 475–530. Wiley-Interscience, 2008.

[3] S. R. Best. Electrically small resonant planar antennas: Optimizing the quality factor and bandwidth. *IEEE Antennas Propag. Mag.*, **57**(3), pp. 38–47, Jun. 2015.

[4] S. R. Best and J. D. Morrow. On the significance of current vector alignment in establishing the resonant frequency of small space-filling wire antennas. *IEEE Antennas Wireless Propag. Lett.*, **2**, pp. 201–204, 2003.

[5] S. R. Best. Low Q electrically small linear and elliptical polarized spherical dipole antennas. *IEEE Trans. Antennas Propag.*, **53**(3), pp. 1047–1053, 2005.

[6] S. R. Best. Optimizing the receiving properties of electrically small HF antennas. *URSI Radio Science Bulletin*, **89**(4), pp. 13–29, 2016.

[7] M. Capek, M. Gustafsson, and K. Schab. Minimization of antenna quality factor. *IEEE Trans. Antennas Propag.*, **65**(8), pp. 4115–4123, 2017.

[8] M. Capek and L. Jelinek. Optimal composition of modal currents for minimal quality factor Q. *IEEE Trans. Antennas Propag.*, **64**(12), pp. 5230–5242, 2016.

[9] L. J. Chu. Physical limitations of omni-directional antennas. *J. Appl. Phys.*, **19**, pp. 1163–1175, 1948.

[10] M. Cismasu and M. Gustafsson. Antenna bandwidth optimization with single frequency simulation. *IEEE Trans. Antennas Propag.*, **62**(3), pp. 1304–1311, 2014.

[11] R. E. Collin. Minimum Q of small antennas. *J. Electromagnet. Waves Appl.*, **12**, pp. 1369–1393, 1998.

[12] R. E. Collin and S. Rothschild. Evaluation of antenna Q. *IEEE Trans. Antennas Propag.*, **12**, pp. 23–27, Jan. 1964.

[13] K. Deb. *Multi-Objective Optimization using Evolutionary Algorithms*. Wiley, 2001.

[14] R. L. Fante. Quality factor of general ideal antennas. *IEEE Trans. Antennas Propag.*, **17**(2), pp. 151–155, Mar. 1969.

[15] F. Ferrero, L. Lizzi, B. L. G. Jonsson, and L. Wang. A two-element parasitic antenna that approach the minimum Q-factor at a given directivity. *ArXiv e-prints, 1705.02281*, pp. 1–11, 2017.

[16] K. Fujimoto and H. Morishita. *Modern Small Antennas*. Cambridge University Press, 2013.

[17] W. Geyi. *Foundations of Applied Electrodynamics*. John Wiley & Sons, 2011.

[18] M. Gustafsson, M. Capek, and K. Schab. Trade-off between antenna efficiency and Q-factor. *IEEE Trans. Antennas Propag.*, **67**(4), pp. 2482–2493, Apr. 2019.

[19] M. Gustafsson and B. L. G. Jonsson. Antenna Q and stored energy expressed in the fields, currents, and input impedance. *IEEE Trans. Antennas Propag.*, **63**(1), pp. 240–249, 2015.

[20] M. Gustafsson and B. L. G. Jonsson. Stored electromagnetic energy and antenna Q. *Prog. Electromagn. Res. (PIER)*, **150**, pp. 13–27, 2015.

[21] M. Gustafsson and S. Nordebo. Optimal antenna currents for Q, superdirectivity, and radiation patterns using convex optimization. *IEEE Trans. Antennas Propag.*, **61**(3), pp. 1109–1118, 2013.

[22] M. Gustafsson, C. Sohl, and G. Kristensson. Physical limitations on antennas of arbitrary shape. *Proc. R. Soc. A*, **463**, pp. 2589–2607, 2007.

[23] M. Gustafsson, C. Sohl, and G. Kristensson. Illustrations of new physical bounds on linearly polarized antennas. *IEEE Trans. Antennas Propag.*, **57**(5), pp. 1319–1327, May 2009.

[24] M. Gustafsson, D. Tayli, C. Ehrenborg, M. Cismasu, and S. Nordebo. Antenna current optimization using MATLAB and CVX. *FERMAT*, **15**(5), pp. 1–29, 2016.

[25] M. Gustafsson, M. Cismasu, and B. L. G. Jonsson. Physical bounds and optimal currents on antennas. *IEEE Trans. Antennas Propag.*, **60**(6), pp. 2672–2681, 2012.

[26] M. Gustafsson, D. Tayli, and M. Cismasu. *Physical bounds of antennas*, pp. 1–32. Springer-Verlag, 2015.

[27] R. F. Harrington. Effect of antenna size on gain, bandwidth and efficiency. *Journal of Research of the National Bureau of Standards – D. Radio Propagation*, **64D**, pp. 1–12, Jan. – Feb. 1960.

[28] R. F. Harrington. Antenna excitation for maximum gain. *IEEE Trans. Antennas Propag.*, **13**(6), pp. 896–903, Nov. 1965.

[29] R. F. Harrington and J. R. Mautz. Control of radar scattering by reactive loading. *IEEE Trans. Antennas Propag.*, **20**(4), pp. 446–454, 1972.

[30] R. L. Haupt and D. H. Werner. *Genetic algorithms in electromagnetics*. John Wiley & Sons, 2007.

[31] IEEE145-1993. *IEEE Standard Definition of Terms for Antennas*. Antenna Standards Committee of the IEEE Antennas and Propagation Society, Mar. 1993.

[32] L. Jelinek and M. Capek. Optimal currents on arbitrarily shaped surfaces. *IEEE Trans. Antennas Propag.*, **65**(1), pp. 329–341, 2017.

[33] L. Jelinek, K. Schab, and M. Capek. The radiation efficiency cost of resonance tuning. *IEEE Trans. Antennas Propag.*, **66**(12), pp. 6716–6723, Dec. 2018. eprint arXiv: 1712.02613.

[34] B. L. G. Jonsson and M. Gustafsson. Stored energies in electric and magnetic current densities for small antennas. *Proc. R. Soc. A*, **471**(2176), pp. 20140897, 2015.

[35] B. L. G. Jonsson and M. Gustafsson. Stored energies for electric and magnetic current densities. *arXiv preprint arXiv:1604.08572*, 2016.

[36] B. L. G. Jonsson, S. Shi, L. Wang, F. Ferrero, and L. Lizzi. On methods to determine bounds on the Q-factor for a given directivity. *IEEE Trans. Antennas Propag.*, **65**(11), pp. 5686–5696, 2017.

[37] O. Kim, S. Pivnenko, and O. Breinbjerg. Superdirective magnetic dipole array as a first-order probe for spherical near-field antenna measurements. *IEEE Trans. Antennas Propag.*, **60**(10), pp. 4670–4676, 2012.

[38] O. Kim. Minimum Q electrically small antennas. *IEEE Trans. Antennas Propag.*, **60**(8), pp. 3551–3558, Aug. 2012.

[39] G. Marrocco. The art of UHF RFID antenna design: impedance-matching and size-reduction techniques. *IEEE Antennas Propag. Mag.*, **50**(1), pp. 66–79, Feb. 2008.

[40] J. S. McLean. A re-examination of the fundamental limits on the radiation Q of electrically small antennas. *IEEE Trans. Antennas Propag.*, **44**(5), pp. 672–676, May 1996.

[41] H. Nagaoka. The inductance coefficients of solenoids. *Journal of the College of Science*, **27**, pp. 1–33, 1909. article 6.

[42] G. C. Onwubolu and B. V. Babu. *New Optimization Techniques in Engineering*. Springer, 2004.

[43] Palmier. *Wikipedia, The Free Encyclopedia*.

[44] M. F. Pantoja, F. G. Ruiz, A. R. Bretones, R. G. Martin, J. M. Gonzalez-Arbesu, J. Romeu, and J. M. Rius. GA design of wire pre-fractal antennas and comparison with other euclidean geometries. *IEEE Antennas Wirel. Propag. Lett.*, **2**, pp. 238–241, 2003.

[45] C. Pfeiffer. Fundamental efficiency limits for small metallic antennas. *IEEE Trans. Antennas Propag.*, **65**(4), pp. 1642–1650, 2017.

[46] M. Pigeon, C. Delaveaud, L. Rudant, and K. Belmkaddem. Miniature directive antennas. *International Journal of Microwave and Wireless Technologies*, **6**(1), pp. 45–50, 2014.

[47] D. M. Pozar. *Microwave Engineering*. John Wiley & Sons, New York, NY, third edition, 2005.

[48] F. J. R. Meys. Measuring the impedance of balanced antennas by an s-parameter method. *IEEE Antennas and Propagation*, **40**(6), pp. 62–65, Dec. 1998.

[49] Y. Rahmat-Samii, J. M. Kovitz, and H. Rajagopalan. Nature-inspired optimization techniques in communication antenna design. *Proc. IEEE*, **100**(7), pp. 2132–2144, Jul. 2012.

[50] Y. Rahmat-Samii and E. Michielssen. *Electromagnetic Optimization by Genetic Algorithms*. Wiley Series in Microwave and Optical Engineering. John Wiley & Sons, 1999.

[51] H. Raza, J. Yang, and A. Hussain. Measurement of radiation efficiency of multiport antennas with feeding network corrections. *IEEE Antennas Wirel. Propag. Lett.*, **11**, pp. 89–92, 2012.

[52] D. R. Rhodes. Observable stored energies of electromagnetic systems. *Journal of the Franklin Institute*, **302**(3), pp. 225–237, 1976.

[53] K. Schab, L. Jelinek, M. Capek, C. Ehrenborg, D. Tayli, G. A. Vandenbosch, and M. Gustafsson. Energy stored by radiating systems. *IEEE Access*, **6**, pp. 10553 – 10568, 2018.

[54] M. Shahpari and D. V. Thiel. Fundamental limitations for antenna radiation efficiency. *IEEE Trans. Antennas Propag.*, **66**(8), pp. 3894–3901, Aug. 2018.

[55] S. Shi, L. Wang, and B. L. G. Jonsson. Antenna current optimization and realizations for far-field pattern shaping. *ArXiv e-print, 1711.09709v2*, 2018.

[56] D. F. Sievenpiper, D. C. Dawson, M. M. Jacob, T. Kanar, S. Kim, J. Long, and R. G. Quarfoth. Experimental validation of performance limits and design guidelines for small antennas. *IEEE Trans. Antennas Propag.*, **60**(1), pp. 8–19, Jan 2012.

[57] G. S. Smith. Efficiency of electrically small antennas combined with matching networks. *IEEE Trans. Antennas Propag.*, **25**, pp. 369–373, 1977.

[58] H. L. Thal. New radiation Q limits for spherical wire antennas. *IEEE Trans. Antennas Propag.*, **54**(10), pp. 2757–2763, Oct. 2006.

[59] H. L. Thal. Q Bounds for Arbitrary Small Antennas: A Circuit Approach. *IEEE Trans. Antennas Propag.*, **60**(7), pp. 3120–3128, 2012.

[60] H. L. Thal. Radiation efficiency limits for elementary antenna shapes. *IEEE Trans. Antennas Propag.*, **66**(5), pp. 2179 – 2187, 2018.

[61] M. Uzsoky and L. Solymár. Theory of super-directive linear arrays. *Acta physica Academiae Scientiarum Hungaricae*, **6**(2), pp. 185–205, 1956.

[62] G. A. E. Vandenbosch. Reactive energies, impedance, and Q factor of radiating structures. *IEEE Trans. Antennas Propag.*, **58**(4), pp. 1112–1127, 2010.

[63] J. Volakis, C. C. Chen, and K. Fujimoto. *Small Antennas: Miniaturization Techniques & Applications*. McGraw-Hill, New York, NY, 2010.

[64] H. A. Wheeler. Fundamental limitations of small antennas. *Proc. IRE*, **35**(12), pp. 1479–1484, 1947.

[65] A. Wood and B. Davidson. RF power device impedances: Practical considerations. Technical Report AN1526, Freescale Semiconductor, Inc., 1991. Rev. 0, 12/1991.

[66] A. D. Yaghjian, M. Gustafsson, and B. L. G. Jonsson. Minimum Q for lossy and lossless electrically small dipole antennas. *Prog. Electromagn. Res.*, **143**, pp. 641–673, 2013.

[67] A. D. Yaghjian and S. R. Best. Impedance, bandwidth, and Q of antennas. *IEEE Trans. Antennas Propag.*, **53**(4), pp. 1298–1324, 2005.

[68] A. D. Yaghjian, T. H. O'Donnell, E. E. Altshuler, and S. R. Best. Electrically small supergain end-fire arrays. *Radio Science*, **43**(3), pp. 1–13, 2008.

[69] R. W. Ziolkowski, M.-C. Tang, and N. Zhu. An efficient, broad bandwidth, high directivity, electrically small antenna. *Microwave and Optical Technology Letters*, **55**(6), pp. 1430–1434, 2013.

Fundamental bounds on MIMO antennas

Paper II

Casimir Ehrenborg and Mats Gustafsson

Published as: C. Ehrenborg and M. Gustafsson, "Fundamental bounds on MIMO antennas," *IEEE Wireless and Propagation Letters*, Vol. 15, No. 1, pp. 21–24, IEEE, 2018.

Abstract

Antenna current optimization is often used to analyze the optimal performance of antennas. Antenna performance can be quantified in *e.g.*, minimum Q-factor and radiation efficiency. The performance of MIMO antennas is more involved and, in general, a single parameter is not sufficient to quantify it. Here, the capacity of an idealized channel is used as the main performance quantity. An optimization problem in the current distribution for optimal capacity, measured in spectral efficiency, given a fixed Q-factor and radiation efficiency is formulated as a semi-definite optimization problem. A model order reduction based on characteristic and energy modes is employed to improve the computational efficiency. The performance bound is illustrated by solving the optimization problem numerically for rectangular plates and spherical shells.

1 Introduction

Wireless communication in modern systems utilize MIMO networks and antennas [15, 17]. These systems consist of two sets of antennas, one transmitting, and one receiving. Normally, one of these sets is situated in a location where space allocation is not an issue, such as a base station. However, the other set is usually contained within a small device, such as a mobile phone, where design space is limited [20]. Naturally, antenna designs aim at maximizing performance in such an environment. However, there is little knowledge of how the performance depends on size, Q-factor, and radiation efficiency restrictions. Having this knowledge *a priori* would enable designers to optimize their antenna designs more efficiently. There has been efforts to bound MIMO antennas performance for spherical surfaces [4, 7] and through information-theoretical approaches [13, 14, 18]. However, in order to create tight bounds for a design region the bounding surface must be arbitrary.

Antenna current optimization can be used to determine physical bounds for antennas of arbitrary shape [11]. These physical bounds are found by maximizing a certain performance parameter by freely placing currents in the design space. By having total control of the current distribution an optimal solution can be reached. While these currents might not necessarily be realizable they provide an upper bound for the considered problem. Construction of such physical bounds are made possible by the ability to formulate convex optimization problems [1] for the performance quantity of interest. The performance of simple antennas can be quantified in *e.g.*, the Q-factor, gain, directivity, and efficiency [9]. MIMO antennas, on the other hand, are more complex and a single parameter is insufficient to determine their performance. The maximization of their main performance quantity, capacity, cannot be formulated as a classical quadratic programming problem. As such, it is a challenging problem to construct physical bounds for MIMO systems. However, it is still possible to utilize antenna current optimization and semi-definite programming [1] to maximize a given performance

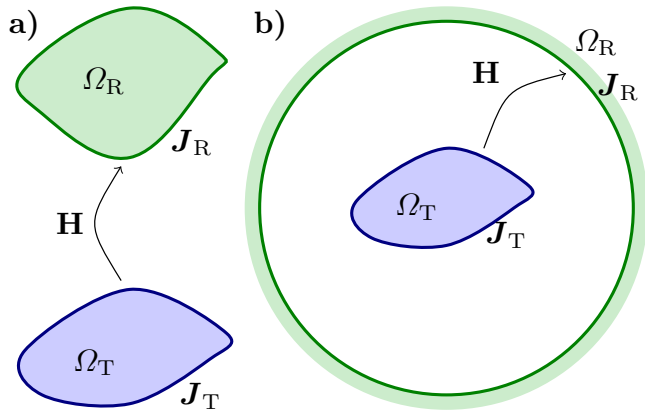

Figure 1: Illustration of the MIMO system model with transmitter region Ω_{T} and receiver region Ω_{R}. Part **(a)** shows the classical MIMO setup with spatially separated regions. Part **(b)** illustrates the idealized case when the receiver region entirely surrounds the transmitter. The system in **(b)** is utilized in this paper to determined performance bounds on MIMO antennas confined to the region Ω_{T}.

quantity, such as capacity, with restrictions on, *e.g.*, the Q-factor and radiation efficiency.

In this letter a method for constructing a performance bound on capacity for arbitrary shaped MIMO antennas using current optimization is presented. Transmitting at maximum capacity is formulated as a convex optimization problem in the current distribution on the MIMO antenna. The problem is constrained by the radiation efficiency and Q-factor. These are expressed as quadratic forms in the current density, where the stored energy in [19] is used. This leads to a convex optimization problem that maximizes the capacity in terms of spectral efficiency for a fixed SNR, radiation efficiency and Q-factor. The convex optimization problem is a semi-definite program [1] expressed in the covariance matrix of the current distribution. In order to bound the performance of a MIMO antenna, rather than a specific channel, the receiver antenna set has been characterized as the spherical modes in the far-field. This leads to an idealized channel in terms of spherical modes [7], which can be thought of as a direct line of sight channel where all radiation is received. Considering such a channel has the benefit of reducing computational complexity. This is further reduced by a model order reduction of the MoM impedance matrix characterizing the antenna.

2 MIMO Model

A classical MIMO system is modeled as [17]

$$\mathbf{y} = \mathbf{H}\mathbf{x} + \mathbf{n}, \tag{1}$$

where $\mathbf{x}$ is a $N \times 1$ matrix of the input signals, $\mathbf{y}$ is a $M \times 1$ matrix of the output signals, $\mathbf{n}$ is a $M \times 1$ matrix of additive noise, and $\mathbf{H}$ is the $M \times N$ channel matrix. The channel matrix models how power is transmitted from the input signals to the output signals, this includes the receiving and transmitting antennas and the wave propagation between them [17].

Fig. 1a displays a classical MIMO setup where two sets of antennas form a channel. Analysis of such systems depend greatly on external factors, such as, scattering phenomena, channel characterization, and antenna location [17]. However, to investigate performance bounds for MIMO antennas we must limit the degrees of freedom to a single antenna. This implies that $\mathbf{H}$ in (1) should model the channel between an arbitrary antenna and an idealized receiver, corresponding to Fig. 1b. The transmitting antenna is modeled with its current distribution using a MoM approximation [9] such that each basis function corresponds to an element of $\mathbf{x}$. The receiver is modeled with the radiated spherical modes, where each mode is an element in $\mathbf{y}$ [7, 10]. This leads to a MIMO system of infinite dimension as N increases with mesh refinement and M increases with the number of included spherical modes. In numerical evaluation N and M are chosen sufficiently large to ensure convergence.

The transmitted signals are modeled as the MoM current elements $\mathbf{I} = \mathbf{T}\mathbf{x}$, where the matrix $\mathbf{T}$ maps the transmitted signals $\mathbf{x}$ to the current distribution on the antenna $\mathbf{I}$. The covariance matrix of the transmitted signal is $\mathbf{P} = \mathcal{E}\left\{\mathbf{x}\mathbf{x}^{\mathrm{H}}\right\}$, where $\mathcal{E}\{\cdot\}$ denotes the temporal average [17]. With this matrix we can calculate the average transmitted power,

$$P = \frac{1}{2}\mathcal{E}\left\{\mathbf{I}^{\mathrm{H}}\mathbf{R}\mathbf{I}\right\} = \frac{1}{2}\mathcal{E}\left\{\mathbf{x}^{\mathrm{H}}\mathbf{T}^{\mathrm{H}}\mathbf{R}\mathbf{T}\mathbf{x}\right\} = \frac{1}{2}\operatorname{Tr}\mathcal{E}\left\{\mathbf{T}^{\mathrm{H}}\mathbf{R}\mathbf{T}\mathbf{x}\mathbf{x}^{\mathrm{H}}\right\} = \frac{1}{2}\operatorname{Tr}(\widehat{\mathbf{R}}\mathbf{P}), \quad (2)$$

where $\widehat{\mathbf{R}} = \mathbf{T}^{\mathrm{H}}\mathbf{R}\mathbf{T}$, and $\mathbf{R}$ is the resistive part of the MoM impedance matrix, $\mathbf{Z} = \mathbf{R} + \mathrm{j}\mathbf{X}$ [9]. Since we are concerned with connecting the currents on the antenna structure to the spherical modes [8] in the idealized receiver we express our channel as

$$\mathbf{y} = \mathbf{M}\mathbf{I} + \mathbf{n} = \mathbf{M}\mathbf{T}\mathbf{x} + \mathbf{n} = \widehat{\mathbf{M}}\mathbf{x} + \mathbf{n}, \quad (3)$$

where $\mathbf{M}$ denotes the map from the currents to the spherical modes. This is a direct channel between the antenna current distribution and the spherical modes [6]. The capacity, expressed as spectral efficiency ($\mathrm{b/(s\,Hz)}$), of this channel is given by [17]

$$C = \max_{\operatorname{Tr}(\widehat{\mathbf{R}}\mathbf{P})=P} \log_2 \det\left(\mathbf{1} + \frac{1}{N_0}\widehat{\mathbf{M}}\mathbf{P}\widehat{\mathbf{M}}^{\mathrm{H}}\right), \quad (4)$$

where $\mathbf{1}$ is the $M \times M$ identity matrix, and N_0 is the noise spectral power density. The noise is modeled as white complex Gaussian noise. The optimal energy allocation in this channel for capacity maximization is given by the water-filling solution [17]. Alternatively, the optimal solution for this problem can be solved

by a semidefinite optimization program,

$$\begin{aligned} \text{maximize} \quad & \log_2 \det(\mathbf{1} + \gamma \widehat{\mathbf{M}} \mathbf{P} \widehat{\mathbf{M}}^{\mathrm{H}}) \\ \text{subject to} \quad & \mathrm{Tr}(\widehat{\mathbf{R}} \mathbf{P}) = 1 \\ & \mathbf{P} \succeq 0, \end{aligned} \tag{5}$$

where the unit transmitted power is considered, and $\gamma = P/N_0$ is the total SNR. Maximizing the capacity of this channel corresponds to focusing the radiation of the antenna to the orthogonal spherical modes.

The solution to (5) is unbounded and increases as mesh refinement and the number of spherical modes are increased if the SNR is scaled with the number of channels in $\widehat{\mathbf{M}}$. Here, we consider the case of a fixed SNR. The solution to (5) can be made more realistic by adding constraints on the losses or Q-factor of the transmitting antenna [7, 16]. The Ohmic losses are calculated as

$$P_\Omega = \frac{1}{2}\mathcal{E}\left\{\mathbf{I}^{\mathrm{H}} \mathbf{R}_\Omega \mathbf{I}\right\} = \frac{1}{2}\mathcal{E}\left\{\mathbf{x}^{\mathrm{H}} \mathbf{T}^{\mathrm{H}} \mathbf{R}_\Omega \mathbf{T} \mathbf{x}\right\} = \frac{1}{2}\,\mathrm{Tr}(\widehat{\mathbf{R}}_\Omega \mathbf{P}), \tag{6}$$

where $\widehat{\mathbf{R}}_\Omega = \mathbf{T}^{\mathrm{H}} \mathbf{R}_\Omega \mathbf{T}$, and $\mathbf{R}_\Omega$ is the loss matrix of the antenna [9]. The stored electric energy is

$$W_{\mathrm{e}} = \frac{1}{4\omega}\mathcal{E}\left\{\mathbf{I}^{\mathrm{H}} \mathbf{X}_{\mathrm{e}} \mathbf{I}\right\} = \frac{1}{4\omega}\,\mathrm{Tr}(\widehat{\mathbf{X}}_{\mathrm{e}} \mathbf{P}), \tag{7}$$

where $\widehat{\mathbf{X}}_{\mathrm{e}} = \mathbf{T}^{\mathrm{H}} \mathbf{X}_{\mathrm{e}} \mathbf{T}$, and $\mathbf{X}_{\mathrm{e}}$ is the electric reactance matrix [9]. The stored magnetic energy W_{m} is similarly defined by the magnetic reactance matrix $\mathbf{X}_{\mathrm{m}}$ as $W_{\mathrm{m}} = \frac{1}{4\omega}\,\mathrm{Tr}(\widehat{\mathbf{X}}_{\mathrm{m}} \mathbf{P})$, where $\widehat{\mathbf{X}}_{\mathrm{m}} = \mathbf{T}^{\mathrm{H}} \mathbf{X}_{\mathrm{m}} \mathbf{T}$.

With these constraints in hand we can formulate our convex optimization problem. We note that the solution is independent of the power P, so it is sufficient to consider the case $P = 1$ giving

$$\begin{aligned} \text{maximize} \quad & \log_2 \det(\mathbf{1} + \gamma \widehat{\mathbf{M}} \mathbf{P} \widehat{\mathbf{M}}^{\mathrm{H}}) \\ \text{subject to} \quad & \mathrm{Tr}((\widehat{\mathbf{X}}_{\mathrm{e}} + \widehat{\mathbf{X}}_{\mathrm{m}})\mathbf{P}) \leq 2Q \\ & \mathrm{Tr}(\widehat{\mathbf{X}} \mathbf{P}) = 0 \\ & \mathrm{Tr}(\widehat{\mathbf{R}}_\Omega \mathbf{P}) \leq 1 - \eta \\ & \mathrm{Tr}(\widehat{\mathbf{R}} \mathbf{P}) = 1 \\ & \mathbf{P} \succeq \mathbf{0}, \end{aligned} \tag{8}$$

where η is the radiation efficiency, and self-resonance is enforced. Here, the problem has been normalized to dissipated power, including losses. The consequence of this is that the Q-factor considered includes losses in its calculation. It is possible, and sometimes advantageous, to normalize to different quantities such as the radiated power. Equation (8) is a semi-definite optimization problem which has a unique solution [1]. However, the problem is non-trivial due to the large number of unknowns for realistic antenna problems. For example a rectangular

plate of size $\ell \times \ell/2$ discretized into 64×32 rectangular elements has $N = 4000$ unknowns. This size is not a problem for convex optimization of type G/Q and Q [2, 8, 9]. However, the semi-definite relaxation has close to $N^2/2 = 8 \cdot 10^6$ unknowns, making the problem much more computationally demanding. Moreover, the logarithm used in the definition of capacity is more involved than the simple quadratic functions in G/Q and Q type problems [8, 9]. Here, the number of unknowns is reduced by expansion of the currents in characteristic, energy, and efficiency modes [9], with similar results.

The expansion includes only the first several dominating modes and as such constitutes a model order reduction. This implies a change of basis $\mathbf{I} \approx \mathbf{U}\tilde{\mathbf{I}}$, where $\mathbf{U}$ maps between the old and the new currents. This reduces the number of unknowns to the included modes $N_1 \ll N$. With this approximation the stored energy, for example, is calculated as

$$\mathbf{I}^{\mathrm{H}}\widehat{\mathbf{X}}_{\mathrm{e}}\mathbf{I} \approx \tilde{\mathbf{I}}^{\mathrm{H}}\mathbf{U}^{\mathrm{T}}\widehat{\mathbf{X}}_{\mathrm{e}}\mathbf{U}\tilde{\mathbf{I}} = \tilde{\mathbf{I}}^{\mathrm{H}}\widetilde{\mathbf{X}}_{\mathrm{e}}\tilde{\mathbf{I}} = \mathrm{Tr}(\widetilde{\mathbf{X}}_{\mathrm{e}}\tilde{\mathbf{I}}\tilde{\mathbf{I}}^{\mathrm{H}}) = \mathrm{Tr}(\widetilde{\mathbf{X}}_{\mathrm{e}}\widetilde{\mathbf{Y}}), \tag{9}$$

where $\widetilde{\mathbf{Y}} = \tilde{\mathbf{I}}\tilde{\mathbf{I}}^{\mathrm{H}}$, and $\widetilde{\mathbf{X}}_{\mathrm{e}} = \mathbf{U}^{\mathrm{T}}\widehat{\mathbf{X}}_{\mathrm{e}}\mathbf{U}$. Similarly $\widehat{\mathbf{X}}_{\mathrm{m}}$, and $\widehat{\mathbf{R}}$, are expressed as $\widetilde{\mathbf{X}}_{\mathrm{m}} = \mathbf{U}^{\mathrm{T}}\widehat{\mathbf{X}}_{\mathrm{m}}\mathbf{U}$, and $\widetilde{\mathbf{R}} = \mathbf{U}^{\mathrm{T}}\widehat{\mathbf{R}}\mathbf{U}$. These replace the corresponding matrices in (8), with $\widetilde{\mathbf{Y}}$ replacing $\mathbf{P}$. This reduces the number of unknowns from approximately $N^2/2$ to $N_1^2/2$.

3 Numerical Examples

In the following examples the optimization problem (8) has been solved for a MIMO system resembling Fig. 1b using the Matlab library CVX [5, 9]. The logarithm in the optimization problem (8) was replaced by a root of order M [5]. After the optimization has been carried out the capacity is calculated as normal with the optimized currents. The energy restriction on the number of transmitter modes and the number of spherical harmonic modes in the receiver have been chosen sufficiently large to ensure convergence and varies from example to example. The number of dominating channels in $\widehat{\mathbf{M}}$ are not many, shown in [3], thus the model order reduction need only include enough modes for these channels to be available. Since the performance of a MIMO antenna cannot be quantified by a single parameter the optimization was run with different constraints. This illustrates how capacity is bounded by different requirements on the transmitting antennas. The optimization has also been run for a spherical shell circumscribing the antenna.

In Fig. 2 the capacity has been optimized for a plate of electrical size $\ell = 0.21\lambda$, and is depicted as a function of the Q-factor restriction. We see a cut-off for $Q \leq 12$ where the optimization problem is unable to realize a feasible current distribution for so low Q-factor, *cf.*, the lower bound on the Q-factor [2]. For higher SNR the capacity increases but the cut-off stays the same, since the SNR does not affect the Q-factor.

We can instead regard the problem with a fixed SNR and investigate how the capacity varies with antenna size, see Fig. 3. Depending on which Q is

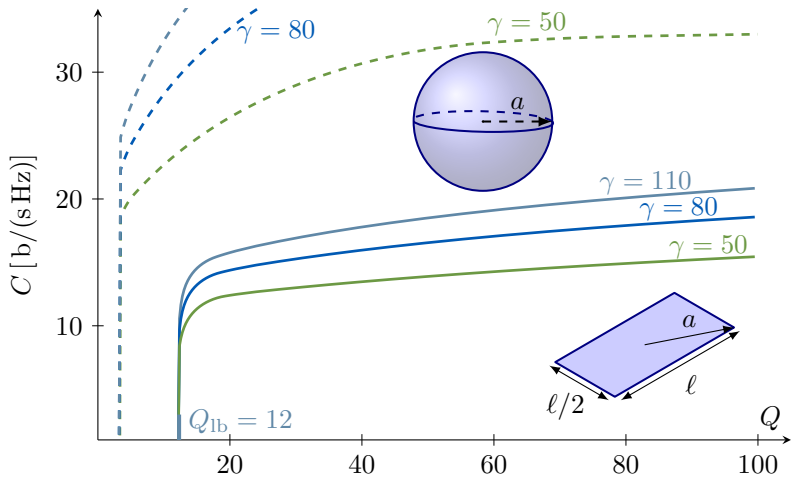

Figure 2: Maximum spectral efficiency achievable for a loss-less rectangular plate of size $\ell \times \ell/2$ for the wavelength $\ell = 0.21\lambda$ given maximum Q-factor on the horizontal axis. The dashed lines show the maximum spectral efficiency achievable for the corresponding circumscribing sphere.

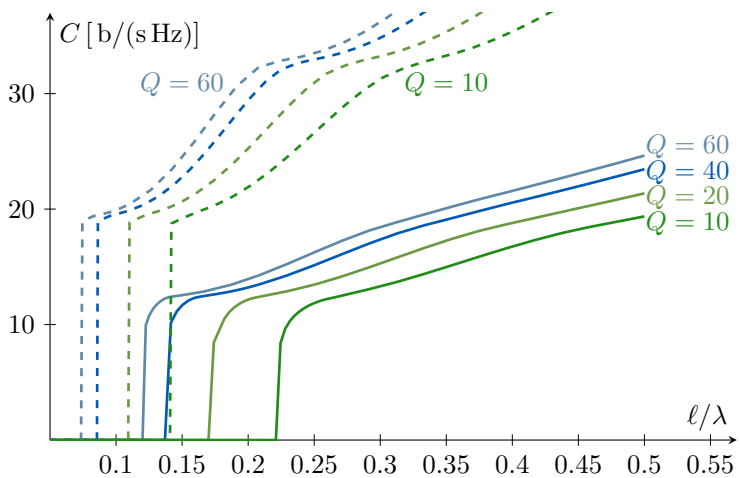

Figure 3: Maximum spectral efficiency achievable for a loss-less rectangular plate of electrical size ℓ/λ for maximum Q-factor with SNR $\gamma = 50$, *cf.*, Fig. 2. The dashed lines show the maximum spectral efficiency achievable for the corresponding circumscribing sphere.

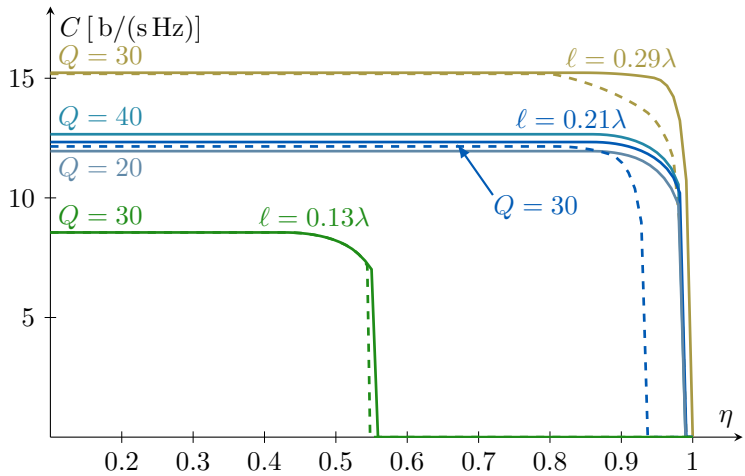

Figure 4: Maximum spectral efficiency achievable for a rectangular plate of electrical size ℓ/λ for minimum radiation efficiency η. The losses are modeled as a resistive sheet with $R = 0.2\,\Omega/\square$. The minimum Q-factor is set to 30 for the three main graphs and SNR $\gamma = 50$. Solid lines are optimized without enforcing resonance and dashed lines are optimized with resonance. For $\ell = 0.21\lambda$ the Q-factors $[20, 30, 40]$ are plotted.

chosen the solution is only realizable for sizes above a certain cut-off. This cut-off corresponds to the size which has the chosen Q as its minimum achievable Q. Above this size the capacity seems to depend linearly on the antenna size. This is consistent with how capacity scales with the number of antennas included in a MIMO system [17].

In Figs. 2 and 3 the dashed lines show the optimization problem solved for a spherical shell circumscribing the planar region. We see that the spectral efficiency achievable by a planar antenna is much less than that of the sphere.

Setting an radiation efficiency requirement on the optimization may restrict which modes are realizable. Fig. 4 illustrates how capacity varies as a function of radiation efficiency. We see that the capacity is unaffected until some cut-off value where the solution is no longer realizable. For electrical sizes $\ell = 0.21\lambda$ and 0.29λ this occurs when the radiation efficiency requirement is high, above 90%. However, for smaller sizes, such as $\ell = 0.13\lambda$, we see that this cut-off occurs at lower radiation efficiencies. The optimization problem has been solved both with and without enforcing resonance. When resonance is enforced, showed in dashed lines, we see that the cut-off occurs at lower radiation efficiencies, this is due to self-resonant currents being inherently less efficient [12]. For the size $\ell = 0.21\lambda$ the Q-factor requirement was varied as well, leading to a slight reduction or increase in capacity. Close to the cut-off efficiency we see a slight decrease in capacity for all cases. This corresponds to the requirement on radiation efficiency limiting the optimization problem. For lower radiation efficiency requirements

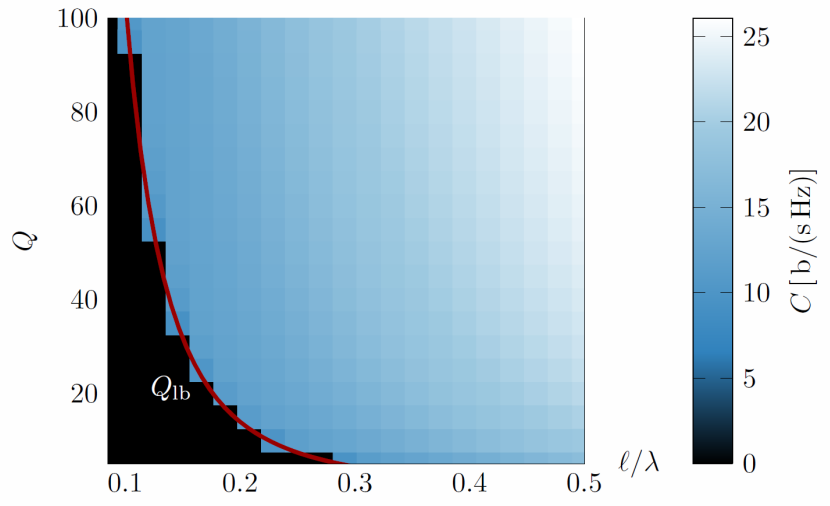

Figure 5: Illustration of the bounding surface of spectral efficiency for a loss less rectangular plate as a function of size and Q-factor with SNR $\gamma = 50$. The red curve shows minimum Q [2]

other constraints limit the optimization and the capacity is unaffected by the bound on radiation efficiency.

In Fig. 5 both the size of the antenna and the Q-factor are varied to create a two dimensional bounding surface. This surface has a sharp cut-off along the minimum Q line [2] seen on the left in Fig. 5. We see that the increase in capacity follows the shape of the minimum Q curve as ℓ/λ and Q are increased. This surface provides a bound on the capacity achievable for MIMO antennas of different sizes and with different bandwidth requirements.

4 Conclusions

In this letter we have presented a framework for constructing performance bounds for MIMO antennas. We simplified the channel problem often considered in communication theory to an idealized channel consisting of a spherical receiver surrounding the antenna region. This enables the formulation of a semi-definite optimization problem that gives a bounding capacity for any antenna that can be constructed within the considered region limited by size, SNR, radiation efficiency, and Q-factor. By utilizing a model order reduction based on energy and characteristic modes the complexity of the problem is reduced such that it is solvable.

These physical boundaries of MIMO antennas represent the ideal solutions possible given complete freedom of current placement within the design area.

While the shape of these current distributions are not easily realizable [12], the bounding values provide an upper limit to what is possible for real antenna topologies. Investigating how these bounds are affected by dielectric materials is very interesting and can be done by including them in the MoM simulation. It remains as future work to explore how these bounds compare to antenna designs and measurements.

Acknowledgment

The support of the Swedish foundation for strategic research under the program applied mathematics and the project Complex analysis and convex optimization for electromagnetic design is gratefully acknowledged.

References

[1] S. P. Boyd and L. Vandenberghe. *Convex Optimization*. Cambridge Univ. Pr., 2004.

[2] M. Capek, M. Gustafsson, and K. Schab. Minimization of antenna quality factor. *IEEE Trans. Antennas Propag.*, **65**(8), pp. 4115–4123, 2017.

[3] C. Ehrenborg and M. Gustafsson. Fundamental bounds on MIMO antennas. Technical Report LUTEDX/(TEAT-7247)/1–9/(2017), Lund University, Department of Electrical and Information Technology, P.O. Box 118, S-221 00 Lund, Sweden, 2017.

[4] A. A. Glazunov, M. Gustafsson, and A. Molisch. On the physical limitations of the interaction of a spherical aperture and a random field. *IEEE Trans. Antennas Propag.*, **59**(1), pp. 119–128, 2011.

[5] M. Grant and S. Boyd. CVX: Matlab software for disciplined convex programming, version 2.1. http://cvxr.com/cvx, Dec. 2018.

[6] M. Gustafsson and S. Nordebo. Bandwidth, Q-factor, and resonance models of antennas. *Prog. Electromagn. Res.*, **62**, pp. 1–20, 2006.

[7] M. Gustafsson and S. Nordebo. On the spectral efficiency of a sphere. *Prog. Electromagn. Res.*, **67**, pp. 275–296, 2007.

[8] M. Gustafsson and S. Nordebo. Optimal antenna currents for Q, superdirectivity, and radiation patterns using convex optimization. *IEEE Trans. Antennas Propag.*, **61**(3), pp. 1109–1118, 2013.

[9] M. Gustafsson, D. Tayli, C. Ehrenborg, M. Cismasu, and S. Nordebo. Antenna current optimization using MATLAB and CVX. *FERMAT*, **15**(5), pp. 1–29, 2016.

[10] M. Gustafsson and S. Nordebo. Characterization of MIMO antennas using spherical vector waves. *IEEE Trans. Antennas Propag.*, **54**(9), pp. 2679–2682, 2006.

[11] M. Gustafsson, D. Tayli, and M. Cismasu. *Physical bounds of antennas*, pp. 1–32. Springer-Verlag, 2015.

[12] L. Jelinek and M. Capek. Optimal currents on arbitrarily shaped surfaces. *IEEE Trans. Antennas Propag.*, **65**(1), pp. 329–341, 2017.

[13] L. Kundu. *Information-Theoretic Limits on MIMO Antennas*. PhD thesis, North Carolina State University, 2016.

[14] M. Migliore. On electromagnetics and information theory. *IEEE Trans. Antennas Propag.*, **56**(10), pp. 3188–3200, Oct. 2008.

[15] A. F. Molisch. *Wireless Communications*. John Wiley & Sons, New York, NY, second edition, 2011.

[16] M. L. Morris, M. Jensen, J. W. Wallace, et al. Superdirectivity in MIMO systems. *IEEE Trans. Antennas Propag.*, **53**(9), pp. 2850–2857, 2005.

[17] A. Paulraj, R. Nabar, and D. Gore. *Introduction to Space-Time Wireless Communications*. Cambridge University Press, Cambridge, 2003.

[18] P. S. Taluja and B. L. Hughes. Fundamental capacity limits on compact MIMO-OFDM systems. In *IEEE International Conference on Communications (ICC)*, pp. 2547–2552, Jun. 2012.

[19] G. A. E. Vandenbosch. Reactive energies, impedance, and Q factor of radiating structures. *IEEE Trans. Antennas Propag.*, **58**(4), pp. 1112–1127, 2010.

[20] Z. Ying. Antennas in cellular phones for mobile communications. *Proceedings of the IEEE*, **100**(7), pp. 2286–2296, Jul. 2012.

Physical Bounds and Radiation Modes for MIMO Antennas

Paper III

Casimir Ehrenborg and Mats Gustafsson

Preprint published as: C. Ehrenborg, and M. Gustafsson, "Physical Bounds and Radiation Modes for MIMO Antennas," Technical Report TEAT-7265, Electromagnetic Theory Department of Electrical and Information Technology, 2018.

Abstract

Modern antenna design for communication systems revolves around two extremes: devices, where only a small region is dedicated to antenna design, and base stations, where design space is not shared with other components. Both imply different restrictions on what performance is realizable. In this paper properties of both ends of the spectrum in terms of MIMO performance is investigated. For small antennas the size restriction dominates the performance parameters. The regions dedicated to antenna design induce currents on the rest of the device. Here a method for studying fundamental bound on spectral efficiency of such configurations is presented. For larger structures the number of degrees of freedom available per unit area is investigated for different shapes. Both of these are achieved by formulating a convex optimization problem for maximum spectral efficiency in the current density on the antenna. A closed form solution for this problem is formulated and investigated in relation to constraining parameters, such as size and efficiency.

1 Introduction

In modern communication technology the use of several antennas organized in MIMO systems have become ubiquitous. This enables much greater bit rate (capacity) to be sent through the link between device and base station [25, 26]. Within smaller devices, such as hand-held electronics, the space allotted for antenna design is extremely limited. Here, both space and power efficiency needs to be utilized as effectively as possible. It is therefore of interest to investigate fundamental bounds on performance of MIMO systems, both in terms of size and efficiency. Previously, bounds on capacity has been investigated for spherical geometries [10, 13], and through information theoretical approaches [6, 8, 9, 21, 28], such as investigating the role of the number of degrees of freedom in the system [7, 12, 23, 24]. Characteristic modes have been utilized to design antennas for maximum capacity and diversity [3, 22]. However, this does not solve the issue of predicting the optimal performance available through antenna design in an arbitrary geometry. A method for calculating optimal spectral efficiency available in an arbitrary volume was presented in [5]. However, in most applications it is effective to use only a small region of the device volume to excite currents over the entire device [17]. Therefore bounding the performance of such sub-regions and finding their optimal placement is of interest.

Current optimization has been utilized to construct fundamental bounds on many different antenna parameters previously, such as, Q, directivity, and efficiency [5, 14–16, 20]. By controlling the current density in the full design space of the antenna an optimal solution can be reached for that configuration. The power of this method comes from the ability to formulate these optimization problems as convex optimization problems. This means that all local minima of the problem are also global minima [1]. Therefore there is no risk of getting caught in local minima and the optimality of the solution can be guaranteed [1]. This method

works very well for single feed, single resonance antennas where their performance, in *e.g.*, Q-factor, can be calculated as simple quadratic forms [15]. Such expressions can be evaluated very efficiently using eigenvalue expressions that enables their optimization [2]. The performance of MIMO antennas on the other hand is usually quantified in terms of capacity, which is not calculated through a quadratic form in the current density, but through a log-determinant of the covariance of the current density. Such an optimization problem is a semi-definite optimization program in the covariance of the current distribution, which has, in general, one more order of unknowns [1]. To solve such optimization problems the number of unknowns need to be reduced [5].

In this paper the method presented in [5] is reformulated in order to find a closed form expression of its solution. A convex optimization problem to maximize the spectral efficiency of an arbitrary transmitter antenna in an ideal channel is formulated in the current density on the antenna. The problem is restricted by the allowed ohmic loss in the structure and normalized by the radiated or dissipated power. This problem is solved by utilizing the good properties of the matrices calculating radiated power and ohmic losses. The solution to this problem is dependent on the radiation modes, which are modes that maximize the fraction between the radiated power and the power dissipated in ohmic losses [27]. These modes are dependent on the geometrical structure of the object they are induced over, therefore the designer has control over how well they can be induced. The relative strength of these modes is investigated for a sphere, a cylinder, a disc, and a plate and its sub-regions. This information is used to analyze how many sub-regions are required to fully utilize the potential of a plate design region. The optimal spectral efficiency of the sub-region configurations is compared to optimizing the currents over the plate and sphere. Larger structures and their number of viable radiation modes are also investigated.

The paper is organized in the following way. In Sec. 2 the MIMO system studied in this paper is introduced and its convex optimization problem is stated. The dual of that problem is formulated and solved in Sec. 3, creating an upper bound for the original problem. In Sec. 4 the results of the optimization problem is illustrated in several examples split into the following sub-sections: Sec. 4.1 where the radiation modes of different shapes are studied, Sec. 4.2 where the radiation modes of a plate are excited by sub-regions, Sec. 4.3 where the optimal spectral efficiency of several structures is investigated, and Sec. 4.4 where the mode availability of larger structures is calculated. The paper is concluded in Sec. 5.

2 MIMO

The received signals in a MIMO system is described by the expression,

$$\mathbf{y} = \mathbf{H}\mathbf{x} + \mathbf{n}, \tag{1}$$

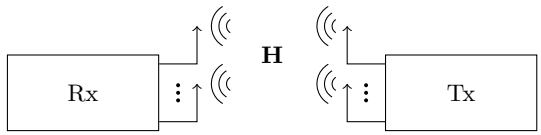

Figure 1: Schematic illustration of a MIMO setup. Rx is the set of receiving antennas, Tx is the set of transmitting antennas, and **H** is the channel matrix describing the propagation between Tx and Rx.

where **y** is a vector containing the received signals, **x** is a vector containing the input signals, **H** is a matrix describing the propagation channel, and **n** contains the noise perturbing the system. In communication theory what is typically optimized is the power distribution in **x** in order to send the maximum number of bits through a channel. However, in that configuration the antennas in the system are assumed fixed [26], see Fig. 1. Here, we are interested in how much performance can be attained from optimizing those antennas for the specific application of transmitting the highest capacity. In order to calculate that performance, the problem must be reformulated slightly. First, the system in (1) concerns two sets of antennas. However, in most cases we are not designing both the antennas in the system simultaneously, such as the base station and the mobile phone. Therefore, we reformulate the problem to optimizing a single device with regards to a general situation. In order to create such conditions, one set of antennas is idealized; here we choose the receiving antennas. Consider a receiving antenna completely circumscribing the transmitting antenna. This is similar to massive MIMO and the intelligent surfaces discussed in [19], covering all surfaces of a room. In such a configuration all radiated energy would be absorbed by the receivers on the walls. This can be characterized by using the spherical modes in the far-field as the receiving antennas [5,10,13], which will be used in this paper, see Fig. 2.

The second issue lies in the method of calculating optimal performance for the antennas. Since we do not know what shape an optimal antenna design would take, we want to incorporate every possible antenna in our solution space. To accomplish this we optimize the currents in the design space of the antenna, as these have the ability to represent every possible antenna within it. Normally a MIMO system is optimized through controlling the input signals to the antennas. These input signals generate the currents on the antenna, that are connected by a fixed mapping. However, since we are controlling the currents directly we simply utilize this map in order to calculate the performance quantities, such as capacity, from the currents [5]. For example, instead of optimizing over the covariance of the input signals, we optimize over the covariance of the currents,

$$\mathbf{P} = \frac{1}{2}\mathcal{E}\left\{\mathbf{I}\mathbf{I}^{\mathrm{H}}\right\}. \tag{2}$$

Essentially, each current element becomes an input signal to the system, whereas for actual antennas the number of inputs is restricted by the number of antenna

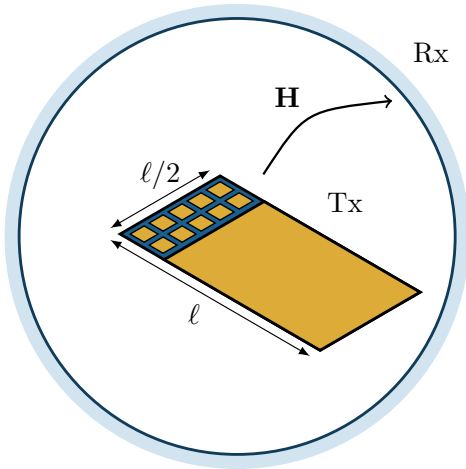

Figure 2: Schematic illustration of the idealized MIMO system where the receiving antennas are the spherical modes in the far-field. The transmitting antennas are illustrated as a plate with antenna design regions marked as small patches.

feeds.

The antenna region is modeled with a MoM code, where each basis function corresponds to an element in $\mathbf{I}$. We call the matrix mapping the current distribution on the plate to spherical modes $\mathbf{S}$ [29], see App. A, which gives a new formulation of (1),

$$\mathbf{y} = \mathbf{S}\mathbf{I} + \mathbf{n}. \tag{3}$$

In this formulation the received signals $\mathbf{y}$ are the radiated spherical modes, see Fig. 2. The average transmitted power of the system is calculated as,

$$P_\mathrm{r} = \frac{1}{2}\mathcal{E}\left\{\mathbf{I}^\mathrm{H}\mathbf{R}_\mathrm{r}\mathbf{I}\right\} = \frac{1}{2}\operatorname{Tr}\mathcal{E}\left\{\mathbf{R}_\mathrm{r}\mathbf{I}\mathbf{I}^\mathrm{H}\right\} = \operatorname{Tr}(\mathbf{R}_\mathrm{r}\mathbf{P}), \tag{4}$$

where $\mathbf{R}_\mathrm{r}$ is the radiation matrix, and we have utilized the cyclic properties of the trace. The capacity of this channel, expressed as spectral efficiency, is calculated as [26]

$$C = \max_{\operatorname{Tr}(\mathbf{R}_\mathrm{r}\mathbf{P})=P_\mathrm{r}} \log_2 \det\left(\mathbf{1} + \frac{1}{N_0}\mathbf{S}\mathbf{P}\mathbf{S}^\mathrm{H}\right), \tag{5}$$

where $\mathbf{1}$ is the identity matrix, and N_0 is the noise spectral power density. The noise is modeled as white complex Gaussian noise. This spectral efficiency is a measure of the capacity per Hz, which can equivalently be viewed as the capacity of a frequency flat channel with a 1 Hz transmission bandwidth [26]. The noise and power considered in (5) have been normalized to that bandwidth. Maximum capacity and optimal energy allocation for (5) can be calculated by the water filling algorithm [26]. However, it can also be written as an optimization problem

solved by semidefinite programming,

$$\begin{aligned} \text{maximize} \quad & \log_2 \det(\mathbf{1} + \gamma \mathbf{S}\mathbf{P}\mathbf{S}^{\mathrm{H}}) \\ \text{subject to} \quad & \mathrm{Tr}(\mathbf{R}_{\mathrm{r}}\mathbf{P}) = 1 \\ & \mathbf{P} \succeq 0, \end{aligned} \tag{6}$$

where the radiated power is normalized to one, and $\gamma = P_{\mathrm{r}}/N_0$ is the total SNR. If the SNR is scaled with the number of included channels, in this case mesh discritization and number of spherical modes, the spectral efficiency is unbounded [5, 26]. However, if the SNR is fixed the problem converges to

$$\log_2 \det(\mathbf{1} + \gamma \mathbf{S}\mathbf{P}\mathbf{S}^{\mathrm{H}}) = M \log_2 \left(1 + \frac{P_{\mathrm{r}}}{M N_0}\right) \approx \frac{\gamma}{\log(2)}, \tag{7}$$

as mesh discretization and number of spherical modes is increased, where M is the number of channels. This problem formulation has the advantage that additional constraints can be added in order to gain a more realistic solution. Here, we can, for example, limit the losses in the structure. Loss is modeled as a uniform impedance sheet with surface resistance R_{s} in $\Omega/\square$ and calculated as,

$$P_\Omega = \frac{1}{2}\mathcal{E}\left\{\mathbf{I}^{\mathrm{H}}\mathbf{R}_\Omega\mathbf{I}\right\} = \mathrm{Tr}(\mathbf{R}_\Omega\mathbf{P}), \tag{8}$$

where $\mathbf{R}_\Omega = R_{\mathrm{s}}\mathbf{\Psi}$ is the loss matrix of the antenna [15], and $\mathbf{\Psi}$ is the Gramian matrix of the MoM basis functions on the antenna. Adding this constraint to (6) gives the formulation

$$\begin{aligned} \text{maximize} \quad & \log_2 \det(\mathbf{1} + \gamma \mathbf{S}\mathbf{P}\mathbf{S}^{\mathrm{H}}) \\ \text{subject to} \quad & \mathrm{Tr}(\mathbf{R}_\Omega\mathbf{P}) \leq \delta \\ & \mathrm{Tr}(\mathbf{R}_{\mathrm{r}}\mathbf{P}) = 1 \\ & \mathbf{P} \succeq \mathbf{0}, \end{aligned} \tag{9}$$

where $\delta = P_\Omega/P_{\mathrm{r}}$ is the dissipation factor of the antenna, which is related to radiation efficiency as,

$$\eta = \frac{P_{\mathrm{r}}}{P_{\mathrm{r}} + P_\Omega} = \frac{1}{1+\delta}. \tag{10}$$

This problem is bounded and converges as the mesh discretization is refined, and the included number of spherical modes is increased [5]. However, it contains many unknowns and is cumbersome to solve numerically. Because it is a semidefinite programming problem the number of unknowns scale as the square of the number of mesh cells, necessitating model order reductions or other numerical procedures to run the optimization [5].

3 Dual Problem

One way of bounding the solution to (9) is to construct a problem that will always have a solution greater than or equal to that of the initial problem. This problem

is known as the dual to (9). The infimum of the dual problem provides an upper bound to the maximum of (9) and they coincide when the duality gap is zero [1].

To construct a dual problem to (9) we can combine the two constraints in (9) into one, as a convex optimization problem with less constraints will always have a greater solution than the same problem with more constraints [1]. A linear combination of the two constraints can be taken to restrict the dual problem

$$\mathrm{Tr}\left(\frac{1}{\delta}\mathbf{R}_\Omega\mathbf{P} + \nu\mathbf{R}_\mathrm{r}\mathbf{P}\right) = 1 + \nu, \tag{11}$$

where ν is a real scalar. Dividing the right-hand side to the left allows the introduction of a new matrix

$$\mathbf{R}_\nu = \frac{1}{1+\nu}\left(\frac{1}{\delta}\mathbf{R}_\Omega + \nu\mathbf{R}_\mathrm{r}\right). \tag{12}$$

The dual to (9) can now be written as

$$\begin{aligned} \min_{\nu}.\max_{\mathbf{P}}. \quad & \log_2\det(\mathbf{1} + \gamma\mathbf{S}\mathbf{P}\mathbf{S}^\mathrm{H}) \\ & \mathrm{Tr}(\mathbf{R}_\nu\mathbf{P}) = 1 \\ & \mathbf{P} \succeq \mathbf{0}. \end{aligned} \tag{13}$$

This problem is valid and convex for all values of ν for which $\mathbf{R}_\nu$ is positive semi-definite.

To solve the dual problem, we rewrite it on such a form that it can be solved by water filling. This can be done by simplifying the condition restricting it. $\mathbf{R}_\nu$ is positive semi-definite by construction and can therefore be Cholesky factorized as $\mathbf{R}_\nu = \mathbf{B}^\mathrm{H}\mathbf{B}$ [1]. By utilizing the cyclic invariance of the trace the condition can be rewritten as $\mathrm{Tr}(\mathbf{B}^\mathrm{H}\mathbf{B}\mathbf{P}) = \mathrm{Tr}(\mathbf{B}\mathbf{P}\mathbf{B}^\mathrm{H})$. The matrix $\mathbf{B}$ can be seen as a coordinate change for $\mathbf{P}$. This allows the introduction of a new variable $\widetilde{\mathbf{P}} = \mathbf{B}\mathbf{P}\mathbf{B}^\mathrm{H}$ to write the optimization problem as,

$$\begin{aligned} \min_{\nu}.\max_{\widetilde{\mathbf{P}}}. \quad & \log_2\det(\mathbf{1} + \gamma\widetilde{\mathbf{H}}\widetilde{\mathbf{P}}\widetilde{\mathbf{H}}^\mathrm{H}) \\ & \mathrm{Tr}(\widetilde{\mathbf{P}}) = 1 \\ & \widetilde{\mathbf{P}} \succeq \mathbf{0}, \end{aligned} \tag{14}$$

where the new channel is $\widetilde{\mathbf{H}} = \mathbf{S}\mathbf{B}^{-1}$. The maximum of this problem can be found by water filling [26]. To perform water filling it is a simple matter of following the same methodology outlined in [26], *i.e.*, find the SVD of the channel matrix $\widetilde{\mathbf{H}}$ and iteratively fill the feeding vector $\widetilde{\mathbf{P}}$ such that the lowest loss channels are utilized the most. With the singular values of the channel matrix, (14) can be

written more simply as

$$\begin{aligned} \min_{\nu} \max_{P_n} \quad & \sum_{n=1}^{N} \log_2(1+\gamma\sigma_n^2 P_n) \\ & \sum_{n=1}^{N} P_n = 1 \\ & P_n \geq 0, \end{aligned} \tag{15}$$

where σ_n, $n = 1 \ldots N$ are the singular values of $\widetilde{\mathbf{H}}$, and P_n is the power allocated to each mode associated with those singular values. These singular values σ_n can be expressed as, see Appendix B,

$$\sigma_n^2 = \frac{\varrho_n(1+\nu)}{\delta^{-1}+\nu\varrho_n}, \tag{16}$$

where ϱ_n are eigenvalues to modes known as radiation modes [27] and are calculated through the generalized eigenvalue problem,

$$\mathbf{R}_{\mathrm{r}}\mathbf{I}_n = \varrho_n \mathbf{R}_{\Omega}\mathbf{I}_n. \tag{17}$$

These modes maximize the fraction between radiated power and power dissipated in ohmic losses, and have orthogonal currents and far-fields. It is evident from (16) that these modes are a dominating factor in the singular values of the optimized channel. With this expression, water filling can be performed fast and efficiently with minimal numerical calculations. The minimization over ν, which can be calculated using conventional minimizers such as *fminbnd* in MATLAB, finally provides an upper bound to the initial problem (9).

4 Results

The solution to the optimization problem (9) provides an upper bound on the spectral efficiency available for different structures. This bound has been verified by optimizing the same problems in CVX [1, 11] for several of the considered cases confirming that the duality gap is zero for these cases. However, it is also interesting to investigate the radiation modes that contribute to the spectral efficiency in (16). To illustrate both of these results this section is divided into four sub-sections. First, the mode strength of different shapes is studied in Sec. 4.1, then feeding a plate through sub-regions is investigated in Sec. 4.2. The optimal spectral efficiency of the same plate is discussed in Sec. 4.3, and finally the mode availability of larger shapes is shown in Sec. 4.4.

4.1 Mode Strength

In the derivation of the optimized channels singular values (16), the radiation modes (17) are the only contributing factors that depend on the geometry of

the structure. All other parameters are either material parameters or design specifications. The influence of antenna design and geometry on the problem is therefore fully described by these radiation modes. Their relative strength can be calculated for different geometries in order to evaluate the availability of these modes. This can serve as a measure of how many orthogonal modes are available to provide diversity for those structures. In Fig. 3 the relative strength of the radiation and loss-less characteristic modes [3, 18] of a $ka = 0.06$, $\ell \times \ell/2$ plate, and the radiation modes of the circumscribing disc and sphere are shown normalized to the first radiation mode of the plate. We see that the two first radiation modes have the same strength and the third and higher order modes are significantly weaker. This means that inducing the first two modes of this plate are enough to harness most of its available diversity. The higher order modes are significantly weaker and require more input power to be utilized, or an increase in the plates size to be effective. The characteristic modes of the plate have been evaluated in the same metric, *cf.*, (17), *i.e.*,

$$\varrho_{\mathrm{c},n} = \frac{\mathbf{I}_{\mathrm{c},n}^{\mathrm{H}} \mathbf{R}_{\Omega} \mathbf{I}_{\mathrm{c},n}}{\mathbf{I}_{\mathrm{c},n}^{\mathrm{H}} \mathbf{R}_{\mathrm{r}} \mathbf{I}_{\mathrm{c},n}}, \tag{18}$$

where $\mathbf{I}_{\mathrm{c},n}$ are the characteristic mode currents, as a comparison. We can see that the characteristic modes preform slightly worse than the radiation modes, and have different radiation patterns for higher order modes. The relative strength of radiation modes for the circumscribing disc and sphere, normalized to the first radiation mode of the plate, have been included as a reference. We see that the disc has slightly higher mode strengths than the plate, whereas the sphere's modes are much stronger and grouped into a set of three for the first modes, rather than two.

4.2 Plate Sub-regions

In wireless communication only a small part of the device is typically dedicated to antenna design. It is therefore interesting to see how well small sub-regions can excite the diversity available from the plate in Fig. 3. The optimization problem in Sec. 3 can be reformulated for a sub-region of a geometry with the rest of the volume acting as a ground plane, see App. E. In Fig. 4, the sub-region problem has been solved for several different orientations of sub-regions on the plate in Fig. 3, where each region covers 1 % of the plate's total area. Here, we can see how well different configurations of sub-regions are able to induce the diversity available in the plate when fed optimally. It is clear that a single sub-region, in case A, is only able to effectively induce the first radiation mode. However, two diagonally situated sub-regions, as in case B, are only marginally better at inducing the second mode. This is due to that the first two radiation and characteristic modes are induced diagonally across the plate [22]. Therefore, the diagonally opposite regions do not effectively induce the second diagonal mode. However, if the two regions are placed on the same side of the plate, as in case

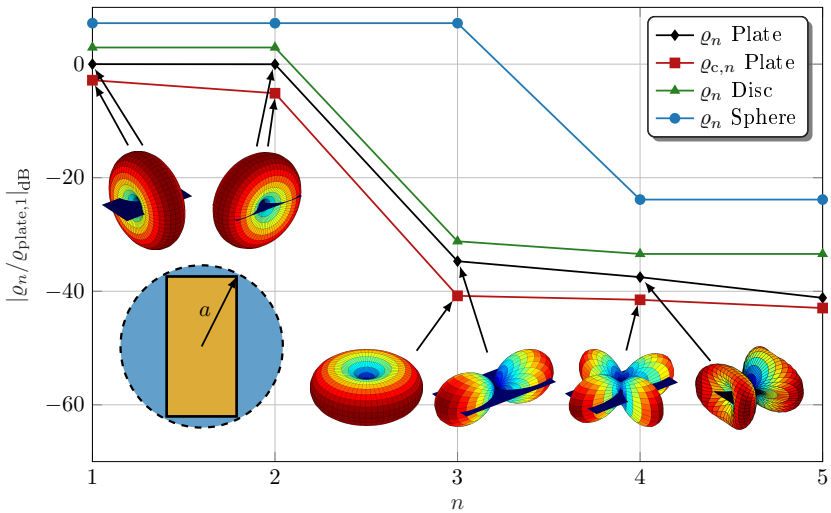

Figure 3: The strength of the first 5 radiation, ϱ_n, and characteristic, $\varrho_{c,n}$, modes of a $ka = 0.06$, $\ell \times \ell/2$ plate, as well as the radiation modes of its circumscribing disc and sphere. All values have been normalized to the first radiation mode of the plate. The corresponding far-fields for the radiation and characteristic modes of the plate can be seen as insets in the figure. The first two radiation and characteristic modes are visually identical and represented by the same patterns.

C, the second order mode is induced effectively. The radiation mode strengths are very similar if these two regions are placed on the long side of the plate. When going to higher order modes, this configuration is no longer as effective, here, the diagonal regions in case B dominate. If three or four sub-regions are utilized, as in cases D and E, we can get both of these properties. However, adding the fourth sub-region only marginally increases the strength of the three first radiation modes.

The values in Fig. 4 have a negligible dependence on the surface resistance R_s. However, the calculation to produce the sub-region problem is dependent on the full impedance matrix $\mathbf{Z}$ and thus the surface resistance, see App. E. This marginally changes the relation between the mode strength. However, the surface resistance plays an important role in which modes are utilized when feeding the structure for optimal spectral efficiency. Fig. 5 illustrates the water-filling procedure for two plates with different surface resistance. When the surface resistance is increased the loss in the higher order modes is increased. This pushes the third order mode out of viability for the signal strength P available in this example. Therefore the number of modes utilized decreases with greater losses.

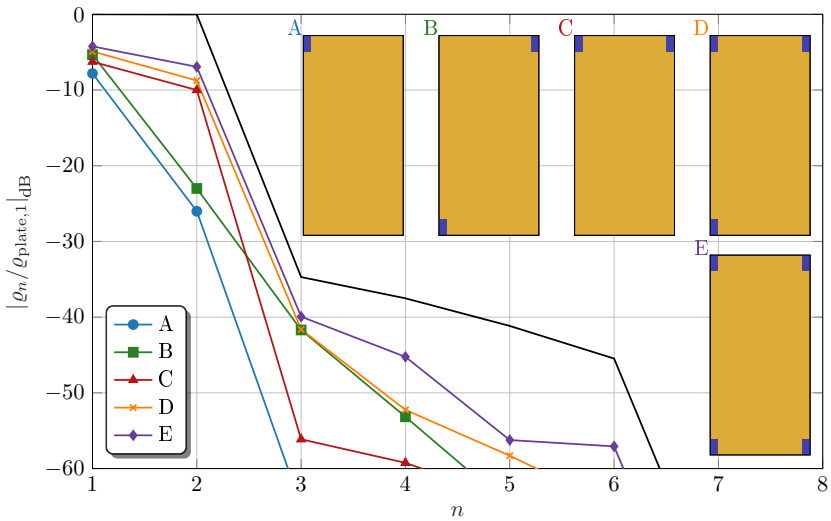

Figure 4: The strength of each mode in Fig. 3 when controlling only the current on sub regions of the $ka = 0.06$, $\ell \times \ell/2$ plate with $R_{\text{s}} = 0.01\,\Omega/\square$. The sub-regions each cover 1% of the plates total area. The current is controlled in the blue regions on the plate and only induced currents live on the yellow part of the plate. The black curve without marks is the strength of each mode for the full plate normalized to the first mode, all other curves have been normalized to the same quantity.

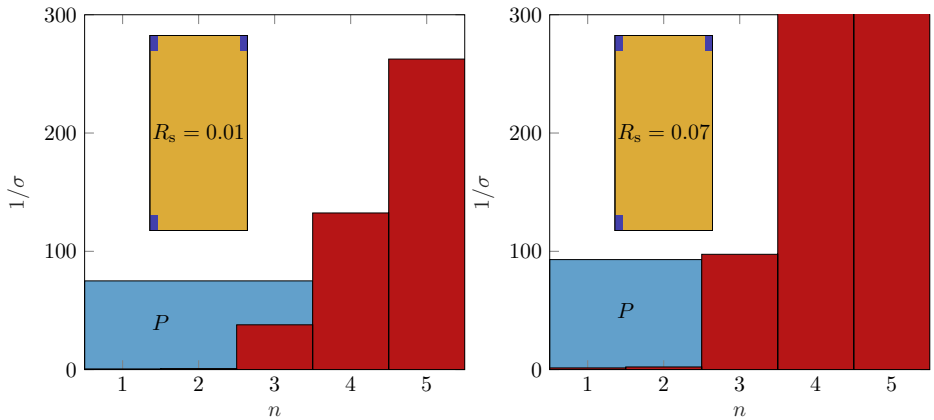

Figure 5: A schematic illustration of water-filling for a plate of size $ka = 0.06$, $\ell \times \ell/2$ with surface resistance $R_{\text{s}} = 0.01\,\Omega/\square$ (left) and $R_{\text{s}} = 0.07\,\Omega/\square$ (right) fed by three sub-regions. The green bars illustrate the loss in each mode. The blue area P represents the total signal strength the system is fed with.

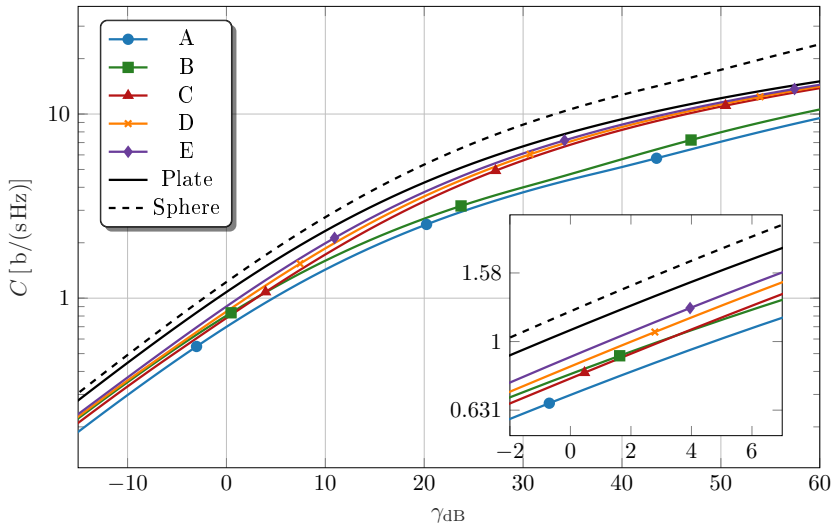

Figure 6: The optimal spectral efficiency solved with the dissipated power normalization for different SNR values for a $ka = 0.06$, $\ell \times \ell/2$ plate, its circumscribing sphere, and the sub-region configurations from Fig. 4. The required radiation efficiency is $\eta = 0.5$.

4.3 Optimal Spectral Efficiency

The optimization problem in (9) is normalized to the radiated power. However, this is only one way of normalizing the power fed to the structure. In App. D the derivation is carried out for the problem normalized to the dissipated power, *i.e.*, changing $\mathbf{R}_{\mathrm{r}}$ in (9) to $\mathbf{R}_{\mathrm{r}} + \mathbf{R}_{\Omega}$, see [5]. The resulting optimized channel is described by (16), but with a more complex dependence on the material parameters. This includes the losses in the structure in the normalization and therefore shifts the results. Notably this normalization shifts the dependence on the SNR γ. When the problem is normalized to radiated power all considered permutations of the same structure produces the same spectral efficiency for low SNR values. This is due to the fact that the power lost in resistive losses is not limited as long as the power radiated to the far-field is the same.

In Fig. 6 the problem normalized to dissipated power has been solved for a $ka = 0.06$, $\ell \times \ell/2$ plate and its circumscribing sphere. Here, the difference between the different sub-regions is visible. The differences in spectral efficiency corresponds to the difference in mode strength shown in Fig. 4. In the inset we can see the point where case B (diagonally opposed sub-regions) and case C (sub-regions on the same side of the plate) cross, around $\gamma_{\mathrm{dB}} = 3.5$. This corresponds to the point where the second order mode, more effectively induced by case C, see Fig. 4, starts to be profitable to excite. For high SNR values we see that the curves from the plate converge to two distinct groups, one containing the configurations

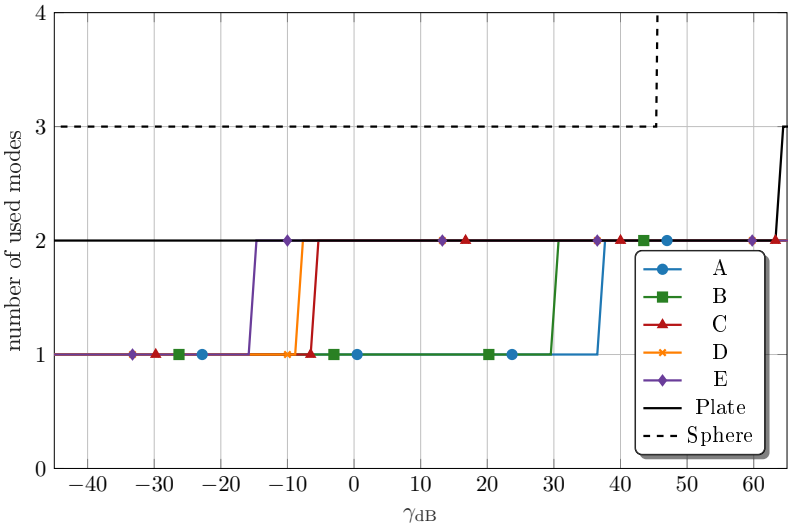

Figure 7: The number of modes used to induce optimal spectral efficiency with normalized dissipated power for different SNR values for a $ka = 0.06$, $\ell \times \ell/2$ plate, its circumscribing sphere, and the sub-region configurations from Fig. 4.

that effectively induce the two first modes, and one with cases A and B which only effectively induce the first mode. The optimal spectral efficiency of the circumscribing sphere has been plotted as a reference. The number of modes that the different cases induce is plotted in Fig. 7. It can be seen that cases C, D, and E induce the second order mode at much lower SNR values than cases A and B. Interestingly, case C starts to induce the second mode around 8 dB before its spectral efficiency passes case B in Fig. 6.

The restriction in (9) can equivalently be expressed as a requirement on the radiation efficiency η, see (10), of the antenna. In Fig. 8, the optimization problem (9) has been solved normalized to radiated power for different required radiation efficiencies. It can be seen that all sub-region orientations except for cases A and B almost fulfill the maximum spectral efficiencies for all radiation efficiencies before their cut-offs. The cut-offs correspond to radiation efficiencies where a solution is no longer feasible. From this it is possible to infer that two or three cleverly placed regions is enough to induce all available spectral efficiency for a $ka = 0.06$ plate. Interestingly case C (two regions on the same side of the plate) has an earlier cut-off than case B (two diagonally opposed regions) even though case C outperforms B for lower radiation efficiency requirements. This most likely corresponds to the slightly higher mode strength of the first mode for case B seen in Fig. 4. For this plate the optimal spectral efficiency of the sphere illustrates that the plate bound is much tighter for planar structures than that of the circumscribing sphere. In Fig. 9 the same optimization problem has been solved for a slightly larger $ka = 0.56$ plate. Here it can be seen that the

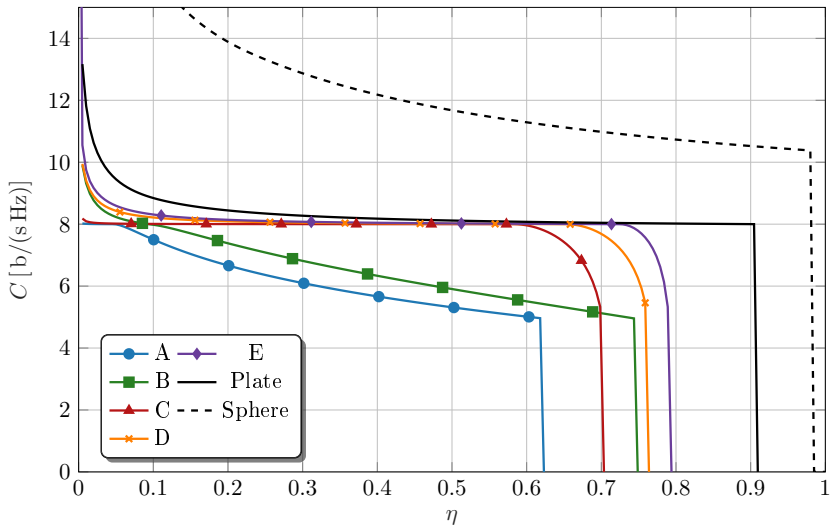

Figure 8: The optimal spectral efficiency with normalized radiated power for a $ka = 0.06$, $\ell \times \ell/2$ plate, its circumscribing sphere, and the sub-region cases in Fig. 4 for different required radiation efficiencies. The SNR is fixed to $\gamma = 30$.

different sub-region configurations start to seperate in terms of performance. It is no longer possible to induce the maximal spectral efficiency of the plate with just a few sub-regions.

4.4 Mode Availability

The examples in Sec. 4.1, 4.2, 4.3 have concerned small structures. The smaller sizes accentuate the availability of the lower order modes. When the size of the structure starts to grow in terms of wavelength a plethora of modes become effective, *i.e.*, have high associated eigenvalues. Through solving the eigenvalue problem (17) the number of viable modes, ϱ_{eff}, can be defined as those with an eigenvalue greater than 1. This is seen as when the excitation of the mode does not accrue more losses. Since (17) depends on the geometry of the structure it is possible to analyze different shapes and study how many modes they have available. However, it is intuitive that shapes with greater surface area will induce more modes. To understand if these shapes are actually inducing these extra modes efficiently per area the number of modes can be normalized to the natural number of degrees of freedom for that area [19, 24]. That number is defined as

$$2L(L+2) \approx 2ka(ka+2) \to 2(ka)^2\,,\; ka \to \infty, \tag{19}$$

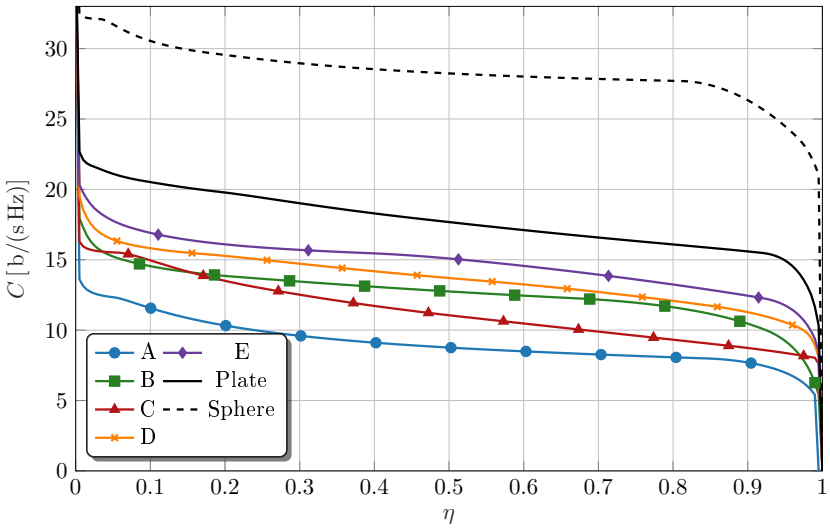

Figure 9: The optimal spectral efficiency with a normalized radiated power for a $ka = 0.56$, $\ell \times \ell/2$ plate, its circumscribing sphere, and the sub-region cases in Fig. 4 for different required radiation efficiencies. The SNR is fixed to $\gamma = 30$.

for a sphere [18]. This term can be rewritten in terms of the area of the sphere A,

$$2(ka)^2 = \frac{k^2 A}{2\pi} = \frac{2\pi A}{\lambda^2}. \tag{20}$$

For the analysis of different shapes presented in Fig. 10 the degrees of freedom for each shape has been calculated by (20) using the surface area of each geometry. We can see that the curves are divided into two distinct groups, the three dimensional shapes A, B, and C, and the two dimensional D and E. This metric shows that a shape such as a cylinder induces modes almost as efficiently per area as a sphere. By arbitrarily permuting the surface of a shape to increase its area, such as for the cylinder F, we can see that the efficiency does not increase with increased area. In fact the efficiency of this shape is much lower. It is reasonable to conclude that convex shapes with maximum area, such as the sphere, will be able to induce the greatest number of modes efficiently. The jagged jumps in the curves are due to the fact that the efficiency of modes is not continuously distributed, *e.g.*, see Fig. 3 where there is a significant jump from the first two modes of the plate to the higher order modes. The consequences of this is that the number of efficient modes is monotonically increasing with frequency, but when it is normalized with the wavelength, as in Fig. 10, discrete jumps will occur when new groups of modes become available. For closed shapes, such as the sphere, the internal resonances produce numerical difficulties in MoM and therefore reduce the number of efficient radiation modes for certain sizes.

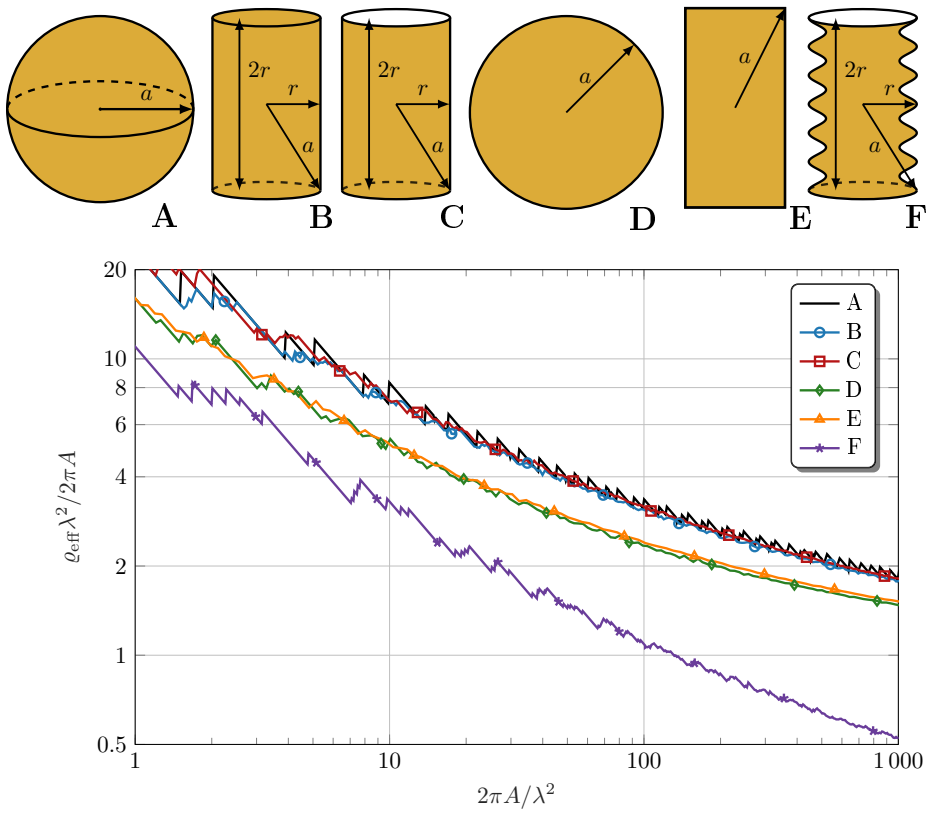

Figure 10: The number of viable modes, ϱ_{eff}, normalized to their natural number of degrees of freedom for different shapes. This is plotted against the surface area normalized to wavelength, see (20). The surface resistance of the shapes is $R_{\text{s}} = 0.01\,\Omega/\square$.

5 Conclusions

In this paper a closed form expression based on water-filling and radiation modes for calculating an upper bound on the optimal spectral efficiency for an arbitrary shape, constrained by the radiation efficiency, was presented. It was illustrated that the radiation modes play an important part in the optimal channel distribution. The strength and availability of the radiation modes were studied for several shapes including a plate, disc, cylinder, and sphere. Through this analysis it was shown that it is possible to excite currents producing optimal spectral efficiency for a plate using only a few small sub-regions. The number of effective modes for large shapes was investigated, and it was illustrated that cylindrical shapes produce roughly as many effective modes per surface area as a sphere.

It remains as an interesting future prospect to formulate similar solutions for

different constraining quantities, such as the Q-factor.

Appendix A Spherical Wave Matrix

The elements of the loss less impedance matrix are calculated by the integral

$$Z_{pq} = \mathrm{j}kZ_0 \int_\Omega \int_\Omega \boldsymbol{\psi}_p(\boldsymbol{r}_1) \cdot \mathbf{G}(\boldsymbol{r}_1, \boldsymbol{r}_2) \cdot \boldsymbol{\psi}_q(\boldsymbol{r}_2)\, \mathrm{d}A_1\, \mathrm{d}A_2, \tag{21}$$

where Z_0 is the free wave impedance, Ω is the source region, $\boldsymbol{\psi}_p$ and $\boldsymbol{\psi}_q$ are the basis and test functions on the antenna, and $\mathrm{d}A$ denotes the area element integrated over [4]. The Greens dyadic inside of this expression can be written as a product between out-going and regular spherical vector waves. The radiation matrix can be found by taking $\mathbf{R} = \mathrm{Re}(\mathbf{Z})$. By taking the real value of (21) both of the spherical vector waves become regular and it is possible to split the double integral into two identical integrals,

$$S_{\alpha p} = k\sqrt{Z_0} \int_\Omega \boldsymbol{\psi}_p(\boldsymbol{r}) \cdot \boldsymbol{u}_\alpha^{(1)}(k\boldsymbol{r})\, \mathrm{d}A, \tag{22}$$

where $\boldsymbol{u}_\alpha^{(1)}$ are the regular spherical vector waves [29]. Those integrals produce a matrix denoted as $\mathbf{S}$ which is the matrix connecting the basis functions in Ω to the spherical modes in the far-field. The radiation matrix can thus be decomposed as $\mathbf{R}_\mathrm{r} = \mathbf{S}^\mathrm{H}\mathbf{S}$.

Appendix B SVD of the New Channel Matrix

The singular values of a matrix can be calculated by taking the positive square root of the eigenvalues of the matrix times itself, $(\mathrm{eig}(\widetilde{\mathbf{H}}\widetilde{\mathbf{H}}^\mathrm{H}))^{1/2}$. By expanding the channel matrix to its component matrices,

$$\mathrm{eig}(\mathbf{S}\mathbf{B}^{-1}\mathbf{B}^{-\mathrm{H}}\mathbf{S}^\mathrm{H}) = \mathrm{eig}(\mathbf{S}\mathbf{R}_\nu^{-1}\mathbf{S}^\mathrm{H}), \tag{23}$$

it can be seen that $\mathbf{R}_\nu^{-1} = (1+\nu)(\frac{1}{\delta}\mathbf{R}_\Omega + \nu\mathbf{R}_\mathrm{r})^{-1}$ needs to be determined independent of ν. Due to their good properties, it is possible to decompose both $\mathbf{R}_\Omega$ and $\mathbf{R}_\mathrm{r}$ into more manageable matrices. Let's start with $\mathbf{R}_\mathrm{r}$, this matrix is the real valued part of the MoM impedance matrix $\mathbf{Z}$. It is possible to decompose $\mathbf{R}_\mathrm{r}$ as a multiplication between two instances of the $\mathbf{S}$ matrix, $\mathbf{R}_\mathrm{r} = \mathbf{S}^\mathrm{H}\mathbf{S}$, see Appendix A. The loss matrix can be decomposed using a Cholesky factorization $\mathbf{R}_\Omega = \boldsymbol{\Upsilon}^\mathrm{H}\boldsymbol{\Upsilon}$. Multiplying the two decomposed matrices together, $\mathbf{C} = \mathbf{S}\boldsymbol{\Upsilon}^{-1}$, the expression in (23) can be written as

$$\begin{aligned}\mathbf{S}\mathbf{R}_\nu^{-1}\mathbf{S}^\mathrm{H} &= (1+\nu)\mathbf{C}(\delta^{-1} + \nu\mathbf{C}^\mathrm{H}\mathbf{C})^{-1}\mathbf{C}^\mathrm{H} \\ &= (1+\nu)\mathbf{U}\boldsymbol{\Sigma}(\delta^{-1} + \nu\boldsymbol{\Sigma}^2)^{-1}\boldsymbol{\Sigma}\mathbf{U}^\mathrm{H}\end{aligned} \tag{24}$$

where an SVD has been taken on $\mathbf{C} = \mathbf{U}\mathbf{\Sigma}\mathbf{V}^{\mathrm{H}}$. Putting this back into the eigenvalue problem (23) a closed form expression can be formed for its solution,

$$\mathrm{eig}(\mathbf{S}\mathbf{R}_{\nu}^{-1}\mathbf{S}^{\mathrm{H}}) = \frac{(1+\nu)\varrho_n}{\delta^{-1}+\nu\varrho_n}, \tag{25}$$

where ϱ_n are the eigenvalues of the generalized eigenvalue problem,

$$\mathbf{R}_{\mathrm{r}}\mathbf{I}_n = \varrho_n\mathbf{R}_{\Omega}\mathbf{I}_n. \tag{26}$$

The solutions to this eigenvalue problem are known as radiation modes [27]. These are related to the singular values of the matrix $\mathbf{C}$ as,

$$\mathrm{svd}(\mathbf{S}\mathbf{\Upsilon}^{-1}) = (\mathrm{eig}(\mathbf{S}\mathbf{R}_{\Omega}^{-1}\mathbf{S}^{\mathrm{H}}))^{1/2} = (\mathrm{eig}(\mathbf{R}_{\mathrm{r}}, \mathbf{R}_{\Omega}))^{1/2} = \varrho_n^{1/2}. \tag{27}$$

It is evident that one of the main contributions to the singular values of the optimal channel are these radiation modes. In fact, the only other part of (25) is a requirement on dissipation factor δ. This is a parameter which the designer does not, in general, have control over. However, the strength of the radiation modes ϱ_n depend on the geometry of the structure, which is controllable.

Appendix C ν Interval

The linear combination of the two conditions in (9) are valid for values of ν that ensure that the resulting matrix $\mathbf{R}_{\nu}$ is positive semidefinite. Since both of its constituent matrices are positive definite this implies that $\nu > \nu_0$. The lower bound can be established by studying the eigenvalue problem in (16),

$$\frac{\varrho_n(1+\nu)}{\delta^{-1}+\nu\varrho_n} \geq 0, \tag{28}$$

ϱ_n is always positive since it is a generalized eigenvalue of two positive semidefinite matrices, therefore the numerator is positive as long as $\nu > -1$. δ and R_{s} are positive constants. Therefore we can study the sign of the denominator

$$\delta^{-1}+\nu\varrho_n \geq 0, \tag{29}$$

giving

$$\nu \geq -\frac{1}{\delta\varrho_n}, \tag{30}$$

which provides two lower limits to the interval. The greatest of the two will provide the limit, *i.e.*, $\nu_0 = \max\{-1, -1/(\delta\varrho_n)\}$.

Appendix D Dissipated Power Normalization

We can alternatively choose to normalize (9) to dissipated power instead of radiated power. This gives the following optimization problem

$$\begin{aligned} \text{maximize} \quad & \log_2 \det(\mathbf{1} + \gamma' \mathbf{S}\mathbf{P}\mathbf{S}^{\mathrm{H}}) \\ \text{subject to} \quad & \mathrm{Tr}(\mathbf{R}_\Omega \mathbf{P}) \leq 1 - \eta \\ & \mathrm{Tr}((\mathbf{R}_\mathrm{r} + \mathbf{R}_\Omega)\mathbf{P}) = 1 \\ & \mathbf{P} \succeq \mathbf{0}. \end{aligned} \tag{31}$$

Combining the two conditions gives,

$$\mathrm{Tr}\left(\left(\frac{1}{1-\eta}\mathbf{R}_\Omega + \nu(\mathbf{R}_\mathrm{r} + \mathbf{R}_\Omega)\right)\mathbf{P}\right) = 1 + \nu \tag{32}$$

which can be simplified by the introduction of a new matrix, as in (12),

$$\mathbf{R}_\nu = \frac{1}{1+\nu}\left(\frac{1}{1-\eta}\mathbf{R}_\Omega + \nu(\mathbf{R}_\mathrm{r} + \mathbf{R}_\Omega)\right). \tag{33}$$

In this case the eigenvalue problem is calculated as in (25) but replacing δ with

$$\frac{1-\eta}{1+\nu(1-\eta)}. \tag{34}$$

The lower limit on ν is thus calculated as

$$\frac{1+\nu(1-\eta)}{1-\eta} + \nu\varrho_n \geq 0, \tag{35}$$

where we can multiply by the denominator since $0 \leq (1-\eta) \leq 1$ because the radiation efficiency exists in the interval $0 \leq \eta \leq 1$. This gives, after simplification,

$$\nu(1-\eta)(\varrho_n + 1) + 1 \geq 0, \tag{36}$$

which provides a lower limit for ν,

$$\nu \geq -\frac{1}{(1-\eta)(\varrho_n + 1)}, \tag{37}$$

or $\nu > -1$ as concluded in App. C.

Appendix E Sub-Regions

In order to simulate embedded antennas the antenna problem must be reformulated in the currents that are controlled [14]. Consider the MoM matrix formulation $\mathbf{Z}\mathbf{I} = \mathbf{V}$, divide it into sub-matrices related to the controlled currents, denoted to subscript a, and induced currents, denoted by subscript g,

$$\begin{pmatrix} \mathbf{Z}_{\mathrm{aa}} & \mathbf{Z}_{\mathrm{ag}} \\ \mathbf{Z}_{\mathrm{ga}} & \mathbf{Z}_{\mathrm{gg}} \end{pmatrix} \begin{pmatrix} \mathbf{I}_\mathrm{a} \\ \mathbf{I}_\mathrm{g} \end{pmatrix} = \begin{pmatrix} \mathbf{V}_\mathrm{a} \\ \mathbf{0} \end{pmatrix}, \tag{38}$$

where $\mathbf{Z}_{\mathrm{ag}}$ connects the controlled region to the induced region, and $\mathbf{Z}_{\mathrm{ga}}$ connects the induced region to the controlled region. The right hand side is only non-zero for the controlled region. The second equation is used to express the induced currents in terms of the controlled ones,

$$\mathbf{I}_{\mathrm{g}} = -\mathbf{Z}_{\mathrm{gg}}^{-1}\mathbf{Z}_{\mathrm{ga}}\mathbf{I}_{\mathrm{a}} = \mathbf{Z}_{\mathrm{t}}\mathbf{I}_{\mathrm{a}}. \tag{39}$$

The MoM matrices of the problem can now be reformulated into forms which only act on controlled currents. Take the Gram matrix $\mathbf{\Psi}$ as an example,

$$\begin{aligned}\mathbf{I}_{\mathrm{a}}^{\mathrm{H}}\mathbf{\Psi}\mathbf{I}_{\mathrm{a}} &= \mathbf{I}_{\mathrm{a}}^{\mathrm{H}}\mathbf{\Psi}_{\mathrm{aa}}\mathbf{I}_{\mathrm{a}} + \mathbf{I}_{\mathrm{a}}^{\mathrm{H}}\mathbf{\Psi}_{\mathrm{ag}}\mathbf{I}_{\mathrm{g}} + \mathbf{I}_{\mathrm{g}}^{\mathrm{H}}\mathbf{\Psi}_{\mathrm{ga}}\mathbf{I}_{\mathrm{a}} + \mathbf{I}_{\mathrm{g}}^{\mathrm{H}}\mathbf{\Psi}_{\mathrm{gg}}\mathbf{I}_{\mathrm{g}} \\ &= \mathbf{I}_{\mathrm{a}}^{\mathrm{H}}(\mathbf{\Psi}_{\mathrm{aa}} + 2\,\mathrm{Re}\{\mathbf{\Psi}_{\mathrm{ag}}\mathbf{Z}_{\mathrm{t}}\} + \mathbf{Z}_{\mathrm{t}}^{\mathrm{H}}\mathbf{\Psi}_{\mathrm{gg}}\mathbf{Z}_{\mathrm{t}})\mathbf{I}_{\mathrm{a}} = \mathbf{I}_{\mathrm{a}}^{\mathrm{H}}\mathbf{\Psi}_{\mathrm{p}}\mathbf{I}_{\mathrm{a}},\end{aligned} \tag{40}$$

where $\mathrm{Re}\{\cdot\}$ is defined as,

$$\mathrm{Re}\{\mathbf{A}\} = \frac{\mathbf{A} + \mathbf{A}^*}{2}. \tag{41}$$

Similarly the $\mathbf{S}$ matrix connecting the currents to the spherical waves in the far-field can be rewritten as,

$$\mathbf{S}^{\mathrm{H}}\mathbf{I} = \mathbf{S}_{\mathrm{a}}^{\mathrm{H}}\mathbf{I}_{\mathrm{a}} + \mathbf{S}_{\mathrm{g}}^{\mathrm{H}}\mathbf{I}_{\mathrm{g}} = \mathbf{S}_{\mathrm{a}}^{\mathrm{H}}\mathbf{I}_{\mathrm{a}} + \mathbf{S}_{\mathrm{g}}^{\mathrm{H}}\mathbf{Z}_{\mathrm{t}}\mathbf{I}_{\mathrm{a}} = \mathbf{S}_{\mathrm{p}}^{\mathrm{H}}\mathbf{I}_{\mathrm{a}}. \tag{42}$$

References

[1] S. P. Boyd and L. Vandenberghe. *Convex Optimization*. Cambridge Univ. Pr., 2004.

[2] M. Capek, M. Gustafsson, and K. Schab. Minimization of antenna quality factor. *IEEE Trans. Antennas Propag.*, **65**(8), pp. 4115–4123, 2017.

[3] Y. Chen and C.-F. Wang. *Characteristic Modes: Theory and Applications in Antenna Engineering*. John Wiley & Sons, 2015.

[4] W. C. Chew, M. S. Tong, and B. Hu. *Integral Equation Methods for Electromagnetic and Elastic Waves*, volume 12. Morgan & Claypool, 2008.

[5] C. Ehrenborg and M. Gustafsson. Fundamental bounds on MIMO antennas. *IEEE Antennas Wireless Propag. Lett.*, **17**(1), pp. 21–24, Jan. 2018.

[6] M. Franceschetti, O. Dousse, D. N. C. Tse, and P. Thiran. Closing the gap in the capacity of wireless networks via percolation theory. *IEEE Trans. Inf. Theory*, **53**(3), pp. 1009–1018, Mar. 2007.

[7] M. Franceschetti, M. D. Migliore, and P. Minero. The capacity of wireless networks: Information-theoretic and physical limits. *IEEE Trans. Inf. Theory*, **55**(8), pp. 3413–3424, Aug. 2009.

[8] M. Franceschetti. *Wave Theory of Information*. Cambridge University Press, 2017.

[9] B. N. Getu and J. B. Andersen. The MIMO cube - a compact MIMO antenna. *IEEE Trans. Wireless Communications*, **4**(3), pp. 1136–1141, 2005.

[10] A. A. Glazunov, M. Gustafsson, and A. Molisch. On the physical limitations of the interaction of a spherical aperture and a random field. *IEEE Trans. Antennas Propag.*, **59**(1), pp. 119–128, 2011.

[11] M. Grant and S. Boyd. CVX: Matlab software for disciplined convex programming, version 2.1. http://cvxr.com/cvx, Dec. 2018.

[12] F. K. Gruber and E. A. Marengo. New aspects of electromagnetic information theory for wireless and antenna systems. *IEEE Trans. Antennas Propag.*, **56**(11), pp. 3470–3484, Nov. 2008.

[13] M. Gustafsson and S. Nordebo. On the spectral efficiency of a sphere. *Prog. Electromagn. Res.*, **67**, pp. 275–296, 2007.

[14] M. Gustafsson and S. Nordebo. Optimal antenna currents for Q, superdirectivity, and radiation patterns using convex optimization. *IEEE Trans. Antennas Propag.*, **61**(3), pp. 1109–1118, 2013.

[15] M. Gustafsson, D. Tayli, C. Ehrenborg, M. Cismasu, and S. Nordebo. Antenna current optimization using MATLAB and CVX. *FERMAT*, **15**(5), pp. 1–29, 2016.

[16] M. Gustafsson, D. Tayli, and M. Cismasu. *Physical bounds of antennas*, pp. 1–32. Springer-Verlag, 2015.

[17] J.-M. Hannula, T. O. Saarinen, A. Lehtovuori, J. Holopainen, and V. Viikari. Tunable eight-element MIMO antenna based on the antenna cluster concept. *arXiv preprint arXiv:1808.07755*, 2018.

[18] R. F. Harrington. *Time Harmonic Electromagnetic Fields*. McGraw-Hill, New York, NY, 1961.

[19] S. Hu, F. Rusek, and O. Edfors. The potential of using large antenna arrays on intelligent surfaces. In *2017 IEEE 85th Vehicular Technology Conference (VTC Spring)*, pp. 1–6, Jun. 2017.

[20] L. Jelinek and M. Capek. Optimal currents on arbitrarily shaped surfaces. *IEEE Trans. Antennas Propag.*, **65**(1), pp. 329–341, 2017.

[21] L. Kundu. *Information-Theoretic Limits on MIMO Antennas*. PhD thesis, North Carolina State University, 2016.

[22] H. Li, Z. Miers, and B. K. Lau. Design of orthogonal MIMO handset antennas based on characteristic mode manipulation at frequency bands below 1 GHz. *IEEE Trans. Antennas Propag.*, **62**(5), pp. 2756–2766, 2014.

[23] M. D. Migliore. On the role of the number of degrees of freedom of the field in MIMO channels. *IEEE Trans. Antennas Propag.*, **54**(2), pp. 620–628, Feb 2006.

[24] M. Migliore. On electromagnetics and information theory. *IEEE Trans. Antennas Propag.*, **56**(10), pp. 3188–3200, Oct. 2008.

[25] A. F. Molisch. *Wireless Communications*. John Wiley & Sons, New York, NY, second edition, 2011.

[26] A. Paulraj, R. Nabar, and D. Gore. *Introduction to Space-Time Wireless Communications*. Cambridge University Press, Cambridge, 2003.

[27] K. R. Schab. *Modal analysis of radiation and energy storage mechanisms on conducting scatterers*. PhD thesis, University of Illinois at Urbana-Champaign, 2016.

[28] P. S. Taluja and B. L. Hughes. Fundamental capacity limits on compact MIMO-OFDM systems. In *IEEE International Conference on Communications (ICC)*, pp. 2547–2552, Jun. 2012.

[29] D. Tayli, M. Capek, L. Akrou, V. Losenicky, L. Jelinek, and M. Gustafsson. Accurate and efficient evaluation of characteristic modes. *IEEE Trans. Antennas Propag.*, pp. 1–10, 2018.

Analysis of Energy Modes for MIMO Antennas

Casimir Ehrenborg, Mats Gustafsson, and Miloslav Capek

Paper IV

Preprint published as: C. Ehrenborg, M. Gustafsson, and M. Capek, "Analysis of Energy Modes for MIMO Antennas," Technical Report TEAT-7266, Electromagnetic Theory Department of Electrical and Information Technology, 2019.

Abstract

The optimal spectral efficiency of MIMO antennas in an ideal line-of-sight channel is investigated when bandwidth requirements are placed on the channel. By posing the problem as a convex optimization problem restricted by the stored energy a semi-analytical expression is formed for its solution. It is shown that this solution is solely dependent on energy modes of the antenna. The ability to induce these modes by utilizing only a few sub-regions of the antenna is analyzed and compared to the full plate. The position of these regions is also investigated when they are raised above the ground plane. The performance of these cases is illustrated by calculating the optimal spectral efficiency of the unrestricted problem and plotting how much is lost when extra constraints are added. It is demonstrated that the spatial diversity of the controlled regions correlates with the number of significant energy modes.

1 Introduction

Design of MIMO antennas is based on effectively exciting discrete communication channels with low correlation [18], in so doing the transmittable bit-rate, or capacity, is increased. A proposed strategy for accomplishing this is to design the antennas such that they effectively induce modes with orthogonal radiation patterns, such as characteristic modes, of the structure which they are embedded in [15–17]. Previously, a method for calculating the optimal performance bound of a MIMO antenna in an ideal channel was presented in [4, 5]. This upper bound serves as a measure of how well a certain configuration is utilizing the total available performance of the design region [5].

Electrically small antennas suffer from a degradation in possible performance as their size is reduced compared to the wavelength. Some of the parameters where this is most evident are radiation efficiency, directivity, and bandwidth [10, 12, 22, 23]. It was shown in [5] that restricting the radiation efficiency of the antenna does not necessarily restrict embedded regions from inducing the full available performance of the entire structure. This could be achieved by analyzing the modes that contribute the most to the performance of the antenna and exciting them effectively. This observation motivates further investigations of the maximum spectral efficiency for a channel with restricted bandwidth, a scenario typically valid in the electrically small regime.

Bandwidth can be estimated, for electrically small systems, through the quotient of the energy stored in a system over the energy dissipated by it [19]. This relation produces accurate estimations and is equal to the Q-factor for single feed, single resonance systems [25]. This classical relation does not hold for multi-port systems, such as MIMO antennas, however, for each individual port feeding a MIMO antenna we have a well defined Q-factor calculated from the stored energy of the current induced by that port [21]. All of the currents these ports induce create a total current distribution on the antenna. Restricting the stored energy calculated from the total current serves as a relaxed problem to limiting

the stored energy of each port. In this way limiting the stored energy of the total current density implicitly imposes a bandwidth requirement on the system.

The ports of a MIMO antenna induce a current distribution across the antenna, optimizing the inputs to those ports is a very restricted way of manipulating the currents on the antenna. Optimizing the current distribution directly is a relaxed problem to optimizing the ports. This means that the optimal value of that optimization will always bound the initial problems solution, therefore providing a performance bound for the antenna. Current optimization is a method used for calculating the optimal performance of a design region by optimizing over the possible currents within that region [10]. These currents have the ability to express all possible solutions that could be created within the considered volume. By formulating the optimization problem as a convex problem the optimality of the solution is guaranteed, as by definition all local minima of a convex problem are also global minima [1]. Previously this method has been used to determine performance bounds for antennas in terms of, *e.g.*, Q-factor [10, 11, 13], efficiency [7, 14], directivity [9], and in multi-objective optimization such as spectral efficiency [4, 5] or trade-off between Q-factor and radiation efficiency [7]. For single feed, single resonance antennas these problems can be solved efficiently due to being expressed as quadratic forms. However, spectral efficiency (capacity), is evaluated based on the covariance of the current distribution and as such cannot be formulated as a quadratic form. The capacity expression creates a semi-definite optimization problem which has one order more of unknowns, making it computationally demanding to solve [4]. In [5] a method for solving such problems was introduced. By formulating a dual of the optimization problem [1] and utilizing the good properties of the matrices restricting it, it is possible to solve them semi-analytically.

In this letter the method from [5] is applied to an optimization problem restricted by the stored energy of an antenna. A convex optimization problem for the maximization of the spectral efficiency in the covariance of the current distribution is stated and solved in Section 2 restricted by the stored energy and radiated power of the structure. This optimization problem is a multi-criteria optimization problem, that forms a Pareto frontier between the spectral efficiency, stored energy, and SNR. The MIMO antenna is optimized in an ideal line-of-sight channel consisting of the spherical modes in the far-field [6, 8]. It is shown that the optimal channel is constructed from the set of modes maximizing radiated energy while minimizing stored energy, denoted here as energy modes [10]. In Section 3 this set of modes is used to analyze the ability of embedded antennas to effectively induce the available performance of the entire structure. The relationship between stored energy restriction and SNR is investigated for these antennas. Finally, regions situated above the ground plane region are considered, mimicking the way common cellphone antennas are designed and fed [24]. The position of these is considered in relation to the edge of the structure.

2 Theory

A MIMO system is described by

$$\mathbf{y} = \mathbf{H}\mathbf{x} + \mathbf{n}, \tag{1}$$

where $\mathbf{y}$ are the received signals, $\mathbf{H}$ is the channel matrix, $\mathbf{x}$ are the transmitted signals, and $\mathbf{n}$ is the noise density in each of the receivers [18]. In order to calculate optimal performance bounds for a MIMO antenna in an arbitrary scenario either the transceiver or receiver needs to be idealized. Here we choose to model the receiver as an idealized absorber perfectly matched to all spherical waves reaching the far-field, characterized as the spherical modes in the far-field. The diversity of the transmitted signal is measured as the diversity in the spherical modes. This configuration lets us bound the performance of one MIMO antenna in terms of its total transmitted power to the far-field [4–6, 8]. The currents induced across the antenna are modeled by MoM [2]. Instead of optimizing the ports inducing these currents, the currents themselves serve as the inputs to the MIMO system in (1).

The optimal spectral efficiency of a MIMO channel can be calculated by solving the optimization problem [5],

$$\begin{aligned} \text{maximize} \quad & \log_2 \det(\mathbf{1} + \frac{1}{N_0}\mathbf{S}\mathbf{P}\mathbf{S}^{\mathrm{H}}) \\ \text{subject to} \quad & \mathrm{Tr}(\mathbf{R}_{\mathrm{r}}\mathbf{P}) = P_{\mathrm{r}} \\ & \mathbf{P} \succeq 0, \end{aligned} \tag{2}$$

where N_0 is the noise spectral density, P_{r} is the radiated power, $\mathbf{S}$ is the channel matrix connecting the antenna to the spherical modes [6, 20], $\mathbf{P}$ is the covariance of the currents [4], and $\mathbf{R}_{\mathrm{r}} = \mathbf{S}^{\mathrm{H}}\mathbf{S}$ is the radiation matrix [2, 20]. Because none of the channels are penalized in this formulation, the optimal solution has equally allocated power [18]. Therefore, the optimal spectral efficiency converges to

$$\log_2 \det(\mathbf{1} + \gamma\mathbf{S}\mathbf{P}\mathbf{S}^{\mathrm{H}}) = M \log_2 \left(1 + \frac{P_{\mathrm{r}}}{M N_0}\right) \approx \frac{\gamma}{\log(2)}, \tag{3}$$

where M is the number of channels, log is the natural logarithm, and $\gamma = P_{\mathrm{r}}/N_0$ is the total SNR. This is the optimal unconstrained spectral efficiency. When adding any constraints or penalties to the channel or antenna we can measure how much is lost in comparison with this ideal spectral efficiency.

Additional constraints must be added to (2) in order to reflect realistic requirements put on the antenna design [4, 5]. Here we want to investigate how the

bandwidth affects the spectral efficiency and thus formulate the problem,

$$\begin{aligned} \text{maximize} \quad & \log_2 \det(\mathbf{1} + \gamma \mathbf{S}\mathbf{P}\mathbf{S}^{\mathrm{H}}) \\ \text{subject to} \quad & \mathrm{Tr}((\mathbf{X}_{\mathrm{e}} + \mathbf{X}_{\mathrm{m}})\mathbf{P}) \leq 2\frac{\omega W_{\mathrm{tot}}}{P_{\mathrm{r}}} \\ & \mathrm{Tr}(\mathbf{R}_{\mathrm{r}}\mathbf{P}) = 1 \\ & \mathbf{P} \succeq \mathbf{0}, \end{aligned} \tag{4}$$

where $\mathbf{X}_{\mathrm{e}}$ and $\mathbf{X}_{\mathrm{m}}$ are the stored electric and magnetic energy matrices, respectively, all equations have been normalized to the radiated power, unit radiated power is considered, ω is the angular frequency, and W_{tot} is the allowed stored energy. This stored energy converges to the Q-factor for single feed, single resonance systems at resonance [10]. However, for a multi-port system, such as a MIMO antenna, this problem is a semi-definite relaxation [1] of the problem where the stored energy is limited for each port feeding the antenna. This means that the solution to (4) will always be an upper bound to the problem limited by the individual stored energies of the ports.

The optimization problem (4) is solved by reformulating it in such a way that the constraints are included into the channel matrix [5]. If this is done (4) can be written in the same form as (2), with the difference that the channels are still penalized by their stored energy. A problem of this form can be solved by taking the singular value decomposition of its channel matrix, and performing water filling to find the optimal energy allocation over those singular values [18]. The water filling optimization is formulated as,

$$\begin{aligned} \text{maximize} \quad & \sum_{n=1}^{M} \log_2 \left(1 + a_n \gamma \sigma_n^2\right) \\ \text{subject to} \quad & \sum_{n=1}^{M} a_n = 1 \end{aligned} \tag{5}$$

where $a_n \geq 0$ is the power allocation fraction in each channel, and σ_n is the singular value of the corresponding channel. The maximum to this problem is easily found by iteratively filling each channel until it is more beneficial to fill the next instead [18].

The singular value decomposition of the channel matrix in (4) can be found by formulating a dual problem which is only restricted by one condition formed from an affine combination of the first two [1,5]. This solution method is reliant on the matrices present in (4) being positive semi-definite which ensures the problem to be convex. The matrices $\mathbf{X}_{\mathrm{e}}$ and $\mathbf{X}_{\mathrm{m}}$ are in general indefinite, however, it was shown in [10,19] that they are positive semi-definite when the electrical size of the considered structure is less than half-a-wavelength. By restricting our problems to that size it allows us to use the method presented in [5] to compute the singular

values of the optimal channel matrix. That method gives the singular values

$$\sigma_n^2 = \frac{w_n(1+\nu)}{\frac{P_\mathrm{r}}{2\omega W_\mathrm{tot}} + w_n\nu}, \tag{6}$$

where ν is the scalar combining the two conditions in (4), and w_n are the eigenvalues of a set of modes we call energy modes [10]. The energy modes are calculated through the generalized eigenvalue problem

$$\mathbf{R}_\mathrm{r}\mathbf{I}_n = w_n(\mathbf{X}_\mathrm{e} + \mathbf{X}_\mathrm{m})\mathbf{I}_n, \tag{7}$$

where $\mathbf{I}_n$ are the mode currents. These modes are similar to characteristic modes in the sense that they have the property of orthogonal radiation patterns. However, instead of being resonant across the structure they minimize the total stored energy in it. This has the effect of implicitly maximizing the bandwidth of the modes. Effectively inducing these modes improves the optimal channel (6), therefore increasing the optimal spectral efficiency. The amplitude of this set of modes is solely dependent on the geometry of the structure, *i.e.*, the design of the antenna.

3 Results

Antennas inside communication devices are in general much smaller than the total device size [24]. This means that only a sub-region is utilized to excite currents over the entire device that are used for communication. It is possible to solve for the optimum solution of (4) when controlling only a sub-region of the device by reformulating the problem in only the controlled currents of the sub-region [5]. This is interesting to investigate since bandwidth and stored energy are usually harshly punished by reducing the size of the structure. By studying the eigenvalues w_n for a few sub-region cases relative to the energy modes of the entire plate we can determine if it is possible to induce the full performance of the plate through them. In Fig. 1 we see that there is a considerable gap between the eigenvalue of the full plate compared to the sub-regions. This contrasts to the results in [5] where it was shown that, when restricting (4) by efficiency, it is possible to induce the entire structures available performance while only feeding a couple of small sub-regions. We can also see that the two diagonally placed elements in case B outperform the two elements in case C for all mode indexes except the second. This is similar to the case in [5] due to the first and second order modes being induced diagonally across the plate. Therefore the two diagonally situated sub-regions do not effectively induce the second mode across the opposite diagonal. The eigenvalues of the circumscribing spherical shell have been included as a reference, and we can see that they are significantly higher than those of the plate.

In Fig. 2 the optimal spectral efficiency loss, in comparison with the ideal (3), for the plate and its sub-regions presented in Fig. 1 is depicted as a function of

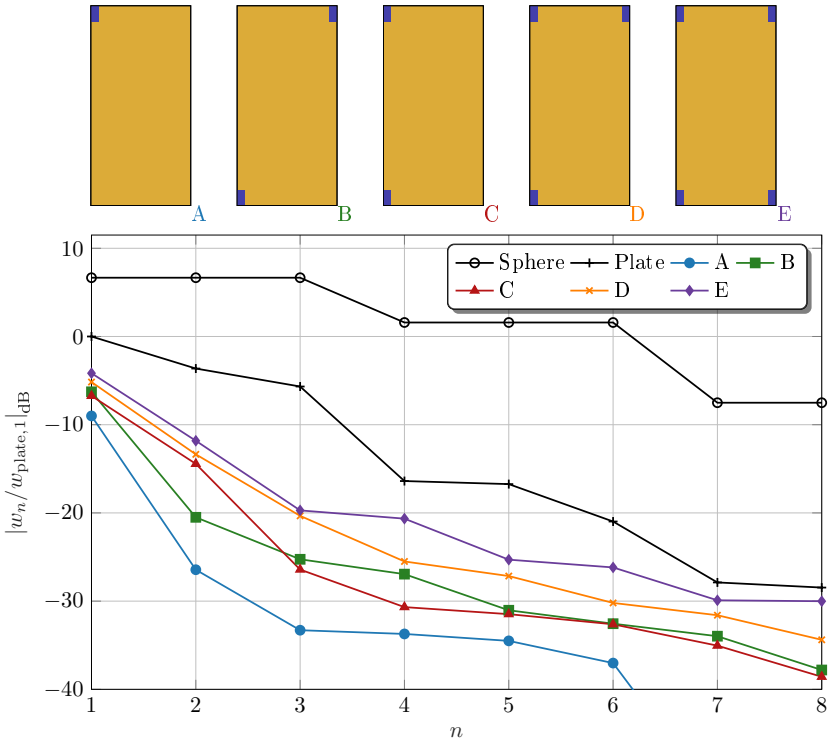

Figure 1: The eigenvalues w_n of a spherical shell, a rectangular plate with aspect ratio $2:1$, and several of its sub-region arrangements. All the eigenvalues have been normalized to the first energy mode of the full plate, the electrical size is $ka = 1$ with k being the wavenumber and a being radius of the smallest sphere circumscribing all the sources.

the maximum allowed stored energy. This Pareto-type curve delimits the feasible region of the problem and reveals that the capacity and the stored energy are strictly conflicting parameters. Here, it is evident that even with four sub-regions placed in the corner of the plate, as in case E, we are far from achieving the optimal spectral efficiency available to the entire plate. In contrast to the case studied in [5] that was restricted by efficiency, this effect remains the same when the size of the plate is reduced. Instead of narrowing the gap between the full plate and its sub-regions, as in [5], a reduction of size makes the sub-region solution unfeasible, due to their lower bound for stored energy increasing [3]. Therefore, we can conclude that the optimal performance of the embedded MIMO antennas is more restricted by the limited bandwidth than the requirements on radiation efficiency.

By picking a value of $\omega W_{\text{tot}}/P_{\text{r}} = 50$ where all sub-region solutions are feasible we can instead study the effect of the SNR on the optimal spectral efficiency

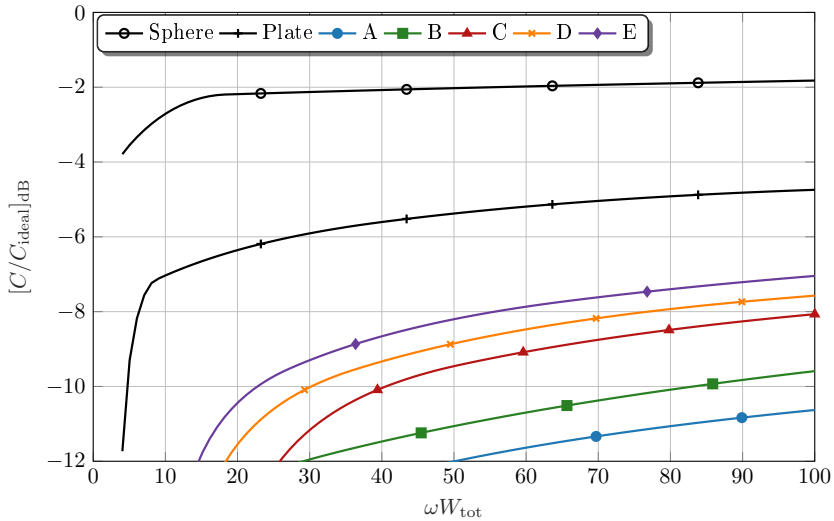

Figure 2: The optimal spectral efficiency loss in comparison to the ideal (3) for the $ka = 1$ spherical shell, plate with aspect ratio $2:1$, and its sub-regions presented in Fig. 1 for different stored energy restrictions. The SNR has been set to $\gamma = 10$.

loss. In Fig. 3 we see that all cases studied converge towards the ideal optimal spectral efficiency when the SNR γ is very small. This is due to the formulation of problem (4) where the radiated power is normalized. All different solutions radiate the same small amount of power at these values without any discernible difference. As SNR increases we see how the cases start to deviate. It is interesting to note that case C, from Fig. 1, outperforms case B, even though case B has a higher mode strength for all modes except the second one, indicating that the two first modes are the two most heavily utilized in this simulation. This has been verified by viewing the power allocation after optimization.

For many applications where embedded antennas are used, such as mobile phones, the antennas are not truly embedded inside the ground plane. Normally there is a substrate layer, or edge that the antennas have been designed upon [24]. In the top of Fig. 4 such a geometry, with regions raised above the ground plane, is illustrated. Here the gap between the regions and the ground plane has not been filled with any material. The placement of the regions has been done in accordance with the intuitive understanding for minimizing stored energy, *i.e.*, maximal charge separation, see Fig. 1. In Fig. 4 the performance of case E, with 4 regions, has been considered when the placement of the regions is shifted in from the edge. Here, it is possible to see the cost of moving away from the edge position considered in the other examples. By shifting incrementally we can see that we quickly loose a significant amount of performance. This effect may be due to the fact that currents need to flow around the outer edges of the regions

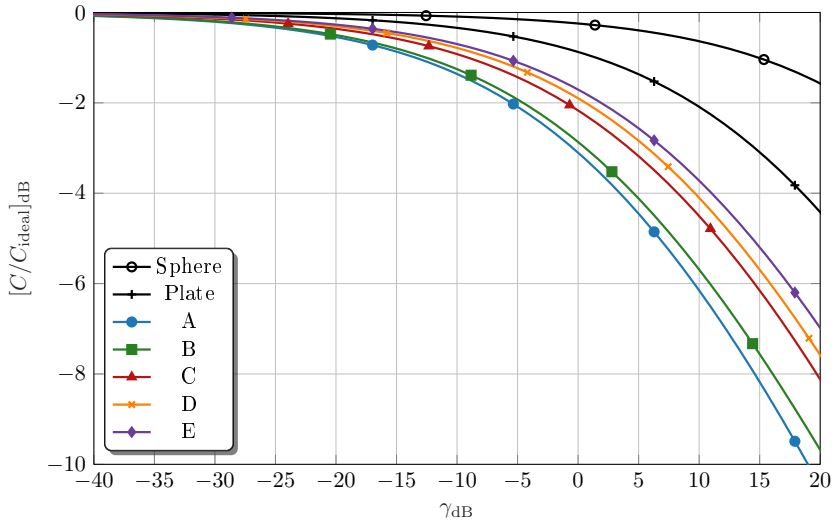

Figure 3: The optimal spectral efficiency loss in comparison to the ideal (3) for a spherical shell, a plate with aspect ratio 2 : 1 and its sub-regions presented in Fig. 1 for different SNR. The stored energy has been chosen as $\omega W_{\text{tot}}/P_{\text{r}} = 50$ and electrical size as $ka = 1$.

rather than being fed directly along the plate. In this case the regions are only connected to the ground plane on two edges, if all edges are connected the loss is even greater. Such a case is similar to when the regions are fully embedded within the ground plane. The raised regions can realize their solution for regions shifted more from the edge, but upon comparison of the case when the regions are placed on the edge, in Figs. 2 and 4, it is clear that the performance does not increase dramatically.

4 Conclusions

The optimal spectral efficiency bound of a MIMO antenna in an ideal channel has been considered when restricted by the stored energy. The Pareto-type bound has been illustrated in comparison to the degradation of the optimal spectral efficiency of the unrestricted problem. It has been shown that a set of modes known as energy modes serves as a useful design tool when analyzing performance of such antennas. However, due to the harsh penalties on stored energy when reducing the design region, it has been concluded that it is not possible to reach the full potential of the plate while only feeding it with a set of small sub-regions. The placement of these regions has also been analyzed, and it could be seen that the performance quickly deteriorated when they were moved away from the edge of the structure.

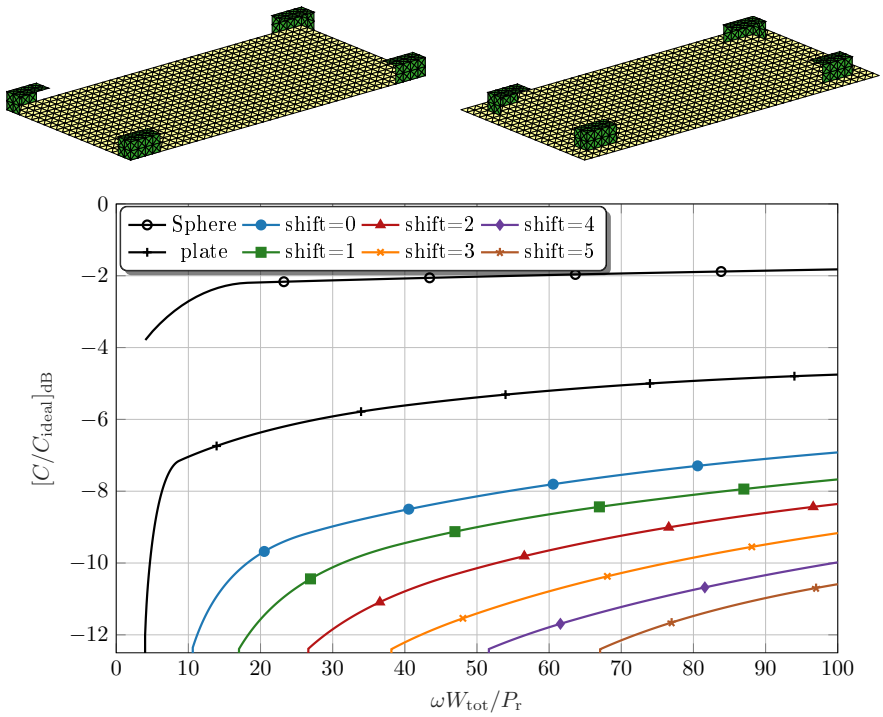

Figure 4: The optimal spectral efficiency loss compared to the ideal case for the $ka = 1$ spherical shell, plate with aspect ratio 2 : 1, and case E, present in Fig. 1 with its regions raised $L/20$ above the ground plane, as well as when those regions are shifted in a number of mesh cells towards the center as shown above. The restricting stored energy W_{tot} has been swept and the SNR has been set to $\gamma = 10$.

While out of the scope of this letter, this method has the potential to include statistical channel models and more realistic scenarios. The modal analysis could also be carried out on designed antennas to evaluate their adherence to the principals suggested here. Generalizing this method to include several different design parameters remains an interesting future prospect.

References

[1] S. P. Boyd and L. Vandenberghe. *Convex Optimization*. Cambridge Univ. Pr., 2004.

[2] W. C. Chew, M. S. Tong, and B. Hu. *Integral Equation Methods for Electromagnetic and Elastic Waves*, volume 12. Morgan & Claypool, 2008.

[3] M. Cismasu and M. Gustafsson. Antenna bandwidth optimization with sin-

gle frequency simulation. *IEEE Trans. Antennas Propag.*, **62**(3), pp. 1304–1311, 2014.

[4] C. Ehrenborg and M. Gustafsson. Fundamental bounds on MIMO antennas. *IEEE Antennas Wireless Propag. Lett.*, **17**(1), pp. 21–24, Jan. 2018.

[5] C. Ehrenborg and M. Gustafsson. Physical bounds and radiation modes for mimo antennas. Technical Report TEAT-7265, Electromagnetic Theory Department of Electrical and Information Technology, 2018.

[6] A. A. Glazunov, M. Gustafsson, and A. Molisch. On the physical limitations of the interaction of a spherical aperture and a random field. *IEEE Trans. Antennas Propag.*, **59**(1), pp. 119–128, 2011.

[7] M. Gustafsson, M. Capek, and K. Schab. Trade-off between antenna efficiency and Q-factor. *IEEE Trans. Antennas Propag.*, **67**(4), pp. 2482–2493, Apr. 2019.

[8] M. Gustafsson and S. Nordebo. On the spectral efficiency of a sphere. *Prog. Electromagn. Res.*, **67**, pp. 275–296, 2007.

[9] M. Gustafsson and S. Nordebo. Optimal antenna currents for Q, superdirectivity, and radiation patterns using convex optimization. *IEEE Trans. Antennas Propag.*, **61**(3), pp. 1109–1118, 2013.

[10] M. Gustafsson, D. Tayli, C. Ehrenborg, M. Cismasu, and S. Nordebo. Antenna current optimization using MATLAB and CVX. *FERMAT*, **15**(5), pp. 1–29, 2016.

[11] M. Gustafsson, D. Tayli, and M. Cismasu. *Physical bounds of antennas*, pp. 1–32. Springer-Verlag, 2015.

[12] R. C. Hansen. *Electrically Small, Superdirective, and Superconductive Antennas*. John Wiley & Sons, Hoboken, NJ, 2006.

[13] L. Jelinek and M. Capek. Optimal currents on arbitrarily shaped surfaces. *IEEE Trans. Antennas Propag.*, **65**(1), pp. 329–341, 2017.

[14] L. Jelinek, K. Schab, and M. Capek. The radiation efficiency cost of resonance tuning. *IEEE Trans. Antennas Propag.*, **66**(12), pp. 6716–6723, Dec. 2018. eprint arXiv: 1712.02613.

[15] H. Li, Z. Miers, and B. K. Lau. Design of orthogonal MIMO handset antennas based on characteristic mode manipulation at frequency bands below 1 GHz. *IEEE Trans. Antennas Propag.*, **62**(5), pp. 2756–2766, 2014.

[16] D. Manteuffel and R. Martens. A concept for MIMO antennas on small terminals based on characteristic modes. In *International Workshop on Antenna Technology (iWAT)*, 2011.

[17] Z. Miers, H. Li, and B. K. Lau. Design of bandwidth-enhanced and multi-band MIMO antennas using characteristic modes. *IEEE Antennas Wirel. Propag. Lett.*, **12**, pp. 1696–1699, 2013.

[18] A. Paulraj, R. Nabar, and D. Gore. *Introduction to Space-Time Wireless Communications*. Cambridge University Press, Cambridge, 2003.

[19] K. Schab, L. Jelinek, M. Capek, C. Ehrenborg, D. Tayli, G. A. Vandenbosch, and M. Gustafsson. Energy stored by radiating systems. *IEEE Access*, **6**, pp. 10553 – 10568, 2018.

[20] D. Tayli, M. Capek, L. Akrou, V. Losenicky, L. Jelinek, and M. Gustafsson. Accurate and efficient evaluation of characteristic modes. *IEEE Trans. Antennas Propag.*, pp. 1–10, 2018.

[21] G. A. E. Vandenbosch. Reactive energies, impedance, and Q factor of radiating structures. *IEEE Trans. Antennas Propag.*, **58**(4), pp. 1112–1127, 2010.

[22] J. Volakis, C. C. Chen, and K. Fujimoto. *Small Antennas: Miniaturization Techniques & Applications*. McGraw-Hill, New York, NY, 2010.

[23] H. A. Wheeler. Small antennas. *IEEE Trans. Antennas Propag.*, **23**(4), pp. 462–469, 1975.

[24] K.-L. Wong. *Planar Antennas for Wireless Communications*. John Wiley & Sons, New York, NY, 2003.

[25] A. D. Yaghjian and S. R. Best. Impedance, bandwidth, and Q of antennas. *IEEE Trans. Antennas Propag.*, **53**(4), pp. 1298–1324, 2005.

Energy Stored by Radiating Systems

Kurt Schab, Lukas Jelinek, Miloslav Capek, Casimir Ehrenborg,
Doruk Tayli, Guy A. E. Vandenbosch, and Mats Gustafsson

Paper V

Published as: K. Schab, L. Jelinek, M. Capek, C. Ehrenborg, D. Tayli, G.A.E. Vandenbosch, M. Gustafsson, "Energy Stored by Radiating Systems," *IEEE Access*, Vol. 6, pp. 10553–10568, IEEE, 2018.

Abstract

Though commonly used to calculate Q-factor and fractional bandwidth, the energy stored by radiating systems (antennas) is a subtle and challenging concept that has perplexed researchers for over half a century. Here, the obstacles in defining and calculating stored energy in general electromagnetic systems are presented from first principles as well as using demonstrative examples from electrostatics, circuits, and radiating systems. Along the way, the concept of unobservable energy is introduced to formalize such challenges. Existing methods of defining stored energy in radiating systems are then reviewed in a framework based on technical commonalities rather than chronological order. Equivalences between some methods under common assumptions are highlighted, along with the strengths, weaknesses, and unique applications of certain techniques. Numerical examples are provided to compare the relative margin between methods on several radiating structures.

1 Introduction

For many in the field of electromagnetics, stored energy is best known by its appearance in the definition of a time-harmonic system's Q-factor (quality factor, antenna Q, radiation Q) [47, 48],

$$Q = \frac{2\pi W_{\text{sto}}}{W_{\text{diss}}}, \tag{1}$$

from which an estimate of fractional bandwidth is available. In the above expression, W_{sto} and W_{diss} denote the cycle-mean stored and dissipated energies within the system, respectively. The dissipated energy is typically well defined and can be easily calculated, while in many cases the definition of stored energy is ambiguous. This issue is particularly troublesome in distributed and radiating systems, where there exists no consistent, physically-intuitive method of delineating the overlap between energy which is stored and that which is propagating. Analogous problems can be encountered in lumped circuits, where specific networks can be arbitrarily inserted to increase the total energy without altering the impedance characteristics as seen from a port. The first of two goals of this paper is to elucidate the challenges involved in defining stored energy within a general electromagnetic system. To do so, we draw upon examples of lumped circuits and radiating systems which exhibit the general issue of "unobservable energy states". Although this concept is somewhat abstract, it provides a consistent framework for understanding what makes defining stored energy in certain systems so difficult.

Because of the powerful relationship between fractional bandwidth and stored energy, many researchers have worked to rigorously define stored energy in an attempt to obtain bounds on the broadband behavior of systems. Of particular practical and historical importance is the study of stored energy in radiating systems, *i.e.*, antennas. Work in this area dates back over half a century and

has given rise to many unique (and sometimes controversial) interpretations and claims. One regime where most methods agree is in the quasi-static limit, *i.e.*, for small antennas. However, for problems involving larger antennas or antennas next to larger objects (*e.g.*, ground planes or human bodies), most methods disagree and there is no consensus on a definition of stored energy. In some cases, the similarities and differences between these existing approaches are clear, though in other instances the technical and philosophical connections between works from different eras are more subtle. The second goal of this paper is to provide a clear summary of the many previously published approaches to defining stored energy, with emphasis on works studying distributed and radiating systems. We aim to provide not a chronological history of this topic, but rather an organized guide to the major themes and concepts used in previous works.

The paper is organized as follows. In Section 2, we present a general definition for stored energy within an electromagnetic system using the concept of unobservable energy states. In Section 3, existing approaches to defining and calculating stored energy within radiating systems are summarized. Where applicable, the similarities and differences between these methods are highlighted, along with their strengths, weaknesses, and relation to the formal definition of stored energy given in Section 2. Analytical and numerical examples are presented in Section 4, giving both quantitative and qualitative insight into the relative results obtained by the methods outlined in Section 3. The paper concludes with a discussion of applications of certain methods in Section 5 and general conclusions in Section 6. Further details are provided on the classical definition of stored energy in Box 1, unobservable states in Boxes 2 and 3, and electrostatic energy in Box 4.

2 Definition and Physical Rationale of Stored EM Energy

The total energy of a dynamic system, see Box 1, represents a well-known and fundamental characteristic describing the energy stored in all of its degrees of freedom. By contrast, the observable part of total energy is a more subtle quantity typically defined in such a way that its value has a direct correspondence with the input / output relation of the system as seen by a fixed observer [89]. In lossless systems, these two quantities are equal due to the Foster's reactance theorem [43, Sec. 8-4], [11]. In general dissipative systems, however, they lose their relation due to the presence of states not observable from outside the system, see Boxes 2 and 3.

The energy supplied to a radiating system is converted into several different forms. Consider a radiator made of non-dispersive isotropic medium with permittivity ε, permeability μ and conductivity σ, which is placed in otherwise free space (effects induced by frequency dispersion are discussed in Appendix A). The radiator is enclosed within a volume V with bounding surface S, see Figure 1. Here we use, $\boldsymbol{\mathcal{E}}$ and $\boldsymbol{\mathcal{H}}$ to represent the time-domain electric and magnetic fields,

Box 1. Stored Energy in Circuits and Systems

Many dynamic systems in nature can be modeled as

$$\frac{\partial}{\partial t}\mathbf{W}\mathbf{u} + \mathbf{P}\mathbf{u} = \mathbf{B}\mathbf{v}_{\text{in}} \quad \text{with} \quad \mathbf{u}_{\text{out}} = \mathbf{B}^{\text{T}}\mathbf{u}, \tag{2}$$

where $\mathbf{v}_{\text{in}}$ and $\mathbf{u}_{\text{out}}$ denote the input and output signals, $\mathbf{u}$ the system's internal states, and $\mathbf{W}$, $\mathbf{P}$, and $\mathbf{B}$ are matrices describing the system [89]. To construct an energy balance of such a system over an interval $[t_1, t_2]$ we multiply with the states $\mathbf{u}$ and integrate to get

$$\left[\frac{\mathbf{u}^{\text{T}}\mathbf{W}\mathbf{u}}{2}\right]_{t_1}^{t_2} + \int_{t_1}^{t_2} \mathbf{u}^{\text{T}}\mathbf{P}\mathbf{u}\,\mathrm{d}t = \int_{t_1}^{t_2} \mathbf{u}_{\text{out}}^{\text{T}}\mathbf{v}_{\text{in}}\,\mathrm{d}t, \tag{3}$$

in which $^{\text{T}}$ denotes matrix transpose. The left-hand side can be identified as the difference in stored energy and dissipation of energy during the interval and the right-hand side is the supplied energy, *cf.*, the definition in Section 2. The definition and interpretation of the stored energy depend on the properties of the matrices $\mathbf{W}$, $\mathbf{P}$, and $\mathbf{B}$.

Systems representable by (2) can contain states that are unobservable to an observer seeing only the input and output signals. These states can contain unobservable energy [89]. The time-average stored energy (3) for time-harmonic signals $\mathbf{u}(t) = \text{Re}\{\mathbf{U}\text{e}^{\text{j}\omega t}\}$ is $\mathbf{U}^{\text{H}}\mathbf{W}\mathbf{U}/4$, where we note that the system matrix $\mathbf{W}$ can be determined by frequency differentiation of the matrix $\mathbf{Z}$ obtained from (2), *i.e.*,

$$\mathbf{Z} = \mathbf{P} + \text{j}\omega\mathbf{W} \quad \text{with} \quad \mathbf{W} = \frac{\partial\,\text{Im}\{\mathbf{Z}\}}{\partial\omega}. \tag{4}$$

By (2), it is implicit that $\mathbf{P}$ and $\mathbf{W}$ are frequency-independent in this classical system model. Probably one of the most familiar systems which follows the form (3) is a lumped circuit. Here, the input and output states are the voltages $\mathbf{V}$ and currents $\mathbf{I}$, respectively. These are related through either the explicit summation of all circuit components or their impedance matrix [70]

$$\mathbf{Z} = \mathbf{R} + \text{j}\omega\mathbf{L} + \frac{1}{\text{j}\omega}\mathbf{C}_{\text{i}}, \tag{5}$$

where $\mathbf{R}$ describes the resistive components of the circuit and matrices $\mathbf{L}$ and $\mathbf{C}_{\text{i}}$ represent the reactive elements. The impedance matrix relates the current to the voltage as $\mathbf{Z}\mathbf{I} = \mathbf{V}$. To reach the stored energy form in (3) we differentiate the impedance matrix with respect to ω and multiply with the current $\mathbf{I}$ and its hermitian conjugate $\mathbf{I}^{\text{H}}$ from the right and left, respectively. This expresses the time-average stored energy, average of the first term in (3) for a time-harmonic signal, as the quadratic form [70]

$$W_{\text{sto}} = \frac{1}{4}\mathbf{I}^{\text{H}}\mathbf{L}\mathbf{I} + \frac{1}{4\omega^2}\mathbf{I}^{\text{H}}\mathbf{C}_{\text{i}}\mathbf{I}, \tag{6}$$

where the classical expressions for the stored energy in inductors and capacitors are recognized [90].

Box 2. Unobservable Energy, Part 1

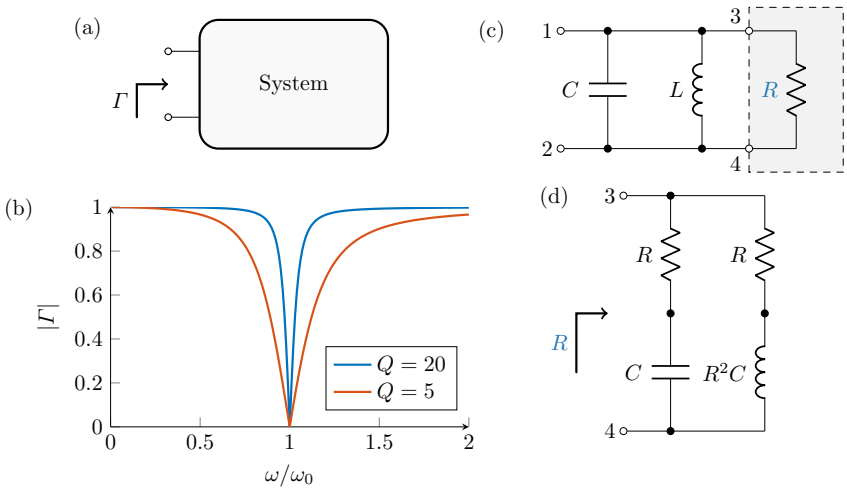

Unobservable states are defined as those states which cannot be identified by an observer performing a macroscopic electromagnetic measurement. To provide an example, let us suppose a yet unknown system, schematically depicted in panel (a). This system is examined by an observer at its input port and quantified by its reflection coefficient Γ, [21]. From the information obtained at the port, we can attempt to construct the system within. The simplest circuit that fits the measured data, depicted in panel (b), is an RLC circuit, see panel (c). However, the resistor in the RLC circuit can be arbitrarily replaced by circuit elements of the Zöbel type [96], see panel (d), without affecting exterior results observed at the port. If we now assume to be able to access the internal structure of the constructed circuits, we can calculate the energy stored in the reactive elements. It then becomes apparent that the added Zöbel circuit does affect the stored energy without changing what is observed at the port. Thus, these two valid circuit realizations for the same mea+sured reflection coefficient predict different values of stored energy. This illustrates that depending on the specific circuit realization, the stored energy, unlike the reflection coefficient, can potentially be altered by states *unobservable* to the outside observer. This is true for all quantities inferred from stored energy, including the Q-factor in (1). It is also important to appreciate that how much of a system's stored energy is observable explicitly depends on the observer. If, for example, the observation procedure would include both measurement of the the reflection coefficient Γ and measurement of heat produced by the circuit, the observer will be able to distinguish circuit (c) from circuit (d), since the time evolution of heat differs in them. Heat however belongs to a microscopic electromagnetism and does not belong the set of measurements allowed in this paper.

Box 3. Unobservable Energy, Part 2

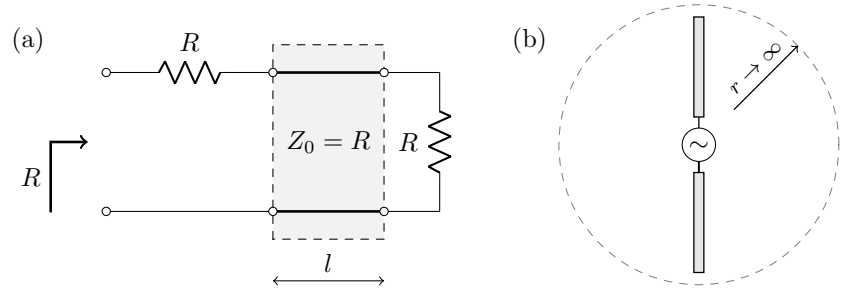

Unobservable energy can be encountered in many basic electromagnetic devices, such as a matched transmission line or a radiating antenna system, see panels (a) and (b) above. In both of these cases, traveling energy exists but is unobservable for an observer at the input port. Specifically, the total energy within the transmission line circuit in panel (a) can be arbitrarily altered through changes to the line length l with no effect on the impedance seen from the input port *cf.*, with lumped circuit models for a transmission line [26]. Similarly, the energy stored within the radiating system in panel (b) depends on the definition of the spatial boundary at which energy "leaves" the system, though this boundary has no effect on the port impedance. For time-harmonic signals and a system boundary chosen at infinity, *i.e.*, the far-field sphere, the system in panel (b) contains an infinite amount of traveling energy.

respectively, while $\boldsymbol{\mathcal{J}}_{\text{source}}$ denotes an impressed current distribution. Assuming the initial conditions $\boldsymbol{\mathcal{E}}(\boldsymbol{r}, t \to -\infty) = \mathbf{0}$, $\boldsymbol{\mathcal{H}}(\boldsymbol{r}, t \to -\infty) = \mathbf{0}$, Poynting's theorem can be written as [49, 66]

$$\mathcal{W}_{\text{supp}}(t_0) = \mathcal{W}_{\text{EM}}(t_0) + \mathcal{W}_{\text{heat}}(t_0) + \mathcal{W}_{\text{rad}}(t_0), \tag{7}$$

where the supplied energy is

$$\mathcal{W}_{\text{supp}}(t_0) = -\int_{-\infty}^{t_0} \int_V \boldsymbol{\mathcal{E}} \cdot \boldsymbol{\mathcal{J}}_{\text{source}} \, \mathrm{d}V \, \mathrm{d}t, \tag{8}$$

the energy lost in heat is

$$\mathcal{W}_{\text{heat}}(t_0) = \int_{-\infty}^{t_0} \int_V \sigma |\boldsymbol{\mathcal{E}}|^2 \, \mathrm{d}V \, \mathrm{d}t, \tag{9}$$

and the net energy escaping the volume through the bounding surface S is

$$\mathcal{W}_{\text{rad}}(t_0) = \int_{-\infty}^{t_0} \int_S (\boldsymbol{\mathcal{E}} \times \boldsymbol{\mathcal{H}}) \cdot \hat{\boldsymbol{n}} \, \mathrm{d}S \, \mathrm{d}t. \tag{10}$$

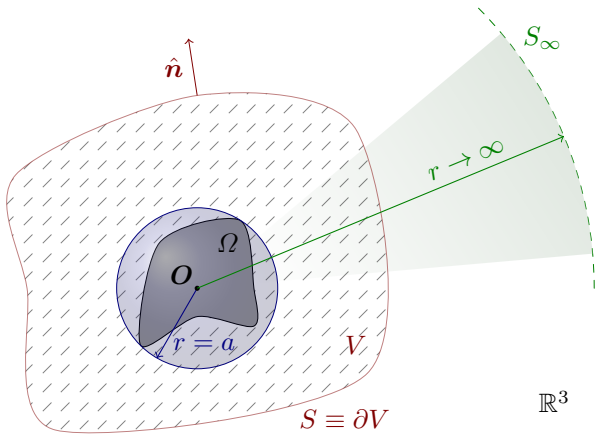

Figure 1: Sketch of an antenna region Ω, a smallest circumscribing sphere of radius a, an arbitrary volume V with its boundary surface S and the far-field sphere bounded by S_∞.

These terms account for energy supplied to and lost from the system, letting us define the remaining term in Poynting's theorem as the total electromagnetic energy stored within the volume V at time $t = t_0$,

$$\mathcal{W}_{\mathrm{EM}}(t_0) = \frac{1}{2} \int_V \left(\varepsilon |\boldsymbol{\mathcal{E}}|^2 + \mu |\boldsymbol{\mathcal{H}}|^2 \right) \mathrm{d}V. \tag{11}$$

All aforementioned quantities depend upon a choice of volume V and its bounding surface S. A specific choice of the surface S lying in the radiation zone[1] [49] leads to (11) representing the total electromagnetic energy and (10) the total radiated energy. This division, however, depends on surface S due to time retardation.

The energy defined in (11) encompasses all electromagnetic energy localized in the chosen volume V containing the system. Nevertheless, for an observer situated at the input port of the system, the entirety of energy W_{EM} is not necessarily observable, see Box 2. By definition, Unobservable energy states cannot affect physical measurements at the location of the observer. For this observer a more sensible definition of the stored energy is,

$$\mathcal{W}_{\mathrm{sto}}(t_0) = \mathcal{W}_{\mathrm{EM}}(t_0) - \mathcal{W}_{\mathrm{unobs}}(t_0), \tag{12}$$

where $\mathcal{W}_{\mathrm{unobs}}(t_0)$ is the energy of all unobservable states. This definition suggests that the value of stored energy depends on the position of the observer. Throughout this paper it is assumed that the observer is positioned at the input port of the electromagnetic system and therefore perceives the minimum stored

[1] Here we make an assumption that electric and magnetic fields are temporarily bandlimited and thus the radiation zone can be defined in a usual manner by the dominance of the $1/r$ field components.

energy from all observers. Note, however, that even the minimum value of energy $\mathcal{W}_{\mathrm{sto}}(t_0)$ is not necessarily recoverable [23, 62] by experiments performed at the location of the observer (recoverable energy $\mathcal{W}_{\mathrm{rec}}(t_0)$ is detailed later in Section 3). The stored energy is fully recoverable only in special cases, the most important being closed lossless systems satisfying $\mathcal{W}_{\mathrm{heat}}(t_0) + \mathcal{W}_{\mathrm{rad}}(t_0) = 0$. Examining the properties of aforementioned energy definitions, we arrive at the following inequality

$$0 \leq \mathcal{W}_{\mathrm{rec}}(t_0) \leq W_{\mathrm{sto}}(t_0) \leq \mathbf{W}_{\mathrm{e}}(t_0) \leq \mathcal{W}_{\mathrm{supp}}(t_0). \tag{13}$$

In the preceding discussion, all quantities are defined in the time domain. However, in many cases cycle mean values of the energies in (10), (11) and (12) in time-harmonic steady state are of interest, where time-harmonic quantities at angular frequency ω are defined as $\mathcal{G}(t) = \mathrm{Re}\{G(\omega)\mathrm{e}^{\mathrm{j}\omega t}\}$ and cycle means are denoted as $\langle\cdot\rangle$. The conversion of all preceding energy terms into time-harmonic domain is straightforward, but induces an issue with potentially unbounded energy values. This happens when the volume V is chosen to consist of all space (denoted V_∞) with bounding surface S being a sphere at infinity (denoted S_∞). In such a case the time-averaged total electromagnetic energy

$$W_{\mathrm{EM}} = \langle \mathcal{W}_{\mathrm{EM}} \rangle = \frac{1}{4}\int_{V_\infty} \left(\varepsilon|\boldsymbol{E}(\omega)|^2 + \mu|\boldsymbol{H}(\omega)|^2\right) \mathrm{d}V \tag{14}$$

is infinite due to the infinite amount of radiation energy contained in propagating fields within the volume V_∞. Subtracting the propagating energy from the total energy W_{EM}, *i.e.*, to identify unobservable energy with radiation, is the aim of several approaches calculating the stored energy $W_{\mathrm{sto}} = \langle W_{\mathrm{sto}}(t_0)\rangle$. These methods rely on the fact that time-averaged radiated power

$$P_{\mathrm{rad}} = \int_{S_\infty} \boldsymbol{P}(\omega)\cdot\hat{\boldsymbol{r}}\,\mathrm{d}S = \frac{1}{2Z_0}\int_{S_\infty} |\boldsymbol{E}(\omega)|^2\,\mathrm{d}S = \frac{1}{2Z_0}\int_{S^2} |\boldsymbol{F}(\omega)|^2\,\mathrm{d}S \tag{15}$$

in time-harmonic steady state is the same for all surfaces enclosing the sources. The quantities

$$\boldsymbol{F}(\omega) = \lim_{r\to\infty} r\mathrm{e}^{\mathrm{j}kr}\boldsymbol{E}(\omega) \tag{16a}$$

$$\boldsymbol{P}(\omega) = \frac{1}{2}\,\mathrm{Re}\{\boldsymbol{E}(\omega)\times\boldsymbol{H}^*(\omega)\} \tag{16b}$$

used above denote the far field and the real part of the Poynting's vector, respectively. In the far right-hand-side of (15), surface S^2 denotes the unit sphere and $k = \omega/c_0$ in (16a) denotes the free-space wavenumber. When used to evaluate Q-factor, the cycle-mean stored energy W_{sto} is normalized by the cycle-mean dissipated energy (see (1)). In radiating systems without ohmic losses, the cycle-mean dissipation reduces to the radiated power P_{rad} in (15).

Note that in many cases, the Q-factor in (1) is assumed to be tuned such that the system as a whole is resonant. In general, a non-resonant system can

Box 4. Electrostatic Energy Expressed in Fields, Circuits, and Charges

Electrostatic energy W_e is thoroughly treated in many classical textbooks [26, 49, 56] with a clear consensus on its definition, see [26] for a discussion. The energy W_e can be expressed in three equivalent ways as

$$W_\mathrm{e} = \frac{1}{2}\int_{\mathbb{R}^3} \varepsilon_0 |\boldsymbol{E}(\boldsymbol{r})|^2 \,\mathrm{dV} = \frac{1}{2}\int_\Omega \phi(\boldsymbol{r})\rho(\boldsymbol{r})\,\mathrm{dV} = \frac{1}{2\varepsilon_0}\int_\Omega\int_\Omega \frac{\rho(\boldsymbol{r}_1)\rho(\boldsymbol{r}_2)}{4\pi|\boldsymbol{r}_1-\boldsymbol{r}_2|}\,\mathrm{dV}_1\,\mathrm{dV}_2, \quad (18)$$

where $\boldsymbol{E}$ denotes electric field intensity, ϕ electric potential and ρ charge density supported in $\Omega \subset \mathbb{R}^3$, see Figure 1. Below, we consider a PEC object Ω with the total charge $\int \rho\,\mathrm{dV} = q_\mathrm{tot}$. From left to right, the terms in (18) represent energy expressed in:

- fields, where the electric energy density $\varepsilon_0|\boldsymbol{E}|^2/2$ is integrated over all space,
- circuits, where a constant potential $\phi = V$ on the PEC object is used to rewrite the energy $W_\mathrm{e} = Vq_\mathrm{tot}/2 = CV^2/2$ in terms of capacitance C,
- charges, where a double integral over the source region is used.

These representations offer alternative expressions and ways to evaluate the energy. Similar interpretations are observed for the electromagnetic energy discussed in Section 3.

be tuned by the addition of a specific reactance, which stores additional energy W_tune. The tuned Q-factor can then be explicitly rewritten as

$$Q = \frac{2\pi\,(W_\mathrm{sto} + W_\mathrm{tune})}{W_\mathrm{diss}}. \quad (17)$$

Since the stored energy in a pure reactance is well-defined, throughout this paper we discuss only the general stored energy W_sto.

3 Existing Methods

So far, we have discussed stored energy only in terms of the abstract definition in (12) involving the total and unobservable energies. For practical purposes, more specific expressions are required to evaluate a system's stored energy. This Section compares many methods developed to calculate the stored energy in electromagnetic systems. These methods vary in approach and generality, though most were motivated by the desire to calculate the Q-factor of radiating systems, as defined in (1).

	Method	Properties			Requirements			Reference
		$\boldsymbol{r}_{\text{ind}}$	$W_{\text{sto}} \geq 0$	$\boldsymbol{J}$-opt	Data	Domain	Region	
Field	W_{P_r}		✓		$\boldsymbol{E}, \boldsymbol{H}$	ω_0	$\mathbb{R}^3$	§3.1.1
	W_{P}	✓	✓		$\boldsymbol{E}, \boldsymbol{H}$	ω_0	$\mathbb{R}^3$	§3.1.2
	W_{F}				$\boldsymbol{E}, \boldsymbol{H}$ or $X_{\text{in}}, \boldsymbol{F}$	ω_0	$\mathbb{R}^3$ or Port, S_∞	§3.1.3
Current	$W_{\mathbf{X}'}$	✓		✓	$\mathbf{Z}$, $\mathbf{I}$	ω_0	Ω	§3.2.1
	W_{reac}	✓		✓	$\boldsymbol{J}$	ω_0	Ω	§3.2.2
	$W_{\widetilde{\mathbf{X}}'}$	✓		✓	$\mathbf{Z}$, $\mathbf{I}$	ω_0	Ω	§3.2.3
	$\mathcal{W}_{\text{td}}(t_0)$	✓	✓		$\boldsymbol{\mathcal{J}}$	t	Ω, S_∞	§3.2.4
System	$W_{\text{Z}^\text{B}_\text{in}}$	✓	✓		Z_{in}, I_{in}	ω	Port	§3.3.1
	$\mathcal{W}_{\text{rec}}(t_0)$	✓	✓		Z_{in}, I_{in}	ω	Port	§3.3.2
	Q_{FBW}	✓	✓		Z_{in}	ω	Port	§3.4.1
	$Q_{\text{Z}'}$	✓	✓		Z_{in}	ω_0	Port	§3.4.2

Table 1: Methods for evaluating stored energy. Rows are grouped by the data required for its evaluation, i.e., methods derived from fields (blue), source distributions (green), and systems (red). The final two uncolored methods are metrics not generally related to stored energy which are used for comparison purposes.

The many attempts at defining and calculating stored energy in radiating systems can be classified and grouped in several ways, *cf.*, the electrostatic case in Box 4. In this section, we briefly discuss these methods using the physical quantities required in each technique as a primary distinguishing feature. All discussed methods are listed in Table 1, where they are grouped using this convention. Specifically, methodologies are grouped into those derived mainly from electromagnetic fields (blue color), those with energy values directly calculable from source current distributions (green color), and those which take a more abstract system-level approach (red and gray color).

This particular division is by no means unique, and throughout this section mathematical equivalences and philosophical similarities between methods are discussed.

The data required for implementing each method are listed in the Requirements column, along with the region over which those data sets are required. These regions are denoted using $\mathbb{R}^3$ to represent all space, Ω the support of sources, S_∞ the far-field sphere, and Port the port of the system. Three salient features are indicated for each method in the Properties column. These features are:

- *coordinate independence*, r_{ind}: A check mark in this column indicates that energy expressions are coordinate independent, *i.e.*, they are independent of an antenna's position within a coordinate system.

- *positive semi-definiteness*, $W_{\text{sto}} \geq 0$: In Section 2 it was argued that the stored energy W_{sto} should always be non-negative. A check mark in this column indicates that energies obtained by a given method obey this re-

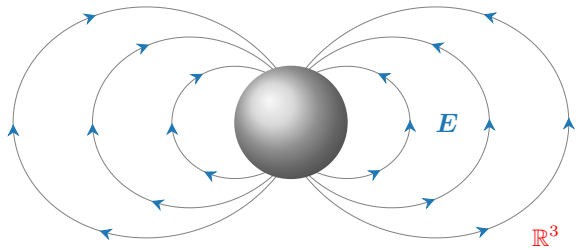

Figure 2: Sketch of electric field intensity $\boldsymbol{E}$ generated by dominant TM_{10} spherical mode.

quirement.

- *applicability to current optimization*, $\boldsymbol{J}$-opt: A check mark in this column indicates that a given formulation of stored energy can be directly applied to source current optimization, useful in determining certain physical bounds.

For the sake of simplicity, all the methods described in Section 3 are presented assuming radiators made only of PEC or assuming electric currents placed in a vacuum environment. All presented methods however allow generalization to non-dispersive inhomogeneous media of finite extent, although validations of such generalizations are scarce. Specific information regarding this procedure for each method is left to corresponding subsections. Similarly, certain methods may be applicable to systems containing dispersive media, though the accuracy and interpretation of results in these cases is still an open area of study.

3.1 Stored Energy Expressed in Terms of Electromagnetic Fields

Methods derived from the fields $\boldsymbol{E}$ and $\boldsymbol{H}$ attempt to calculate stored energy (12) by subtracting unobservable energy from the total energy locally at the level of electromagnetic fields around the radiator, see Figure 2. These procedures commonly allow for the definition of a local stored energy density by identifying energy in radiating fields as unobservable energy. An explicit relation for the unobservable energy density can be identified in these methods, and is given by the subtraction terms in (19), (20) and (21). An advantage of these methods is that they require only field quantities, not the physical structure of the radiator. However, these methods are typically computationally demanding, rendering even simple optimization tasks prohibitively expensive. Other common issues are the unknown form of unobservable energy within the smallest sphere circumscribing a source region Ω (which can lead to over-subtraction [38]) and omission of other forms of unobservable energy such as non-radiating currents [79], see also Boxes 2 and 3. In all known cases, general dispersive materials cannot be treated with these methods. The inclusion of non-dispersive materials can be

made [18,20,94] in all methods described in this subsection by changing $\varepsilon_0 \to \varepsilon$ and $\mu_0 \to \mu$ in the first two terms in (19), (20) and (21).

The published results are dominated by analytic evaluation of the stored energy for spherical modes in the exterior region of a sphere circumscribing the radiator [18,20,25]. The radiated power (15) expressed in the power flux and the far field are identical for this case and the classical expressions can be extended to arbitrary shapes in several ways. Here, we consider radiated energy expressed as the: power flux in the radial direction, magnitude of the power flux, and far-field amplitude, see first three rows in Table 1.

3.1.1 Subtraction of the radial power flow $\hat{\boldsymbol{r}} \cdot \boldsymbol{P}$

Collin and Rothschild [20] suggested identification of radiated energy with the power flux in the radial direction to define the stored energy as

$$W_{\mathrm{P_r}} = \frac{1}{4} \int_{\mathbb{R}^3} \left(\varepsilon_0 |\boldsymbol{E}|^2 + \mu_0 |\boldsymbol{H}|^2 - 4\sqrt{\varepsilon_0 \mu_0}\, \hat{\boldsymbol{r}} \cdot \boldsymbol{P} \right) \mathrm{d}V. \tag{19}$$

They used this expression to evaluate the stored energy in the exterior of a sphere using mode expansions and produced explicit results on the Chu [15] lower bound, see also [18] for a time-domain extension. The expression (19) is non-negative and does not subtract energy for standing waves, *e.g.*, in the interior of a sphere for spherical mode expansions [20, 25]. The main drawbacks of (19) are the coordinate dependence and the need for numerical integration for general fields, see [71, 72] for spheroidal geometries and [17] for an FDTD approach.

3.1.2 Subtraction of the magnitude of the power flow $|\boldsymbol{P}|$

The problem with coordinate dependence in (19) can be resolved by subtraction of the magnitude of the power flow $|\boldsymbol{P}|$, *i.e.*,

$$W_{\mathrm{P}} = \frac{1}{4} \int_{\mathbb{R}^3} \left(\varepsilon_0 |\boldsymbol{E}|^2 + \mu_0 |\boldsymbol{H}|^2 - 4\sqrt{\varepsilon_0 \mu_0} |\boldsymbol{P}| \right) \mathrm{d}V. \tag{20}$$

This expression for the stored energy was originally proposed in an equivalent form by Counter [22]. The expression is identical to (19) for fields expressed as a single spherical mode [22]. It is non-negative and less than or equal to (19) for general fields with a power flow in non-radial directions. The main drawback with (20) is the numerical evaluation of the energy density over $\mathbb{R}^3$.

3.1.3 Subtraction of the far-field amplitude $|\boldsymbol{F}|^2$

The energy of the radial component of the power flow, subtracted in the previous method (19), can be expressed in the far-field amplitude $|\boldsymbol{F}|^2$ outside a

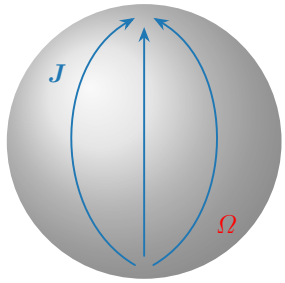

Figure 3: Illustration of surface current of dominant TM_{10} mode on a spherical shell Ω.

circumscribing sphere. This leads to the formulation [25, 29, 30, 33, 57, 65, 94]

$$W_{\mathrm{F}} = \frac{1}{4}\int_{\mathbb{R}^3}\left(\varepsilon_0|\boldsymbol{E}|^2 + \mu_0|\boldsymbol{H}|^2 - 2\varepsilon_0\frac{|\boldsymbol{F}|^2}{|\boldsymbol{r}|^2}\right)\mathrm{d}V$$
$$= \frac{1}{4}\frac{\partial X_{\mathrm{in}}}{\partial\omega}|I_0|^2 - \frac{\mathrm{Im}}{2Z_0}\int_{S^2}\frac{\partial\boldsymbol{F}}{\partial\omega}\cdot\boldsymbol{F}^*\,\mathrm{d}S \quad (21)$$

for the stored energy, where S^2 denotes the unit sphere and the frequency derivatives are evaluated for a frequency independent input current I_0. Here, all radiated energy is subtracted and the expression makes no difference between standing and radiating waves, *e.g.*, in the interior of the smallest circumscribing sphere. Hence, the energy W_{F} differs from $W_{\mathrm{P_r}}$ by kaP_{rad} for spherical modes and implies a difference of the Chu bound by ka, *i.e.*, $Q_{\mathrm{Chu}} - ka$. Variations of (21) exist in the literature and, *e.g.*, Rhodes [65] suggested to use subtraction (21) only in the exterior region, keeping the total electromagnetic energy in the interior region. A shielded power supply is also often excluded from the integration in (21), [94]. This is equivalent to setting the $\boldsymbol{E}$ and $\boldsymbol{H}$ to zero in the region of the power supply.

The stored energy W_{F} in (21) can be rewritten using the frequency-differentiated input reactance X'_{in} and far field $\boldsymbol{F}'$ for antennas with a fixed feeding current I_0 using a reactance theorem [25, 65, 94]. This form of the stored energy is shown in the far right of (21) and simplifies the numerical evaluation from a volume integral to a surface integral. Moreover, it shows that the energy W_{F} is coordinate dependent for non-symmetric radiation patterns [33, 94]. The reactance theorem is extended to complex media in [91, 94]. The formula (21) is also rewritten in the current density in [33], see Section 3.2.2.

3.2 Stored Energy Expressed in Currents

Several methods exist for calculating the energy stored by a source current distribution $\boldsymbol{J}$ placed in vacuum, see Figure 3. These methods can be used to evaluate

stored energy from any system (including materials, feeds, and ports) which can be represented by an equivalent current distribution $\boldsymbol{J}$. A powerful feature of this approach is an immense reduction of information needed to evaluate stored energy. Commonly, only current densities on finite surfaces are needed. These methods are also well suited for various tasks in antenna design [37], since the feeding which leads to the current density $\boldsymbol{J}$ need not be known. This makes it possible to determine fundamental performance bounds on antennas with given support [8, 35, 37, 50] or to utilize modal decomposition methods [4].

Similarly to field approaches, the methods discussed in this subsection identify radiation energy as unobservable energy. In contrast to the field-based methods, however, the explicit form of the unobservable energy is, with an exception of Sec. 3.2.4, not known for current-based methods. Their use for evaluation of (12) for lumped circuits will thus always count the entire electromagnetic energy W_{EM} regardless of the complexity of the circuit. The formulation of the methods for general dispersive materials is not well studied except for the state-space MoM approach in Section 3.2.3. In the case of non-dispersive materials, electric polarization can be included in the current density $\boldsymbol{J}$.

3.2.1 Differentiated MoM reactance matrix $\mathbf{X}'$

Harrington and Mautz [46] proposed to use frequency differentiation of the MoM reactance matrix

$$W_{\mathbf{X}'} = \frac{1}{4}\mathbf{I}^{\mathrm{H}}\frac{\partial \mathbf{X}}{\partial \omega}\mathbf{I} = \frac{1}{4}\mathbf{I}^{\mathrm{H}}\mathbf{X}'\mathbf{I} \tag{22}$$

to estimate the stored energy. The reactance matrix is determined from the impedance matrix $\mathbf{Z} = \mathbf{R} + \mathrm{j}\mathbf{X}$ derived from the MoM approximation of the Electric Field Integral Equation (EFIE) [14]. The expression (22) is not derived in [46], but is merely motivated by the analogous expression of Foster's reactance theorem for lossless systems [44], see also (30). The stored energy for lumped circuit networks can be determined with the formula (22) by substituting the MoM impedance matrix with the lumped circuit impedance matrix, see (5) and [70].

For currents in free space, the expression (22) is identical to the MoM state-space approach in Section 3.2.3 and the MoM approximation of the stored energy expressions by Vandenbosch [80]. Hence, it also suffers from the matrix $\mathbf{X}'$ being indefinite for large structures and potentially producing negative values for the stored energy [38]. The expression (22) is easily applied to temporally dispersive materials but is inaccurate for many cases [40], *cf.*, the state-space MoM approach in Section 3.2.3.

3.2.2 Reactive energy

The expressions in the frequency domain introduced by Vandenbosch [80] start from the same classical idea as described by Collin and Rothschild [20]: the subtraction of the radiated energy density from the total energy density. However,

the subtracted term is defined in a slightly different way on the basis of an energy balance equation involving the derivatives of Maxwell's laws. The resulting difference is analytically integrated over all space, yielding closed-form expressions for the reactive energy (both the electric and magnetic part) in terms of the currents flowing on the radiator. The new definition thus eliminates the coordinate dependency, resulting in the expression

$$W_{\text{reac}} = \frac{Z_0}{4\omega} \int_{\Omega} \int_{\Omega} \Big(\big(k^2 \boldsymbol{J}_1 \cdot \boldsymbol{J}_2^* + \nabla_1 \cdot \boldsymbol{J}_1 \nabla_2 \cdot \boldsymbol{J}_2^*\big) \frac{\cos(kr_{12})}{4\pi r_{12}} - k\big(k^2 \boldsymbol{J}_1 \cdot \boldsymbol{J}_2^* - \nabla_1 \cdot \boldsymbol{J}_1 \nabla_2 \cdot \boldsymbol{J}_2^*\big) \frac{\sin(kr_{12})}{4\pi} \Big) \, \mathrm{d}V_1 \, \mathrm{d}V_2. \quad (23)$$

This expression was later found to conform [33] to the coordinate independent part of energy W_{F} given by (21). The same expression is found also from a line of reasoning starting in time domain [83], [84]. The expression is positive semi-definite for circuits and small radiators but indefinite for larger structures [38]. This method essentially can be seen as a "transformation" of the original field based definition (21), acting on all space, into a current based interpretation, acting only within the volume of the radiator. The MoM approximation of (23) is identical to (22) for the free-space case and hence (23) offers a rigorous motivation for (22). The first term in (23) is also similar to the time-domain formulation using the product of sources and potentials proposed by Carpenter in [12]. Moreover, Geyi presented an approximation of (23) for small antennas in [28]. This small regime formulation was also addressed in [81], [82]. The formulation based on (23) is generalized to electric and magnetic current densities in [51, 53].

3.2.3 State-space MoM model $\widetilde{\mathbf{X}}'$

The state-space method is based on the classical approach to define stored energy in a dynamic system, see (3). The stored energy for a radiating system is more complex as the dynamics are not described by the simple system in (3). In [39], a state-space model

$$\widetilde{\mathbf{Z}}\widetilde{\mathbf{I}} = \begin{pmatrix} \mathrm{j}\omega\mu\mathbf{L} & \mathbf{1} \\ -\mathbf{1} & \mathrm{j}\omega\varepsilon\mathbf{C} \end{pmatrix} \begin{pmatrix} \mathbf{I} \\ \mathbf{U} \end{pmatrix} = \begin{pmatrix} \mathbf{B} \\ \mathbf{0} \end{pmatrix} V_{\text{in}} \quad (24)$$

is derived from the MoM impedance matrix $\mathbf{Z} = \mathrm{j}\omega\mu\mathbf{L} + \mathbf{C}_{\text{i}}/(\mathrm{j}\omega\varepsilon)$, where $\mathbf{U}$ is the voltage state and $\mathbf{V} = \mathbf{B}V_{\text{in}} = \mathbf{ZI}$ is the excitation. The stored energy is constructed by differentiation of the state-space reactance matrix $\widetilde{\mathbf{X}} = \mathrm{Im}\{\widetilde{\mathbf{Z}}\}$ with respect to the frequency, *cf.*, (4). The resulting stored energy is identical to the $\mathbf{X}'$-formulation in Section 3.2.1 for PEC structures in free space and suffers from the same problem of being indefinite for larger structures. The advantage of the state-space approach is that the quadratic forms for the stored energy are derived for small structures in temporally dispersive and inhomogeneous materials.

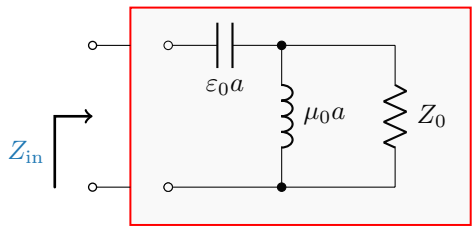

Figure 4: Synthetized circuit for dominant TM_{10} mode of a spherical shell with radius a [15].

3.2.4 Subtraction of the radiated power in time domain

The subtraction of unobservable energy (12) in the form of radiation can advantageously be applied in time domain [10]. In this paradigm the system is brought into a given state (for example time-harmonic steady state) during time $t < t_0$ and then its excitation is switched off. The system is then let to pass a subsequent transient state in which all its energy is lost via radiation and heat. With the time-dependent current density $\boldsymbol{\mathcal{J}}(t)$ existing in the system, which has been recorded during the entire time course, the stored energy can be calculated as

$$\mathcal{W}_{\text{td}}(t_0) = \int_{t_0}^{\infty} \left(\mathcal{P}_{\text{heat}}(\boldsymbol{\mathcal{J}}) + \mathcal{P}_{\text{rad}}(\boldsymbol{\mathcal{J}}) - \mathcal{P}_{\text{rad}}(\boldsymbol{\mathcal{J}}_{\text{freeze}}) \right) \mathrm{d}t, \tag{25}$$

where $\mathcal{P}_{\text{heat}}$ and $\mathcal{P}_{\text{rad}}$ are the power lost and power radiated corresponding to the lost and radiated energy $\mathcal{W}_{\text{heat}}$ and $\mathcal{W}_{\text{rad}}$ defined by (9), (10), with bounding surface S_{far} located in the far field. The current density $\boldsymbol{\mathcal{J}}_{\text{freeze}}(t)$ is defined as the current density at time $t = t_0$ artificially frozen for times $t > t_0$, *i.e.*, $\boldsymbol{\mathcal{J}}_{\text{freeze}}(t > t_0) = \boldsymbol{\mathcal{J}}(t_0)$. Cycle-mean stored energy in time-harmonic case is achieved by moving time t_0 within one period and averaging. Note that although the power terms in (25) are evaluated for time $t > t_0$, the time retardation demands knowledge of the current density also in preceding times.

This subtraction technique closely follows the stored energy definition (12) and its more detailed exposition [10] also shows that the method gives non-negative stored energy, is coordinate independent, and can subtract the radiation energy inside the smallest circumscribing sphere. The unobservable energy can in this case be identified with the subtracted term in (25). The major disadvantage of this approach is that it requires numerically expensive evaluation.

3.3 Approaches Using System, Port, or Feed

System-level approaches evaluate energy storage directly from quantities available in the input/output ports of the system, see Figure 4. Grounded in thermodynamic principles, energy balance calculations of this kind preceded local approaches in mechanics, however, they are not commonly seen in the domain

of electromagnetic stored energy evaluation. The oldest application of system-level energy quantification in electromagnetics uses circuit synthesis [15, 70] and is also tightly related to the concept of recoverable energy [62]. The generality of these approaches is unprecedented as they are applicable to arbitrarily complex electromagnetic systems. Unfortunately, this generality comes at the price of losing all physical interpretation of the unobservable energy content. Additionally, application of these techniques require systems with well defined input ports. This latter restriction makes these techniques inappropriate for evaluating the Q-factors of currents without a well-defined port, such as those encountered in modal decompositions and current optimization.

3.3.1 Circuit synthesis

Chu's classical antenna bound was originally derived using the stored energy in lumped inductors and capacitors within circuit models representing wave impedances of spherical modes [15]. Thal has extended this approach to hollow spheres [75] and arbitrarily shaped radiators [77]. The stored energy for arbitrarily shaped antennas can analogously be estimated from equivalent circuit networks synthesized solely from the input impedance [32], where Brune synthesis [3, 90] is used. Alternative synthesis methods [90] can be used but it is essential that the synthesized circuit is a reciprocal minimal representation [89]. Non-reciprocal methods such as the minimum-phase Darlington synthesis [69, 70] can be used to estimate the recoverable energy in Section 3.3.2.

It is hypothesized [32] that the Brune circuit synthesis procedure produces a circuit with minimal stored energy from all reciprocal realizations, and thus best estimates the stored energy W_{sto}. By definition, this means the procedure only includes the observable part of the stored energy. Note that this is zero for the Zöbel network in Box. 2. The formulation can be used for arbitrary antennas and material models, but its application requires approximation of the input impedance $Z_{\text{in}}(\omega)$ as a positive-real function. This approximation is computationally difficult for electrically large antennas that require high-order rational functions.

3.3.2 Recoverable energy

The recoverable energy $\mathcal{W}_{\text{rec}}(t_0)$ is defined as the maximum energy which can be extracted from a system which has been driven for times $t < t_0$ by a known set of sources [23, 62]. In the most general sense, calculating $\mathcal{W}_{\text{rec}}(t_0)$ involves finding the optimal "recovery source" [62] as a function of time $t > t_0$. This recovery signal implicitly depends on the sources applied at times $t < t_0$ and the locations where recovery is allowed to occur. The optimal recovery source extracts maximum energy from the system and equivalently minimizes energy lost by the system during recovery. When both driving and recovery sources are confined to a single port as they are in many antenna systems, the task of finding the optimal recovery source is greatly simplified [24]. Given a port impedance

Z_c and a system reflection coefficient $\Gamma(\omega)$, the recovery source (in the form of an incident voltage $u_{in}^{+}(t)$) is obtained by solving

$$\mathcal{F}^{-1}\left\{\frac{1}{Z_c}\left(1-|\Gamma(\omega)|^2\right)\right\} * u_{in}^{+}(t) = 0 \tag{26}$$

for times $t > t_0$, where $*$ denotes convolution and $\mathcal{F}^{-1}\{\cdot\}$ denotes the inverse Fourier transform.

Applying this recovery source to the antenna port, the recoverable energy is given by

$$\mathcal{W}_{rec}(t_0) = -\int_{t_0}^{\infty} u_{in}(t) i_{in}(t)\,\mathrm{d}t, \tag{27}$$

where u_{in} and i_{in} are the total port voltage and current corresponding to the optimal time course $u_{in}^{+}(t)$ from (26).

For time-harmonic excitation prior to time t_0, the cycle-mean recoverable energy can be calculated directly in closed-form from a rational function fit of the system's input impedance [24]. The process of approximating an antenna's input impedance as a rational function, however, suffers from the same problems as Brune synthesis for electrically large antennas. The formulation of energy $\mathcal{W}_{rec}$ in terms of field quantities can be found in [62] and an overview of its physical properties and more detailed exposition can be found in [67]. A first generalization of the concept to more arbitrary excitations of radiators can be found in [95].

3.4 System-level Metrics not Directly Derived from Stored Energy

Determining the stored energy in a system is largely motivated by its approximate inverse proportionality[2] to frequency selectivity of a single resonant system, which is most commonly described by its Fractional Bandwidth (FBW) or Q-factor. There are however methods which attempt to evaluate Q-factor without knowledge of stored electromagnetic energy. The most well known are the Q-factors $Q_{Z'}$ derived from the frequency derivative of an input impedance and Q_{FBW} derived directly from the fractional bandwidth of the system. Both of these methods belong to the system-based class of approaches and share those properties. For comparison purposes, both methods will be calculated alongside Q-factors derived from stored energy.

[2] Often, this inverse proportionality is taken for granted. It is, however, important to stress that a strict functional relation of Q-factor based on stored energy and fractional bandwidth does not exist [34], and the discrepancy from the inverse proportionality can in specific cases be enormous [6]. On the other hand, in many cases, including practically all electrically small radiators, the inverse proportionality is almost exact.

3.4.1 Fractional bandwidth

The Q-factor Q_{FBW} is calculated directly from the fractional bandwidth B as [94]

$$Q_{\mathrm{FBW}} = \frac{2\Gamma_0}{\sqrt{1-\Gamma_0^2}} \frac{1}{B_{\Gamma_0}}, \tag{28}$$

where Γ_0 denotes the level of the reflection coefficient $|\Gamma|$ at which the fractional bandwidth B_{Γ_0} is evaluated. The relation assumes that the system is matched and tuned to resonance at the evaluation frequency, *i.e.*, $\Gamma(\omega) = 0$. The most important merit of the Q-factor Q_{FBW} is its exact proportionality to fractional bandwidth. The major drawback of this method is its inability to evaluate Q-factor from data at a single frequency and its dependence on the choice of parameter Γ_0.

3.4.2 Differentiated input impedance

The Q-factor $Q_{\mathrm{Z}'}$ has been derived [94] from Q_{FBW} in the limit where $\Gamma_0 \to 0$ and it represents the differential fractional bandwidth of the system. Similarly to Q_{FBW}, it assumes the system is matched and tuned to resonance. It is most commonly defined as [94]

$$Q_{\mathrm{Z}'} = \frac{\omega}{2R_{\mathrm{in}}} \left| \frac{\partial Z_{\mathrm{in}}}{\partial \omega} \right| = \omega \left| \frac{\partial \Gamma}{\partial \omega} \right|. \tag{29}$$

Alternatively, $Q_{\mathrm{Z}'}$ can be viewed as the classical Q-factor (1) derived from a local approximation of an input impedance by a single resonance (RLC) circuit [61, 94] for which relation $Q_{\mathrm{Z}'} = Q \approx Q_{\mathrm{FBW}}$ holds. The advantage of $Q_{\mathrm{Z}'}$ over Q_{FBW} is its much simpler evaluation and its independence of the parameter Γ_0. However, the cost of this simplification is the loss of a direct relation to fractional bandwidth [94], the possibility of predicting $Q_{\mathrm{Z}'} = 0$ [6,34], and the problematic interpretation in cases of closely spaced resonances [73]. The Q-factor $Q_{\mathrm{Z}'}$ can also be written solely in terms of source current density [7,40] which relates it to the Q-factor based on energies W_{F} and W_{reac}, see Section 4.1.

In systems which are not self-resonant, tuning via an ideal series or parallel lumped reactance is commonly assumed [94]. The values of the corresponding $Q_{\mathrm{Z}'}$ factors differs in those two scenarios, but in practical cases (including those shown in this paper), the differences are minor. The evaluation of $Q_{\mathrm{Z}'}$ factor with parallel reactance tuning can also be seen as evaluating the tuned $Q_{\mathrm{Y}'}$ factor which would result from using (29) on the input admittance and input conductance [40].

3.5 Other Methods

The list of methods discussed above is not complete and we have intentionally selected those which follow the definition (12) and at the same time exhibit generality. In this subsection we briefly comment on those not explicitly treated.

First concept is that of employing angular field decomposition, identifying stored energy with the energy of the evanescent (invisible) part of the spectra [19,64]. A similar concept was proposed in [78] to evaluate Q-factors of electrically small dipole radiators and in [55] to evaluate Q-factors of arrays. This spectral decomposition method is an interesting scheme which gives important insight into the subtraction of the radiation part of unobservable energy. Its most important drawback is its applicability solely to planar radiators. A generalization to general radiators has been proposed in [59, 60], but has not been tested.

The second concept, proposed by Kaiser [52], bears similarity to the time domain version of the method of Collin and Rothschild [18] and claims to be its relativistic generalization. The major difference from (20) is the use of squared instead of linear subtraction which was introduced as an analogy to relativistic energy-momentum relation [1, 52]. The merit of this concept is positive semi-definiteness, coordinate independence, and the capability to deliver a local stored energy density. In canonical cases it leads to stored energy values [5] very close to (20), but its testing in more general scenarios is not available.

The last presented concept is based on a fact that the stored energy in a lossless network can be determined by differentiation of the input reactance $\mathbf{X}_{\text{in}}$ or susceptance $\mathbf{B}_{\text{in}}$ [44] as

$$W_{\mathbf{X}'_{\text{in}}} = \frac{1}{4}\mathbf{I}^{\text{H}}_{\text{in}}\frac{\partial \mathbf{X}_{\text{in}}}{\partial \omega}\mathbf{I}_{\text{in}} \tag{30a}$$

$$W_{\mathbf{B}'_{\text{in}}} = \frac{1}{4}\mathbf{V}^{\text{H}}_{\text{in}}\frac{\partial \mathbf{B}_{\text{in}}}{\partial \omega}\mathbf{V}_{\text{in}}, \tag{30b}$$

respectively. This formula is related to the Foster's reactance theorem [27] where a positive energy implies a positive slope of the reactance. The input resistance of antennas is, however, non-zero and the approximation (30) is hence generally inadequate. This is also concluded from (21), as (30) neglects the far-field term in (21). Moreover, it is necessary to include the input resistance to accurately estimate the fractional bandwidth as shown by $Q_{Z'}$ expression in (29). Although the expression (30) has the same form as the differentiated reactance matrices in Sections 3.2.1 and 3.2.3 there are substantial differences. It is sufficient to know only the input-output relation for the lossless system in (30) whereas (22) requires knowledge of the internal dynamics of the system.

4 Analytic and Numerical Comparisons

In this section, two classes of comparisons are made between the methods described in the preceding section. First, we study the analytic relation between some methods under certain specific conditions. Following that, numerical examples are presented where the Q-factor of driven antennas are calculated and compared.

4.1 Analytical Comparison of Various Methods

When methods from Table 1 are applied to fields and currents generated by PEC structures operating in the quasi-static limit where radiation is negligible, the stored energy predicted by them reduces to the electro- and magnetostatic expressions, see Box 4. They however start to differ for electrically larger structures. Here, the methods are analytically compared for canonical cases such as spherical geometries, PEC structures, and single-resonance models.

Spherical modes have dominated evaluation of stored energy and Q-factors since the publication by Chu [15]. Collin and Rothschild [20], see Section 3.1.1, presented closed form expressions of the Q-factor and stored energy $W_{\mathrm{P_r}}$ for a single radiating spherical mode outside a sphere with radius a. Comparing the definitions of the methods in Table 1 for this case reveals the identities

$$W_{\mathrm{P_r}} = W_{\mathrm{F}} + \frac{a}{c_0} P_{\mathrm{rad}} = W_{\mathrm{P}} = W_{\mathsf{Z}^{\mathrm{B}}_{\mathrm{in}}}, \tag{31}$$

where the difference with aP_{rad}/c_0 (ka for the Q-factor) for the subtracted far-field expression W_{F} originates from the subtraction of the radiated power inside of the sphere in (21) and the equality for the Brune circuit follows from the circuit model of the spherical modes [15]. Thal [75] analyzed the corresponding case with electric currents by inclusion of the stored energy in standing waves inside the sphere. This case is identical to (31) for the field-based methods but with an added connection to W_{reac}, *i.e.*,

$$W_{\mathrm{P_r}} = W_{\mathrm{F}} + \frac{a}{c_0} P_{\mathrm{rad}} = W_{\mathrm{P}} = W_{\mathrm{reac}} + \frac{a}{c_0} P_{\mathrm{rad}}, \tag{32}$$

where the spherical mode expansion in [33] is used for W_{reac} in (23). The identity (32) can be generalized to arbitrary electric current densities on the sphere with exception for W_{P}.

When stored energy W_{F} given by (21) is written as a bilinear form of source current density [33], it relates to energy (23) as $W_{\mathrm{F}} = W_{\mathrm{reac}} + W_{\mathrm{coord}}$, where coordinate-dependent term W_{coord} is given by [33, Eq. 26]. The coordinate dependent part vanishes in the important case of equiphase current densities, *i.e.*, $|\mathbf{I}^{\mathrm{T}}\mathbf{I}| = \mathbf{I}^{\mathrm{H}}\mathbf{I}$, which appear as a result of characteristic mode decomposition [4], minimum Q-factor modes [8], and often approximately for small self-resonant antennas. The equiphase case is also related to differentiation of the input admittance (30) for a fixed voltage source [40] revealing the following connection between the field, current, and port based methods:

$$W_{\mathrm{F}} = W_{\mathrm{reac}} = |W_{\mathbf{B}'_{\mathrm{in}}}| \approx Q_{\mathsf{Z}'} \frac{P_{\mathrm{rad}}}{\omega}, \tag{33}$$

where the final step is valid for self-resonant cases for which the change of reactance dominates over the resistance.

The MoM discretized version of (23) for PEC structures is also identical to the differentiated reactance matrix (22) and the state-space MoM (24), *i.e.*,

$$W_{\mathrm{reac}} = W_{\mathbf{X}'} = W_{\widetilde{\mathbf{X}}'}. \tag{34}$$

This equality is used for the presented numerical results in Section 4.2, where the energy W_{reac} is used to indicate all three methods in (34).

Finally, the system methods agree for single-resonance RLC circuit networks

$$Q_{\mathrm{Z}^{\mathrm{B}}_{\mathrm{in}}} = Q_{\text{rec}} = Q_{\mathrm{Z}'} \approx Q_{\text{FBW}}, \tag{35}$$

where the subscripts used are the same as for corresponding energies.

The above comparison suggests that the proposed methods agree for many cases. However, the identities are based on specific assumptions and discarding the imposed restrictions on the geometries, equiphase currents, and single resonance can produce very different estimates of the stored energy. For an example designed to demonstrate the effects of breaking these assumptions, we generalize the single mode case (32) to to a TM_{01} electric current mode distributed on two spherical shells with radii a_1 and $a_2 > a_1$. Let the inner current have amplitude J_1 and normalize the outer current amplitude with J_0 such that $J_2 = J_0$ cancels the radiation from the inner surface. This non-radiation current has no dissipated power and hence an infinite Q-factor. Lowering the amplitude to $J_2 = 0.5J_0$ increases total the radiation as only half of the radiated field is canceled. Figure 5a depicts the case $a_2 = 6a_1$ with $J_2 = (0.5 + 0.05\text{j})J_0$, where the small imaginary part is added to invalidate the equiphase identity (33). In the figure, we observe that $Q_{\text{F}} \approx Q_{\text{reac}} \approx Q_{\mathrm{Z}'}$ as expected from (33) as the current is approximately equiphase. The Q-factors from the subtracted power flow (19) and (20) are substantially lower than the other Q-factors around $ka_2 \approx 5$. This is contrary to the expectation from the single mode case (32) and can be explained by the power flow between the spherical shells that is not subtracted by the far field in (21). The effects on the Q-factors of an increased phase shift between the current is depicted in Figure 5b, where $J_2 = (1-0.5\text{j})J_0$ is used. Here, all considered methods produce different results. These simple examples illustrate the challenges to define stored energy and that the challenge increases with the electrical size of the object and phase variation of the current.

4.2 Numerical Comparison of Various Methods

Numerical results for different antenna types are presented in this section. The examples are: a center fed cylindrical dipole, an off-center fed cylindrical dipole, a strip folded dipole, and a Yagi-Uda antenna. The tuned Q-factor (17) is chosen as an appropriate measure to compare the different methods, as it is only a renormalization of the stored energy along with an addition of a known tuning energy, see Section 2. This permits us to compare and contrast methods for evaluating the stored energy with the methods in Section 3.4 which only calculate the tuned Q-factor, such as $Q_{\mathrm{Z}'}$ and Q_{FBW}. All example structures are modeled as PEC in free space and are each fed by a single delta-gap voltage source. In this case many of the methods described in Section 3 are formally equivalent, see Section 4.1. Hence, only one representative of each such group is presented here. Each method follows the notation introduced in Table 1. The frequency axis of

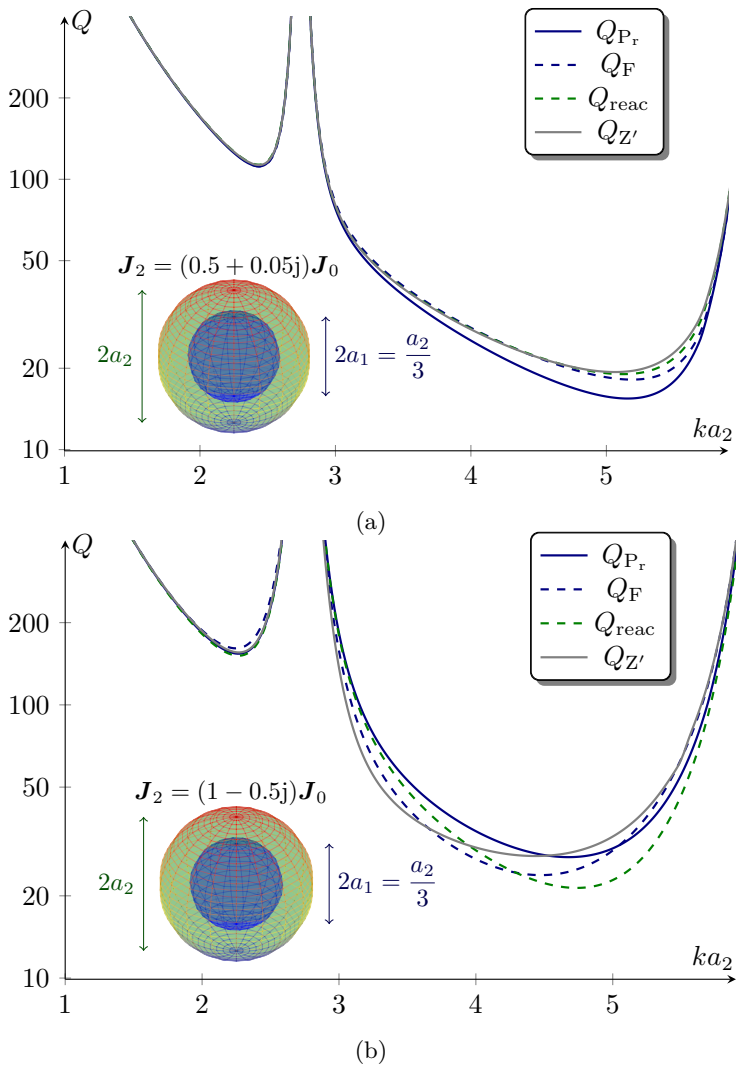

Figure 5: Q-factors for concentric spherical current shells radiating the spherical TM_{01} mode with $a_2 = 6a_1$: a) $J_2 = (0.5 + 0.05\mathrm{j})J_0$, b) $J_2 = (1 - 0.5\mathrm{j})J_0$. Note that the energy W_F has been evaluated according to the first line of (21) which does not demand the frequency normalization of the current and $Q_{\mathrm{Z}'}$ is calculated using the current based formulation in [40].

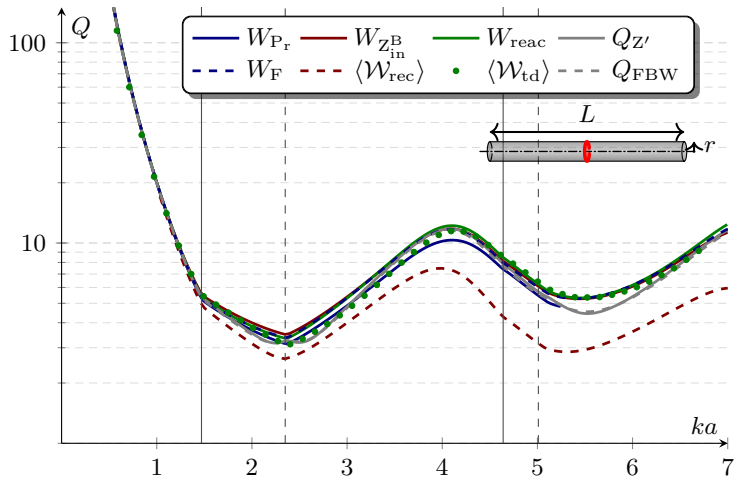

Figure 6: Q-factors of a hollow cylindrical dipole of length L and radius $r = L/200$, fed at its center. The gray solid and dashed vertical lines denote resonance and anti-resonances of the antenna.

all plots is expressed in the dimensionless quantity ka, where a is the radius of the smallest sphere that circumscribes each antenna. The Q-factor Q_{FBW} has been calculated at the level $\Gamma_0 = 1/3 \approx -10\,\mathrm{dB}$ in (28).

4.2.1 Center fed cylindrical dipole

Figure 6 depicts the Q-factors calculated by the methods discussed in Section 3 for a hollow cylindrical dipole. All the methods agree well for low ka values, which are typical dimensions for electrically small antennas. The methods start to diverge for electrically larger structures, when $ka \gg 1.5$. It should be noted that the relative difference in Q-factor is very small, even for larger structures. The only major divergence is the Q-factor from the recoverable energy W_{rec} which predicts significantly lower values than the other methods for $ka > 3$. This, however, is to be expected as the recoverable energy is the lower bound to the stored energy, see (13).

4.2.2 Off-center fed cylindrical dipole

The dipole examined here is identical to the center fed dipole in Section 4.2.1 except that its feeding point is shifted by a distance $l = 0.23L$ from the center. This gives rise to a phase shift which changes the stored energy and Q-factor. If we compare Figures 6 and 7 we see that the Q-factors fluctuate much more than observed in the center fed dipole. However, the Q-factors retain the same behavior with respect to each other as for the center fed dipole for most of the simulated interval. They predict essentially the same results for low values of ka

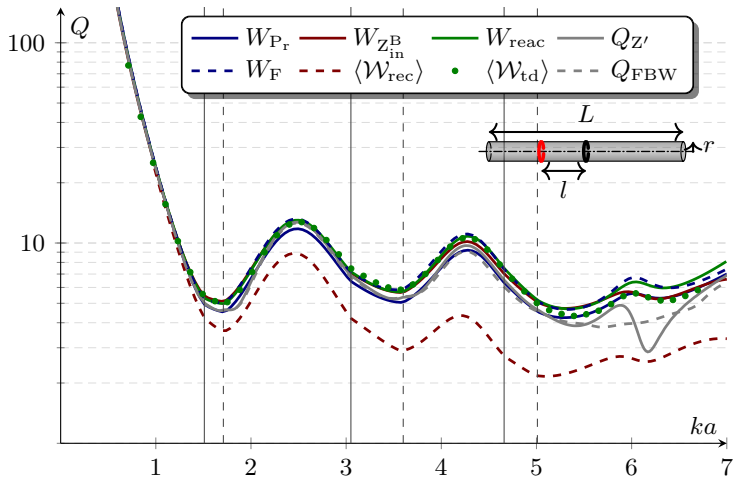

Figure 7: Q-factors for a hollow cylindrical dipole of length L and radius $r = L/200$, with an off-center feed $l = 0.23L$ from the center. The gray solid and dashed vertical lines denote resonance and anti-resonances of the antenna.

and diverge slightly for $ka > 1.5$. However, around $ka = 6.2$ the Q-factor $Q_{\mathrm{Z'}}$ has a dip which is not mimicked by the other methods. The recoverable energy W_{rec} predicts lower values of Q-factor than the other methods but seems to follow the behavior of the curves with smaller fluctuations.

4.2.3 Strip folded dipole

In Figure 8, Q-factors are depicted for a folded strip dipole. Due to computational complexity the subtraction of the power flow $|\boldsymbol{P}|$, the energy W_{P} has not been calculated for this example. With exception of recoverable energy, the depicted methods shown agree well for $ka < 4$, above this point the Q-factors $Q_{\mathrm{Z'}}$ and Q_{FBW} start to diverge from the other methods.

4.2.4 Yagi-Uda

Figure 9 depicts Q-factors calculated for a Yagi-Uda antenna, again the subtraction of the power flow, $|\boldsymbol{P}|$ has not been calculated due to computational complexity. All methods presented agree well over the entire interval, excluding a small dip from Q-factor $Q_{\mathrm{Z'}}$ at $ka = 1.8$ and some small divergence at $ka > 6$. This can be explained by the off resonance behavior of the Yagi-Uda antenna. When the parasitic elements are no longer active, the antenna essentially behaves as a center-fed dipole. Because of this simple behavior the relative difference between the methods becomes very small.

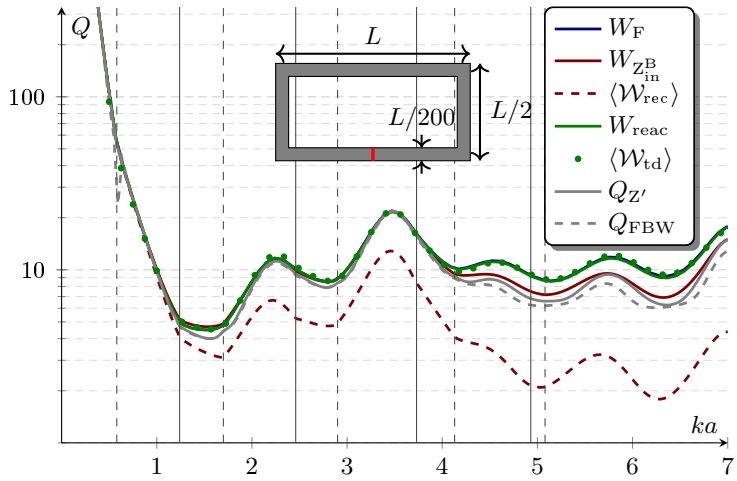

Figure 8: Q-factors for a folded strip dipole of circumscribing dimensions $L \times L/2$, with strip width $L/200$. The gray solid and dashed vertical lines denote resonance and anti-resonances of the antenna.

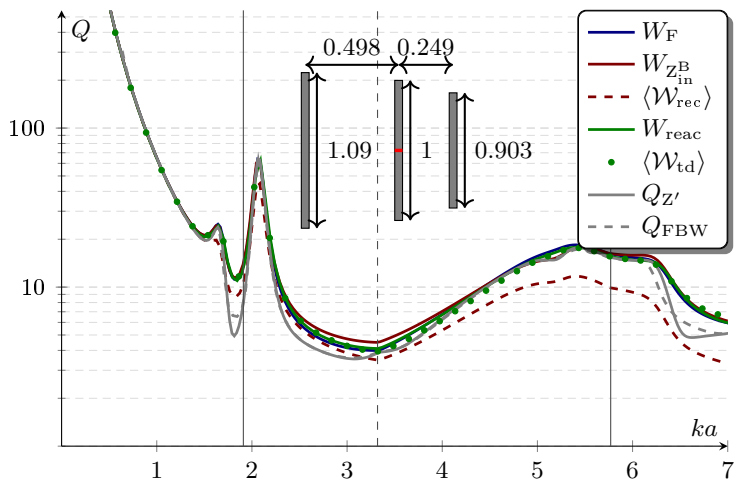

Figure 9: Q-factors for a Yagi-Uda antenna specified in the upper right corner of the figure. All the dimensions of the Yagi-Uda antenna are normalized to the center dipole length L. The elements have been modeled as strips of width $L/200$. The gray solid and dashed vertical lines denote resonance and anti-resonances of the antenna.

5 Applications

Stored energy for radiating systems was initially used by Chu [15] to derive his classical antenna bounds for spherical shapes. Bounds have continued to be a major driving force for research into stored energy [42, 87, 88] as antenna designers are, naturally, interested in how good their antennas are and how far they are from the optima [41, 68, 86]. The Chu bound was originally derived with a circuit model for spherical modes 3.3.1, see also [75–77]. The model was reformulated in fields (19) by Collin and Rothschild [20] and subsequently refined in [25,58,94], see [41,68,86] for an overview. Formulations as optimization problems has generalized the classical bounds on the Q-factor to a multitude of problems formulated as combinations of stored energy, radiated fields, induced currents, and losses [8, 35, 37, 50]. Many problems are formulated as convex optimization problems [8,31,35,37,74] which are efficiently solved with standard algorithms. Here, it is essential that the quadratic forms for the stored energy are positive semidefinite, see Table 1. Unfortunately, several presented methods are indefinite for electrically large structures. This restricts the problems to sub-wavelength structures where the expressions are positive semidefinite. Apart from convex optimization and considering mainly sub-wavelength radiators, other techniques like parameter sweeps [81, 82], polarizabilities [51, 92, 93], or modal decomposition [9, 13, 50, 53] can be applied to determine bounds.

Although stored energy has so far mainly been used to determine physical bounds, stored energy has great potential to be an important concept also for an antenna design. The results by Chu [15] showed that small antennas are dipole radiators and the explicit shape of the current distribution can give insight to design. Thal [75] showed how the stored energy in the interior of a sphere contributes [2, 54]. The importance of the polarizability and its associated charge separation was shown in [36, 92]. With the current-based formulations in Section 3.2 and optimization of the current distribution we get suggestions for optimal currents for many antenna parameters [8, 35, 37, 38, 50].

Another direction from which the problem of minimization of Q-factor was attacked is characteristic mode theory [45] as it provides favorable separation of reactive stored energy (23), constituting thus modal Q-factors for arbitrary bodies [4]. Mixing rules similar to those used with spherical modes can be applied, leading to approximative, but straightforward rules for fundamental bounds on Q-factor of arbitrarily-shaped radiators. Stored energy expressions are also used to construct new type of modes with properties differing from those of characteristic modes. Energy modes formed from eigenvalue problems involving the matrix $\mathbf{X}'$ in (22) were introduced in [46]. These types of modes are also useful to determine and interpret the physical bounds discussed above [9,37]. Moreover, as these modes are real-valued many of the proposed expressions for stored energy agree (33) and the resulting Q-factor is also a good estimate of the fractional bandwidth for single mode antennas.

Stored energy can also be used to simplify some antenna optimization by

replacing simulations over a bandwidth with a single frequency calculation of the Q-factor [16]. This single frequency optimization increases the computational efficiency but is restricted to narrow band cases. A typical representative of an application which can benefit from this approach is a design and optimization of Radio Frequency Identification (RFID) tags with minimal mutual coupling [63, 85].

6 Summary

A definition of stored energy in a general electromagnetic system was proposed and discussed using the concept of unobservable energy. Various aspects of subtracting the unobservable energy have been pointed out in the examples of Zöbel's network, matched transmission lines, and, most importantly, radiating structures. It has been shown that a majority of the well-established concepts for evaluating stored energy in radiating systems can be categorized into three different groups – whether they used field quantities, source currents, or rely solely on knowledge in system as a whole without possibility to probe its internal structure. An important outcome of this paper is understanding that all existent concepts, in fact, attempt to define unobservable energy. Nevertheless, the common association of unobservable energy purely with radiated energy is insufficient. By the proposed definition, the unobservable energy represents the difference between the total electromagnetic energy W_{EM} and the stored energy W_{sto} so that it contains the energy of all unobservable states.

Careful analysis of the presented results revealed good agreement between all evaluated methods for equiphased currents and electrically small ($ka < 1.5$) antenna structures, though simple analytically-constructed examples and larger objects revealed significant disagreements. The systematic difference between recoverable energy W_{rec} and stored energy W_{sto} is due to reciprocity of the resulting realizations. While the recoverable energy allows for non-reciprocal circuits, the stored energy approaches, as illustrated by Brune synthesis, deal with reciprocal systems only. Taking Q_{FBW} as reference measure of fractional bandwidth, it is obvious that the Q-factor resulting from recoverable energy considerably overestimates the fractional bandwidth. The other presented methods have much better agreement with fractional bandwidth. However, from this point of view, the best predictor of bandwidth potential is Q-factor $Q_{\mathrm{Z}'}$, but only when the system under study can be approximated as a single resonance system.

For practical aspects of stored energy evaluation, the method evaluating energy W_{reac} or, alternatively, energy $W_{\mathbf{X}'}$, gives precise approximation of stored energy for electrically small structures, offers simple implementation, and, in addition, is fully compatible with present approaches to minimization of Q-factor like convex optimization and pixeling. Whenever negative values of stored energy could be an issue, an alternative method, possibly Brune synthesis, is recommended since the breaking point at which stored energy W_{reac} fails is not exactly known. As confirmed by all treated examples, Brune synthesis is capable of dis-

tilling the maximum amount of unobservable energy from the total energy, thus surpassing other contemporary approaches. However, complications in performing Brune synthesis for electrically large antennas may be an obstacle limiting its application.

Though many researchers have contributed to the study of stored energy with corresponding indisputable achievements, several fundamental questions remain open. The missing proof of the minimal reciprocal realizations generated by Brune synthesis as well as closely related reformulation of this circuit synthesis in terms of the electromagnetic quantities, may open the final stage to explicit, coherent, and exact definition and evaluation of unobservable energy. Additionally, further work is needed on the calculation, verification, and interpretation of stored energy in general dispersive media.

Appendix A Stored Energy in Dispersive Media

The definition in Section 2 covers antennas in a non-dispersive background. Consider instead a radiator embedded in an isotropic dielectric material described by a Lorentz dispersion model

$$\frac{\partial^2 \boldsymbol{\mathcal{P}}}{\partial t^2} + \Gamma \frac{\partial \boldsymbol{\mathcal{P}}}{\partial t} + \omega_\mathrm{r}^2 \boldsymbol{\mathcal{P}} = \varepsilon_0 \omega_\mathrm{p}^2 \boldsymbol{\mathcal{E}}, \tag{36}$$

where $\boldsymbol{\mathcal{P}}$ is the polarization, Γ is the loss factor, ω_r is the resonance frequency of the material, and ω_p is the coupling constant [49]. If we divide the energy analogously to (7), the material properties influence the heat and total energy terms [66]. The new heat term reads

$$\mathcal{W}_\mathrm{heat}\left(t_0\right) = \int_{-\infty}^{t_0} \int_V \sigma \left|\boldsymbol{\mathcal{E}}\right|^2 + \frac{\Gamma}{\varepsilon_0 \omega_\mathrm{p}^2} \left| \frac{\partial \boldsymbol{\mathcal{P}}}{\partial t} \right|^2 \mathrm{d}V \, \mathrm{d}t, \tag{37}$$

and the total energy reads

$$\mathcal{W}_\mathrm{EM}\left(t_0\right) = \frac{1}{2} \int_V \varepsilon_0 \left|\boldsymbol{\mathcal{E}}\right|^2 + \mu_0 \left|\boldsymbol{\mathcal{H}}\right|^2 + \frac{1}{\varepsilon_0 \omega_\mathrm{p}^2} \left[\left| \frac{\partial \boldsymbol{\mathcal{P}}}{\partial t} \right|^2 + \omega_\mathrm{r}^2 |\boldsymbol{\mathcal{P}}|^2 \right] \mathrm{d}V. \tag{38}$$

The stored energy definition (12) still applies, but the dispersion generally rise the energy of unobservable states. The subtraction of unobservable energy states becomes especially problematic in dispersive background since in a such case far field is no longer well defined and many classical methods break down. System based methods, see Table 1, and engineering metrics $Q_{\mathrm{Z}'}$ and Q_FBW are unaffected, in principle, but, in certain cases, they are more likely to predict unphysical results, see [40]. Extensive comparison of the relation between Q-factor and fractional bandwidth in dispersive environments are scarce but the case of antennas in Lorentz media (36) is treated in [39] using state-space models.

References

[1] H. Bateman. *The mathematical analysis of electrical and optical wave-motion on the basis of Maxwell's equations (1915)*. Forgotten Books, 2010.

[2] S. R. Best. The radiation properties of electrically small folded spherical helix antennas. *IEEE Trans. Antennas Propag.*, **52**(4), pp. 953–960, 2004.

[3] O. Brune. Synthesis of a finite two-terminal network whose driving-point impedance is a prescribed function of frequency. *MIT J. Math. Phys.*, **10**, pp. 191–236, 1931.

[4] M. Capek, P. Hazdra, and J. Eichler. A method for the evaluation of radiation Q based on modal approach. *IEEE Trans. Antennas Propag.*, **60**(10), pp. 4556–4567, 2012.

[5] M. Capek and L. Jelinek. Various interpretations of the stored and the radiated energy density. 2015. eprint arXiv: 1503.06752.

[6] M. Capek, L. Jelinek, and P. Hazdra. On the functional relation between quality factor and fractional bandwidth. *IEEE Trans. Antennas Propag.*, **63**(6), pp. 2787–2790, Jun. 2015.

[7] M. Capek, L. Jelinek, P. Hazdra, and J. Eichler. The measurable Q factor and observable energies of radiating structures. *IEEE Trans. Antennas Propag.*, **62**(1), pp. 311–318, Jan. 2014.

[8] M. Capek, M. Gustafsson, and K. Schab. Minimization of antenna quality factor. *IEEE Trans. Antennas Propag.*, **65**(8), pp. 4115–4123, 2017.

[9] M. Capek and L. Jelinek. Optimal composition of modal currents for minimal quality factor Q. *IEEE Trans. Antennas Propag.*, **64**(12), pp. 5230–5242, 2016.

[10] M. Capek, L. Jelinek, and G. A. E. Vandenbosch. Stored electromagnetic energy and quality factor of radiating structures. *Proc. R. Soc. A*, **472**(2188), 2016.

[11] H. J. Carlin. Network theory without circuit elements. *Proceedings of the IEEE*, **55**(4), pp. 482–497, Apr. 1967.

[12] C. J. Carpenter. Electromagnetic energy and power in terms of charges and potentials instead of fields. *IEE Proc. A*, **136**(2), pp. 55–65, 1989.

[13] J. Chalas, K. Sertel, and J. L. Volakis. Computation of the Q limits for arbitrary-shaped antennas using characteristic modes. *IEEE Trans. Antennas Propag.*, **64**(7), pp. 2637–2647, 2016.

[14] W. C. Chew, M. S. Tong, and B. Hu. *Integral Equation Methods for Electromagnetic and Elastic Waves*, volume 12. Morgan & Claypool, 2008.

[15] L. J. Chu. Physical limitations of omni-directional antennas. *J. Appl. Phys.*, **19**, pp. 1163–1175, 1948.

[16] M. Cismasu and M. Gustafsson. Antenna bandwidth optimization with single frequency simulation. *IEEE Trans. Antennas Propag.*, **62**(3), pp. 1304–1311, 2014.

[17] S. Collardey, A. Sharaiha, and K. Mahdjoubi. Evaluation of antenna radiation Q using FDTD method. *Electronics Letters*, **41**(12), pp. 675–677, 2005.

[18] R. E. Collin. Minimum Q of small antennas. *J. Electromagnet. Waves Appl.*, **12**, pp. 1369–1393, 1998.

[19] R. E. Collin and S. Rothschild. Reactive energy in aperture fields and apperture Q. *Canadian Journal of Physics*, **41**(12), pp. 1967–1979, 1963.

[20] R. E. Collin and S. Rothschild. Evaluation of antenna Q. *IEEE Trans. Antennas Propag.*, **12**, pp. 23–27, Jan. 1964.

[21] R. E. Collin. *Foundations for Microwave Engineering.* McGraw-Hill, New York, NY, second edition, 1992.

[22] V. A. Counter. Miniature cavity antenna. Technical Report 2, Microwave Lab, 1948. Contract No. W28-099-ac-382.

[23] W. A. Day. Reversibility, recoverable work and free energy in linear viscoelasticity. *Quart. Journ. Mech. and Applied Math.*, **23**, pp. 1–15, 1970.

[24] R. H. Direen. *Fundamental Limitations on the Terminal Behavior of Antennas and Nonuniform Transmission Lines.* PhD thesis, University of Colorado, 2010.

[25] R. L. Fante. Quality factor of general ideal antennas. *IEEE Trans. Antennas Propag.*, **17**(2), pp. 151–155, Mar. 1969.

[26] R. P. Feynman, R. B. Leighton, and M. Sands. *The Feynman Lectures on Physics.* Addison-Wesley, Reading, MA, 1965.

[27] R. M. Foster. A reactance theorem. *Bell Labs Technical Journal*, **3**(2), pp. 259–267, 1924.

[28] W. Geyi. A method for the evaluation of small antenna Q. *IEEE Trans. Antennas Propag.*, **51**(8), pp. 2124–2129, 2003.

[29] W. Geyi. Physical limitations of antenna. *IEEE Trans. Antennas Propag.*, **51**(8), pp. 2116–2123, Aug. 2003.

[30] W. Geyi. *Foundations of Applied Electrodynamics.* John Wiley & Sons, 2011.

[31] M. Gustafsson, J. Friden, and D. Colombi. Antenna current optimization for lossy media with near field constraints. *IEEE Antennas Wirel. Propag. Lett.*, **14**, pp. 1538–1541, 2015.

[32] M. Gustafsson and B. L. G. Jonsson. Antenna Q and stored energy expressed in the fields, currents, and input impedance. *IEEE Trans. Antennas Propag.*, **63**(1), pp. 240–249, 2015.

[33] M. Gustafsson and B. L. G. Jonsson. Stored electromagnetic energy and antenna Q. *Prog. Electromagn. Res. (PIER)*, **150**, pp. 13–27, 2015.

[34] M. Gustafsson and S. Nordebo. Bandwidth, Q-factor, and resonance models of antennas. *Prog. Electromagn. Res.*, **62**, pp. 1–20, 2006.

[35] M. Gustafsson and S. Nordebo. Optimal antenna currents for Q, superdirectivity, and radiation patterns using convex optimization. *IEEE Trans. Antennas Propag.*, **61**(3), pp. 1109–1118, 2013.

[36] M. Gustafsson, C. Sohl, and G. Kristensson. Physical limitations on antennas of arbitrary shape. *Proc. R. Soc. A*, **463**, pp. 2589–2607, 2007.

[37] M. Gustafsson, D. Tayli, C. Ehrenborg, M. Cismasu, and S. Nordebo. Antenna current optimization using MATLAB and CVX. *FERMAT*, **15**(5), pp. 1–29, 2016.

[38] M. Gustafsson, M. Cismasu, and B. L. G. Jonsson. Physical bounds and optimal currents on antennas. *IEEE Trans. Antennas Propag.*, **60**(6), pp. 2672–2681, 2012.

[39] M. Gustafsson and C. Ehrenborg. State-space models and stored electromagnetic energy for antennas in dispersive and heterogeneous media. *Radio Sci.*, **52**, 2017.

[40] M. Gustafsson, D. Tayli, and M. Cismasu. Q factors for antennas in dispersive media. Technical Report LUTEDX/(TEAT-7232)/1–24/(2014), Lund University, Department of Electrical and Information Technology and P.O. Box 118 and S-221 00 Lund, Sweden, 2014. http://www.eit.lth.se.

[41] M. Gustafsson, D. Tayli, and M. Cismasu. *Physical bounds of antennas*, pp. 1–32. Springer-Verlag, 2015.

[42] R. C. Hansen. Fundamental limitations in antennas. *Proc. IEEE*, **69**(2), pp. 170–182, 1981.

[43] R. F. Harrington. *Time Harmonic Electromagnetic Fields.* McGraw-Hill, New York, NY, 1961.

[44] R. F. Harrington. *Field Computation by Moment Methods.* Macmillan, New York, NY, 1968.

[45] R. F. Harrington and J. R. Mautz. Theory of characteristic modes for conducting bodies. *IEEE Trans. Antennas Propag.*, **19**(5), pp. 622–628, 1971.

[46] R. F. Harrington and J. R. Mautz. Control of radar scattering by reactive loading. *IEEE Trans. Antennas Propag.*, **20**(4), pp. 446–454, 1972.

[47] IEEE. *1549-2011 – IEEE Standard for Microwave Filter Definitions*, 2011.

[48] IEEE145-1993. *IEEE Standard Definition of Terms for Antennas.* Antenna Standards Committee of the IEEE Antennas and Propagation Society, Mar. 1993.

[49] J. D. Jackson. *Classical Electrodynamics.* John Wiley & Sons, New York, NY, third edition, 1999.

[50] L. Jelinek and M. Capek. Optimal currents on arbitrarily shaped surfaces. *IEEE Trans. Antennas Propag.*, **65**(1), pp. 329–341, 2017.

[51] B. L. G. Jonsson and M. Gustafsson. Stored energies in electric and magnetic current densities for small antennas. *Proc. R. Soc. A*, **471**(2176), pp. 20140897, 2015.

[52] G. Kaiser. Electromagnetic inertia, reactive energy and energy flow velocity. *J. Phys. A: Math. Theor.*, **44**(34), pp. 345206, 2011.

[53] O. S. Kim. Lower bounds on Q for finite size antennas of arbitrary shape. *IEEE Trans. Antennas Propag.*, **64**(1), pp. 146–154, 2016.

[54] O. Kim, O. Breinbjerg, and A. Yaghjian. Electrically small magnetic dipole antennas with quality factors approaching the Chu lower bound. *IEEE Trans. Antennas Propag.*, **58**(6), pp. 1898–1906, Jun. 2010.

[55] D.-H. Kwon and D. M. Pozar. Energy storage and radiation Q of infinite planar dipole phased arrays. *IEEE Trans. Antennas Propag.*, **62**(1), pp. 153–162, 2014.

[56] L. D. Landau, E. M. Lifshitz, and L. P. Pitaevskiĭ. *Electrodynamics of Continuous Media.* Pergamon Press, Oxford, second edition, 1984.

[57] C. Levis. A reactance theorem for antennas. *Proceedings of the IRE*, **45**(8), pp. 1128–1134, 1957.

[58] J. S. McLean. A re-examination of the fundamental limits on the radiation Q of electrically small antennas. *IEEE Trans. Antennas Propag.*, **44**(5), pp. 672–676, May 1996.

[59] S. M. Mikki and Y. M. Antar. A theory of antenna electromagnetic near field part I. *IEEE Trans. Antennas Propag.*, **59**(12), pp. 4691–4705, 2011.

[60] S. M. Mikki and Y. M. Antar. A theory of antenna electromagnetic near field-part II. *IEEE Trans. Antennas Propag.*, **59**(12), pp. 4706–4724, 2011.

[61] T. Ohira. What in the world is Q? *IEEE Microw. Mag.*, **17**(6), pp. 42–49, Jun. 2016.

[62] V. G. Polevoi. Maximum energy extractable from an electromagnetic field. *Radiophysics and Quantum Electronics*, **33**(7), pp. 603–609, 1990.

[63] M. Polivka, J. Havlicek, M. Svanda, and J. Machac. Improvement in robustness and recognizability of RCS response of u-shaped strip-based chipless RFID tags. *IEEE Antennas Wireless Propag. Lett.*, **15**, pp. 2000–2003, 2016.

[64] D. Rhodes. On the stored energy of planar apertures. *IEEE Trans. Antennas Propag.*, **14**(6), pp. 676–683, 1966.

[65] D. R. Rhodes. Observable stored energies of electromagnetic systems. *Journal of the Franklin Institute*, **302**(3), pp. 225–237, 1976.

[66] R. Ruppin. Electromagnetic energy density in a dispersive and absorptive material. *Physics letters A*, **299**(2), pp. 309–312, 2002.

[67] K. Schab, L. Jelinek, and M. Capek. Recoverable energy of dissipative electromagnetic systems. 2017. eprint arXiv: 1701.06313.

[68] D. F. Sievenpiper, D. C. Dawson, M. M. Jacob, T. Kanar, S. Kim, J. Long, and R. G. Quarfoth. Experimental validation of performance limits and design guidelines for small antennas. *IEEE Trans. Antennas Propag.*, **60**(1), pp. 8–19, Jan 2012.

[69] W. Smith. Average energy storage by a one-port and minimum energy synthesis. *IEEE Transactions on Circuit Theory*, **17**(3), pp. 427–430, 1970.

[70] W. E. Smith. The energy storage of a prescribed impedance. *Proceedings of the Royal Society of New South Wales*, **102**, pp. 203—-218, 1969.

[71] J. C.-E. Sten. Reconstruction of electromagnetic minimum energy sources in a prolate spheroid. *Radio Sci.*, **39**(2), 2004.

[72] J. C.-E. Sten, P. K. Koivisto, and A. Hujanen. Limitations for the radiation Q of a small antenna enclosed in a spheroidal volume: axial polarisation. *AEÜ Int. J. Electron. Commun.*, **55**(3), pp. 198–204, 2001.

[73] H. Stuart, S. Best, and A. Yaghjian. Limitations in relating quality factor to bandwidth in a double resonance small antenna. *IEEE Antennas Wirel. Propag. Lett.*, **6**, 2007.

[74] D. Tayli and M. Gustafsson. Physical bounds for antennas above a ground plane. *IEEE Antennas Wirel. Propag. Lett.*, **15**, pp. 1281–1284, 2016.

[75] H. L. Thal. New radiation Q limits for spherical wire antennas. *IEEE Trans. Antennas Propag.*, **54**(10), pp. 2757–2763, Oct. 2006.

[76] H. L. Thal. Gain and Q bounds for coupled TM-TE modes. *IEEE Trans. Antennas Propag.*, **57**(7), pp. 1879–1885, Jul. 2009.

[77] H. L. Thal. Q Bounds for Arbitrary Small Antennas: A Circuit Approach. *IEEE Trans. Antennas Propag.*, **60**(7), pp. 3120–3128, 2012.

[78] G. Thiele, P. Detweiler, and R. Penno. On the lower bound of the radiation Q for electrically small antennas. *IEEE Trans. Antennas Propag.*, **51**(6), pp. 1263–1269, Jun. 2003.

[79] J. G. van Bladel. *Electromagnetic Fields*. IEEE Press, Piscataway, NJ, second edition edition, 2007.

[80] G. A. E. Vandenbosch. Reactive energies, impedance, and Q factor of radiating structures. *IEEE Trans. Antennas Propag.*, **58**(4), pp. 1112–1127, 2010.

[81] G. A. E. Vandenbosch. Simple procedure to derive lower bounds for radiation Q of electrically small devices of arbitrary topology. *IEEE Trans. Antennas Propag.*, **59**(6), pp. 2217–2225, 2011.

[82] G. A. E. Vandenbosch. Explicit relation between volume and lower bound for Q for small dipole topologies. *IEEE Trans. Antennas Propag.*, **60**(2), pp. 1147–1152, Feb. 2012.

[83] G. A. E. Vandenbosch. Radiators in time domain, part I: electric, magnetic, and radiated energies. *IEEE Trans. Antennas Propag.*, **61**(8), pp. 3995–4003, 2013.

[84] G. A. E. Vandenbosch. Radiators in time domain, part II: finite pulses, sinusoidal regime and Q factor. *IEEE Trans. Antennas Propag.*, **61**(8), pp. 4004–4012, 2013.

[85] A. Vena, E. Perret, and S. Tedjini. A fully printable chipless RFID tag with detuning correction technique. *IEEE Microwave and Wireless Components Letters*, **22**(4), pp. 209–211, 2012.

[86] J. Volakis, C. C. Chen, and K. Fujimoto. *Small Antennas: Miniaturization Techniques & Applications*. McGraw-Hill, New York, NY, 2010.

[87] H. A. Wheeler. Fundamental limitations of small antennas. *Proc. IRE*, **35**(12), pp. 1479–1484, 1947.

[88] H. Wheeler. The radiansphere around a small antenna. *Proc. IRE*, **47**(8), pp. 1325–1331, 1959.

[89] J. C. Willems. Dissipative dynamical systems part II: Linear systems with quadratic supply rates. *Arch. Rational Mech. Anal.*, **45**(5), pp. 352–393, 1972.

[90] O. Wing. *Classical Circuit Theory*. Springer, New York, 2008.

[91] A. D. Yaghjian. Internal energy, Q-energy, Poynting's theorem, and the stress dyadic in dispersive material. *IEEE Trans. Antennas Propag.*, **55**(6), pp. 1495–1505, 2007.

[92] A. D. Yaghjian, M. Gustafsson, and B. L. G. Jonsson. Minimum Q for lossy and lossless electrically small dipole antennas. *Prog. Electromagn. Res.*, **143**, pp. 641–673, 2013.

[93] A. D. Yaghjian and H. R. Stuart. Lower bounds on the Q of electrically small dipole antennas. *IEEE Trans. Antennas Propag.*, **58**(10), pp. 3114–3121, 2010.

[94] A. D. Yaghjian and S. R. Best. Impedance, bandwidth, and Q of antennas. *IEEE Trans. Antennas Propag.*, **53**(4), pp. 1298–1324, 2005.

[95] X. Zheng, G. A. E. Vandenbosch, and V. V. Moshchalkov. Recoverable energy of antennas. In *International Conference on Electromagnetics in Advanced Applications (ICEAA)*, pp. 1–3, 2016.

[96] O. J. Zobel. Theory and design of uniform and composite electric wave filters. *Bell System Technical Journal*, **2**, pp. 1–46, 1923.

State-Space Models and Stored Electromagnetic Energy for Antennas in Dispersive and Heterogeneous Media

Mats Gustafsson and Casimir Ehrenborg

Paper VI

Published as: M. Gustafsson, C. Ehrenborg, "State-space models and stored electromagnetic energy for antennas in dispersive and heterogeneous media,"*Radio Science*, Vol 52, No. 11, pp. 1325–1343, 2017.

Abstract

Accurate and efficient evaluation of the stored energy is essential for Q-factors, physical bounds, and antenna current optimization. Here, it is shown that the stored energy can be estimated from quadratic forms based on a state-space representation derived from the electric and magnetic field integral equations. The derived expressions are valid for small antennas embedded in temporally dispersive and inhomogeneous media. The quadratic forms also provide simple single frequency formulas for the corresponding Q-factors. Numerical examples comparing the different Q-factors are presented for dipole and meander line antennas in conductive, Debye, and Lorentz media for homogeneous and inhomogeneous media. The computed Q-factors are also verified with the Q-factor obtained from the stored energy in Brune synthesized circuit models.

1 Introduction

Antennas are placed in the proximity of, or inside, lossy media in applications involving mobile phones, body area networks, implants, submarines, and plasmonics [2, 41, 58]. The losses in such systems are associated with conduction or relaxation phenomena. These effects lead to a frequency dependent permittivity, and hence temporal dispersion. Temporal dispersion is present in natural [33, 39, 52] and artificial materials [5, 8, 15]. Dispersion is often neglected for antenna modeling in the microwave range by considering antennas in free space or embedded in non-dispersive dielectrics, however it is usually necessary for modeling of phenomena in the mm, THz, and optical range. Electromagnetic energy density in dispersive media builds on the classical results in [39] with extensions to applications such as antennas, metamaterials, and photonics [45, 51, 57, 62].

Stored energy is instrumental for antenna analysis in terms of the Q-factor [7, 10,13,24,28,46,55,63]. In [29,61,62] stored energy is considered for small antennas composed of dispersive or lossy media, embedded in free space. However, when calculating stored energy for antennas embedded in lossy background media, new challenges arise. The classical subtraction technique, where the energy in the far-field is subtracted from the total energy density, is difficult to generalize to lossy media due to the exponential decay of the far-field and its associated coordinate dependence [42]. Here, we follow the approach in [17, 31, 53] and express the stored energy and Q-factors in terms of the current density on the antenna structure. The derivation is based on a state-space representation [59] together with frequency differentiation of the MoM impedance matrix.

Stored energy is investigated for state-space models in [59], where it is shown that the stored energy is associated with minimal systems having internal symmetry, *i.e.*, reciprocity. We use this approach to construct symmetric state-space models for antennas in dispersive media, and calculate their stored energy. The explicit results are given for conductivity, Debye, Drude, and Lorentz models and are simply generalized to models with multiple terms [33, 39, 52]. The resulting models are classical state-space models for small antennas, but contain a phase

shift (time delay) for larger structures that is not considered in [59]. Here, we use a local approximation based on differentiation with respect to the frequency to include time-delay effects [26]. In total, this offers a stored energy that is identical to the stored energy defined by subtraction of the far-field energy term for the free space coordinate independent case [22]. Moreover, the stored energy derived from the state-space model in dispersive media equals the stored energy determined from synthesized circuit models for small antennas.

This paper is organized as follows. In Sec. 2, the Q-factor and stored energies are discussed. A state-space model based on the MoM impedance matrix and its stored energy is introduced in Sec. 3. The state-space models and stored energies are generalized to temporally dispersive and inhomogeneous media in Secs 4 and 5, respectively. The paper is concluded in Sec. 6.

2 Stored Energy, Q-Factor, and State-Space Models

Stored energy for antennas is a concept which arose by necessity to calculate the Q-factor [10, 28, 43, 55, 63]. The Q-factor measures how well an oscillating system stores energy as opposed to dissipating it. The Q-factor for an antenna tuned to resonance is defined as [28, 55, 63]

$$Q = \frac{2\omega \max\{W_\mathrm{e}, W_\mathrm{m}\}}{P_\mathrm{d}} = \omega \frac{W + |W_\mathrm{m} - W_\mathrm{e}|}{P_\mathrm{d}}, \tag{1}$$

where $W = W_\mathrm{e} + W_\mathrm{m}$, W_e, and W_m denote the stored electromagnetic, electric, and magnetic energies, respectively, ω is the angular frequency, and P_d is the dissipated power. The dissipated power P_d and energy difference $W_\mathrm{m} - W_\mathrm{e}$ are well defined and follows directly from Poynting's theorem [19, 22]. Because of its relation to the bandwidth the Q-factor is an important parameter for antenna design. Thus it has become imperative to define stored energy for antennas [7, 10, 28, 46, 55, 63]. However, this is not trivial as electromagnetic fields, current densities, and circuit models can give different interpretations of the stored energy, see Fig. 1. In this section follows a brief overview of previous methods used to define stored energy.

The classical way of interpreting stored energy is as the energy stored in the fields that radiate from the antenna, but do not escape its vicinity, see Fig. 1b. This naturally leads to the subtraction calculation method, where the stored energy, W_F, is calculated by subtracting the power flow or the far-field power from the total energy [13, 16, 28, 55, 63]. Subtraction of the far-field term yields

$$W_\mathrm{F} = \frac{1}{4} \int_{\mathbb{R}^3_\mathrm{r}} \epsilon |\boldsymbol{E}(\boldsymbol{r})|^2 + \mu |\boldsymbol{H}(\boldsymbol{r})|^2 - 2\epsilon \frac{|\boldsymbol{F}(\hat{\boldsymbol{r}})|^2}{r^2} \,\mathrm{dV}, \tag{2}$$

where ϵ is the permittivity, μ is the permeability, $\boldsymbol{E}$ and $\boldsymbol{H}$ are the electric and magnetic fields, and $\boldsymbol{F}(\hat{\boldsymbol{r}})$ is the electric far-field; $\boldsymbol{F} \sim \mathrm{e}^{\mathrm{j}kr} r \boldsymbol{E}$ as $r \to \infty$ with

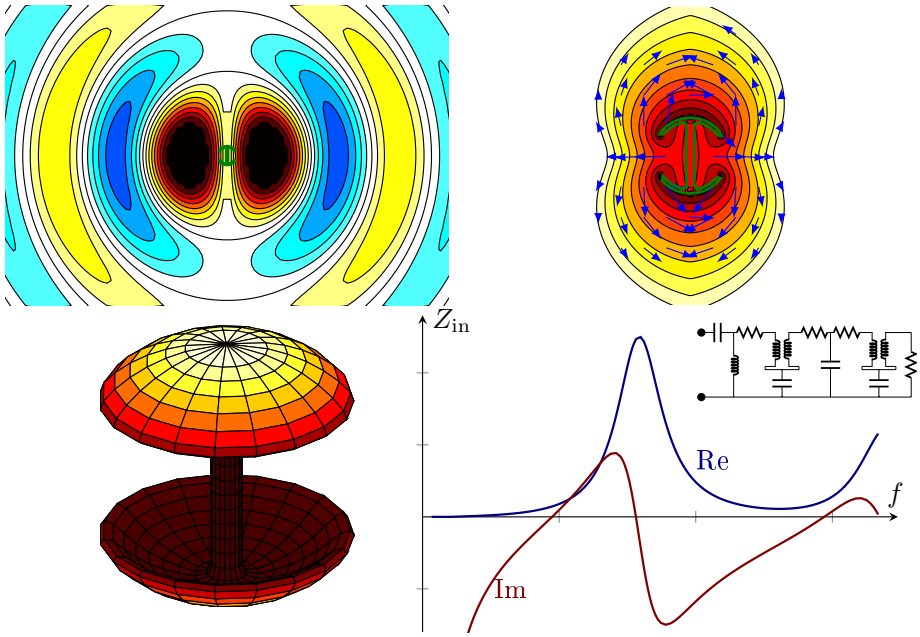

Figure 1: The three different approaches to express stored energy, electromagnetic fields, current density, and input impedance. Here, all are illustrated for the same capacitive dipole. a) snapshot of the magnetic field around the antenna. b) stored energy density around the antenna. c) current density on the antenna. d) input impedance and circuit model for the antenna.

$r = |\boldsymbol{r}|$ and $\hat{\boldsymbol{r}} = \boldsymbol{r}/r$. This definition of stored energy has been generally accepted since the classical work by [13], see also [16, 40, 63]. The stored energy (2) can also be expressed in the current density on the antenna structure [18, 22, 53, 54], see Fig. 1c. This simplifies the evaluation of stored energy and enables antenna current optimization [6, 23–25, 34]. The main drawbacks with (2) are possible coordinate dependence [22, 63] and negative stored energies [25, 63]. Moreover, as soon as losses are introduced in the background material, the far-field vanishes, *i.e.*, $\boldsymbol{F}(\hat{\boldsymbol{r}}) = \boldsymbol{0}$. This implies that W_{F} equals the total energy and it is hence not possible to distinguish the stored energy from the total energy in lossy backgrounds using (2) [63].

Using the same concept of stored energy defined as energy in the fields around the antenna, subtraction of the power flow from the energy density suggests the stored energy [14]

$$W_{\text{P}} = \frac{1}{4}\int_{\mathbb{R}^3_{\text{r}}} \epsilon|\boldsymbol{E}(\boldsymbol{r})|^2 + \mu|\boldsymbol{H}(\boldsymbol{r})|^2 - 4|\sqrt{\epsilon\mu}\boldsymbol{P}(\boldsymbol{r})|\,\mathrm{dV}, \tag{3}$$

where $\boldsymbol{P} = \frac{1}{2}\,\mathrm{Re}\{\boldsymbol{E} \times \boldsymbol{H}^*\}$ is the time-average Poynting vector. This definition

is coordinate independent and can be used in inhomogeneous and lossy backgrounds. However, the integral needs to be evaluated numerically and it is not clear how to generalize the formulation to temporally dispersive backgrounds. As an alternative, the radial component of the Poynting vector $\hat{\boldsymbol{r}} \cdot \boldsymbol{P}$ can be subtracted instead of the far-field amplitude [13, 40]. This leads to a coordinate dependent expression that differs from (2) by the radiated energy of the standing waves within the structure [22].

The problems with (2) and (3) call for alternative methodologies to define and evaluate the stored energy. To circumvent some of these problems, we consider the stored energy for the antenna as the stored energy seen from the input impedance, Z_{in}, see Fig. 1d. This has several advantages, such as being related to the impedance bandwidth, coordinate independent, and valid in arbitrary surrounding materials.

The input-impedance is separated into a resistive and reactive part, where the resistive part relates to dissipated energy and the reactive part relates to stored energy. For a lumped circuit network the reactance is proportional to the difference between energy stored capacitively and energy stored inductively

$$Z_{\text{in}} = R_{\text{in}} + \mathrm{j}X_{\text{in}} = \frac{2P_{\text{d}} + 4\mathrm{j}\omega(W_{\text{m}} - W_{\text{e}})}{|I_{\text{in}}|^2}, \tag{4}$$

where R_{in} is the input resistance, X_{in} the input reactance, and I_{in} the input current. The input impedance of the antenna can be modeled with circuit elements using, *e.g.*, Brune synthesis [4, 21], see also Fig. 1d. Kirchoff's laws are used to relate the currents $\mathbf{I}$ and voltages $\mathbf{V} = \mathbf{ZI}$ via the impedance matrix $\mathbf{Z}$, in the circuit network. The impedance matrix is further decomposed in its resistance $\mathbf{R}$, inductance $\mathbf{L}$, and capacitance $\mathbf{C} = \mathbf{C}_{\text{i}}^{-1}$ matrices [47, 48]:

$$\mathbf{Z} = \mathbf{R} + \mathrm{j}\mathbf{X} = \mathbf{R} + \mathrm{j}\omega\mathbf{L} + \frac{1}{\mathrm{j}\omega}\mathbf{C}_{\text{i}} = \mathbf{R} + s\mathbf{L} + \frac{1}{s}\mathbf{C}_{\text{i}}, \tag{5}$$

where $s = \mathrm{j}\omega$ is the Laplace parameter. The impedance matrix (5) can be considered as a second order state-space model for the input impedance $Z_{\text{in}} = V_{\text{in}}/I_{\text{in}}$ with the input $\mathbf{V} = \mathbf{B}V_{\text{in}}$ and output $I_{\text{in}} = \mathbf{B}^{\text{T}}\mathbf{I}$, where $\mathbf{B}$ is the feeding matrix, and the superscript $^{\text{T}}$ denotes the transpose. State-space models are used to model input output systems by ordinary differential equations [59]. They can be written in many forms and the order (degree of $s \to \frac{\partial}{\partial t}$) can be traded to the dimension of the system (number of states). For the analysis in the paper, the second order state-space model (5) is rewritten as the first order model [59]

$$s\begin{pmatrix}\mathbf{L} & \mathbf{0}\\ \mathbf{0} & \mathbf{C}\end{pmatrix}\begin{pmatrix}\mathbf{I}\\ \mathbf{U}\end{pmatrix} + \begin{pmatrix}\mathbf{R} & \mathbf{1}\\ -\mathbf{1} & \mathbf{0}\end{pmatrix}\begin{pmatrix}\mathbf{I}\\ \mathbf{U}\end{pmatrix} = \begin{pmatrix}s\mathbf{L}+\mathbf{R} & \mathbf{1}\\ -\mathbf{1} & s\mathbf{C}\end{pmatrix}\begin{pmatrix}\mathbf{I}\\ \mathbf{U}\end{pmatrix} = \begin{pmatrix}\mathbf{V}\\ \mathbf{0}\end{pmatrix}$$
$$\text{or } \widetilde{\mathbf{Z}}\widetilde{\mathbf{I}} = \widetilde{\mathbf{V}}, \tag{6}$$

where the voltage state $\mathbf{U} = \frac{1}{s}\mathbf{C}_{\text{i}}\mathbf{I}$ is introduced, and $\mathbf{1}$ is the identity matrix. The time-domain ($s \to \frac{\partial}{\partial t}$) stored energy is defined from the energy balance that

is derived by multiplication of (6) with the states, $(\mathbf{I}^{\mathrm{T}}\ \mathbf{U}^{\mathrm{T}})$, from the left and temporal integration, *i.e.*,

$$\left[\frac{\mathbf{I}^{\mathrm{T}}(t)\mathbf{L}\mathbf{I}(t)+\mathbf{U}^{\mathrm{T}}(t)\mathbf{C}\mathbf{U}(t)}{2}\right]_{t_1}^{t_2}+\int_{t_1}^{t_2}\mathbf{I}^{\mathrm{T}}(t)\mathbf{R}\mathbf{I}(t)\,\mathrm{d}t = \int_{t_1}^{t_2}\mathbf{I}^{\mathrm{T}}(t)\mathbf{V}(t)\,\mathrm{d}t=\int_{t_1}^{t_2}I_{\mathrm{in}}(t)V_{\mathrm{in}}(t)\,\mathrm{d}t, \quad (7)$$

where for notational simplicity time t is used to define time-domain quantities. The first and second terms in the left-hand side are identified as the change of stored energy and dissipated energy during the time interval $[t_1, t_2]$, respectively. The right-hand side is the supplied energy during the same period. The time-average stored energy for a time-harmonic signal in (7) is alternatively obtained from the quadratic form constructed from the matrix multiplying s in (6), *i.e.*,

$$W=\frac{\mathbf{I}^{\mathrm{H}}\mathbf{L}\mathbf{I}}{4}+\frac{\mathbf{U}^{\mathrm{H}}\mathbf{C}\mathbf{U}}{4}=\frac{\mathbf{I}^{\mathrm{H}}\mathbf{L}\mathbf{I}}{4}+\frac{\mathbf{I}^{\mathrm{H}}\mathbf{C}_{\mathrm{i}}^{\mathrm{H}}\mathbf{C}\mathbf{C}_{\mathrm{i}}\mathbf{I}}{4\omega^2} = \frac{1}{4}\mathbf{I}^{\mathrm{H}}\left(\mathbf{L}+\frac{\mathbf{C}_{\mathrm{i}}}{\omega^2}\right)\mathbf{I}=\frac{\mathbf{I}^{\mathrm{H}}\mathbf{X}'\mathbf{I}}{4}=\frac{\tilde{\mathbf{I}}^{\mathrm{H}}\widetilde{\mathbf{X}}'\tilde{\mathbf{I}}}{4}, \quad (8)$$

where the superscripts $^{\mathrm{H}}$ and prime $'$ denote the conjugate transpose and differentiation with respect to ω, respectively, we have used that $\mathbf{C}_{\mathrm{i}}^{\mathrm{H}}=\mathbf{C}_{\mathrm{i}}$, and $\widetilde{\mathbf{Z}}=\widetilde{\mathbf{R}}+\mathrm{j}\widetilde{\mathbf{X}}$. It is essential that the matrices $\mathbf{L}=\mathbf{L}^{\mathrm{T}}$ and $\mathbf{C}_{\mathrm{i}}=\mathbf{C}_{\mathrm{i}}^{\mathrm{T}}$ are symmetric, frequency independent, and real valued to determine the stored energy [59].

The stored energy expression (8) is a Hermitian quadratic form in terms of the frequency derivative of the reactance or state-space reactance matrix. The difference between the stored magnetic and electric energies are directly proportional to the quadratic form of the reactance matrix, $W_{\mathrm{m}}-W_{\mathrm{e}}=\dfrac{\mathbf{I}^{\mathrm{H}}\mathbf{X}\mathbf{I}}{4\omega}$ *cf.*, (4). This gives us explicit formulas for the stored magnetic and electric energies

$$W_{\mathrm{m}}=\frac{1}{8}\mathbf{I}^{\mathrm{H}}\left(\frac{\partial\mathbf{X}}{\partial\omega}+\frac{\mathbf{X}}{\omega}\right)\mathbf{I}=\frac{1}{4}\mathbf{I}^{\mathrm{H}}\mathbf{L}\mathbf{I} \quad (9)$$

and

$$W_{\mathrm{e}}=\frac{1}{8}\mathbf{I}^{\mathrm{H}}\left(\frac{\partial\mathbf{X}}{\partial\omega}-\frac{\mathbf{X}}{\omega}\right)\mathbf{I}=\frac{1}{4\omega^2}\mathbf{I}^{\mathrm{H}}\mathbf{C}_{\mathrm{i}}\mathbf{I}, \quad (10)$$

respectively. The stored energy (8) can hence be interpreted as the sum of the electric energy in the capacitors and the magnetic energy in the inductors. The relations (9) and (10) resemble the expressions in [19,30] for the input impedance of single and array antennas. Here, it is essential to note that (9) and (10) are expressed in the state-space matrix and not in the input impedance, *cf.*, [19,30]. The expressions based on the input impedance are only valid for single resonance RLC circuits and lossless circuit networks [30]. The Brune synthesized circuit and the state-space representation are mathematical models created from a rational

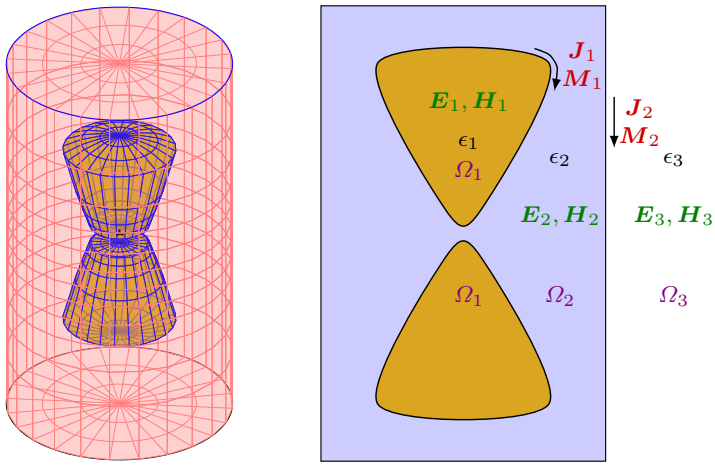

Figure 2: Illustration of an antenna geometry composed of three materials modeled by their permittivity ϵ_n and permeability μ_n, $n = 1, 2, 3$ in the regions Ω_n. The electromagnetic fields are denoted $\boldsymbol{E}_n$ and $\boldsymbol{H}_n$ in Ω_n. The equivalent (surface) currents $\boldsymbol{J}_m$ and $\boldsymbol{M}_m$ have support on the boundary between Ω_m and Ω_{m+1}, $m = 1, 2$. (left) three dimensional and (right) two dimensional cut.

approximation of the input impedance. Here, it is also important to realize that the circuit model is non-unique and that there are several methods to synthesize circuit models [60], see also [46, 59] for discussions about minimum realizations and unobservable energy. The Zöbel network [64] is a classical example that illustrates these properties. The unobservable stored energy does not contribute to the input impedance and the bandwidth of the system. Hence, we are seeking the observable part or equivalently the minimum stored energy in the system.

The Q-factor (1) is expressed in the reactance matrix and its frequency derivative as

$$Q = \frac{\max\{\mathbf{I}^{\mathrm{H}}(\omega\mathbf{X}' \pm \mathbf{X})\mathbf{I}\}}{2\mathbf{I}^{\mathrm{H}}\mathbf{R}\mathbf{I}} = \frac{\omega\mathbf{I}^{\mathrm{H}}\mathbf{X}'\mathbf{I} + |\mathbf{I}^{\mathrm{H}}\mathbf{X}\mathbf{I}|}{2\mathbf{I}^{\mathrm{H}}\mathbf{R}\mathbf{I}}, \tag{11}$$

where we used the time average dissipated power $P_{\mathrm{d}} = \frac{1}{2}\operatorname{Re}\{\mathbf{I}^{\mathrm{H}}\mathbf{V}\} = \frac{1}{2}\mathbf{I}^{\mathrm{H}}\mathbf{R}\mathbf{I}$, with $\mathbf{R} = \operatorname{Re}\mathbf{Z}$. The Q-factor (11) is determined from the input impedance (4) and hence related to the fractional bandwidth of the antenna. However, the dependence on the input impedance is also the main draw back of this method, as it is based on the antenna geometry including its feed. In this paper we view the antenna as a input output system, but instead of synthesizing an equivalent circuit model we create a state-space model from the MoM impedance matrix. This model is based on Maxwell equations, includes the antenna geometry, and can be used for antenna current optimization.

We consider antennas in an inhomogeneous temporally dispersive background medium, see Fig. 2. The background medium has permittivity $\epsilon = \epsilon_0\epsilon_{\mathrm{r}}$ and

permeability $\mu = \mu_0\mu_\mathrm{r}$ which depend on the angular frequency ω or Laplace parameter $s = \mathrm{j}\omega$. The wave impedance $\eta = \sqrt{\mu/\epsilon}$, the index of refraction $n = \sqrt{s^2\epsilon_\mathrm{r}\mu_\mathrm{r}}/s$, the wavenumber $k = -\mathrm{j}\kappa$, where $\kappa = \sqrt{s^2\epsilon\mu}$, speed of light $\mathrm{c}_0 = 1/\sqrt{\epsilon_0\mu_0}$, and the intrinsic impedance of vacuum $\eta_0 = \sqrt{\mu_0/\epsilon_0}$ are also used to simplify the notation. To start, we restrict the analysis to electric surface current densities in free space in Sec. 3. This case is thoroughly analyzed using (2) in [21, 22, 53, 54]. The background material is subsequently generalized to temporally dispersive in Sec. 4, piecewise inhomogeneous in Sec. 5.1, and inhomogeneous in Sec. 5.2.

3 Stored Energy for Antennas in Free Space

The state-space model is based on the EFIE impedance matrix $\mathbf{Z}$. A standard MoM implementation of the EFIE determines the impedance matrix [9, 44, 56] which can be written as

$$\mathbf{Z} = s\mu\mathbf{L} + \frac{1}{s\epsilon}\mathbf{C}_\mathrm{i} = \eta\kappa\mathbf{L} + \frac{\eta}{\kappa}\mathbf{C}_\mathrm{i}, \tag{12}$$

where the matrices $\mathbf{L}$ and $\mathbf{C}_\mathrm{i}$ depend on the wavenumber and have the elements

$$L_{mn} = \int_{\partial\Omega}\int_{\partial\Omega} \boldsymbol{\psi}_m(\boldsymbol{r}_1)\cdot\boldsymbol{\psi}_n(\boldsymbol{r}_2)\frac{\mathrm{e}^{-\mathrm{j}kR_{12}}}{4\pi R_{12}}\,\mathrm{dS}_1\,\mathrm{dS}_2 \tag{13}$$

and

$$C_{imn} = \int_{\partial\Omega}\int_{\partial\Omega} \nabla_1\cdot\boldsymbol{\psi}_m(\boldsymbol{r}_1)\nabla_2\cdot\boldsymbol{\psi}_n(\boldsymbol{r}_2)\frac{\mathrm{e}^{-\mathrm{j}kR_{12}}}{4\pi R_{12}}\,\mathrm{dS}_1\,\mathrm{dS}_2, \tag{14}$$

where $R_{12} = |\boldsymbol{r}_1 - \boldsymbol{r}_2|$ is the distance between the spatial points $\boldsymbol{r}_1$ and $\boldsymbol{r}_2$ and $\partial\Omega$ denotes the antenna boundary modeled as a PEC. The material parameters are $\epsilon = \epsilon_0$ and $\mu = \mu_0$ for the free space case. The basis functions, $\boldsymbol{\psi}_m(\boldsymbol{r})$, are assumed to be real valued and divergence conforming with vanishing normal components at the antenna boundary [30, 44]. The decomposition of the MoM impedance matrix (12) resembles the impedance matrix for lumped circuits (5) with the major differences that $\mathbf{R}$ is missing and that $\mathbf{L}$ and $\mathbf{C}_\mathrm{i}$ are complex valued and depend on k (or s) in (12). The MoM impedance matrix (12) can alternatively be decomposed as (5) using the real and imaginary parts, see App. B. It is however advantageous to keep (12) for the presentation in this paper.

The state-space model is constructed for the input impedance, $Z_\mathrm{in} = V_\mathrm{in}/I_\mathrm{in}$, with the voltage excitation V_in and current output I_in. The current column matrix $\mathbf{I}$ contains the expansion coefficients I_n for the current density $\boldsymbol{J}(\boldsymbol{r}) = \sum_{n=1}^{N} I_n\boldsymbol{\psi}_n(\boldsymbol{r})$ that is determined from the linear system

$$\mathbf{ZI} = \mathbf{V} = \mathbf{B}V_\mathrm{in} \quad \text{and } I_\mathrm{in} = \mathbf{B}^\mathrm{T}\mathbf{I}, \tag{15}$$

where $\mathbf{B}$ is the matrix containing feed position of the antenna. Inspired by the stored energy in circuit models (8) and more general state-space models [59], we use a state-space approach based on a MoM formulation to determine the stored energy for antennas. This changes the interpretation of stored energy from energy expressed in the electromagnetic fields to energy expressed in the states. These states (in the MoM formulations) are the current densities and hence the sources of the fields, see Fig.1. The state-space model also shows that the stored energy determined from the current density is related to the stored energy determined from the input impedance for small antennas $ka \ll 1$, where a denotes the radius of the smallest circumscribing sphere [10].

A PEC antenna structure embedded in a homogeneous isotropic media is modeled by the EFIE (12) and (15). The system can be written

$$\mathbf{Z}\mathbf{I} = (s\mu\mathbf{L} + \frac{1}{s\epsilon}\mathbf{C}_\mathrm{i})\mathbf{I} = s\mu\mathbf{L}\mathbf{I} + \mathbf{U} = \mathbf{V} = \mathbf{B}V_\mathrm{in} \quad \text{and } I_\mathrm{in} = \mathbf{B}^\mathrm{T}\mathbf{I}, \tag{16}$$

where a voltage state $\mathbf{U} = \frac{1}{s\epsilon}\mathbf{C}_\mathrm{i}\mathbf{I}$ is introduced, *cf.*, (6), to rewrite the second order system (16) to the first order system

$$s\begin{pmatrix}\mu\mathbf{L} & \mathbf{0}\\ \mathbf{0} & \epsilon\mathbf{C}\end{pmatrix}\begin{pmatrix}\mathbf{I}\\ \mathbf{U}\end{pmatrix} = \begin{pmatrix}\mathbf{0} & -\mathbf{1}\\ \mathbf{1} & \mathbf{0}\end{pmatrix}\begin{pmatrix}\mathbf{I}\\ \mathbf{U}\end{pmatrix} + \begin{pmatrix}\mathbf{B}\\ \mathbf{0}\end{pmatrix}V_\mathrm{in}. \tag{17}$$

The system is a classical state-space model for the free space case, $\epsilon = \epsilon_0$ and $\mu = \mu_0$, in the limit of small antennas $ka \ll 1$. Moreover the symmetry of the system implies that the stored energy is defined for minimal representations [59]. Following the approach in Sec. 2, the stored energy is given by the quadratic form generated by the matrix that multiples s (temporal derivative). However, the frequency dependence of $\mathbf{L}$ and $\mathbf{C}_\mathrm{i}$ cannot be neglected for finite sized antennas. Moreover, the matrices $\mathbf{L}$ and $\mathbf{C}_\mathrm{i}$ have an imaginary part for $\omega > 0$, see App. B. To resolve the issue of frequency dependence, we use differentiation with respect to s of the state-space model to estimate the term that is proportional to s. This expresses the time average stored energy as

$$\begin{aligned} W_{\widetilde{\mathbf{X}}'} &= \frac{1}{4}\widetilde{\mathbf{I}}^\mathrm{H}\frac{\partial\widetilde{\mathbf{X}}}{\partial\omega}\widetilde{\mathbf{I}} = \frac{\mathrm{Re}}{4}\begin{pmatrix}\mathbf{I}\\ \mathbf{U}\end{pmatrix}^\mathrm{H}\begin{pmatrix}\mu_0(\mathbf{L}+\omega\mathbf{L}') & \mathbf{0}\\ \mathbf{0} & \epsilon_0(\mathbf{C}+\omega\mathbf{C}')\end{pmatrix}\begin{pmatrix}\mathbf{I}\\ \mathbf{U}\end{pmatrix}\\ &= \frac{\mathrm{Re}}{4}\big(\mu_0\mathbf{I}^\mathrm{H}(\mathbf{L}+\omega\mathbf{L}')\mathbf{I} + \epsilon_0\mathbf{U}^\mathrm{H}(\mathbf{C}+\omega\mathbf{C}')\mathbf{U}\big)\\ &\simeq \frac{\mathrm{Re}}{4}\mathbf{I}^\mathrm{H}\big(\mu_0(\mathbf{L}+\omega\mathbf{L}') + \frac{1}{\omega^2\epsilon_0}(\mathbf{C}_\mathrm{i}-\omega\mathbf{C}_\mathrm{i}')\big)\mathbf{I} = \frac{1}{4}\mathbf{I}^\mathrm{H}\frac{\partial\mathbf{X}}{\partial\omega}\mathbf{I}, \end{aligned} \tag{18}$$

where $\mathbf{C}' = -\mathbf{C}\mathbf{C}_\mathrm{i}'\mathbf{C}$ and $\mathrm{Re}\{\frac{\partial\mathbf{Z}}{\partial s}\} = \frac{\partial\mathbf{X}}{\partial\omega}$ are used and the differentiated matrices have the entries

$$L'_{mn} = \frac{\partial L_{mn}}{\partial\omega} = -\mathrm{j}\frac{\partial k}{\partial\omega}\int_{\partial\Omega}\int_{\partial\Omega}\boldsymbol{\psi}_m(\boldsymbol{r}_1)\cdot\boldsymbol{\psi}_n(\boldsymbol{r}_2)\frac{\mathrm{e}^{-\mathrm{j}kR_{12}}}{4\pi}\,\mathrm{dS}_1\,\mathrm{dS}_2, \tag{19}$$

and

$$C'_{imn} = \frac{\partial C_{imn}}{\partial\omega} = -\mathrm{j}\frac{\partial k}{\partial\omega}\int_{\partial\Omega}\int_{\partial\Omega}\nabla_1\cdot\boldsymbol{\psi}_m(\boldsymbol{r}_1)\nabla_2\cdot\boldsymbol{\psi}_n(\boldsymbol{r}_2)\frac{\mathrm{e}^{-\mathrm{j}kR_{12}}}{4\pi}\,\mathrm{dS}_1\,\mathrm{dS}_2. \tag{20}$$

The use of frequency differentiation is an approximation to handle the frequency dependence of $\mathbf{L}$ and $\mathbf{C}_\mathrm{i}$. The stored energy (18) is dominated by the contribution from $\mathbf{L}$ and $\mathbf{C}_\mathrm{i}$ for small antennas [22] and the contributions from $\mathbf{L}'$ and $\mathbf{C}_\mathrm{i}'$ are lower order corrections. The $\simeq$ in (18) is used to indicate that we neglect the low order correction term $\mathrm{Re}\{\mathbf{I}^\mathrm{H}(\mathbf{1}-\mathbf{C}_\mathrm{i}^\mathrm{H}\mathbf{C}_\mathrm{i}^{-1})\mathbf{C}_\mathrm{i}'\mathbf{I}\} \approx 0$. These terms are neglected in the remainder of this paper.

The expression (18) for the stored energy is identical to the expressions proposed by [31], and [53] which is equal to the stored energy W_F in (2) for the cases where (2) is coordinate independent [22]. The stored electric and magnetic energies, and Q-factor are determined as for the circuit network case in (9) to (11). The time average dissipated power is determined from the Poynting vector and can be expressed as the quadratic form [19, 22, 53] $P_\mathrm{d} = \frac{1}{2}\,\mathrm{Re}\{\mathbf{I}^\mathrm{H}\mathbf{V}\} = \frac{1}{2}\mathbf{I}^\mathrm{H}\mathbf{R}\mathbf{I}$, where $\mathbf{R} = \mathrm{Re}\,\mathbf{Z}$, as in (72). The stored energy expression (18) is compared with the stored energy determined from Brune synthesized circuit models in [21], see also [11, 12, 24, 32]. The results agree very well for antenna sizes up to approximately half-a-wavelength and Q-factors above 5. The problems with larger antennas are caused by the frequency dependence of the matrices $\mathbf{L}$ (13) and $\mathbf{C}_\mathrm{i}$ (14). This frequency dependence implies that (16) is not a first order state-space model, hence, the frequency differentiation in (18) is only an approximation. This interpretation is analogous to the difficulties to define the radiated energy in (2) and (3) for larger antenna structures and originates in the wave nature of the electromagnetic fields that causes phase, or equivalently time, shifts. The state-space approach suggest a possible remedy using rational approximations of the Green's function in (13) and (14). The problem with the frequency dependence of $\mathbf{L}$ and $\mathbf{C}_\mathrm{i}$ is, however, negligible for small antennas with $Q \gg 1$ that are the main focus of this paper.

4 Stored Energy for Temporally Dispersive Background Media

The classical approach to define stored energy by subtraction of the far-field (2) is difficult to generalize to lossy background materials as the far-field vanishes. This implies that W_F equals the total energy in a lossy background and that $W_\mathrm{F} \to \infty$ as the losses approach zero. Here, we use the state-space approach to generalize the expressions for the stored energy in Sec. 3 to background materials with losses and temporally dispersive permittivity in Sec. 4.1, and combined permittivity and permeability in Sec. 4.2.

4.1 Temporally Dispersive Permittivity

The MoM impedance matrix in temporally dispersive media is formally identical to the free space case (12) with the use of the complex-valued wavenumber k in

the background medium. Consider for simplicity a non-magnetic media with the permittivity described by a single Lorentz resonance [33, 52]

$$\epsilon(s) = \epsilon_\infty + \frac{\alpha^2}{\beta^2 + \gamma s + \delta s^2} = \epsilon_\infty + \frac{\alpha^2}{\chi}, \tag{21}$$

where ϵ_∞ is the instantaneous response, $\alpha, \beta, \gamma, \delta$ are the Lorentz parameters, and χ is introduced for notational simplicity. This model reduces to conductivity ($\beta = \delta = 0$), Debye ($\delta = 0$), and Drude ($\beta = 0$) models with specific parameter choices and is easily extended to multiple resonances. The system (16) is rewritten to a first order system by introduction of the voltage state $\mathbf{U}$, polarization state $\mathbf{P}$, and its temporal derivative $\dot{\mathbf{P}} = \beta^{-1} s\mathbf{P}$, *i.e.*,

$$\mathbf{I} = s\epsilon\mathbf{C}\mathbf{U} = \Big(s\epsilon_\infty + \frac{s\alpha^2}{\beta^2 + \gamma s + \delta s^2}\Big)\mathbf{C}\mathbf{U} = s\epsilon_\infty\mathbf{C}\mathbf{U} + \alpha\dot{\mathbf{P}}, \tag{22}$$

where $\mathbf{C} = \mathbf{C}_\mathrm{i}^{-1}$ is used for simplicity. Note that $\mathbf{C}_\mathrm{i}$ has a null space and is not invertible. This is resolved in the final expressions for the stored energy below. The rational and second order s-term in $\alpha\dot{\mathbf{P}}$ are removed by multiplication with $\chi\mathbf{C}_\mathrm{i}/(s\alpha)$, *i.e.*,

$$\alpha\mathbf{U} = (\beta^2 + \gamma s + \delta s^2)\frac{1}{s}\mathbf{C}_\mathrm{i}\dot{\mathbf{P}} = \beta\mathbf{C}_\mathrm{i}\mathbf{P} + (\gamma + \delta s)\mathbf{C}_\mathrm{i}\dot{\mathbf{P}}. \tag{23}$$

Collecting the equations (16), (22), $s\mathbf{C}_\mathrm{i}\mathbf{P} = \beta\mathbf{C}_\mathrm{i}\dot{\mathbf{P}}$, and (23) gives the linear system

$$\widetilde{\mathbf{Z}}\widetilde{\mathbf{I}} = \begin{pmatrix} s\mu\mathbf{L} & \mathbf{1} & \mathbf{0} & \mathbf{0} \\ -\mathbf{1} & s\epsilon_\infty\mathbf{C} & \mathbf{0} & \mathbf{1}\alpha \\ \mathbf{0} & \mathbf{0} & s\mathbf{C}_\mathrm{i} & -\beta\mathbf{C}_\mathrm{i} \\ \mathbf{0} & -\mathbf{1}\alpha & \beta\mathbf{C}_\mathrm{i} & (s\delta + \gamma)\mathbf{C}_\mathrm{i} \end{pmatrix} \begin{pmatrix} \mathbf{I} \\ \mathbf{U} \\ \mathbf{P} \\ \dot{\mathbf{P}} \end{pmatrix} = \begin{pmatrix} \mathbf{V} \\ \mathbf{0} \\ \mathbf{0} \\ \mathbf{0} \end{pmatrix} = \widetilde{\mathbf{B}}V_\mathrm{in}, \tag{24}$$

with the output $I_\mathrm{in} = \mathbf{B}^\mathrm{T}\mathbf{I} = \widetilde{\mathbf{B}}^\mathrm{T}\widetilde{\mathbf{I}}$, and input V_in. This is a classical state-space representation [59] in the limit of small antennas, where the s-dependence of the matrices $\mathbf{L}$ and $\mathbf{C}_\mathrm{i}$ is negligible. Furthermore, the representation is reciprocal with internal symmetry $\mathrm{diag}(\mathbf{1}, -\mathbf{1}, -\mathbf{1}, \mathbf{1})$, see [59].

To calculate the stored energy of the system (24), the term proportional to s is estimated by differentiation with respect to s

$$\frac{\partial\widetilde{\mathbf{Z}}}{\partial s} = \begin{pmatrix} \mu\mathbf{L} + \omega\mu\mathbf{L}' & \mathbf{0} & \mathbf{0} & \mathbf{0} \\ \mathbf{0} & \epsilon_\infty\mathbf{C} + \omega\epsilon_\infty\mathbf{C}' & \mathbf{0} & \mathbf{0} \\ \mathbf{0} & \mathbf{0} & \mathbf{C}_\mathrm{i} + \omega\mathbf{C}_\mathrm{i}' & \mathrm{j}\beta\mathbf{C}_\mathrm{i}' \\ \mathbf{0} & \mathbf{0} & -\mathrm{j}\beta\mathbf{C}_\mathrm{i}' & \delta\mathbf{C}_\mathrm{i} + (\omega\delta - \mathrm{j}\gamma)\mathbf{C}_\mathrm{i}' \end{pmatrix}, \tag{25}$$

where frequency dependence of the matrices $\mathbf{L}$ and $\mathbf{C}_\mathrm{i}$ are approximated locally using frequency differentiation [26]. The stored energy is finally calculated by the quadratic form obtained by multiplication of (25) with the states from the

left and right. A closed form expressions is derived by back substitution of the explicit expressions of the states expressed in the current $\mathbf{I}$. Use that $\mathbf{CU} = \frac{1}{s\epsilon}\mathbf{I}$, $\dot{\mathbf{P}} = \frac{s}{\beta}\mathbf{P}$, $\mathbf{P} = \frac{\alpha\beta}{s\epsilon\chi}\mathbf{I}$, and

$$\mathrm{j}\beta\left(\mathbf{P}^{\mathrm{H}}\mathbf{C}_{\mathrm{i}}'\dot{\mathbf{P}} - \dot{\mathbf{P}}^{\mathrm{H}}\mathbf{C}_{\mathrm{i}}'\mathbf{P}\right) = \left(-\omega\mathbf{P}^{\mathrm{H}}\mathbf{C}_{\mathrm{i}}'\mathbf{P} - \omega\mathbf{P}^{\mathrm{H}}\mathbf{C}_{\mathrm{i}}'\mathbf{P}\right) = -2\omega\mathbf{P}^{\mathrm{H}}\mathbf{C}_{\mathrm{i}}'\mathbf{P} \tag{26}$$

to express the stored energy as

$$\begin{aligned} W_{\widetilde{\mathbf{X}}'} = {} & \frac{\mathrm{Re}}{4}\mathbf{I}^{\mathrm{H}}\left(\mu\mathbf{L} + \frac{\epsilon_\infty}{|\omega\epsilon|^2}\mathbf{C}_{\mathrm{i}} + \omega\mu\mathbf{L}' - \frac{\omega\epsilon_\infty}{|\omega\epsilon|^2}\mathbf{C}_{\mathrm{i}}'\right)\mathbf{I} \\ & + \frac{\mathrm{Re}}{4}\mathbf{P}^{\mathrm{H}}\left(\mathbf{C}_{\mathrm{i}} + \mathbf{C}_{\mathrm{i}}\delta\frac{\omega^2}{\beta^2} + \omega\mathbf{C}_{\mathrm{i}}' + \omega^2\frac{\omega\delta - \mathrm{j}\gamma}{\beta^2}\mathbf{C}_{\mathrm{i}}' - 2\omega\mathbf{C}_{\mathrm{i}}'\right)\mathbf{P}, \end{aligned} \tag{27}$$

where the low-order term in (18) is neglected. The second part multiplying $\mathbf{P}$ can be written as

$$(\beta^2 + \delta\omega^2)\mathbf{C}_{\mathrm{i}} - \omega(\beta^2 - \omega^2\delta + \mathrm{j}\omega\gamma)\mathbf{C}_{\mathrm{i}}' = (\beta^2 + \delta\omega^2)\mathbf{C}_{\mathrm{i}} - \omega\chi\mathbf{C}_{\mathrm{i}}', \tag{28}$$

that together with elimination of $\mathbf{P}$ express the stored energy as the quadratic form

$$W_{\widetilde{\mathbf{X}}'} = \frac{\mathrm{Re}}{4}\mathbf{I}^{\mathrm{H}}\left(\mu\mathbf{L} + \frac{\epsilon_\infty}{|\omega\epsilon|^2}\mathbf{C}_{\mathrm{i}} + \omega\mu\mathbf{L}' - \frac{\omega\epsilon_\infty}{|\omega\epsilon|^2}\mathbf{C}_{\mathrm{i}}' + \frac{\alpha^2\left((\beta^2 + \omega^2\delta)\mathbf{C}_{\mathrm{i}} - \omega\chi\mathbf{C}_{\mathrm{i}}'\right)}{|\omega\epsilon|^2|\chi|^2}\right)\mathbf{I} \tag{29}$$

in the current $\mathbf{I}$. The solution simplifies for the reduced models, *e.g.*, the conductivity model $\epsilon = \epsilon_\infty + \sigma/s$ with $\alpha^2/\gamma = \sigma$, $\beta = \delta = 0$, and $\chi = s\gamma$ has the stored energy

$$W_{\widetilde{\mathbf{X}}'} = \frac{\mathrm{Re}}{4}\mathbf{I}^{\mathrm{H}}\left(\mu\mathbf{L} + \frac{\epsilon_\infty}{\omega^2\epsilon_\infty^2 + \sigma^2}\mathbf{C}_{\mathrm{i}} + \omega\mu\mathbf{L}' - \frac{\mathrm{j}\sigma + \omega\epsilon_\infty}{\omega^2\epsilon_\infty^2 + \sigma^2}\mathbf{C}_{\mathrm{i}}'\right)\mathbf{I}. \tag{30}$$

It is also straight forward to generalize the stored energy expressions to multiple resonances by adding multiple polarization states.

We follow (9), (10), and (11) to determine the stored electric and magnetic energies and Q-factor for the state-space model. The frequency derivative of the state-space matrix $\widetilde{\mathbf{X}}'$ produces the quadratic forms for the stored energies in (18), *i.e.*,

$$W_{\widetilde{\mathbf{X}}'} = W_{\mathrm{e}\widetilde{\mathbf{X}}'} + W_{\mathrm{m}\widetilde{\mathbf{X}}'} = \frac{1}{4}\widetilde{\mathbf{I}}^{\mathrm{H}}\frac{\partial\widetilde{\mathbf{X}}}{\partial\omega}\widetilde{\mathbf{I}} = \frac{1}{4\omega}\mathbf{I}^{\mathrm{H}}(\mathbf{X}_{\mathrm{e}} + \mathbf{X}_{\mathrm{m}})\mathbf{I}, \tag{31}$$

where (29) is used to introduce the electric, $\mathbf{X}_{\mathrm{e}}$, and magnetic, $\mathbf{X}_{\mathrm{m}}$, reactance matrices for dispersive media [23,24]. The difference between the stored magnetic and electric energies give the explicit formulas for the stored magnetic and electric energies

$$W_{\mathrm{m}\widetilde{\mathbf{X}}'} = \frac{1}{8}\widetilde{\mathbf{I}}^{\mathrm{H}}\left(\frac{\partial\widetilde{\mathbf{X}}}{\partial\omega} + \frac{\widetilde{\mathbf{X}}}{\omega}\right)\widetilde{\mathbf{I}} = \frac{1}{4\omega}\mathbf{I}^{\mathrm{H}}\mathbf{X}_{\mathrm{m}}\mathbf{I} \tag{32}$$

and

$$W_{\mathrm{e}\widetilde{\mathbf{X}}'} = \frac{1}{8}\widetilde{\mathbf{I}}^{\mathrm{H}}\left(\frac{\partial\widetilde{\mathbf{X}}}{\partial\omega} - \frac{\widetilde{\mathbf{X}}}{\omega}\right)\widetilde{\mathbf{I}} = \frac{1}{4\omega}\mathbf{I}^{\mathrm{H}}\mathbf{X}_{\mathrm{e}}\mathbf{I}, \tag{33}$$

respectively. The relations (32) and (33) are formally identical to the stored energy expressions for the lumped circuit networks (9) and (10). The Q-factor for antennas tuned to resonance (1) is

$$Q_{\widetilde{\mathbf{X}}'} = \frac{\max\{\widetilde{\mathbf{I}}^{\mathrm{H}}(\omega\widetilde{\mathbf{X}}' \pm \widetilde{\mathbf{X}})\widetilde{\mathbf{I}}\}}{2\mathbf{I}^{\mathrm{H}}\mathbf{R}\mathbf{I}} = \frac{\omega\widetilde{\mathbf{I}}^{\mathrm{H}}\widetilde{\mathbf{X}}'\widetilde{\mathbf{I}} + |\mathbf{I}^{\mathrm{H}}\mathbf{X}\mathbf{I}|}{2\mathbf{I}^{\mathrm{H}}\mathbf{R}\mathbf{I}} = \frac{\max\{\mathbf{I}^{\mathrm{H}}\mathbf{X}_{\mathrm{e}}\mathbf{I}, \mathbf{I}^{\mathrm{H}}\mathbf{X}_{\mathrm{m}}\mathbf{I}\}}{\mathbf{I}^{\mathrm{H}}\mathbf{R}\mathbf{I}} \tag{34}$$

for the stored energy (31).

We compare the Q-factor determined from the state-space model $Q_{\widetilde{\mathbf{X}}'}$ using (29) with the differentiated input impedance $Q_{\mathrm{Z}'_{\mathrm{in}}}$ (66), Brune synthesis $Q_{\mathrm{Z}^{\mathrm{B}}_{\mathrm{in}}}$ [21], and $\Gamma_0 = 0.3$ reflection coefficient $Q_{0.3}$ (68) in Figs. 3, 4, and 5. The antenna parameters are computed using a MoM code based on rectangular elements for planar (negligible thickness) structures modeled as PECs. We consider non-dispersive, conductivity, and Lorentz permittivity models for dipole antennas with length ℓ and width 0.01ℓ in Figs 3 and 4. The results are presented in the dimensionless parameter ℓ/λ, where λ is the free space wavelength. The material parameters are functions of the dimensionless parameter $\omega = 2\pi\ell/\lambda$.

Fig. 3 depicts strip dipoles, fed at the center and 0.27ℓ from the center, in a homogenous medium with relative permittivity $\epsilon_{\mathrm{r}} = 1 - \mathrm{j}2\pi\alpha/\omega$. The off-center feed is chosen to eliminate some of the symmetries of the induced current density distribution in comparison to the center-fed case, and increase the phase shift of the induced current density. The calculated Q-factors are depicted in Fig. 3 for free space and background media with relative permittivity $\epsilon_{\mathrm{r}} = 1 - \mathrm{j}0.25/\omega \approx 1 - \mathrm{j}0.04\lambda/\ell$. All Q-factors seem to agree well for the center fed dipole in the left hand figure. For the off-center fed dipole in the right hand figure the Q-factors agree well for low frequencies, but tend to deviate slightly at higher frequencies. At low frequencies the loss tangent $0.25/\omega$ is high and thus all Q-factors are small. The Q-factor from the Brune circuit $Q_{\mathrm{Z}^{\mathrm{B}}_{\mathrm{in}}}$ follow $Q_{\widetilde{\mathbf{X}}'}$ but gives slightly lower values. The Q-factor from the differentiated input impedance $Q_{\mathrm{Z}'_{\mathrm{in}}}$ is similar to $Q_{\mathrm{Z}^{\mathrm{B}}_{\mathrm{in}}}$ except for $\ell/\lambda \approx 2$ in the off-center fed case, where $Q_{\mathrm{Z}'}$ has a dip. This dip is mimicked in the free space case where $Q_{\mathrm{Z}'} \approx 0$, see also [21]. $Q_{0.3}$ also deviates from $Q_{\widetilde{\mathbf{X}}'}$ at $\ell/\lambda \approx 2$ where it has a fixed lower level. $Q_{\widetilde{\mathbf{X}}'}$ and $Q_{\mathrm{Z}^{\mathrm{B}}_{\mathrm{in}}}$ do not seem to be affected by these effects and predict values of around 7 in this region.

Fig. 4 shows the Q-factors for a center fed dipole in a background Lorentz media. The background has been modeled by the Lorentz model

$$\epsilon_{\mathrm{r}} = 1 + \frac{\nu^2\omega_0^2/2}{\omega_0^2 + s\nu\omega_0 + s^2}, \tag{35}$$

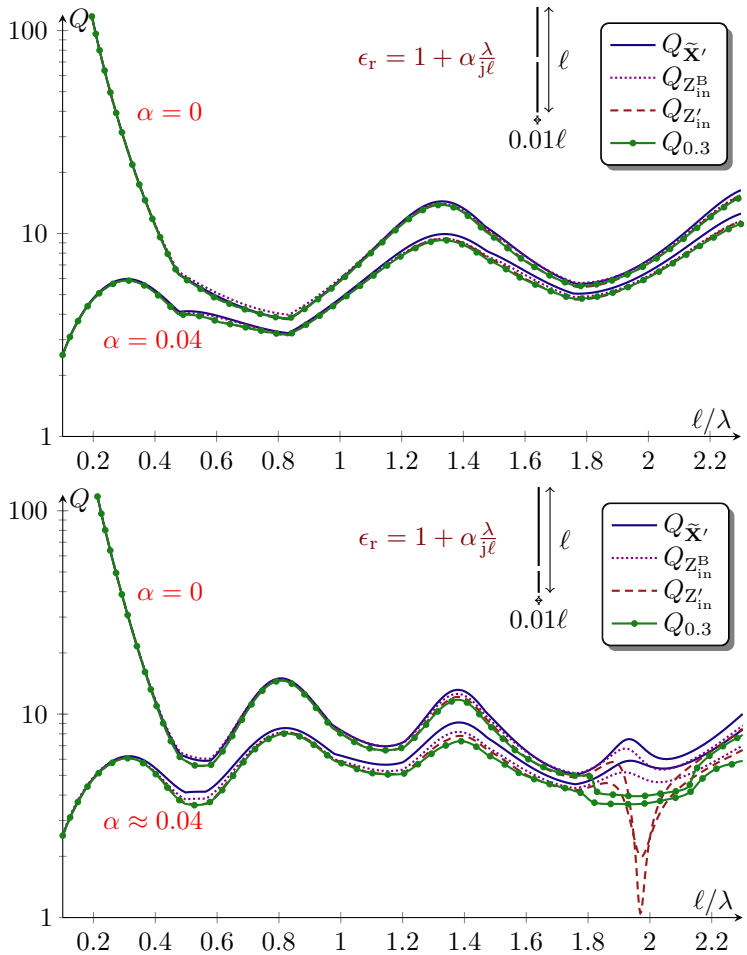

Figure 3: Q-factors for strip dipoles with length ℓ, width $\ell/100$, and fed in the center and 0.27ℓ from the center in the top and bottom figure, respectively. The antennas are placed in a homogeneous medium with relative permittivity $\epsilon_r = 1 - 2\pi\alpha j/\omega$, where $\omega = 2\pi\ell/\lambda$. The Q-factors are determined from the state-space matrix $Q_{\widetilde{\mathbf{X}}'}$ in (34), the Brune synthesized circuit model $Q_{Z_{in}^B}$ as in [21], the differentiated input impedance $Q_{Z_{in}'}$ in (66), and fractional bandwidth $Q_{0.3}$ (68) with $\Gamma_0 = 0.3$.

with the values

$$\epsilon_r(\omega_0) = 1 - j\nu/2 \quad \text{and} \quad (\omega\epsilon_r)'|_{\omega=\omega_0} = 0, \tag{36}$$

where ω_0 is the resonance frequency of the material. All Q-factors agree well outside the resonance $\omega_0 \approx 0.25$. The state-space model $Q_{\widetilde{\mathbf{X}}'}$ and Brune circuit

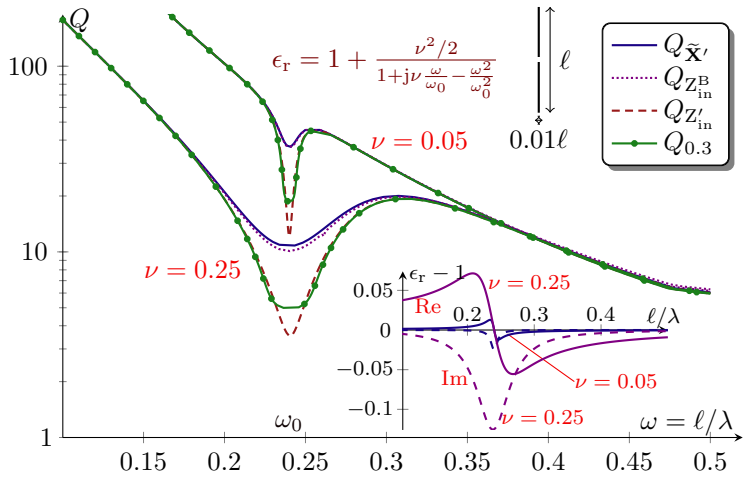

Figure 4: Q-factors for a center fed strip dipole with length ℓ, and width $\ell/100$, placed in a homogeneous medium with relative permittivity (35), where $\omega = 2\pi\ell/\lambda$ and $\nu = \{0.25, 0.05\}$. The permittivity is depicted in the bottom right. The Q-factors are determined from the state-space matrix $Q_{\widetilde{\mathbf{X}}'}$ in (34), the Brune synthesized circuit model $Q_{Z_{in}^B}$ as in [21], the differentiated input impedance $Q_{Z'_{in}}$ in (66), and fractional bandwidth $Q_{0.3}$ (68) with $\Gamma_0 = 0.3$.

$Q_{Z_{in}^B}$ are similar at ω_0, whereas $Q_{Z'_{in}}$ and $Q_{0.3}$ are lower. The similarities between $Q_{\widetilde{\mathbf{X}}'}$ and $Q_{Z_{in}^B}$ indicate that (29) is accurate for small antennas in highly dispersive backgrounds. The lower values for $Q_{Z'_{in}}$ show that Z_{in} is not well approximated with a single resonances model around ω_0. The fractional bandwidth $Q_{0.3}$ agrees with $Q_{Z'_{in}}$ as $\Gamma_0 \to 0$, but is closer to $Q_{Z_{in}^B}$ for larger values of Γ_0.

Fig. 5 depicts the Q-factors for a meander line antenna following the design in [3]. The Q-factors have been calculated for an interval around the operating frequency of the antenna and seem to agree well with $Q_{Z_{in}^B}$ and $Q_{Z'_{in}}$ predicting slightly lower values than $Q_{\widetilde{\mathbf{X}}'}$ for greater losses. This illustrates the state-space methods ability to also accurately calculate the Q-factor for more advanced antenna structures.

4.2 Temporally Dispersive Permittivity and Permeability

Temporally dispersive permittivity and permeability are used to model metamaterials and can produce exotic phenomena such as negative refraction [1, 2, 8]. These are very challenging material models and good cases to verify the accuracy of the stored energy expressions [27]. Here, the state-space model is generalized

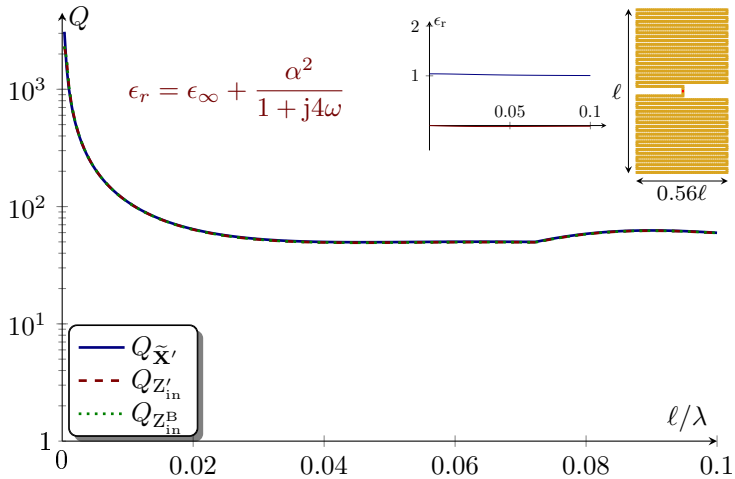

Figure 5: Q-factors for meander line antenna 'M1' in [3], with height ℓ, width 0.56ℓ, and placed in a homogeneous Debye medium with relative permittivity (21). The Lorentz parameters are chosen as $\alpha = 0.2, \beta = 1, \gamma = 4, \delta = 0$. The antenna geometry is depicted in the upper right hand corner as well as the permittivity over the frequency interval. The Q-factor has been calculated with the state-space model $Q_{\widetilde{\mathbf{X}}'}$, Brune synthesis $Q_{\mathrm{Z}^{\mathrm{B}}_{\mathrm{in}}}$, and differentiation of the impedance matrix $Q_{\mathrm{Z}'_{\mathrm{in}}}$.

to Lorentz models in the permittivity and permeability, *i.e.*,

$$\epsilon(s) = \epsilon_\infty + \frac{\alpha^2}{\beta^2 + \gamma s + \delta s^2} \quad \text{and } \mu(s) = \mu_\infty + \frac{\alpha_1^2}{\beta_1^2 + \gamma_1 s + \delta_1 s^2}, \tag{37}$$

where the parameters are defined in analogy to (21), and are assumed to be non-negative. Following the approach in Sec. 4.1, we introduce the voltage state $\mathbf{U}$, electric polarizability $\mathbf{P}$ and $\dot{\mathbf{P}}$, and the magnetic polarizability $\mathbf{P}_{\mathrm{m}}$ and $\dot{\mathbf{P}}_{\mathrm{m}}$. The EFIE MoM system is rewritten,

$$\mathbf{ZI} = (s\mu\mathbf{L} + \frac{1}{s\epsilon}\mathbf{C}_{\mathrm{i}})\mathbf{I} = s\mu_\infty\mathbf{LI} + \alpha_1\dot{\mathbf{P}}_{\mathrm{m}} + \mathbf{U} = \mathbf{V} = \mathbf{B}V_{\mathrm{in}}, \tag{38}$$

with the magnetic polarizability $\dot{\mathbf{P}}_{\mathrm{m}} = \frac{s\alpha_1}{\beta_1^2+\gamma_1 s+\delta_1 s^2}\mathbf{LI}$. The equation is divided into its electric and magnetic parts relating to the permittivity and permeability, respectively. The electric part is identical to (22) and analyzed as in Sec. 4.1. The magnetic part is similarly rewritten using

$$\alpha_1\mathbf{LI} = (\frac{\beta_1^2}{s} + \gamma_1 + \delta_1 s)\dot{\mathbf{P}}_{\mathrm{m}} = \beta_1\mathbf{P}_{\mathrm{m}} + \gamma_1\dot{\mathbf{P}}_{\mathrm{m}} + \delta_1 s\dot{\mathbf{P}}_{\mathrm{m}}. \tag{39}$$

Collecting the terms gives the state-space model

$$\begin{pmatrix} s\mu_\infty\mathbf{L} & \mathbf{1} & \mathbf{0} & \mathbf{0} & \mathbf{0} & \alpha_1\mathbf{1} \\ -\mathbf{1} & s\epsilon_\infty\mathbf{C} & \mathbf{0} & \mathbf{1}\alpha & \mathbf{0} & \mathbf{0} \\ \mathbf{0} & \mathbf{0} & s\mathbf{C}_\mathrm{i} & -\beta\mathbf{C}_\mathrm{i} & \mathbf{0} & \mathbf{0} \\ \mathbf{0} & -\alpha\mathbf{1} & \beta\mathbf{C}_\mathrm{i} & (s\delta+\gamma)\mathbf{C}_\mathrm{i} & \mathbf{0} & \mathbf{0} \\ \mathbf{0} & \mathbf{0} & \mathbf{0} & \mathbf{0} & s\mathbf{L}^{-1} & -\beta_1\mathbf{L}^{-1} \\ -\alpha_1\mathbf{1} & \mathbf{0} & \mathbf{0} & \mathbf{0} & \beta_1\mathbf{L}^{-1} & (s\delta_1+\gamma_1)\mathbf{L}^{-1} \end{pmatrix} \begin{pmatrix} \mathbf{I} \\ \mathbf{U} \\ \mathbf{P} \\ \dot{\mathbf{P}} \\ \mathbf{P}_\mathrm{m} \\ \dot{\mathbf{P}}_\mathrm{m} \end{pmatrix} = \begin{pmatrix} \mathbf{B} \\ \mathbf{0} \\ \mathbf{0} \\ \mathbf{0} \\ \mathbf{0} \\ \mathbf{0} \end{pmatrix} V_\mathrm{in}. \tag{40}$$

The stored energy is approximated as the quadratic form generated by the differentiated system matrix in (40),

$$\begin{pmatrix} \mu_\infty\mathbf{L}+\omega\mu_\infty\mathbf{L}' & \mathbf{0} & \mathbf{0} & \mathbf{0} & \mathbf{0} & \mathbf{0} \\ \mathbf{0} & \epsilon_\infty\mathbf{C}+\omega\epsilon_\infty\mathbf{C}' & \mathbf{0} & \mathbf{0} & \mathbf{0} & \mathbf{0} \\ \mathbf{0} & \mathbf{0} & \mathbf{C}_\mathrm{i}+\omega\mathbf{C}_\mathrm{i}' & \mathrm{j}\beta\mathbf{C}_\mathrm{i}' & \mathbf{0} & \mathbf{0} \\ \mathbf{0} & \mathbf{0} & -\mathrm{j}\beta\mathbf{C}_\mathrm{i}' & \delta\mathbf{C}_\mathrm{i}+(\omega\delta-\mathrm{j}\gamma)\mathbf{C}_\mathrm{i}' & \mathbf{0} & \mathbf{0} \\ \mathbf{0} & \mathbf{0} & \mathbf{0} & \mathbf{0} & \mathbf{L}_\mathrm{i}+\omega\mathbf{L}_\mathrm{i}' & \mathrm{j}\beta_1\mathbf{L}_\mathrm{i}' \\ \mathbf{0} & \mathbf{0} & \mathbf{0} & \mathbf{0} & -\mathrm{j}\beta_1\mathbf{L}_\mathrm{i}' & \delta_1\mathbf{L}_\mathrm{i}+(\omega\delta_1-\mathrm{j}\gamma_1)\mathbf{L}_\mathrm{i}' \end{pmatrix}.$$

The electric terms are analyzed in Sec. 4.1 and the magnetic terms are similarly simplified as

$$\begin{aligned} &\begin{pmatrix} \mathbf{P}_\mathrm{m} \\ \dot{\mathbf{P}}_\mathrm{m} \end{pmatrix}^\mathrm{H} \begin{pmatrix} \mathbf{L}^{-1}-\omega\mathbf{L}^{-1}\mathbf{L}'\mathbf{L}^{-1} & -\mathrm{j}\beta_1\mathbf{L}^{-1}\mathbf{L}'\mathbf{L}^{-1} \\ \mathrm{j}\beta_1\mathbf{L}^{-1}\mathbf{L}'\mathbf{L}^{-1} & \delta_1\mathbf{L}^{-1}-(\omega\delta_1-\mathrm{j}\gamma_1)\mathbf{L}^{-1}\mathbf{L}'\mathbf{L}^{-1} \end{pmatrix} \begin{pmatrix} \mathbf{P}_\mathrm{m} \\ \dot{\mathbf{P}}_\mathrm{m} \end{pmatrix} \\ &= \begin{pmatrix} \frac{\alpha_1\beta_1}{\chi_1}\mathbf{L}\mathbf{I} \\ \frac{\alpha_1 s}{\chi_1}\mathbf{L}\mathbf{I} \end{pmatrix}^\mathrm{H} \begin{pmatrix} \mathbf{L}^{-1}-\omega\mathbf{L}^{-1}\mathbf{L}'\mathbf{L}^{-1} & -\mathrm{j}\beta_1\mathbf{L}^{-1}\mathbf{L}'\mathbf{L}^{-1} \\ \mathrm{j}\beta_1\mathbf{L}^{-1}\mathbf{L}'\mathbf{L}^{-1} & \delta_1\mathbf{L}^{-1}-(\omega\delta_1-\mathrm{j}\gamma_1)\mathbf{L}^{-1}\mathbf{L}'\mathbf{L}^{-1} \end{pmatrix} \begin{pmatrix} \frac{\alpha_1\beta_1}{\chi_1}\mathbf{L}\mathbf{I} \\ \frac{\alpha_1 s}{\chi_1}\mathbf{L}\mathbf{I} \end{pmatrix} \\ &\simeq \begin{pmatrix} \frac{\alpha_1\beta_1}{\chi_1}\mathbf{I} \\ \frac{\alpha_1 s}{\chi_1}\mathbf{I} \end{pmatrix}^\mathrm{H} \begin{pmatrix} \mathbf{L}-\omega\mathbf{L}' & -\mathrm{j}\beta_1\mathbf{L}' \\ \mathrm{j}\beta_1\mathbf{L}' & \delta_1\mathbf{L}-(\omega\delta_1-\mathrm{j}\gamma_1)\mathbf{L}' \end{pmatrix} \begin{pmatrix} \frac{\alpha_1\beta_1}{\chi_1}\mathbf{I} \\ \frac{\alpha_1 s}{\chi_1}\mathbf{I} \end{pmatrix} \\ &= \frac{\alpha_1^2}{|\chi_1^2|}\mathbf{I}^\mathrm{H}\big(\beta_1^2(\mathbf{L}-\omega\mathbf{L}')+2\omega\beta_1^2\mathbf{L}'+\omega^2(\delta_1\mathbf{L}-(\omega\delta_1-\mathrm{j}\gamma_1)\mathbf{L}')\big)\mathbf{I} \\ &= \frac{\alpha_1^2}{|\chi_1^2|}\mathbf{I}^\mathrm{H}\big((\beta_1^2+\omega^2\delta_1)\mathbf{L}+\omega(\beta_1^2-\omega^2\delta_1+\mathrm{j}\omega\gamma_1)\mathbf{L}')\big)\mathbf{I} \\ &= \frac{\alpha_1^2}{|\chi_1^2|}\mathbf{I}^\mathrm{H}\big((\beta_1^2+\omega^2\delta_1)\mathbf{L}+\omega\chi_1\mathbf{L}'\big)\mathbf{I}, \end{aligned} \tag{41}$$

where we again neglect the lower order terms.

If we consider a medium with permittivity and permeability according to the Lorentz model (37) and $\mu_\mathrm{r} = \epsilon_\mathrm{r}$. This synthesizes a case where $\mathbf{Z}' \approx \mathbf{0}$ for antennas that are resonant at ω_0 [27] for any $\nu > 0$. Furthermore, the corresponding impedance matrix does not change significantly as $\nu \to 0$, *i.e.*, $\mathbf{Z}_\nu \approx \mathbf{Z}_{\nu=0}$ as $\nu \ll 1$. Therefore, the energy distribution in the fields, currents, or circuit models of the antenna depend weakly on ν as $\nu \ll 1$.

In Fig. 6 a strip dipole with length ℓ and width 0.01ℓ are used to illustrate the estimated Q-factors. Consider the resonance frequency $\omega_0 = 2\pi\ell/\lambda = 3$ and the damping $\nu = 0.1$ in the Lorentz model (37). The maximal susceptibility is $|1-\epsilon_\mathrm{r}| = \nu/\sqrt{4-\nu^2} \approx \nu/2$ for $\nu \ll 1$. The Q-factors give similar results away

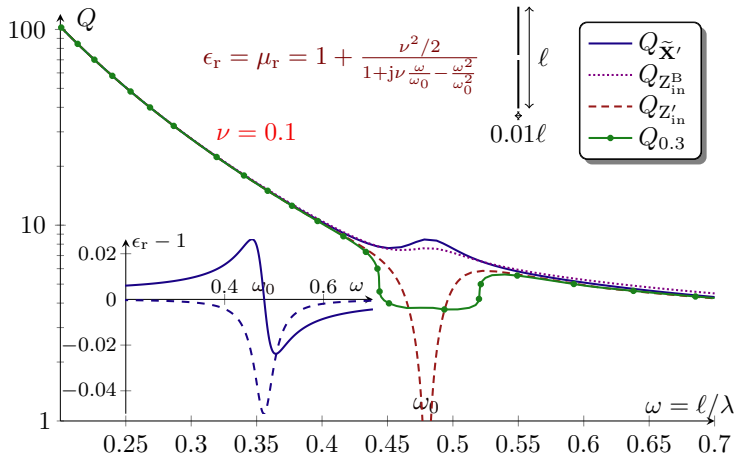

Figure 6: Q-factors for a strip dipole with length ℓ, width $\ell/100$, fed at the center, and placed in a homogeneous electric and magnetic Lorentz medium with relative permittivity and permeability (37) as depicted in the bottom left inset, where $\omega = 2\pi\ell/\lambda$ and $\nu = 10^{-1}$. The Q-factors are determined from the state-space matrix $Q_{\widetilde{\mathbf{X}}'}$, the Brune synthesized circuit model $Q_{Z_{in}^B}$, the differentiated input impedance $Q_{Z'_{in}}$, and fractional bandwidth $Q_{0.3}$.

from the resonance frequency ω_0, which coincides with the dipole resonance of the antenna. At ω_0 $Q_{Z'_{in}}$ has a substantial dip, whereas $Q_{\widetilde{\mathbf{X}}'}$ and $Q_{Z_{in}^B}$ increase slightly. $Q_{Z_{in}^B}$ has slightly lower values than $Q_{\widetilde{\mathbf{X}}'}$ at the resonance ω_0. $Q_{0.3}$ on the other hand also displays a bottoming out of its values around the resonance, *cf.*, with [27]. This in conjunction with $Q_{Z'_{in}}$ behavior indicate that the single resonance approximation for Z_{in} is not satisfied in this kind of resonant media. The multiple resonance also increases the fractional bandwidth and invalidates the simple relation (68).

5 Stored Energy for Inhomogeneous Media

The numerical examples in Sec. 4 indicate that the state-space approach produces accurate estimates of the stored energy for homogeneous background media. Following this approach, we analyze piecewise homogeneous background media using the surface equivalence principle, and inhomogeneous media with volume integral equations in Secs 5.1 and 5.2, respectively.

5.1 Piecewise Homogeneous Media

The surface equivalence principle is used to express the electromagnetic fields in piecewise homogeneous media [9, 35, 44, 52, 56]. Consider for simplicity a PEC antenna structure embedded in a media with permittivity and permeability as depicted in Fig. 2. The geometry is divided into three regions Ω_p $p = 1, 2, 3$, with corresponding material parameters ϵ_p and μ_p. Let $\partial\Omega_p$ denote the exterior surface of Ω_p, *i.e.*, the boundary of $\bigcup_{q=1}^{p} \Omega_q$. The field in region Ω_p is expressed by the equivalent currents $\boldsymbol{J}_{p-1}, \boldsymbol{J}_p, \boldsymbol{M}_{p-1}$, and $\boldsymbol{M}_p$, where $\boldsymbol{J}_0 = \boldsymbol{M}_0 = \mathbf{0}$. We follow the state-space approach and construct a system for the input impedance $Z_{\text{in}} = V_{\text{in}}/I_{\text{in}}$.

The EFIE and Magnetic Field Integral Equation (MFIE) for the inner region Ω_2 is written

$$\begin{pmatrix} \mathbf{Z}_{2,11} & \mathbf{Z}_{2,12} & \mathbf{K}_{2,12} \\ \mathbf{Z}_{2,21} & \mathbf{Z}_{2,22} & \mathbf{K}_0 + \mathbf{K}_{2,22} \\ -\mathbf{K}_{2,21} & \mathbf{K}_0 - \mathbf{K}_{2,22} & \frac{1}{\eta_2^2}\mathbf{Z}_{2,22} \end{pmatrix} \begin{pmatrix} \mathbf{I}_1 \\ \mathbf{I}_2 \\ \mathbf{M}_2 \end{pmatrix} = \begin{pmatrix} \mathbf{V}_1 \\ \mathbf{0} \\ \mathbf{0} \end{pmatrix}, \tag{42}$$

where $\mathbf{Z}_{p,oq}$ denotes the EFIE impedance matrix (12) connecting the surfaces o and q through their respective currents, evaluated using materials ϵ_p and μ_p. $\mathbf{K}_{p,oq}$ is the corresponding MFIE operator with elements

$$K_{p,oq,mn} = \int_{\partial\Omega_o} \int_{\partial\Omega_q} \boldsymbol{\psi}_m(\boldsymbol{r}_1) \cdot \boldsymbol{\psi}_n(\boldsymbol{r}_2) \times \nabla_1 G_{12} \, \mathrm{dS}_1 \, \mathrm{dS}_2 \tag{43}$$

and $\mathbf{K}_0$ is the free term of the MFIE. Since region 1 is a PEC, there exists no magnetic surface current $\mathbf{M}_1$. The EFIE and MFIE for the exterior region Ω_3 is similarly

$$\begin{pmatrix} \mathbf{Z}_{3,22} & -\mathbf{K}_0 + \mathbf{K}_{3,22} \\ -\mathbf{K}_0 - \mathbf{K}_{3,22} & \frac{1}{\eta_3^2}\mathbf{Z}_{3,22} \end{pmatrix} \begin{pmatrix} \mathbf{I}_2 \\ \mathbf{M}_2 \end{pmatrix} = \begin{pmatrix} \mathbf{0} \\ \mathbf{0} \end{pmatrix}. \tag{44}$$

The EFIE and MFIE in (42) and (44) can be combined in different ways to mitigate internal resonance problems of the MoM solution, *e.g.*, the PMCHWT and Müller integral equations [9,35]. Here, we choose the PMCHWT formulation and add the equations (42) and (44) together to get

$$\begin{pmatrix} \mathbf{Z}_{2,11} & \mathbf{Z}_{2,12} & \mathbf{K}_{2,12} \\ \mathbf{Z}_{2,21} & \mathbf{Z}_{2,22} + \mathbf{Z}_{3,22} & \mathbf{K}_{2,22} + \mathbf{K}_{3,22} \\ -\mathbf{K}_{2,21} & -\mathbf{K}_{2,22} - \mathbf{K}_{3,22} & \frac{1}{\eta_2^2}\mathbf{Z}_{2,22} + \frac{1}{\eta_3^2}\mathbf{Z}_{3,22} \end{pmatrix} \begin{pmatrix} \mathbf{I}_1 \\ \mathbf{I}_2 \\ \mathbf{M}_2 \end{pmatrix} = \begin{pmatrix} \mathbf{V}_1 \\ \mathbf{0} \\ \mathbf{0} \end{pmatrix}, \tag{45}$$

where the $\mathbf{K}_0$ term cancels out. This can be considered as a second order state-space model for the input impedance with the decomposition (12). Because the material parameters are different in the two regions it is, however, advantageous to first divide (45) as a sum of its inner and outer parts. This creates two parts that are formally identical and can be written as

$$\begin{pmatrix} \mathbf{Z} & \mathbf{K} \\ -\mathbf{K} & \mathbf{Z} \end{pmatrix} \begin{pmatrix} \mathbf{I} \\ \mathbf{M} \end{pmatrix} = \begin{pmatrix} s\mu\mathbf{L} + \frac{\mathbf{C}_{\text{i}}}{s\epsilon} & \mathbf{K} \\ -\mathbf{K} & s\epsilon\mathbf{L} + \frac{\mathbf{C}_{\text{i}}}{s\mu} \end{pmatrix} \begin{pmatrix} \mathbf{I} \\ \mathbf{M} \end{pmatrix}, \tag{46}$$

where the material parameters ϵ_p and μ_p are used in region Ω_p. The second order system (46) is rewritten as a first order system, in analogy with (16), by the introduction of a magnetic voltage state $\mathbf{U}_\mathrm{m} = \frac{1}{s\mu}\mathbf{C}_\mathrm{i}\mathbf{M}$,

$$\begin{pmatrix} s\mu\mathbf{L} & \mathbf{1} & \mathbf{K} & \mathbf{0} \\ -\mathbf{1} & s\epsilon\mathbf{C} & \mathbf{0} & \mathbf{0} \\ -\mathbf{K} & \mathbf{0} & s\epsilon\mathbf{L} & \mathbf{1} \\ \mathbf{0} & \mathbf{0} & -\mathbf{1} & s\mu\mathbf{C} \end{pmatrix} \begin{pmatrix} \mathbf{I} \\ \mathbf{U} \\ \mathbf{M} \\ \mathbf{U}_\mathrm{m} \end{pmatrix}. \tag{47}$$

This system can determine the stored energy of each region with the same approximation used in (18). For simplicity, we consider first non-dispersive material models. It is sufficient to use differentiation with respect to the Laplace parameter s for the non-dispersive cases to illustrate the method, giving

$$\begin{pmatrix} \mu\mathbf{L} + \omega\mu\mathbf{L}' & \mathbf{0} & -\mathrm{j}\mathbf{K}' & \mathbf{0} \\ \mathbf{0} & \epsilon\mathbf{C} + \omega\epsilon\mathbf{C}' & \mathbf{0} & \mathbf{0} \\ \mathrm{j}\mathbf{K}' & \mathbf{0} & \epsilon\mathbf{L} + \omega\epsilon\mathbf{L}' & \mathbf{0} \\ \mathbf{0} & \mathbf{0} & \mathbf{0} & \mu\mathbf{C} + \omega\mu\mathbf{C}' \end{pmatrix} \tag{48}$$

with $\mathbf{L}'$ as in (19), $\mathbf{C}' = -\mathbf{C}\mathbf{C}_\mathrm{i}'\mathbf{C}$ as in (20), and

$$K'_{p,mn} = \kappa'\kappa \int_{\partial\Omega_p}\int_{\partial\Omega_p} \boldsymbol{\psi}_n(\boldsymbol{r}_1)\cdot\boldsymbol{\psi}_m(\boldsymbol{r}_2)\times(\boldsymbol{r}_1-\boldsymbol{r}_2)G\,\mathrm{dS}_1\,\mathrm{dS}_2, \tag{49}$$

where we used

$$\frac{\partial}{\partial\kappa}\nabla_2 G = \nabla_2\frac{\partial}{\partial\kappa}G = -\nabla_2\frac{\mathrm{e}^{-\kappa R}}{4\pi} = -\frac{\kappa\mathrm{e}^{-\kappa R}(\boldsymbol{r}_1-\boldsymbol{r}_2)}{4\pi R} = -\kappa(\boldsymbol{r}_1-\boldsymbol{r}_2)G. \tag{50}$$

The $\mathbf{K}'$ term in vacuum is recognized as being proportional to the $\mathbf{K}_2$ term used in [36], see also [38]. The terms that contribute to the stored energy are expanded in the wavenumber k in [37] and it is shown that the $\mathbf{K}_1$-term and the potentially coordinate dependent terms $\mathbf{K}_3$ and $\mathbf{K}_4$ used in [36] are one order smaller than the $\mathbf{K}_2$-term. These terms are not present in the state-space based approach presented here. The contribution to the stored energy from the region Ω_p is finally given by the real part of the quadratic form

$$\begin{pmatrix} \mathbf{I} \\ \mathbf{U} \\ \mathbf{M} \\ \mathbf{U}_\mathrm{m} \end{pmatrix}^\mathrm{H} \begin{pmatrix} \mu\mathbf{L} + \omega\mu\mathbf{L}' & \mathbf{0} & -\mathrm{j}\mathbf{K}' & \mathbf{0} \\ \mathbf{0} & \epsilon\mathbf{C} + \omega\epsilon\mathbf{C}' & \mathbf{0} & \mathbf{0} \\ \mathrm{j}\mathbf{K}' & \mathbf{0} & \epsilon\mathbf{L} + \omega\epsilon\mathbf{L}' & \mathbf{0} \\ \mathbf{0} & \mathbf{0} & \mathbf{0} & \mu\mathbf{C} + \omega\mu\mathbf{C}' \end{pmatrix} \begin{pmatrix} \mathbf{I} \\ \mathbf{U} \\ \mathbf{M} \\ \mathbf{U}_\mathrm{m} \end{pmatrix} \tag{51}$$

and the total stored energy by summation over all regions. This can be expressed as a quadratic form in the electric and magnetic current by substituting back the voltage states.

The expression (51) resembles the stored energy from electric and magnetic current densities [36–38]. The stored energies in [36–38] are derived from the

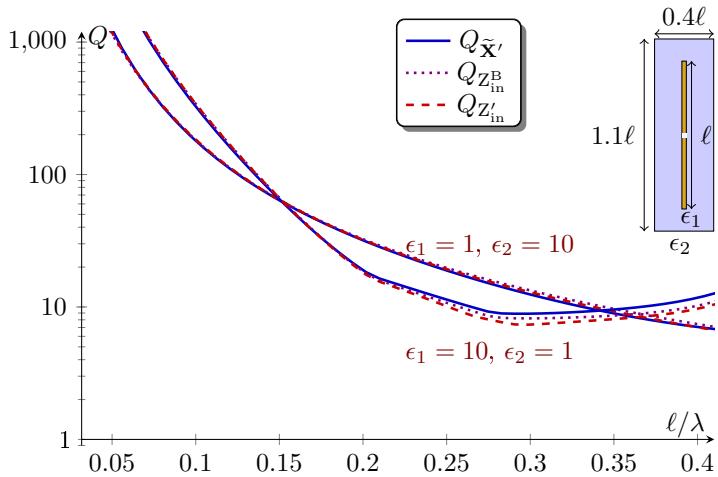

Figure 7: Q-factors for a cylindrical dipole with length ℓ, width $\ell/100$, fed at the center, and placed in a dielectric cylinder with permittivity ϵ_1 and background permittivity ϵ_2. The cylinder has height 1.1ℓ and diameter 0.4ℓ. The Q-factors are computed using (51), Brune synthesized circuits [21], and (66) for the two cases $\{\epsilon_1, \epsilon_2\} = \{1, 10\}$ and $\{\epsilon_1, \epsilon_2\} = \{10, 1\}$.

subtraction of the far-field in a non-dispersive homogeneous background as in (2). The equivalence principle states that the fields generated by currents at $\partial\Omega_n$ vanish outside Ω_n and for that reason produces the total energy in Ω_n. The exterior region is an exception for which the energy produced is similar to the case of far-field subtraction. Consequently, the stored energy (51) resembles (2) with spatially dependent permittivity and permeability in the energy density terms, and the exterior permittivity in the subtracted far-field energy term, for small structures. The expressions differ for larger structures, where $\mathbf{K}_1$ together with the coordinate dependent terms in [37] contribute.

Figs. 7 and 8 depicts Q-factors $Q_{\widetilde{\mathbf{X}}'}$ based on the energy expressions (51) for multilayer structures. Fig. 7 shows Q-factors for a cylindrical dipole embedded in a dielectric cylinder. The figure contains two cases, when the permittivity of the cylinder is higher than the background, and when the permittivity of the background is higher than the cylinder. For both cases $Q_{\widetilde{\mathbf{X}}'}$ agrees very well with $Q_{\mathrm{Z}^{\mathrm{B}}_{\mathrm{in}}}$ and $Q_{\mathrm{Z}'_{\mathrm{in}}}$. However, $Q_{\mathrm{Z}^{\mathrm{B}}_{\mathrm{in}}}$ and $Q_{\mathrm{Z}'_{\mathrm{in}}}$ have slightly lower values than $Q_{\widetilde{\mathbf{X}}'}$ for $\{\epsilon_1, \epsilon_2\} = \{10, 1\}$ at higher frequencies. Fig. 8 instead shows what occurs when the dielectric cylinder encasing the dipole is much larger, for the two cases. The Q-factors agree well except for higher frequencies when the cylinder is large. There is also a dip in $Q_{\mathrm{Z}'_{\mathrm{in}}}$ at $0.2\ell/\lambda$ for cylinder size $2.6\ell \times 1.6\ell$.

The piecewise inhomogeneous case can be expanded to temporally dispersive permittivity and permeability as was done for homogeneous media in Sec. 4.1. The system matrix (47) is expanded to a first order state-space model for the

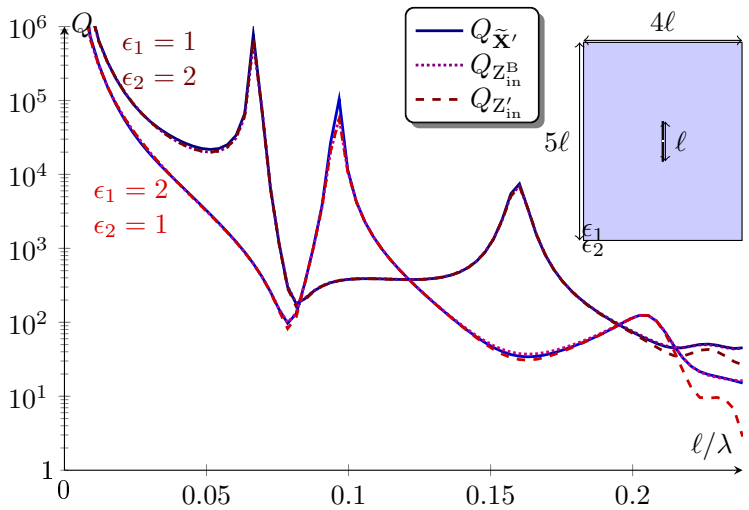

Figure 8: Q-factors for a cylindrical dipole with length ℓ, width $\ell/100$, fed at the center, and placed in a dielectric cylinder with permittivity ϵ_1 and background permittivity ϵ_2. The cylinder has heights 5ℓ and diameters 4ℓ. The Q-factors are computed using (51), Brune synthesized circuits [21], and (66) for the two cases $\{\epsilon_1, \epsilon_2\} = \{1, 2\}$ and $\{\epsilon_1, \epsilon_2\} = \{2, 1\}$.

Lorentz model (21) in analog with (24). However, the magnetic currents give rise to the states $\mathbf{U}_\mathrm{m}, \mathbf{P}_\mathrm{m}, \dot{\mathbf{P}}_\mathrm{m}$ in addition to the voltage $\mathbf{U}$ and polarization states $\mathbf{P}$ and $\dot{\mathbf{P}}$ used in (24). The resulting system matrix is

$$\begin{pmatrix} s\mu\mathbf{L} & \mathbf{1} & \mathbf{K} & \mathbf{0} & \mathbf{0} & \mathbf{0} & \mathbf{0} & \mathbf{0} \\ -\mathbf{1} & s\epsilon_\infty\mathbf{C} & \mathbf{0} & \mathbf{0} & \mathbf{0} & \mathbf{1}\alpha & \mathbf{0} & \mathbf{0} \\ -\mathbf{K} & \mathbf{0} & s\epsilon_\infty\mathbf{L} & \mathbf{1} & \mathbf{0} & \mathbf{0} & \mathbf{0} & \mathbf{1}\alpha \\ \mathbf{0} & \mathbf{0} & -\mathbf{1} & s\mu\mathbf{C} & \mathbf{0} & \mathbf{0} & \mathbf{0} & \mathbf{0} \\ \mathbf{0} & \mathbf{0} & \mathbf{0} & \mathbf{0} & s\mathbf{C}_\mathrm{i} & -\beta\mathbf{C}_\mathrm{i} & \mathbf{0} & \mathbf{0} \\ \mathbf{0} & -\mathbf{1}\alpha & \mathbf{0} & \mathbf{0} & \beta\mathbf{C}_\mathrm{i} & (s\delta+\gamma)\mathbf{C}_\mathrm{i} & \mathbf{0} & \mathbf{0} \\ \mathbf{0} & \mathbf{0} & \mathbf{0} & \mathbf{0} & \mathbf{0} & \mathbf{0} & s\mathbf{L}_\mathrm{i} & -\beta\mathbf{L}_\mathrm{i} \\ \mathbf{0} & \mathbf{0} & -\mathbf{1}\alpha & \mathbf{0} & \mathbf{0} & \mathbf{0} & \beta\mathbf{L}_\mathrm{i} & (s\delta+\gamma)\mathbf{L}_\mathrm{i} \end{pmatrix} \begin{pmatrix} \mathbf{I} \\ \mathbf{U} \\ \mathbf{M} \\ \mathbf{U}_\mathrm{m} \\ \mathbf{P} \\ \dot{\mathbf{P}} \\ \mathbf{P}_\mathrm{m} \\ \dot{\mathbf{P}}_\mathrm{m} \end{pmatrix}, \tag{52}$$

where we used

$$(s\epsilon\mathbf{L} + \frac{\mathbf{C}_\mathrm{i}}{s\mu})\mathbf{M} = (s\epsilon_\infty\mathbf{L} + \frac{\mathbf{C}_\mathrm{i}}{s\mu} + \frac{s\alpha^2}{\chi}\mathbf{L})\mathbf{M} = s\epsilon_\infty\mathbf{L}\mathbf{M} + \mathbf{U}_\mathrm{m} + \alpha\dot{\mathbf{P}}_\mathrm{m}, \tag{53}$$

and $s\alpha\mathbf{L}\mathbf{M} = \chi\dot{\mathbf{P}}_\mathrm{m} = \chi s\mathbf{P}_\mathrm{m}\beta^{-1}$ with $\mathbf{L}\mathbf{M}\alpha = \chi\mathbf{P}_\mathrm{m}\beta^{-1}$ to get

$$\alpha\mathbf{L}\mathbf{M} = (\beta^2 + s\gamma + s^2\delta)\mathbf{P}_\mathrm{m}\beta^{-1} = \beta\mathbf{P}_\mathrm{m} + (\gamma + s\delta)\dot{\mathbf{P}}_\mathrm{m}. \tag{54}$$

From here the electric and magnetic terms are analyzed as in 4.2.

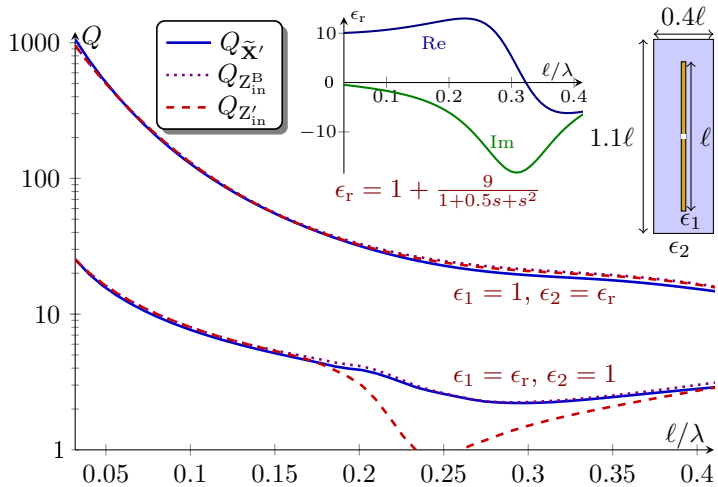

Figure 9: Q-factors for a cylindrical dipole with length ℓ, width $\ell/100$, fed at the center, and placed in a dielectric cylinder with permittivity ϵ_1 and background permittivity ϵ_2. The cylinder has height 1.1ℓ and diameter 0.4ℓ. The Q-factors are computed using (51), Brune synthesized circuits [21], and (66) for the two cases $\{\epsilon_1, \epsilon_2\} = \{1, \epsilon_{\mathrm{r}}\}$ and $\{\epsilon_1, \epsilon_2\} = \{\epsilon_{\mathrm{r}}, 1\}$, $\epsilon_{\mathrm{r}} = 1 + 9/(1 + 0.5s + s^2)$.

Fig. 9 displays Q-factors calculated for a cylindrical dipole encased in both a dielectric cylinder with dispersive permittivity in a normal background and a vacuum cylinder in a dispersive background. The dispersive permittivity is modeled by the Lorentz model (21). For the case when the background is dispersive and the cylinder is vacuum, the Q-factors agree well. For the second case, when the cylinder is dispersive, $Q_{\widetilde{\mathbf{X}}'}$ and $Q_{\mathrm{Z}^{\mathrm{B}}_{\mathrm{in}}}$ agree for the whole interval. However, $Q_{\mathrm{Z}'_{\mathrm{in}}}$ has a dip around 0.2 to 0.35ℓ. This is most likely caused by multiple resonances in the input impedance.

5.2 Inhomogeneous Media

To handle fully inhomogeneous background media we use volume integral equations [9], the implementation of which is much more arduous than surface based integral equations. However, the method for constructing the state-space system and calculating the stored energy is principally the same. For completeness, we present here the analysis needed to calculate the stored energy with volume integral equations.

Consider a dielectric body with relative permittivity $\epsilon_{\mathrm{r}}(\boldsymbol{r})$. The volume EFIE is

$$\boldsymbol{E}(\boldsymbol{r}_1) = \boldsymbol{E}^{(\mathrm{i})}(\boldsymbol{r}_1) - k^2 \int_{\Omega} \mathbf{G}(\boldsymbol{r}_1 - \boldsymbol{r}_2) \cdot (1 - \epsilon_{\mathrm{r}}(\boldsymbol{r}_2)) \boldsymbol{E}(\boldsymbol{r}_2)\, \mathrm{dV}_2, \qquad (55)$$

where $\mathbf{G} = (\mathbf{1} + k^{-2}\nabla\nabla)G$ is the Green dyadic, k the free-space wavenumber, and $\boldsymbol{E}^{(\mathrm{i})}$ the incident electric field. Introduce the contrast current density $\boldsymbol{J} = \kappa(1 - \epsilon_{\mathrm{r}})\boldsymbol{E}$ to reformulate (55) to an integral equation in that quantity

$$\frac{\boldsymbol{J}(\boldsymbol{r}_1)}{\kappa(1 - \epsilon_{\mathrm{r}}(\boldsymbol{r}_1))} = \boldsymbol{E}^{(\mathrm{i})}(\boldsymbol{r}_1) + \kappa \int_\Omega \mathbf{G}(\boldsymbol{r}_1 - \boldsymbol{r}_2) \cdot \boldsymbol{J}(\boldsymbol{r}_2)\,\mathrm{dV}_2. \tag{56}$$

Multiply both sides with test functions $\boldsymbol{\Psi}$ and integrate over the volume

$$\begin{aligned}\int_\Omega \frac{\boldsymbol{\Psi}(\boldsymbol{r}) \cdot \boldsymbol{J}(\boldsymbol{r})}{\kappa(1 - \epsilon_{\mathrm{r}}(\boldsymbol{r}))}\,\mathrm{dV} &= \int_\Omega \boldsymbol{\Psi}(\boldsymbol{r}) \cdot \boldsymbol{E}^{(\mathrm{i})}(\boldsymbol{r})\,\mathrm{dV} \\ + \int_\Omega \int_\Omega \kappa G(\boldsymbol{r}_1 - \boldsymbol{r}_2)\boldsymbol{\Psi}(\boldsymbol{r}_1) \cdot \boldsymbol{J}(\boldsymbol{r}_2) &+ \frac{1}{\kappa} G(\boldsymbol{r}_1 - \boldsymbol{r}_2)\nabla_1 \cdot \boldsymbol{\Psi}(\boldsymbol{r}_1)\nabla_2 \cdot \boldsymbol{J}(\boldsymbol{r}_2)\,\mathrm{dV}_1\,\mathrm{dV}_2,\end{aligned} \tag{57}$$

where we split the Green's dyadic $\mathbf{G}$ into two parts. The differentiated term is partially integrated to reduce the singularity of the Green's function

$$\begin{aligned}\int_\Omega \int_\Omega \boldsymbol{J}(\boldsymbol{r}_1) \cdot \nabla\nabla G \cdot \boldsymbol{J}(\boldsymbol{r}_2)\,\mathrm{dV}_1\,\mathrm{dV}_2 \\ = -\int_\Omega \int_\Omega \nabla_1 \cdot \boldsymbol{J}(\boldsymbol{r}_1) G \nabla_2 \cdot \boldsymbol{J}(\boldsymbol{r}_2)\,\mathrm{dV}_1\,\mathrm{dV}_2.\end{aligned} \tag{58}$$

To obtain the MoM formulation we expand the contrast current density $\boldsymbol{J}$ in basis functions $\boldsymbol{\Psi}_n$ as

$$I_n = \int_\Omega \boldsymbol{\Psi}_n(\boldsymbol{r}) \cdot \boldsymbol{J}(\boldsymbol{r})\,\mathrm{dV} = \int \boldsymbol{\Psi}_n(\boldsymbol{r}) \cdot \kappa\big(1 - \epsilon_{\mathrm{r}}(\boldsymbol{r})\big)\boldsymbol{E}(\boldsymbol{r})\,\mathrm{dV}. \tag{59}$$

This enables the introduction of matrix quantities similar to those used in (12), and thus, the construction of the state-space system. The inductance matrix is defined as

$$L_{mn} = \int_\Omega \int_\Omega G(\boldsymbol{r}_1 - \boldsymbol{r}_2)\boldsymbol{\Psi}_m(\boldsymbol{r}_1) \cdot \boldsymbol{\Psi}_n(\boldsymbol{r}_2)\,\mathrm{dV}_1\,\mathrm{dV}_2, \tag{60}$$

the capacitance matrix as

$$C_{imn} = \int_\Omega \int_\Omega G(\boldsymbol{r}_1 - \boldsymbol{r}_2)\nabla_1 \cdot \boldsymbol{\Psi}_m(\boldsymbol{r}_1)\nabla_2 \cdot \boldsymbol{\Psi}_n(\boldsymbol{r}_2)\,\mathrm{dV}_1\,\mathrm{dV}_2, \tag{61}$$

and the material matrix as

$$M_{mn} = \int_\Omega \frac{\boldsymbol{\Psi}_m(\boldsymbol{r}) \cdot \boldsymbol{\Psi}_n(\boldsymbol{r})}{1 - \epsilon_{\mathrm{r}}(\boldsymbol{r})}\,\mathrm{dV}. \tag{62}$$

With these three matrices equation (57) can be written as the second order system

$$\big(s\mu_0\mathbf{L} + \frac{\mathbf{C}_{\mathrm{i}} + \mathbf{M}}{s\epsilon_0}\big)\mathbf{I} = \mathbf{V}. \tag{63}$$

Similarly to previous sections it can be transformed to the first order state-space model by the introduction of a voltage state $\mathbf{U} = \frac{1}{s\epsilon_0}(\mathbf{C}_\mathrm{i} + \mathbf{M})\mathbf{I}$

$$\begin{pmatrix} s\mu_0\mathbf{L} & \mathbf{1} \\ -\mathbf{1} & s\epsilon_0(\mathbf{C}_\mathrm{i} + \mathbf{M})^{-1} \end{pmatrix} \begin{pmatrix} \mathbf{I} \\ \mathbf{U} \end{pmatrix} = \begin{pmatrix} \mathbf{V} \\ \mathbf{0} \end{pmatrix}. \tag{64}$$

Finally, the stored energy is given by the quadratic form of the frequency differentiation of the state-space matrix

$$\begin{aligned} \frac{\mathrm{Re}}{4} \begin{pmatrix} \mathbf{I} \\ \mathbf{U} \end{pmatrix}^\mathrm{H} \begin{pmatrix} \mu_0(\mathbf{L} + \omega\mathbf{L}') & \mathbf{0} \\ \mathbf{0} & \epsilon_0(\mathbf{C}_\mathrm{i} + \mathbf{M})^{-1} - \epsilon_0\omega(\mathbf{C}_\mathrm{i} + \mathbf{M})^{-1}\mathbf{C}_\mathrm{i}'(\mathbf{C}_\mathrm{i} + \mathbf{M})^{-1} \end{pmatrix} \begin{pmatrix} \mathbf{I} \\ \mathbf{U} \end{pmatrix} \\ = \frac{\mathrm{Re}}{4}\mathbf{I}^\mathrm{H}\big(\mu_0(\mathbf{L} + \omega\mathbf{L}') + \frac{1}{\omega^2\epsilon_0}(\mathbf{C}_\mathrm{i} + \mathbf{M} - \omega\mathbf{C}_\mathrm{i}')\big)\mathbf{I} = \frac{1}{4}\mathbf{I}^\mathrm{H}\frac{\partial\mathbf{X}}{\partial\omega}\mathbf{I}. \end{aligned} \tag{65}$$

6 Conclusions

State-space models for the input impedance based on the integral equations EFIE and MFIE have been used to determine the stored electromagnetic energy for small antennas. These expressions have been calculated by synthesizing first order state-space models. The stored energy is expressed as a quadratic form of the frequency differentiated system matrix and the states. This quadratic form is advantageous because it enables us to utilize these stored energy expressions in fast and efficient optimization techniques [6, 11, 23, 24].

For the free-space case it is shown in Sec. 3 that the proposed expression is identical to the stored energy introduced by [53], see also [31]. This energy expression has been verified for several antennas with good results [11,12,21,32]. In [25], it is, however, shown that the quadratic form can be indefinite for sufficiently large structures. This partly questions the validity of the energy expression, although the same problem appears in the commonly used stored energy in [63] defined by subtraction of the far-field [22]. The energy expressions presented here are restricted to electrically small antennas where they are positive definite. The open question of defining and efficiently evaluating the stored energy for electrically large structures remains, as of yet, unsolved, see also [46].

In Sec. 4 the state-space models are generalized to temporally dispersive background media. The results produced by the state-space method seem to be reliable and produce similar values as Brune circuit synthesis [21] and differentiation of the input impedance $Q_{\mathrm{Z}'_\mathrm{in}}$ for single resonance cases. However, the main advantage over other contemporary methods is that the state-space model is written as a quadratic form in the current, and hence enables fast and effective use in antenna current optimization to determine physical bounds [7, 11, 20, 23, 24, 34].

The state-space model was further generalized to piecewise inhomogeneous media in Sec. 5. Here it was shown that the method is stable for cases where there are lossy media present but radiation still exists. These cases are of special interest since they have similarities with applications such as implanted antenna

system. By offering a stable method of calculating the Q-factor for inhomogeneous media the state-space method opens up avenues of research for calculating optimal Q values for application based cases. This suggests the possibility to construct Q-factor bounds for more applications than free space [23, 24] and infinite ground planes [50].

Appendix A Q-factors $Q_{\mathrm{Z}'_{\mathrm{in}}}$ and Q_{Γ_0}

By taking the frequency derivative of the input impedance, the stored energy can be approximated through the Q-factor [43, 63],

$$Q_{\mathrm{Z}'_{\mathrm{in}}} = \frac{\omega}{2R_{\mathrm{in}}(\omega)} |Z'_{\mathrm{in0}}(\omega)|, \tag{66}$$

where Z_{in0} is the input impedance tuned to resonance. This simple expression (66) gives an accurate measure of the fractional bandwidth, but can overestimate the bandwidth for multiple resonance cases [26, 49].

The corresponding fractional bandwidth, B, is

$$B \approx \frac{2}{Q} \frac{\Gamma_0}{\sqrt{1-\Gamma_0^2}}, \tag{67}$$

for single resonance antennas [63], where Γ_0 denotes the threshold for the reflection coefficient. The relationship between the fractional bandwidth and Q-factor (67) for the RLC resonance circuit can also be used to define an equivalent Q-factor for a given threshold level Γ_0 *i.e.*,

$$Q_{\Gamma_0} = \frac{2}{B_{\Gamma_0}} \frac{\Gamma_0}{\sqrt{1-\Gamma_0^2}}, \tag{68}$$

where B_{Γ_0} denotes the fractional bandwidth for the threshold Γ_0.

Appendix B MoM Impedance Matrix

The MoM impedance matrix is divided into two parts in (12). This decomposition is non-unique and $\mathbf{Z}$ can alternatively be divided as

$$\mathbf{Z} = \mathrm{j}\omega\mu_0\mathbf{L} + \frac{1}{\mathrm{j}\omega\epsilon_0}\mathbf{C}_{\mathrm{i}} + \eta_0\mathbf{R} \tag{69}$$

for the free space case, where

$$L_{mn} = \int_{\partial\Omega}\int_{\partial\Omega} \boldsymbol{\psi}_{m1} \cdot \boldsymbol{\psi}_{n2} \frac{\cos(kR_{12})}{4\pi R_{12}} \,\mathrm{dS}_1 \,\mathrm{dS}_2, \tag{70}$$

$$C_{\mathrm{i}mn} = \int_{\partial\Omega}\int_{\partial\Omega} \nabla_1 \cdot \boldsymbol{\psi}_{m1} \nabla_2 \cdot \boldsymbol{\psi}_{n2} \frac{\cos(kR_{12})}{4\pi R_{12}} \,\mathrm{dS}_1 \,\mathrm{dS}_2, \tag{71}$$

and

$$R_{mn} = \int_{\partial\Omega}\int_{\partial\Omega} (k\boldsymbol{\psi}_{m1}\cdot\boldsymbol{\psi}_{n2} - \frac{1}{k}\nabla_1\cdot\boldsymbol{\psi}_{m1}\nabla_2\cdot\boldsymbol{\psi}_{n2})\frac{\sin(kR_{12})}{4\pi R_{12}}\,\mathrm{dS}_1\,\mathrm{dS}_2, \quad (72)$$

Here, $\boldsymbol{\psi}_{ni}$ is a short hand notation for basis functions $\boldsymbol{\psi}_n(\boldsymbol{r}_i)$ with $n = 1, ..., N$, $i = 1, 2$, $\boldsymbol{r}_i$ denotes the position vector, and $R_{12} = |\boldsymbol{r}_1 - \boldsymbol{r}_2|$.

Appendix Acknowledgments

The support of the Swedish foundation for strategic research under the program Applied Mathematics and the project Complex analysis and convex optimization for Electromagnetic design is gratefully acknowledged.

References

[1] A. Alù, M. G. Silveirinha, A. Salandrino, and N. Engheta. Epsilon-near-zero metamaterials and electromagnetic sources: Tailoring the radiation phase pattern. *Physical Review B*, **75**(15), pp. 155410, 2007.

[2] S. Arslanagic, R. W. Ziolkowski, and O. Breinbjerg. Analytical and numerical investigation of the radiation and scattering from concentric metamaterial cylinders excited by an electric line source. *Radio Sci.*, **42**(6), 2007.

[3] S. R. Best. Electrically small resonant planar antennas: Optimizing the quality factor and bandwidth. *IEEE Antennas Propag. Mag.*, **57**(3), pp. 38–47, Jun. 2015.

[4] O. Brune. Synthesis of a finite two-terminal network whose driving-point impedance is a prescribed function of frequency. *MIT J. Math. Phys.*, **10**, pp. 191–236, 1931.

[5] C. Caloz. Metamaterial dispersion engineering concepts and applications. *Proc. IEEE*, **99**(10), pp. 1711–1719, 2011.

[6] M. Capek, M. Gustafsson, and K. Schab. Minimization of antenna quality factor. *IEEE Trans. Antennas Propag.*, **65**(8), pp. 4115–4123, 2017.

[7] M. Capek, L. Jelinek, and G. A. E. Vandenbosch. Stored electromagnetic energy and quality factor of radiating structures. *Proc. R. Soc. A*, **472**(2188), 2016.

[8] F. Capolino, editor. *Theory and Phenomena of Metamaterials.* CRC Press, 2009.

[9] W. C. Chew, M. S. Tong, and B. Hu. *Integral Equation Methods for Electromagnetic and Elastic Waves*, volume 12. Morgan & Claypool, 2008.

[10] L. J. Chu. Physical limitations of omni-directional antennas. *J. Appl. Phys.*, **19**, pp. 1163–1175, 1948.

[11] M. Cismasu and M. Gustafsson. Antenna bandwidth optimization with single frequency simulation. *IEEE Trans. Antennas Propag.*, **62**(3), pp. 1304–1311, 2014.

[12] M. Cismasu and M. Gustafsson. Multiband antenna Q optimization using stored energy expressions. *IEEE Antennas Wirel. Propag. Lett.*, **13**(2014), pp. 646–649, 2014.

[13] R. E. Collin and S. Rothschild. Evaluation of antenna Q. *IEEE Trans. Antennas Propag.*, **12**, pp. 23–27, Jan. 1964.

[14] V. A. Counter. Miniature cavity antenna. Technical Report 2, Microwave Lab, 1948. Contract No. W28-099-ac-382.

[15] N. Engheta and R. W. Ziolkowski. *Metamaterials: physics and engineering explorations*. John Wiley & Sons, 2006.

[16] R. L. Fante. Quality factor of general ideal antennas. *IEEE Trans. Antennas Propag.*, **17**(2), pp. 151–155, Mar. 1969.

[17] W. Geyi. A method for the evaluation of small antenna Q. *IEEE Trans. Antennas Propag.*, **51**(8), pp. 2124–2129, 2003.

[18] W. Geyi. Physical limitations of antenna. *IEEE Trans. Antennas Propag.*, **51**(8), pp. 2116–2123, Aug. 2003.

[19] W. Geyi. *Foundations of Applied Electrodynamics*. John Wiley & Sons, 2011.

[20] M. Gustafsson, J. Friden, and D. Colombi. Antenna current optimization for lossy media with near field constraints. *IEEE Antennas Wirel. Propag. Lett.*, **14**, pp. 1538–1541, 2015.

[21] M. Gustafsson and B. L. G. Jonsson. Antenna Q and stored energy expressed in the fields, currents, and input impedance. *IEEE Trans. Antennas Propag.*, **63**(1), pp. 240–249, 2015.

[22] M. Gustafsson and B. L. G. Jonsson. Stored electromagnetic energy and antenna Q. *Prog. Electromagn. Res. (PIER)*, **150**, pp. 13–27, 2015.

[23] M. Gustafsson and S. Nordebo. Optimal antenna currents for Q, superdirectivity, and radiation patterns using convex optimization. *IEEE Trans. Antennas Propag.*, **61**(3), pp. 1109–1118, 2013.

[24] M. Gustafsson, D. Tayli, C. Ehrenborg, M. Cismasu, and S. Nordebo. Antenna current optimization using MATLAB and CVX. *FERMAT*, **15**(5), pp. 1–29, 2016.

[25] M. Gustafsson, M. Cismasu, and B. L. G. Jonsson. Physical bounds and optimal currents on antennas. *IEEE Trans. Antennas Propag.*, **60**(6), pp. 2672–2681, 2012.

[26] M. Gustafsson and S. Nordebo. Bandwidth, Q factor, and resonance models of antennas. *Prog. Electromagn. Res.*, **62**, pp. 1–20, 2006.

[27] M. Gustafsson, D. Tayli, and M. Cismasu. Q factors for antennas in dispersive media. Technical Report LUTEDX/(TEAT-7232)/1–24/(2014), Lund University, Department of Electrical and Information Technology and P.O. Box 118 and S-221 00 Lund, Sweden, 2014. http://www.eit.lth.se.

[28] M. Gustafsson, D. Tayli, and M. Cismasu. *Physical bounds of antennas*, pp. 1–32. Springer-Verlag, 2015.

[29] T. V. Hansen, O. S. Kim, and O. Breinbjerg. Properties of sub-wavelength spherical antennas with arbitrarily lossy magnetodielectric cores approaching the Chu lower bound. *IEEE Trans. Antennas Propag.*, **62**(3), pp. 1456–1460, 2014.

[30] R. F. Harrington. *Field Computation by Moment Methods.* Macmillan, New York, NY, 1968.

[31] R. F. Harrington and J. R. Mautz. Control of radar scattering by reactive loading. *IEEE Trans. Antennas Propag.*, **20**(4), pp. 446–454, 1972.

[32] P. Hazdra, M. Capek, and J. Eichler. Radiation Q-factors of thin-wire dipole arrangements. *IEEE Antennas Wirel. Propag. Lett.*, **10**, pp. 556–560, 2011.

[33] J. D. Jackson. *Classical Electrodynamics.* John Wiley & Sons, New York, NY, third edition, 1999.

[34] L. Jelinek and M. Capek. Optimal currents on arbitrarily shaped surfaces. *IEEE Trans. Antennas Propag.*, **65**(1), pp. 329–341, 2017.

[35] J. M. Jin. *Theory and Computation of Electromagnetic Fields.* Wiley Online Library, 2010.

[36] B. L. G. Jonsson and M. Gustafsson. Stored energies in electric and magnetic current densities for small antennas. *Proc. R. Soc. A*, **471**(2176), pp. 20140897, 2015.

[37] B. L. G. Jonsson and M. Gustafsson. Stored energies for electric and magnetic current densities. *arXiv preprint arXiv:1604.08572*, 2016.

[38] O. S. Kim. Lower bounds on Q for finite size antennas of arbitrary shape. *IEEE Trans. Antennas Propag.*, **64**(1), pp. 146–154, 2016.

[39] L. D. Landau and E. M. Lifshitz. *Electrodynamics of Continuous Media.* Pergamon Press, Oxford, first edition, 1960.

[40] J. S. McLean. A re-examination of the fundamental limits on the radiation Q of electrically small antennas. *IEEE Trans. Antennas Propag.*, **44**(5), pp. 672–676, May 1996.

[41] F. Merli, L. Bolomey, J. Zurcher, G. Corradini, E. Meurville, and A. Skrivervik. Design, realization and measurements of a miniature antenna for implantable wireless communication systems. *IEEE Trans. Antennas Propag.*, **59**(10), pp. 3544–3555, 2011.

[42] R. K. Moore. Effects of a surrounding conducting medium on antenna analysis. *IEEE Trans. Antennas Propag.*, **11**(3), pp. 216–225, 1963.

[43] T. Ohira. What in the world is Q? *IEEE Microw. Mag.*, **17**(6), pp. 42–49, Jun. 2016.

[44] A. F. Peterson, S. L. Ray, and R. Mittra. *Computational Methods for Electromagnetics*. IEEE Press, New York, NY, 1998.

[45] R. Ruppin. Electromagnetic energy density in a dispersive and absorptive material. *Physics letters A*, **299**(2), pp. 309–312, 2002.

[46] K. Schab, L. Jelinek, M. Capek, C. Ehrenborg, D. Tayli, G. Vandenbosch, and M. Gustafsson. Energy stored by radiating systems. Technical Report LUTEDX/(TEAT-7251)/1–32/(2017), Lund University, Department of Electrical and Information Technology, P.O. Box 118, S-221 00 Lund, Sweden, 2017.

[47] W. Smith. Average energy storage by a one-port and minimum energy synthesis. *IEEE Transactions on Circuit Theory*, **17**(3), pp. 427–430, 1970.

[48] W. E. Smith. The energy storage of a prescribed impedance. *Proceedings of the Royal Society of New South Wales*, **102**, pp. 203—-218, 1969.

[49] H. Stuart, S. Best, and A. Yaghjian. Limitations in relating quality factor to bandwidth in a double resonance small antenna. *IEEE Antennas Wirel. Propag. Lett.*, **6**, 2007.

[50] D. Tayli and M. Gustafsson. Physical bounds for antennas above a ground plane. *IEEE Antennas Wirel. Propag. Lett.*, **15**, pp. 1281–1284, 2016.

[51] S. Tretyakov. Electromagnetic field energy density in artificial microwave materials with strong dispersion and loss. *Physics Letters A*, **343**(1), pp. 231–237, 2005.

[52] J. G. van Bladel. *Electromagnetic Fields*. IEEE Press, Piscataway, NJ, second edition edition, 2007.

[53] G. A. E. Vandenbosch. Reactive energies, impedance, and Q factor of radiating structures. *IEEE Trans. Antennas Propag.*, **58**(4), pp. 1112–1127, 2010.

[54] G. A. E. Vandenbosch. Radiators in time domain, part II: finite pulses, sinusoidal regime and Q factor. *IEEE Trans. Antennas Propag.*, **61**(8), pp. 4004–4012, 2013.

[55] J. Volakis, C. C. Chen, and K. Fujimoto. *Small Antennas: Miniaturization Techniques & Applications.* McGraw-Hill, New York, NY, 2010.

[56] J. L. Volakis and K. Sertel. *Integral Equation Methods for Electromagnetics.* SciTech Publishing Inc., 2012.

[57] O. B. Vorobyev. Energy density of macroscopic electric and magnetic fields in dispersive medium with losses. *Prog. Electromagn. Res. B*, **40**, pp. 343–360, 2012.

[58] H. A. Wheeler. Fundamental limitations of a small VLF antenna for submarines. *IRE Trans. on Antennas and Propagation*, **6**, pp. 123–125, 1958.

[59] J. C. Willems. Dissipative dynamical systems part II: Linear systems with quadratic supply rates. *Arch. Rational Mech. Anal.*, **45**(5), pp. 352–393, 1972.

[60] O. Wing. *Classical Circuit Theory.* Springer, New York, 2008.

[61] A. D. Yaghjian. Internal energy, Q-energy, Poynting's theorem, and the stress dyadic in dispersive material. *IEEE Trans. Antennas Propag.*, **55**(6), pp. 1495–1505, 2007.

[62] A. D. Yaghjian, M. Gustafsson, and B. L. G. Jonsson. Minimum Q for lossy and lossless electrically small dipole antennas. *Prog. Electromagn. Res.*, **143**, pp. 641–673, 2013.

[63] A. D. Yaghjian and S. R. Best. Impedance, bandwidth, and Q of antennas. *IEEE Trans. Antennas Propag.*, **53**(4), pp. 1298–1324, 2005.

[64] O. J. Zobel. Theory and design of uniform and composite electric wave filters. *Bell System Technical Journal*, **2**, pp. 1–46, 1923.

"Ceterum autem censeo Carthaginem esse delendam"

-Cato the Elder